# THEORETICAL STUDY OF NUCLEAR FLOW AND STOPPING AT INTERMEDIATE ENERGIES

**A THESIS**

submitted to the

**THAPAR INSTITUTE OF ENGINEERING AND TECHNOLOGY, PATIALA**

for the degree of

**DOCTOR OF PHILOSOPHY**

IN THE FACULTY OF SCIENCE

By

**Deepshikha**

**Regn. No. 901412010**


**SCHOOL OF PHYSICS AND MATERIALS SCIENCE**

**THAPAR INSTITUTE OF ENGINEERING AND TECHNOLOGY**

**PATIALA-147004, PUNJAB (INDIA)**

.

*Dedicated to*

**My Beloved Mother**

*who left this materialistic world on 21st, February, 2016.*

THAPAR INSTITUTE
OF ENGINEERING & TECHNOLOGY
(Deemed to be University)

TIET, PATIALA

# CANDIDATE'S DECLARATION

I hereby certify that the work in this thesis entitled "**THEORETICAL STUDY OF NUCLEAR FLOW AND STOPPING AT INTERMEDIATE ENERGIES**" is partial fulfillment of the requirements for the award of degree of Doctor of Philosophy and submitted in the School of Physics and Materials Science, Thapar Institute of Engineering and Technology, Patiala, is an authentic record of my own work carried out during a period from July 2014 to October 2018 under the supervision of **Dr. Suneel Kumar**, Associate Professor, Department of Physics, Central University of Haryana, Jant-Pali Mahendergarh (India). The matter presented in this thesis has not been submitted by me in part or full for the award of any other degree in any other university or institute.

Deepshikha

(Deepshikha)

(Regn. No. 901412010)

This is to certify that the above statement made by the candidate is correct to the best of our knowledge.

Supervisor

S Kumar
26/4/2019

(Dr. Suneel Kumar)
Associate Professor
Department of Physics
Central University of Haryana
Jant-Pali Mahendergarh (India)

Administrative Supervisor

O Pandey

(Dr. O. P. Pandey)
Senior Professor and Head SPMS
School of Physics and Materials Science
TIET Patiala
Punjab (India)

# Acknowledgments

Upon attaining this goal of a doctorate degree, I must reflect back upon what has brought me to this point. I would like to pay high regards to Saraswati the Goddess of knowledge who gave me some intellect and wisdom to reach where I am today. It is a great pleasure and privilege to express my deepest sense of gratitude to all the truly remarkable people, I have met during my doctoral study.

First, I would like to express my everlasting indebtedness to my supervisor **Dr. Suneel Kumar**. I am immensely grateful to him for his enthusiasm. His observations and critical comments helped me to establish the overall direction of the research and make me to move forward with investigation in depth during my doctoral study. I am forever indebted thanks to my Administrative Supervisor **Prof. O. P. Pandey**, for guiding me often with big doses of patience.

I would like to thank Director TIET, **Prof. Prakash Gopalan** for allowing me to grow as a researcher. Their advice in shaping my career has been priceless. Without their precious support it would not be possible to conduct the research so efficiently and timely. I am also thankful to Registrar TIET, **Dr. Gurbinder Singh** for encouraging me time to time and my research attitude. Thanks to **Prof. Rafat Siddique** Dean, Research and sponsored projects for providing best possible research facilities.

I offer thanks to Prof. Rajeev K. Puri, Panjab University, Chandigarh for his support during my whole work. I acknowledge the useful suggestions from the members of my doctoral committee **Dr. Manoj Sharma, Dr. Debabrata Deb and Dr. Arvind Kumar Lal**. Their guidance has served me well and I owe them my heartfelt appreciation. I wish to express humble and special thanks to faculty of School of Physics and Materials Science Dr. Kulvir Singh, Dr. Puneet Sharma, Dr. Soumendu Jana, Dr. Poonam Uniyal, Dr. Alka Upadhyay and Dr. Loveleen Kaur Brar. My sincere thanks also goes to all the faculty and staff of the SPMS for their kind support and motivation. I would like to thank administrative and technical staff members of the Thapar Institute who has been kind enough to advise and help in their respective roles.

No research is possible without the Library, the center of learning resources. I take this time to express my gratitude to all the library staff for their services.

I am thankful to my dearest friend **Ms. Richa** and her husband **Dr. Munish Aggarwal**, Dean Research and HOD Applied Science of Lyallpur Khalsa College of Engineering, Jalandhar, for his valuable and necessary support. In the later stage of my research work, Dr. Munish offered a great amount of help, numerous advices on writing papers and thesis. His numerous advice, insight and enriching comments help me in improving the quality of my research papers and thesis. He spent his invaluable time in reading my thesis comprehensively and bringing the document in publishing form is acknowledged.

I am highly thankful to my best teacher **Dr. Varinder Kaur** (Principal) GTB Khalsa College, Dasuya for her support and constant source of inspiration. It has been an honor for me to be her student. Her steady encouragement and conviction will always inspire me. I am thankful to Associate professor, **Dr. Rohit Mehra** National Institute of Technology, Jalandhar, who introduces me with the research and enlightening me as a first glance of research. He has guided and encouraged me to carry on through these years. I offer special thanks to **Dr. H. M. Mittal** National Institute of Technology, Jalandhar who taught me nuclear Physics. I am also thankful to **Prof. Arun Bharti** University of Jammu, for vision, encouragement and advice. I am highly thankful to **Prof. Anju Bhasin** Vice-Chancellor of Cluster University, Jammu, for the helping hands whenever I needed the most.

I would like to thank my seniors **Dr. Mani Mahajan** and **Dr. Gourav Singla** for their guidance and help whenever I bothered them. I am also thankful to **Dr. Karan Singh Vinayak** for his support. A warm word for my colleague and great friend Shoiab Noor, Neeraj Sharma, Jaspreet Kaur Naggi, Navneet Singh and Kundan that always managed to make me feel special and with whom I had the best tea breaks. I also wish to extend my thanks to all my friends, juniors and seniors at Thapar for all the memorable moments. I would also greatly appreciate the help of Rajni di, Kamal di, Navjot di, Gurjeet Kaur, Neha Grover, Kanishka Sharma, Ishita Sharma, Pallavi Gupta, Navneet Kaur, Shobha, Nisha di, Ruby Priya, Jagroop, Bharti, Shivani Jain

and Shinavi Punj mam. I highly appreciate Amandeep Randhawa mam for her pleasant company.

I can't think of achieving this stage without the support of my best friends **Dr. Sonia Sharma**, **Dr. Anuuradha Gupta** and **Ms. Monika Sharma** who helped me 24×7 during my Ph.D. I am thankful to all of them for having the doors open to any of my questions and problems. I highly appreciate the support of **Mr. Jagjeet singh** who always motivated and guided me. I am also thankful to the little kids **Anahita**, **Reyansh** and **Radhika**, they always made me feel like a kid and helped me relieving the stress whenever I felt so. I am thankful to Ms. Shalpa mam for giving some cherishable and unforgettable moments. I am also thankful to **Ms. Harsh** mam and **Mr. Suresh Metha** sir, for special love and care.

I am very much thankful to the **Council of Scientific and Industrial Research (CSIR)**, Government of India for providing me the Senior Research fellowship (SRF) during my doctoral study and **Thapar Institute of Engineering and Technology (TIET)** for Teaching Associateship. I am also thankful to **Department of Science and Technology (DST)**, Government of India and **Thapar Institute of Engineering and Technology (TIET)** for the financial support to present my research work in 23rd Workshop 'Marie & Pierre Curie' on Essential Problems in Nuclear Physics: Kazimierz Dolny, Poland. I am extremely thankful to the **Galileo Galilei Institute** (GGI) for theoretical Physics Florence, Italy, given me the opportunity to attend the school.

I would like to thank my grandparents and my extensive set of relatives, all of whom lofted me above their heads and made me feel like the center of attention, providing motivation to continue climbing. I owe you all much more than German chocolate. I am also thankful to my cousins **Abhishek Sharma** and **Atul Sharma**, who helped me to look at the lighter side of all situations, filling my life with love and laughter.

Finally, I'd like to thank my mother **Ms. Parveen Sharad** and my father **Mr. Satya Varat Sharad**, who gave me a great start to my education by letting me read anything I could get my hands on. I would not be able to go through all the challenges during my Ph.D. research without their support and understanding. They always believed in

me and gave me words of encouragement. I am wholeheartedly thankful to you for making me realize that how meaningful and beautiful my life is. Thank you **Abhinav Sharad** my loving brother, for always helping me with fun and crazy ideas in hard times. He is always ready to help with a smile and faithful support during all the stages of my Ph.D.

I am grateful to numerous local and global peers who have contributed towards shaping this thesis. Without the help of all these people, this thesis would not have seen the light of the day. Lastly, I am thankful to all those whose names have been left unintentionally.

Thanks for all of you for your encouragement !!!!!!!!!

Deepshikha

Date : 26.04.2019 (Deepshikha)

Patiala

# List of Publications:

## A. Journals:

1. Memory loss in central heavy-ion collisions at intermediate energy.
   Deepshikha and Suneel Kumar
   **Nuclear Physics A 982, 89 (2019).**
   doi.org/10.1016/j.nuclphysa.2018.11.007.

2. Comprehensive study of memory loss for mass symmetric colliding nuclei at intermediate energy.
   Deepshikha and Suneel Kumar
   **Nuclear Physics A 978, 13 (2018).**
   doi.org/10.1016/j.nuclphysa.2018.07.007.

3. Heavy-Ion collision dynamics: Correlation with elliptic flow and nuclear stopping.
   Deepshikha and Suneel Kumar
   **Nuclear Physics A 977, 69 (2018).**
   doi.org/10.1016/j.nuclphysa.2018.06.003.

4. Investigation of nuclear stopping observable in heavy ion collisions.
   Deepshikha and Suneel Kumar
   **Nuclear Physics A 975, 29 (2018).**
   doi.org/10.1016/j.nuclphysa.2018.04.002.

5. Participation of nucleons among different harmonics of anisotropic flow.
   Deepshikha and Suneel Kumar
   **Canadian Journal of Physics 96, 1092 (2018).**
   doi.org/10.1139/cjp-2017-0607.

6. On the inadequate equilibrium accomplished in mass asymmetric reactions at intermediate energies.
   Deepshikha and Suneel Kumar

**Modern Physics Letters A 33, 1850201 (2018).**
doi.org/10.1142/S0217732318502012.

7. Various characteristics of transition energy for nearly symmetric colliding nuclei
Deepshikha and Suneel Kumar
**International Journal of Modern Physics E 27, 1850084 (2018)**.
doi.org/10.1142/S0218301318500842.

8. Analyzing the fragment production in mass asymmetric reaction as a function of density dependent part of symmetry energy.
Amandeep, Deepshikha, Karan Singh Vinayak and Suneel Kumar
**Phys. of Atomic Nuclei 4, 474 (2016).**
doi.org/10.1134/S1063778816040153.

9. To study the effect of mass asymmetry by compensating the colliding geometry at intermediate energies.
Deepshikha and Suneel Kumar (to be submitted).

## B. Publications in AIP Proceedings:

10. On the contribution of Symmetry and Coulomb components of nucleon nucleon potentials in estimation of transition energy.
Deepshikha and Suneel Kumar
**AIP Conf. Proc. 1953, 140027 (2018).**
DOI:10.1063/1.5033202.

11. Transition energy as a probe to study the mass asymmetric nuclear reactions at intermediate energies.
Deepshikha and Suneel Kumar
**AIP Conf. Proc. 2006, 030005 (2018).**
DOI:10.1063/1.5051261.

12. Interconnection between balance energy and transition energy for light charged particles in heavy-ion collisions.

Deepshikha and Suneel Kumar

**AIP Conf. Proc. 2050, 020014 (2018).**

DOI:10.1063/1.5083601.

13. Density and Temperature Evolution in Mass Asymmetric Reactions.
    Deepshikha, Amandeep, Karan Singh Vinayak and Suneel Kumar
    **AIP Conf. Proc. 1728, 020232 (2016).**
    DOI:10.1063/1.4946283.

## C. Symposia/Workshops/Conferences:

14. Interdependence between balance energy and transition energy for nearly symmetric colliding nuclei.
    Deepshikha and Suneel Kumar
    **National Conference on Advanced Materials and Devices for Futuristic Applications, Chandigarh University, 20 (2018) (Best Poster Award)**.

15. Strength of directed to the elliptic flow at intermediate energies.
    Deepshikha and Suneel Kumar
    **Proceedings of DAE Symposium on Nuclear Physics, Vol. 63, 528-529 (2018)**.

16. Effect of Cross-section and Gaussian width on nuclear stopping.
    Deepshikha and Suneel Kumar
    **Proceedings of DAE Symposium on Nuclear Physics, Vol. 62, 528-529 (2017)**.

17. The study of Participant and Spectator matter for asymmetric collisions.
    Deepshikha and Suneel Kumar
    **National Conference On Recent Trends in Nuclear Physics, Aligarh Muslim university, 25 (2016).**

18. Temperature evolution in mass asymmetric reactions in heavy ion collision.
    Deepshikha and Suneel Kumar

**National Conference On Recent Trends in Nuclear Physics, Aligarh Muslim university, 26 (2016).**

19. Relative contribution of nucleons among different harmonics of anisotropic flow.
    Deepshikha and Suneel Kumar
    **23rd Nuclear Physics Workshop Marie and Pierre Curie, Poland 29 (2016)**.

20. Interrelation between Energy of Vanishing flow and Transition Energy.
    Deepshikha, Amandeep Kaur and Suneel Kumar
    **Proceedings of DAE Symposium on Nuclear Physics Vol. 60, 460-461 (2015).**

21. Neutron/Proton emission in mass-asymmetric intermediate energy heavy-ion collisions.
    Amandeep, Karan Singh Vinayak, Deepshikha and Suneel Kumar
    **Proceedings of DAE Symposium on Nuclear Physics Vol. 60, 458-459 (2015).**

22. Role of different momentum dependent interaction on energy dependence of directed flow.
    Amandeep Kaur and Deepshikha
    **Proceedings of National Conference on Emerging Challenges in Nuclear and Many-body Physics, University of Jammu, 30 (2014).**

23. Influence of isospin momentum interaction on transverse flow.
    Amandeep Kaur, Deepshikha and Suneel Kumar
    **Proceedings of DAE Symposium on Nuclear Physics Vol. 59, 474-475 (2014).**

| Abbreviations | |
|---|---|
| EOS | equation of state |
| QGP | quark gluon plasma |
| TDHF | time dependent hartree-fock |
| BUU | boltzmann uehling uhlenbeck |
| IBUU | isospin dependent boltzmann uehling uhlenbeck |
| INC | intranuclear cascade calculations |
| CMD | classical molecular dynamics |
| FMD | fermionic molecular dynamics |
| AMD | antisymmetrized molecular dynamics |
| QMD | quantum molecular dynamics |
| IQMD | isospin dependent quantum molecular dynamics |
| ImQMD | improved quantum molecular dynamics |
| FN | free nucleons |
| LCP | light charged particles |
| MMF | medium mass fragments |
| IMF | intermediate mass fragments |
| HMF | heavy mass fragments |
| MST | minimum spanning tree |
| MDI | momentum dependent interactions |

# Contents

# List of Figures

# List of Tables

# ABSTRACT

The nuclear physics field promises a rich variety of interesting phenomena studied both by experimental observations and theoretical calculations. While switching from low incident energy to higher incident energy plenty of phenomenon have been observed. In the present study we have explored different aspects of two phenomena namely collective flow and nuclear stopping using isospin-dependent Quantum Molecular Dynamics (IQMD) model.

Initially, author has tried to ruminate the basic collision dynamics and shed light on influence of centrality of nuclear reactions before and after collisions. The central collisions, peripheral collisions and three dimensional trajectory of nucleons have been discussed in detail. The phase space of nucleons in nuclear reactions have also been discussed.

The detailed analysis has been made on nuclear stopping using various observable for the mass symmetric and asymmetric reactions. Our study proves that the ratio of width of transverse to longitudinal rapidity distribution i.e., $< varxz >$ is the most suitable parameter to study nuclear stopping. Also, it has been observed that light mass fragments (LMF's) emitted from participant region can be used as a barometer to study nuclear stopping. Attempts have been made to recognize the aspect of nucleon-nucleon cross-sections, equation of state and width of Gaussian wave packet on memory loss of nucleons. Finally, correlations among nucleons and memory loss have been explored thoroughly.

It has been observed that effect of mass asymmetry can be compensated by changing the impact parameter of nuclear reactions. In a comparative study, various mass asymmetric reactions with total mass fixed have been also analyzed and knock off that mass asymmetry of the reaction has a remarkable influence on the dynamics of the reaction. Thus, while studying various phenomena of the heavy-ion reactions at intermediate energies, the mass asymmetry of the reaction should be properly taken into account.

Nuclear flow observable have been investigated systematically for the collision of nearly

symmetric nuclei. Both balance and transition energies have shown their dependence on various input parameters of the reaction like the composite mass of the colliding nuclei, incident energy and impact parameter. In addition to this, it has been concluded that power law behavior is perceived for both the balance and transition energies. Transition energy is more expedient to analyzing the behavior of compressed nuclear matter. Further, squeeze out phenomenon is helpful to understand the reaction dynamics. The higher harmonics i.e., $< v_3 >$ and $< v_4 >$ have smaller contribution than $< v_1 >$ and $< v_2 >$. The percentage of nucleons participating in flow decreases with increasing order of the harmonics.

Lastly, author summarize the work carried out in this thesis along with the future prospects for the extension of present work.

# Chapter 1

# Introduction

*" Take up one idea. Make that one idea your life - think of it, a dream of it, live on that idea. Let the brain, muscles, nerves, every part of your body, be full of that idea, and just leave every other idea alone. This is the way to success."*.....*Swami Vivekananda.*

## 1.1 Evolution of nuclear physics

The elucidation of the nuclear physics stems basically with the discovery of X-rays by Rontgen in 1895 and the discovery of natural radioactivity in 1896 by Antoine Henri Becquerel [1]. These discoveries may be regarded as birth of the nuclear physics. The phenomenon of natural radioactivity suggests that unstable nuclei are capable of emitting different particles like $\alpha$, $\beta$ and $\gamma$-rays. When the nucleus disintegrates by emitting these particles or capturing an electron, the process is called radioactive decay [2–8]. Fig 1.1, represents the relation between the relative activity of radioactive substance with time.

In the early fifties, one was able to accelerate only light charged particles due to which nuclear physics was confined to study limited phenomena like fusion, fission, cluster radioactivity and deep inelastic scattering. Now a days accelerators are able to accelerate the nuclei up to several hundreds of GeV. In terms of energy domain, the nuclear reactions may be classified into three different categories varying from few MeV/nucleon to GeV/nucleon namely low, intermediate and high energy nuclear physics. The heavy-

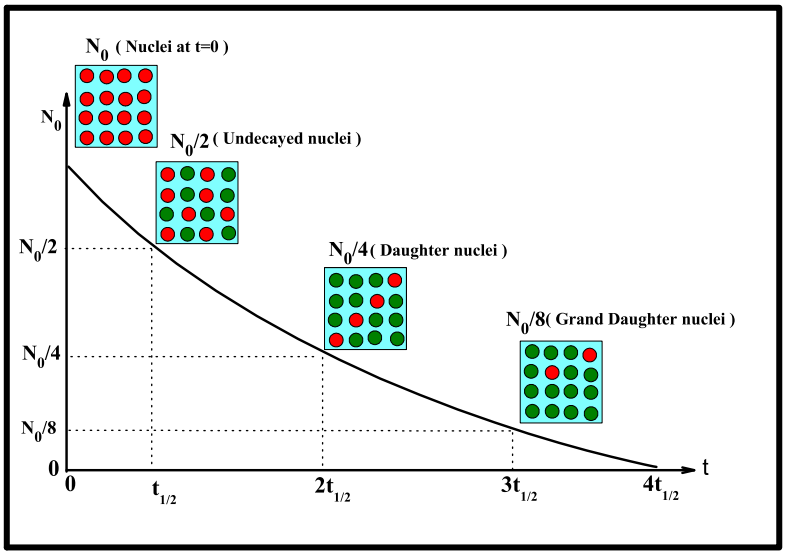


**Figure 1.1:** Exponential decay curve of the nuclei in a radioactive sample with respect to half-life.

ion nuclear reactions at low incident energy give unique possibility to study nucleus-nucleus interactions such as fusion, fission, cluster decay, formation of super heavy nuclei and the halo-nuclei etc [9–12]. The heavy-ion collisions at intermediate energy (10 MeV/nucleon $<$ E $\leq$ 2GeV/nucleon) is the domain selected for the present study. Several phenomena like nuclear stopping [13–22], collective flow [20, 23–25], multi-fragmentation [26–34], sub-threshold particle production [35] and isospin dynamics [19, 36] are observed at intermediate energies. On the other hand, the main interest to study high energy (E $>$ 2 GeV/nucleon) nuclear reactions is to explore the world of deconfinement and quark-gluon plasma [37, 38]. Thus, each type of reaction with its own specific scenario provides information that are crucial to understand clear picture of nuclear reaction dynamics and nuclear physics as a whole.

Experimental discovery by Ernest Rutherford [39–41] were obligatory to account for structure, properties and interaction of nuclei. In order to understand the properties of the nucleus, pictorial view of elementary parts of an atom are presented in the Fig 1.2. The atom consists of a small but massive nucleus surrounded by a cloud of

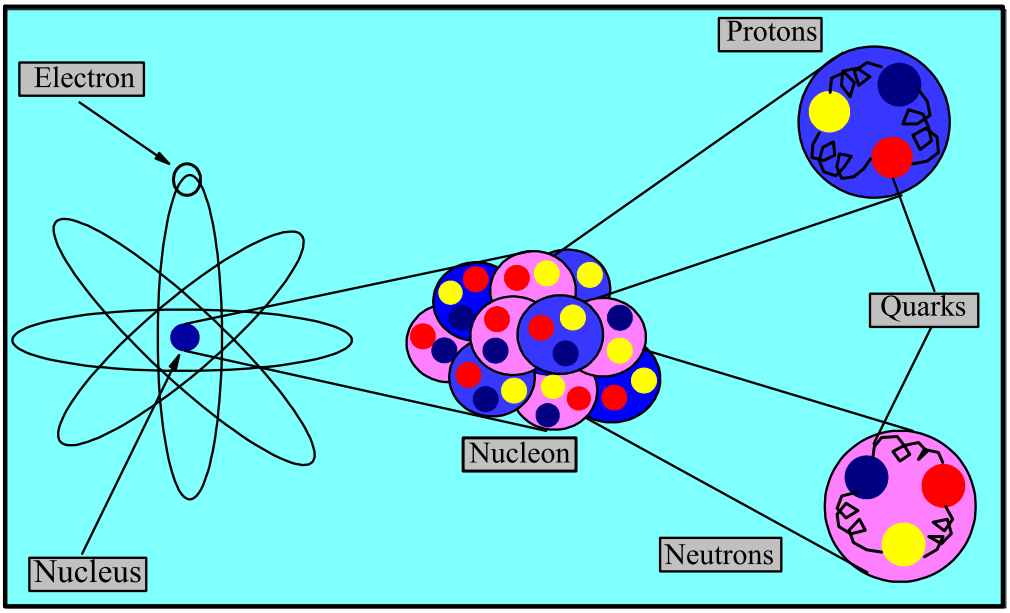


**Figure 1.2:** Pictorial view of elementary parts of an atom.

rapidly moving electrons. Neutrons and protons make up the nucleus held together by the strong interactions known as nuclear force. Nucleon consists of quarks [42] as per standard model, the interactions among the quarks are exchanged by the basic particle known as gluon [43]. The standard model in particle physics describes the theory concerning the three fundamental forces i.e., electromagnetic, weak and strong nuclear forces. The quantum chromo-dynamics (QCD) [44] is primary element of the standard model. QCD have two peculiar properties i.e., confinement and asymptotic freedom [45, 46]. The state in which matter consists of high density of quarks and gluons is called quark-gluon plasma state (QGP) [47].

## 1.2 Significance of Heavy-ion reactions

During the early stage of the universe, the interior constitution of neutron star and evolution of nuclear matter strongly depends upon the density and temperature of hadron matter. To understand many unanswered questions about the origin of universe, the

situation at t = 0, of big bang must be considered. The atoms, molecules, elements and compounds were originated from the Big Bang and scattered throughout the universe billions year ago. Occurrence of astrophysical happening are remote in space and time, therefore to study nuclear matter at extreme temperature and densities is quite difficult. Also, it is very difficult to accumulate data from cosmic rays, which is an another source of heavy ions. Heavy-ion collisions (HICs) are used to study some of these theories for instance, knowing about the nature of the strong forces and about the state of matter in the first few microsecond after the Big Bang. The study of HICs at intermediate energies give us the possibility to understand and explain the characteristics of nuclear matter under the conditions of temperature and density similar to what was existed at the time of early universe. The heavy-ion reactions at intermediate energy regime are best suited to investigation for the nuclear equation of state (NEOS). Other possible phenomenon which are accomplished with heavy ion collisions:

- Produce nuclear matter with high angular momentum/excitation energy.
- Produce nuclear matter with large neutron or proton deficiency.
- Produce nuclei away from the dripline.

## 1.3 The mean field theory (MFT)

The concept of mean field theory is an approximation method which is applicable for many-body problem of identical particles like atoms and nucleus [48]. For a many-body system Schrodinger wave equation can not be solved to obtain the energy spectrum and wave functions analytically [48] and in such a situations average potential is used, which is a mean potential of all interactions acting upon a single particle. Using this mean potential Schrodinger equation can be solved and known as mean field method. The concept of mean field theory [49] is widely used for the description of many-body interacting systems. The idea is to treat the many-body system not by summing up all mutual two-body interactions of the particles but to describe the interaction of one particle with the remaining particles by an average potential created by the other particles. Mean field theory is very efficient for the description of many body systems like finite nuclei or infinite nuclear matter and neutron matter which occurs in the interior

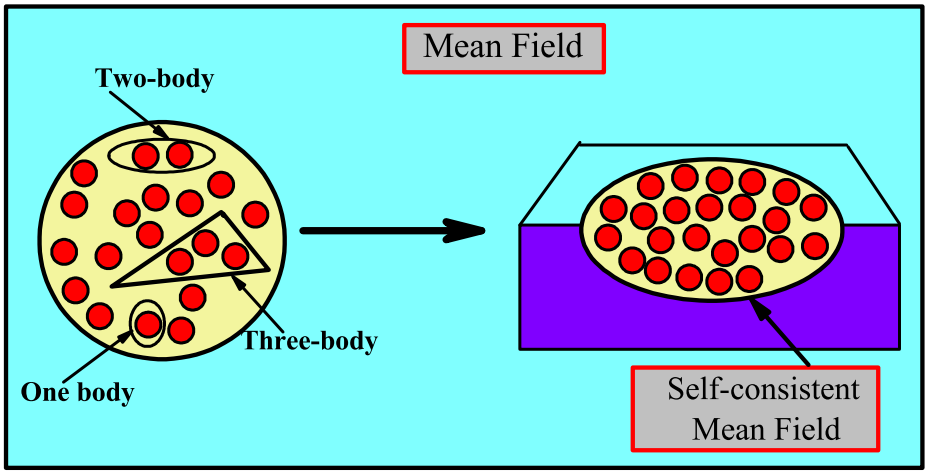


**Figure 1.3:** Schematic diagram for the mean field.

of neutron star. At low energies, this is an excellent approximation method to study nuclear structure. In the Fig 1.3, schematic diagram of mean field is shown. To convert many-body system into a non-interacting system of quasi-particles external mean field potential is a powerful approximation. The remaining interactions are known as residual interactions and that can be served as a perturbation potential in the base of perturbation approximation [50].

## 1.4 Nucleus-Nucleus (NN) collision to hydrodynamics

A heavy-ion collision is a step by step process and each step demands its own explanation, representation and interpretation. Hydrodynamics [51] is a convenient and applicable tool to describe one of these steps. A schematic evolution of the system is shown in the Fig 1.4, which shows four different phases of heavy-ion collision. Initially two nuclei collide with each other. After the collision phase, protons and neutrons

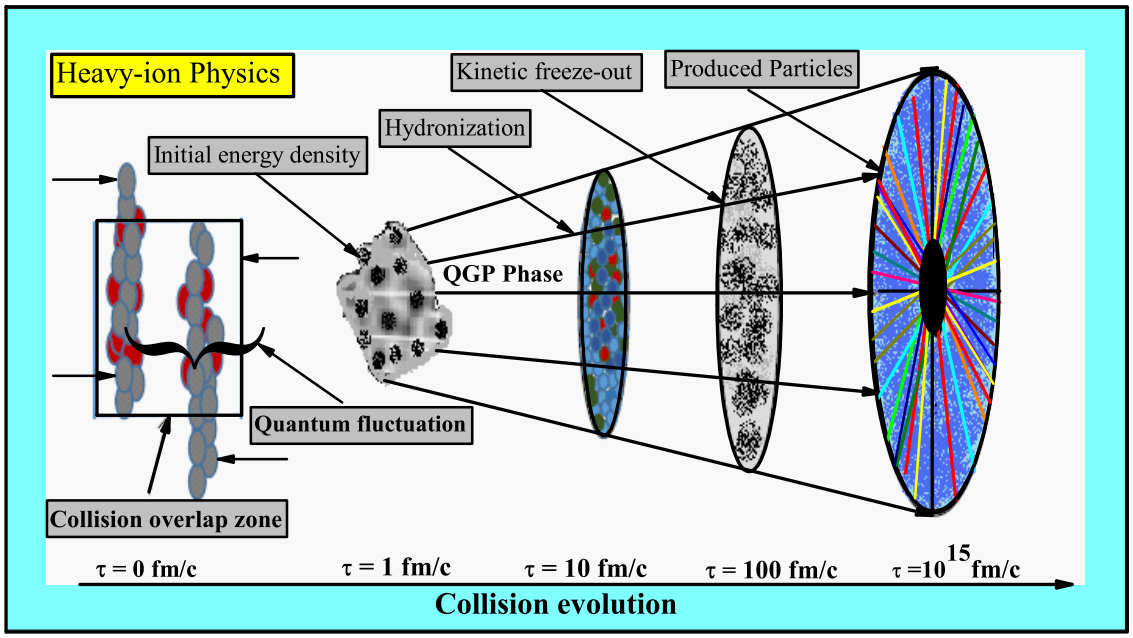


**Figure 1.4:** Schematic diagram for the evolution of heavy-ion collision.

of the colliding nuclei collapse with each other and form a fireball during the early times in the collisions. This stage is called quark deconfinement. This fireball created in the second step expands and cools with time. Then the system undergoes for the third stage, which is called hydronization and the last step is kinetic freeze-out. In the kinetic freeze-out stage [52] in which the individual quarks and gluons interact with the ordinary matter and spread away in all the directions.

In the Fig 1.5, the same process is shown in the space time diagram. After the primary interaction of two colliding nuclei, pre-equilibrium occurs. Pre-equilibrium emission takes place after the collisions of two nuclei. Pre-equilibrium stage leads to the creation of heavy quarks and photons etc. Thermal equilibrium takes place due to multiple scattering between nucleons. In the interacting system, the mean free path of nucleons is expected to be narrow in comparison to the system size, if energy density is high, thermalized quark gluon plasma (QGP) [53,54] expands hydrodynamically. Tem-

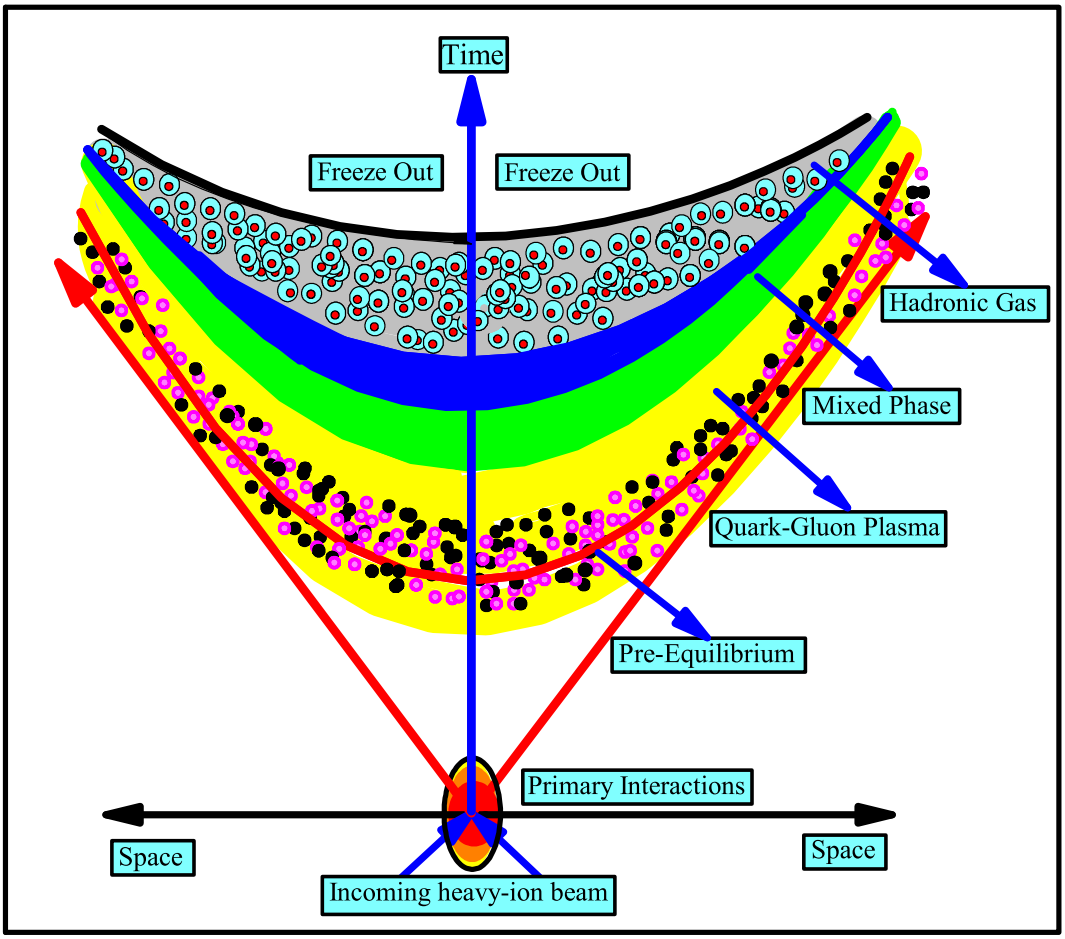


**Figure 1.5:** The space time evolution of heavy-ion collision which undergoes a phase transition to a QGP.

perature of the medium decreases with its expansion. Lastly the system achieves freeze out state which strongly depends upon the temperature and the centrality. Chemical freeze-out describes the point where inelastic processes converts one kind of hadronic species. The point where the momentum of the produced particles are fixed is known as thermal or kinetic freeze-out.

## 1.5 Equation of State for isospin symmetric nuclear matter

Nucleon-nucleon (NN) collision provides the unique way of exploring interesting topic such as nuclear equation of state (EOS) [55, 56] and EOS describes the relationship between temperature, pressure and density. The equation of state (EOS) of nuclear matter is useful and significant tool to study the properties of nuclear matter at and far from the line of stability of structures and evolution of compact astrophysical objects such as neutron stars [57] and core-collapse supernovae [58]. The nuclear equation of state is valid only if it reproduces the properties like saturation density and binding energy per nucleon. The maximum density of nucleons in finite nuclei is called saturation density and maximum value of saturation density is equal to $\rho_0 = 0.16 \pm 0.02$ nucleons/fm$^3$. The binding energy per nucleon of a nucleus is a measure of the stability of a nucleus. The distance traveled by nucleons between two successive collisions is known as mean free path. Nuclear compressibility $\kappa$, is an empirical property that

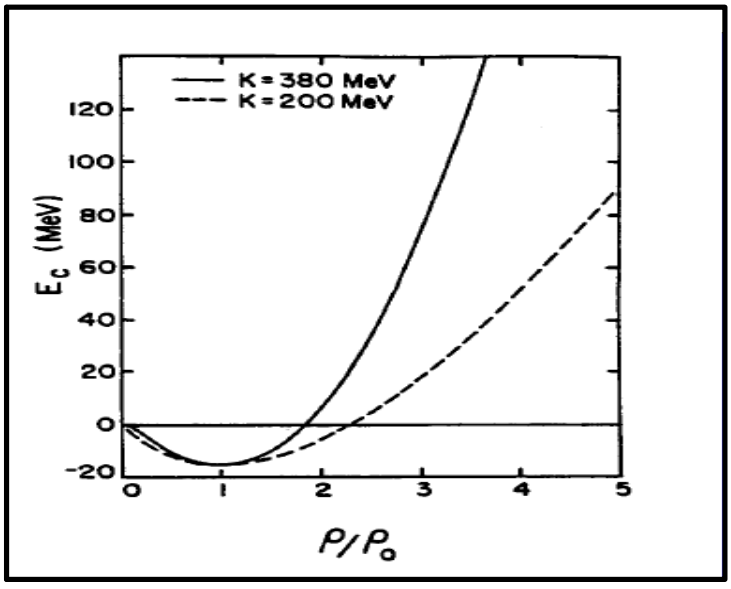


**Figure 1.6:** The equation of state for two different values of the compressibility of nuclear matter [59].

characterize the equation of state (EOS) and is represented as:

$$\kappa \;=\; 9\rho_o^2 \frac{d^2}{d\rho^2}\left(\frac{E}{A}\right). \tag{1.1}$$

here E/A, represents the energy per particle at normal nuclear matter density. Two possible equation of state (EOS) are, soft equation of state with $\kappa = 200$ MeV and hard equation of state with $\kappa = 380$ MeV, corresponding to two different incompressibility [60] are shown in Fig 1.6. The detail regarding the equation of state has been discussed in chapter 2.

## 1.6 Observables to study heavy-ion collisions

The study of heavy-ion reactions achieved great impetus with the evolution of the various phenomenon which revolutionized the understanding of nuclear matter at intermediate energies. Moreover such phenomena are highly specific towards the input parameters like incident energy and impact parameter of the reaction. These phenomenon are potentially significant and details regarding these phenomena are discussed in the succeeding sections.

### 1.6.1 Multi-fragmentation

Multi-fragmentation is a phenomenon, which is associated with breakup of the highly excited nuclear matter into fragments of different masses depending on the incident energy, system mass and impact parameter of the reaction [61–71]. According to the theoretical point of view, phenomenon of multi-fragmentation is the process in which excitation energy is deposited in compressed matter which leads to breaks up of excited nuclear matter into fragments. The mass symmetric reactions result in higher compression and mass asymmetric reactions lead to rotation of colliding nuclear matter. At a smaller value of impact parameter and due to maximum overlap there are frequent nucleon-nucleon collisions, so maximum part of the nuclear matter is emitted in the form of free nucleons while most of the initial correlations among the nucleons are destroyed. This leads to the formation of light mass fragments and free nucleons. In contrast, the scenario for peripheral collisions i.e., at higher value of impact parameter

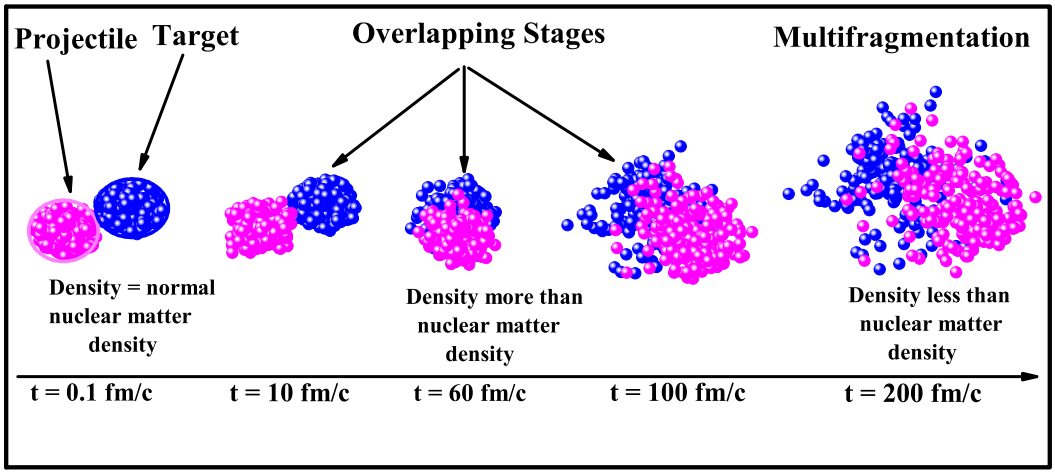


**Figure 1.7:** A schematic representation of nuclear multi-fragmentation process.

is quite different because many of the initial correlations are preserved. It has been observed that nucleons from the target and projectile form fragments of different size such as free nucleons (FN's) A = 1, light mass fragments (LMF's) $2 \leq A \leq 4$ and intermediate mass fragments (IMF's) $5 \leq A \leq \frac{A_{tot}}{3}$.

### 1.6.2 Anisotropic flow

Anisotropic flow term is used to describe the collective evolution of the nucleons observed as an overall pattern which correlates with the momentum of the final state nucleons. The pattern is believed to be developed due to the initial asymmetry of the nuclear collisions. The azimuthal anisotropy of the transverse momentum distribution in non-central heavy-ion collisions, suggested as a signature of collective flow [72]. Mathematically, anisotropic flow can be defined with the help of Fourier expansion [73]:

$$\frac{dN}{d\phi} \propto [1 + 2\sum_{n=1}^{\infty} v_n \cos(n\phi)] \tag{1.2}$$

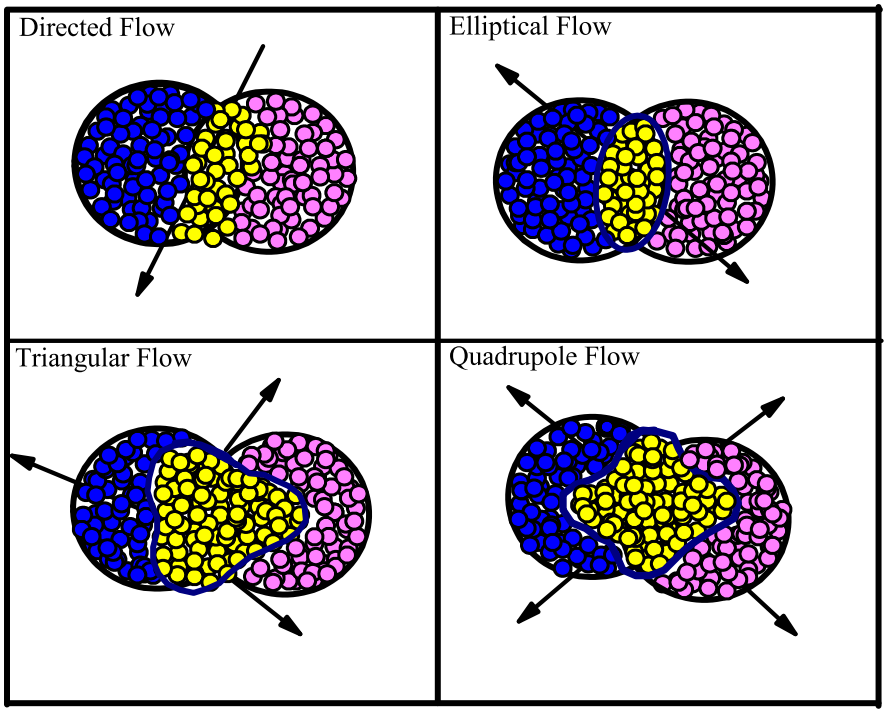


**Figure 1.8:** Schematic representation of different types of flow

where $\phi$ is the azimuthal angle between the transverse momentum of the particles and the reaction plane. The first harmonic coefficient $< v_1 >$ known as the directed flow, second harmonic coefficient $< v_2 >$ represents elliptical flow, third harmonic coefficient $< v_3 >$ represents triangular flow and fourth harmonic coefficient $< v_4 >$ represents the quadrangular flow respectively. Fig 1.8, represent the distribution of nucleons involved in directed flow ($< v_1 >$), elliptic flow ($< v_2 >$), triangular ($< v_3 >$), and quadrangular ($< v_4 >$) flow. The first harmonic coefficient corresponds to drift of nucleons and such a flow is called directed flow. Elliptic flow is represented by the elliptical distribution of nucleons. If the azimuthal distribution is of triangular shape then such flow is called triangular flow and in the last quadrangular distribution is presented. The anisotropic flow can be influenced by the transverse momentum of the nucleons and found to be a promising tool for elucidating flow. Such type of study is useful to understand the reaction dynamics and the flow shapes. The theoretical

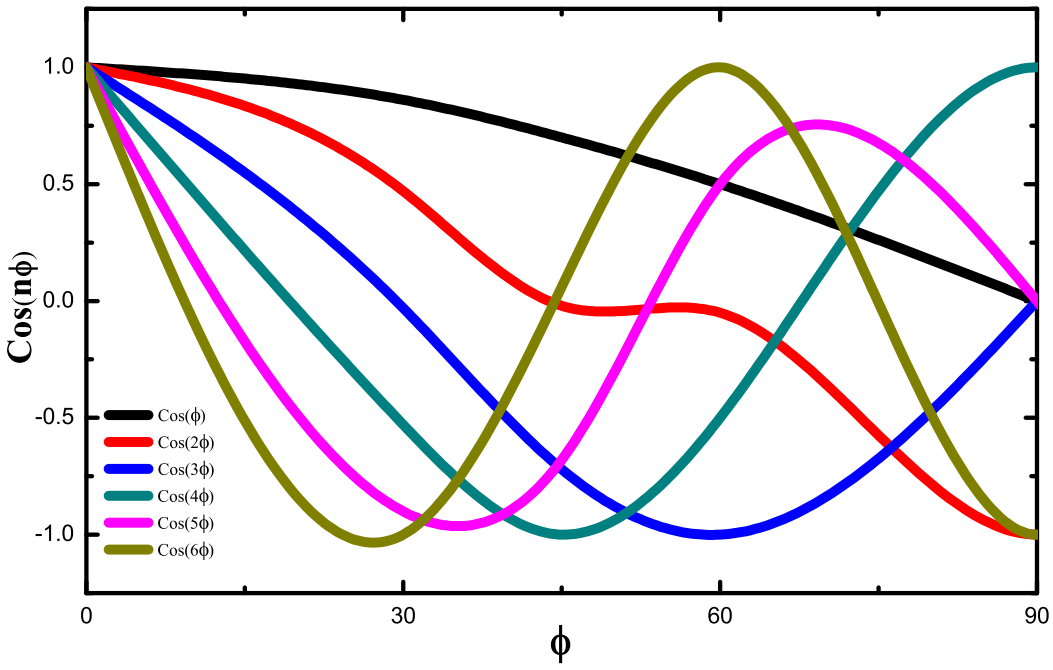


**Figure 1.9:** Representation of different harmonic coefficients with azimuthal angle.

azimuthal angular variation for different flow harmonics is shown in Fig 1.9. The maxima of azimuthal distributions have a peak value at $0^0$ shows in-plane emissions of nucleons. All the harmonic components behave differently at each azimuthal angle. Different harmonics of flow have been described briefly in the preceding subsections.

### 1.6.3 Directed flow

The appearance of collective flow is due to pressure gradient generated by the collision of two nuclei and is one of the key cognition in heavy ion collisions. In 1985, P. Danielewicz and Odyniec [74] developed a technique for analyzing the directed flow. When both the attractive and repulsive interactions balance each other at a particular incident energy, net flow disappears. This incident energy at which net flow disappears is termed as Balance energy or the energy of vanishing flow ($E_{bal}$) [75]. In the Fig 1.10, schematic representation of directed flow at three incident energies is shown:

- E $< E_{bal}$

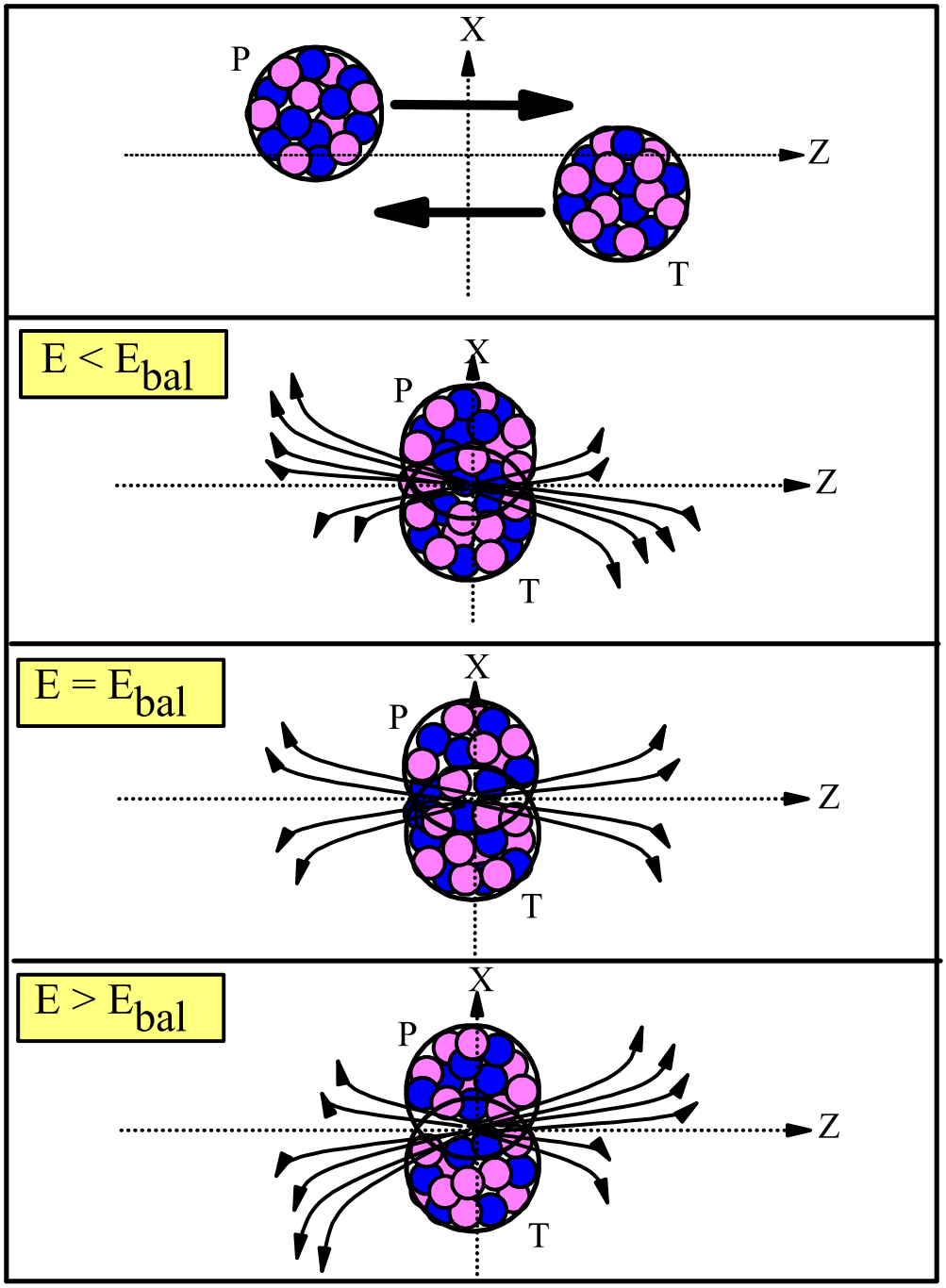


**Figure 1.10:** Schematic representation of directed flow at incident energies below, near and above the balance energy.

- E = $E_{bal}$
- E > $E_{bal}$

Initially, projectile and target approach each other from the opposite direction.

1. In the first case i.e., at low incident energies when E < $E_{bal}$, interactions among the nucleons are dominated due to the attractive mean field. The nucleons in this case are scattered away from the projectile side of the reaction and leads to negative directed flow. When the incident energy is found to less than the balance energy, the phenomenon of fusion and cluster radioactivity is dominant [76, 77].

2. In the second case, when incident energy is equal to the balance energy i.e., $E = E_{bal}$, the nucleons are symmetrically deflected in the reaction plane and the directed transverse flow vanishes.

3. Lastly, when $E > E_{bal}$ with increasing incident energy repulsive nucleon-nucleon scattering dominates and the particles are scattered towards the projectile side of reaction plane and leads to positive directed flow.

### 1.6.4 Elliptical flow

The second harmonic coefficient of the Fourier expansion of the azimuthal distribution of the emitted particles is called elliptic flow [78–80]. The directed flow is antisymmetric with respect to $\phi$ distribution for the forward rapidity ($Yc.m. > 0.0$) as well as backward rapidity ($Yc.m. < 0.0$) [81], whereas elliptic flow shows similar distribution in both the rapidity regions, for the mass symmetric nuclear reactions. Squeeze out phenomenon was observed by two collaborations nearly at the same time. Diogene collaboration [82] have observed the squeeze out effect in case of Ne-induced reactions for mid rapidity range at 400 MeV/nucleons. The second collaboration Plastic Ball Group [83] have observed out-of-plane emission [82, 83] for the reaction $^{197}_{79}Au +^{197}_{79} Au$ at energy 800 MeV/nucleons. Collective flow was observed initially in azimuthal distributions by Gesellschaft fur Schwerionenforschung (GSI) Lawrence Berkeley National Laboratory (LBNL) Collaborations at Bevalac accelerator [84]. The ratio $R_N$ [85]

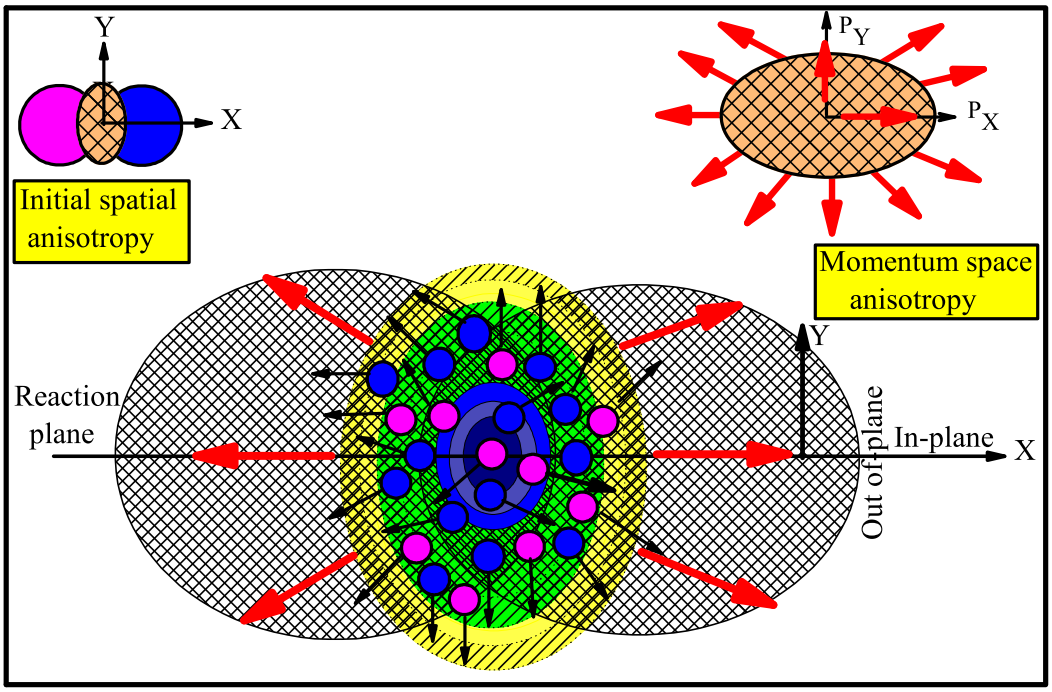


**Figure 1.11:** Schematic representation of elliptic flow.

measures the strength of squeeze out effect and is given by:

$$R_n = \frac{dN/d\Phi(90^0) + dN/d\Phi(-90^0)}{dN/d\Phi(0^0) + dN/d\Phi(180^0)} = \frac{1 - 2v_2}{1 + 2v_2}. \tag{1.3}$$

An attempt was made by A. M. Poskanzer and S. Voloshin [86] to study the flow, using Fourier Expansion of azimuthal particle distributions. The collective flow indicates the strong multiple interactions among nucleons and fragments created after the collision phase is over. The experimental analysis provided the evidence for the presence of anisotropic flow, which is the anisotropic distribution of particle momentum distributions with in the reaction plane. In non-central collisions the distribution of nucleons in the interaction region depends on the impact parameter.

Elliptic flow refers to the anisotropic distribution at mid-rapidity i.e., transition from in-plane or out-of-plane. In the Fig 1.11, Illustration of elliptic flow shows the possible movement of nucleons from the compressed zone. Azimuthal distributions at $0^o$ and $180^o$ exhibit predominantly in-plane emission, while distributions at $\pm$ $90^o$ signifies out-of-plane emission. Ellipse with its major axis along the x-axis represents the in-

plane emission and along y-axis represents the out-of-plane emission. With an increase in incident energy in-plane emission to out-of-plane emission occurred and the elliptic flow shows a transition from positive to negative flow. Incident energy at which transition occurs is called the transition energy $E_{Trans}$ [87]. Transition energy depends on participant expansion, rotation and the shadowing of the spectator matter [88].

### 1.6.5 The correlation between balance energy and transition energy

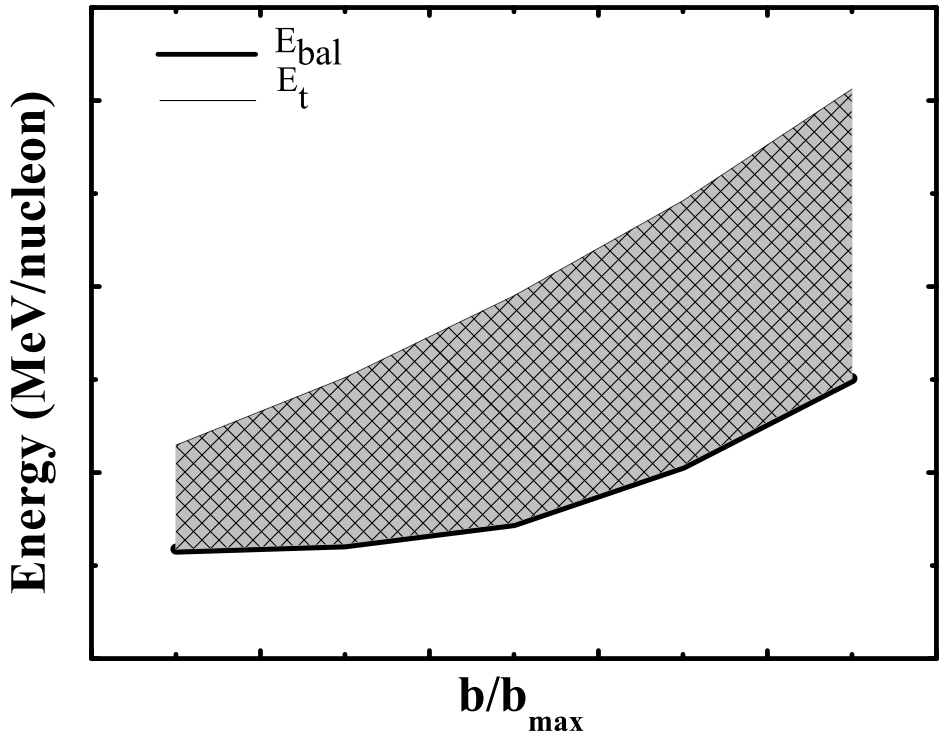


**Figure 1.12:** The correlation between balance energy and transition energy.

In the Fig 1.12, the correlation between balance and transition energy is shown. Both the balance and transition energy are found to increase with increase in the impact parameter but transition energy increases at a faster pace. Because as the

impact parameter increases, less participation of nuclear matter is involved which leads to jet like distribution of nucleons. Squeeze out effect can be visualized by studying the observable that depends on impact parameter. Correlation between balance energy and transition energy is presented in Fig 1.12, for one set of reaction with variation in scaled impact parameter. One can see that both balance as well as transition energy does not show any interdependence on varying the scaled impact parameter. The correlation between transition energy and balance energy can be helpful in understanding the role of Coulomb interactions and Symmetry energy on the reaction dynamics [89–91].

### 1.6.6 Triangular flow and Quadrangular flow

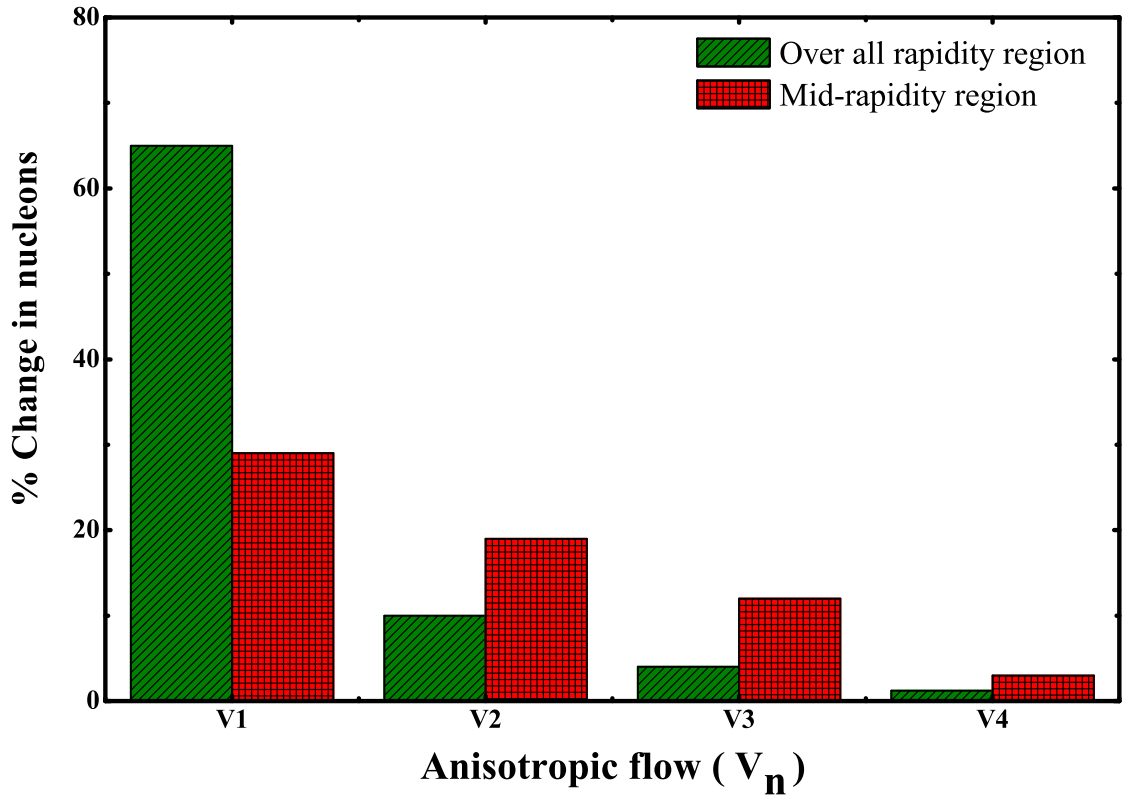


**Figure 1.13:** Anisotropic flow as a function of the percentage change in the flow corresponding to the over all rapidity region and mid-rapidity region.

In the Fig 1.13, we have displayed the relative contribution of nucleons participating

among different harmonics. More specifically, we have made an attempt to find the correlation between whole rapidity region nucleons and mid-rapidity region nucleons participating in the nuclear flow. Less than 50% of the total nucleons involved in transverse flow $< v_1 >$ actually comes from mid-rapidity region. The nucleons in the mid-rapidity region actually suffered strong interactions. Therefore, one can say that the participant region (mid-rapidity) can be used helpful in studying the compressibility of the nuclear matter. While the situation is not same in case of higher harmonics i.e., $< v_2 >$, $< v_3 >$ and $< v_4 >$. However, these harmonics are very useful to estimate the influence of isospin content, isospin dependent of nucleon-nucleon cross section and EOS of nuclear matter. In case of higher harmonics $< v_3 >$ and $< v_4 >$, very less number of nucleons contribute in the flow. One can see that in the mid-rapidity region nucleons still contribute in the triangular and quadrangular flow. Relativistic Heavy Ion Collider (RHIC) have demonstrated the presence of higher order flows [92–94]. Recently, the scaling of these anisotropic flows [95] have also been studied and is found to be originated from nucleonic coalescence.

### 1.6.7 Nuclear stopping

Strength of nuclear interactions can be estimated through the phenomenon known as nuclear stopping [96]. In the participant zone, the nucleons lose a larger part of their energy due to two body or three body collisions. Further, nucleons slow down as they passes through the nucleus, this energy loss is called nuclear stopping. In heavy-ion collisions, using rapidity distributions [97, 98] nuclear stopping has been also studied. It is also well accepted that nuclear stopping governs most of the energy dissipated in a central heavy-ion collision at intermediate energies. The degree of nuclear stopping is affected by various input parameters like incident energy, colliding geometry and system mass. It is influenced by both binary collisions [99] as well as by the in-medium effects such as Fermi motion and Pauli-blocking [100–102]. Nuclear stopping has been studied theoretically as well as experimentally [14–21] by various researchers throughout the globe.

In the Fig 1.14, schematic diagram of possible nuclear stopping scenarios has been

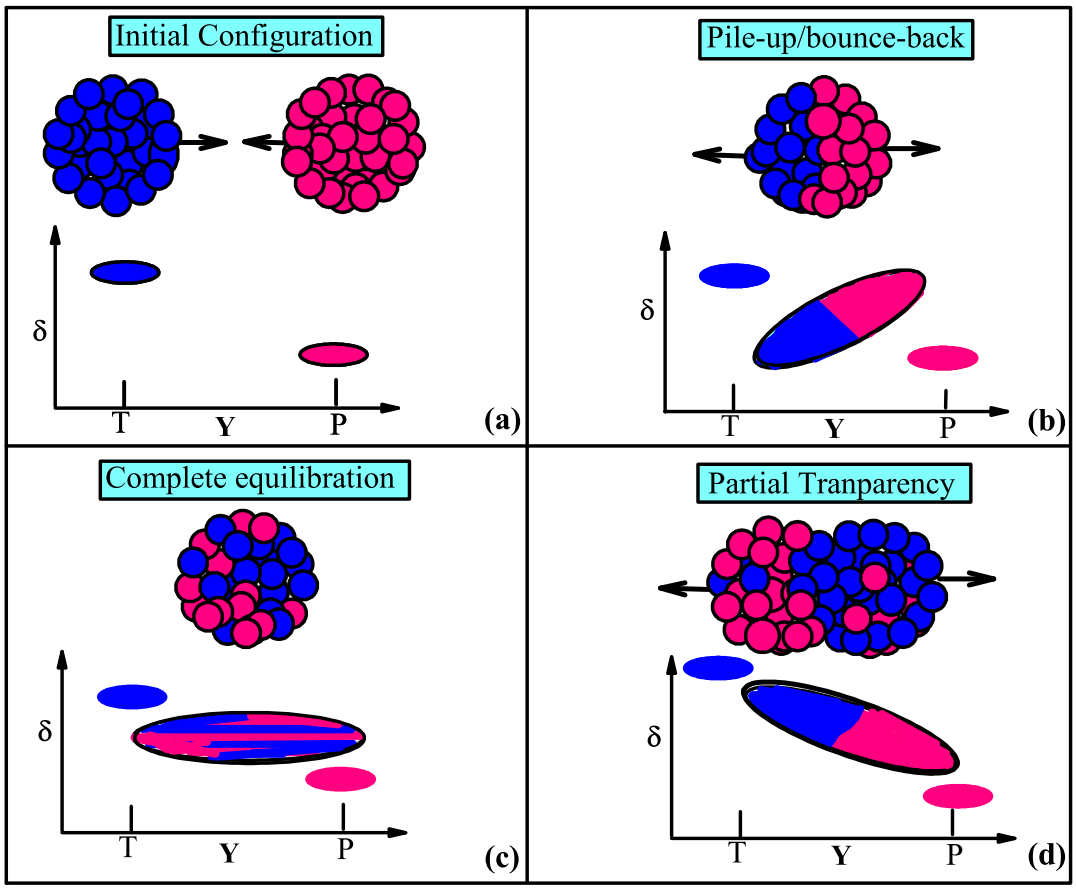


**Figure 1.14:** Schematic diagram of nuclear stopping.

displayed. We have shown initial configuration where:

• The nucleons of target and projectile approaches each other

• In the second case nuclei repled each other just like two hard spheres

• The third one shows the complete memory loss due to breakage of correlations among the nucleons and colliding nuclei which also heats the matter.

• Last case is related to partial transparency, where the nuclei are passing each other without interactions.

## 1.7 Review of experimental attempts on nuclear stopping

Nuclear stopping is one of the vital attention requisite to define the essential reaction dynamics in heavy-ion collisions. Nuclear stopping governs most of the dissipated energy in central heavy-ion collisions and constitute the incomparable reaction mechanisms over large domains of incident energies. Advantageous and fruitful attempts have been made to essence about the nuclear equation of state and isospin effects on the nuclear stopping.

Nuclear stopping using FOPI detector [103–107] was to examine the isospin dependence of various physical observables, therefore four projectile and target combination were taken into account i.e., ${}^{96}_{44}Ru+{}^{96}_{44}Ru$, ${}^{96}_{40}Zr+{}^{96}_{40}Zr$, ${}^{96}_{44}Ru+{}^{96}_{40}Zr$ and ${}^{96}_{40}Zr+{}^{96}_{44}Ru$. Two drift chambers i.e., CDC and HELITRON were used for the tracking of charged particles. Both CDC and HELITRON are placed inside a uniform solenoidal field. Quantitative measurement of stopping and mixing were extracted from the data. FOPI collaboration also studied the central collision for the reaction ${}^{58}_{26}Ni+{}^{58}_{26}Ni$, at incident energies between 1 GeV/nucleon to 2 GeV/nucleon. The rapidity spectra and transverse momentum dependence on the beam energy and centrality of the collisions were presented in the above mentioned studies. At different energies similar shapes of rapidity spectra for protons and deuterons were seen under the same impact parameter constraints.

Proton rapidity distribution in symmetric nuclear collisions was studied by Bhong et al., [108]. The results expose the incomplete mixing and partial transparency of the projectile and target nuclei at SIS energies. At central collisions, even at high energies 0.4 GeV/nucleon - 1.5 GeV/nucleon. It has been observed that global equilibrium was not achieved.

The FOPI collaboration [109] presented a complete systematics of global stopping. A total of 5 systems at 25 energies were analyzed for this work ${}^{40}_{20}Ca+{}^{40}_{20}Ca$ (0.4, 0.6, 0.8, 1.0, 1.5, 1.93), ${}^{58}_{28}Ni+{}^{58}_{28}Ni$ (0.09, 0.15, 0.25, 0.4), ${}^{96}_{44}Ru+{}^{96}_{44}Ru$ (0.4, 1.5), ${}^{129}_{54}Xe+{}^{127}_{53}I$ (0.15, 0.25, 0.4), ${}^{197}_{79}Au+{}^{197}_{79}Au$ (0.09, 0.12, 0.15, 0.25, 0.4, 0.6, 0.8, 1.0, 1.2, 1.5). This idea gave an insight to understand in-medium effects on mesonic and baryonic parti-

cles, since the effective densities in the early phase of the reactions were expected to be strongly correlated to the degree of nuclear stopping.

Systematic study of nuclear stopping for the system $^{197}_{97}Au +^{197}_{97} Au$, was conducted by INDRA and FOPI collaboration [110]. Their study concluded that there exist a strong correlation between the nuclear stopping and the directed flow. Experimentally Lehaut et al., [18] (INDRA and ALADIN collaborations) studied the nuclear stopping at intermediate energies for mass symmetric and mass asymmetric reactions such as $^{197}_{79}Au +^{197}_{79} Au$, $^{129}_{54}Xe +^{118}_{50} Sn$, $^{58}_{28}Ni +^{58}_{28} Ni$, $^{36}_{18}Ar +^{36}_{18} KCl$. The behavior of isotropic ratios $R_E$ and $R_P$ were studied. In the Fermi-energy domain, in-medium effects for nuclear matter were studied by INDRA collaboration [111] for mass symmetric as well as mass asymmetric reactions $^{36}_{18}Ar +^{36}_{18} KCl$, $^{36}_{18}Ar +^{58}_{28} Ni$, $^{58}_{28}Ni +^{58}_{28} Ni$, $^{129}_{54}Xe +^{118}_{50} Sn$, $^{181}_{73}Ta +^{197}_{79} Au$, $^{155}_{64}Gd +^{238}_{92} U$, $^{155}_{82}Pb +^{197}_{79} Au$, $^{197}_{79}Au +^{197}_{79} Au$ and $^{238}_{92}U +^{238}_{92} U$. Their study concluded that nuclear stopping is not completely observed above $E_{inc} = 30$ MeV/nucleon, whatever be the system size. It was found that mean-free path exhibits a maximum at $\lambda_{NN} = 9.5 \pm 2$ fm at $E_{inc} = 40$ MeV/nucleon and $\lambda_{NN} = 4.5 \pm 1$ fm at $E_{inc} = 100$ MeV/nucleon and are in agreement with theoretical predictions.

### 1.7.1 Theoretical review

Numerous attempts have been reported regarding the theoretical study of nuclear stopping. Micghal Gryzinski [112] studied the stopping power. For studying the absolute stopping power, equations were derived on the basis of Classical Mechanics. Nuclear stopping power showed dependence on density and momentum of the electron. Calculations of nuclear stopping, ranges and straggling in low energy region was studied by W. D. Wilson et al., [113]. In the free electron approximation interatomic potentials were calculated and these calculated potentials are accurate for the prediction of the energy ranges.

Nuclear stopping was further carried out by Renfordt et al., [99] for the reaction $^{36}_{18}Ar+^{155}_{82}Pb$ at 0.8 GeV/nucleon. Distribution of nucleons in heavy-ion collision have spherical shapes and resulting in complete stopping of projectile nucleons. These ob-

servations were compared with the hydrodynamical model [114].

W. Bauer [96] studied the nuclear stopping at incident energies around 100 MeV/nucleon. Boltzmann-Uehling-Uhlenbeck theory was used for numerical calculation and later compared with an approximate scaling function. B. A. Li et al., [115] studied the excitation function of nuclear stopping using a relativistic transport model for the reaction ${}^{197}_{79}Au + {}^{197}_{79}Au$. They observed that complete stopping can be achieved in the whole beam momentum range.

Nuclear stopping was studied by Liu et al., [116] for different systems ${}^{20}_{10}Ne + {}^{20}_{10}Ne$, ${}^{40}_{18}Ar + {}^{40}_{18}Ar$, ${}^{80}_{40}Zn + {}^{80}_{40}Zn$, ${}^{112}_{50}Sn + {}^{112}_{50}Sn$ and ${}^{124}_{50}Sn + {}^{124}_{50}Sn$. They proposed that nuclear stopping can be used to extract information on the isospin dependence of in-medium nucleon-nucleon cross section.

Yang et al., [117] studied the entrance channel dependence of the isospin effects on nuclear stopping. The colliding systems are ${}^{40}_{18}Ar + {}^{68}_{40}Zn$, ${}^{58}_{28}Ni + {}^{58}_{28}Ni$, ${}^{58}_{26}Fe + {}^{58}_{26}Fe$, ${}^{58}_{24}Cr + {}^{58}_{24}Cr$, ${}^{76}_{40}Zn + {}^{76}_{40}Zn$, ${}^{80}_{40}Zn + {}^{80}_{40}Zn$ and ${}^{112}_{50}Sn + {}^{112}_{50}Sn$ at E = 100 MeV/nucleon and impact parameter b = 0.0, 1.0, 2.0, 3.0, 4.0 and 5.0 fm. Nuclear stopping was found to be sensitive towards the incident energy, impact parameter, mass of the colliding nuclei and in-medium nucleon nucleon cross section, but is insensitive to the symmetry potential and the isospin asymmetry of the colliding nuclei. Momentum-dependent interactions (MDI) strongly suppresses the sensitivity of nuclear stopping [117].

Isospin effects of Coulomb interaction and symmetry potential using the isospin-dependent quantum molecular dynamics model was studied by Liu et al., [118]. Isospin effects have been used to obtain the information for the NN cross section and mean field.

Dhawan et al., [119] investigated the emission of light complex particles. In their work different symmetric reactions were considered i.e., ${}^{20}_{10}Ne + {}^{20}_{10}Ne$, ${}^{40}_{20}Ca + {}^{40}_{20}Ca$, ${}^{58}_{28}Ni + {}^{58}_{28}Ni$, ${}^{93}_{41}Nb + {}^{93}_{41}Nb$, ${}^{139}_{57}La + {}^{139}_{57}La$ and ${}^{197}_{79}Au + {}^{197}_{79}Au$. They concluded that nuclear stopping in central collisions are better randomized than peripheral ones.

Y. Zhang et al., [120] reported that binary nucleon-nucleon cross-section (NNCS) and mean field are the two important ingredients of nuclear transport model. In medium NNCS was explored using the symmetric system ${}^{197}_{79}Au + {}^{197}_{79}Au$ and results were com-

pared with quantum molecular dynamics simulation. Also, stopping parameter vartl, rapidity variance in the transverse direction to the longitudinal direction was used to measure the nuclear stopping.

The phenomenon of nuclear stopping and compression had been wonderfully explained by Fen Fu et al., [121]. Two symmetric systems ${}^{58}_{28}Ni + {}^{58}_{28}Ni$, and ${}^{155}_{82}Pb + {}^{155}_{82}Pb$ were used to calculate the nuclear stopping. The ratio between the flow energy and the total available energy in center of mass of the colliding systems shows strong relation with degree of nuclear stopping.

Kumar et al., [122] studied global nuclear stopping for the reactions ${}^{40}_{20}Ca + {}^{40}_{20}Ca$, ${}^{58}_{28}Ni + {}^{58}_{28}Ni$, ${}^{93}_{41}Nb + {}^{93}_{41}Nb$, ${}^{131}_{54}Xe + {}^{131}_{54}Xe$, and ${}^{197}_{79}Au + {}^{197}_{79}Au$ at different energies. Role of momentum-dependent interactions and symmetry energy were checked. Nuclear stopping is found to be sensitive towards the momentum-dependent interactions and symmetry energy at low incident energies. Maximum stopping is observed at the central collisions. It was proves that [123] the light mass fragments (LMF's) production was highly correlated with global stopping. They further studied the nuclear stopping parameter's R and $Q_{ZZ}$ using both the hard and soft equation of states. From their results, it was concluded that nuclear stopping can be studied in term of anisotropy ratio and quadrupole moment depends weakly on the symmetry energy and strongly on the isospin-dependent cross-section.

Effect of charge asymmetry and isospin-dependent cross section on nuclear stopping were studied by Jain et al., [124, 125] and the reaction ${}^{124}_{m}X + {}^{124}_{m}X$, where m varies from 47 to 59 and for the reactions ${}^{40}_{n}Y + {}^{40}_{n}Y$, where n varies from 14 to 23 respectively. Their finding concludes that nuclear stopping is strongly depend upon the isospin-dependent cross section. Theoretical results followed the similar trend as recorded by INDRA collaboration. In another study simulations were carried out for the reactions ${}^{124}_{59}Pr + {}^{124}_{59}Pr$ (N/Z = 1.101), ${}^{124}_{56}Ba + {}^{124}_{56}Ba$ (N/Z = 1.214), ${}^{124}_{53}I + {}^{124}_{53}I$ (N/Z = 1.33), ${}^{124}_{50}I + {}^{124}_{50}I$ (N/Z = 1.48) and ${}^{124}_{47}Ag + {}^{124}_{47}I$ (N/Z = 1.638). The participant matter and anisotropic ratio decreases and the spectator matter and relative momentum increases with an increases in N/Z of the system.

Nuclear stopping in asymmetric colliding nuclei were studied by Varinder et al., [126].

The reactions are ${}^{56}_{26}Fe + {}^{96}_{44}Ru$ ($\eta = 0.2$), ${}^{50}_{24}Cr + {}^{102}_{56}Ru$ ($\eta = 0.3$), ${}^{40}_{20}Ca + {}^{112}_{50}Sn$ ($\eta = 0.4$), ${}^{32}_{16}S + {}^{120}_{50}Sn$ ($\eta = 0.5$), ${}^{28}_{14}Si + {}^{124}_{54}Xe$ ($\eta = 0.6$) and ${}^{16}_{8}O + {}^{136}_{54}Xe$ ($\eta = 0.7$). Maximum nuclear stopping was obtained in case of nearly symmetric systems. Individual contribution of neutron and proton were investigated in terms of stopping observable, anisotropic ratio and the quadrupole moment.

The effect of density-dependent symmetry energy on nuclear stopping was studied by Vinayak et al., [127]. The reactions ${}^{40}_{20}Ca + {}^{40}_{20}Ca$ (N/Z = 1), ${}^{48}_{20}Ca + {}^{48}_{20}Ca$ (N/Z = 1.5), ${}^{60}_{20}Ca + {}^{60}_{20}Ca$ (N/Z = 2), ${}^{58}_{28}Ni + {}^{58}_{28}Ni$ (N/Z = 1.07), ${}^{72}_{28}Ni + {}^{72}_{28}Ni$ (N/Z = 1.5), ${}^{84}_{28}Ni + {}^{84}_{28}Ni$ (N/Z = 2), ${}^{100}_{50}Sn + {}^{100}_{50}Sn$ (N/Z = 1), ${}^{124}_{50}Sn + {}^{124}_{50}Sn$ (N/Z = 1.5) and ${}^{150}_{50}Sn + {}^{150}_{50}Sn$ (N/Z = 2) were choosen. The nuclear stopping is found to decrease with increase in stiffness of density-dependent symmetry energy. In Ref. [128,129], the effect of rapidity distributions on nuclear stopping was investigated with density-dependent symmetry energy using isospin-dependent quantum molecular dynamics model.

In 2013, a new concept of memory loss, in nuclear stopping was introduced by Jun Su and Feng-Shou Zhang [13]. They calculated stopping parameters $< vartl >$ and $R_E$. Results of stopping parameters were compared with the entrance channels isotropic ratio $R_E^{entr}$. Their study concluded that in the central collision the complete global equilibrium can not be achieved.

Nuclear stopping and Pauli blocking for the symmetric reaction ${}^{129}_{54}Xe + {}^{129}_{50}Sn$ were studied by Yong-Zhong Xing et al., [130]. In the Fermi energy domain they calculated the isotropy ratio $R_P^E$ for the free protons. Their study revealed that the isotropy ratio $R_P^E$, evaluated using IQMD model is very sensitive to the Pauli-blocking effects.

The isotropy ratio $R^E$ for the reaction, ${}^{129}_{54}Xe + {}^{129}_{50}Sn$ using semiclassical Landau-Vlasov transport model was studied by Z. Basrak et al., [131]. They investigated the impacts of the nuclear mean field on reaction centrality and modified nucleon-nucleon (NN) cross section.

Anti-symmetric molecular dynamics (AMD) model was used to study nuclear stopping and light charged particle emission for the reaction ${}^{12}_{6}C + {}^{12}_{6}C$ at 95 MeV/nucleon by G. Tain et al., [132]. Energy spectra and angular distributions using AMD for light charged particles with $Z \leq 2$ was produced. In their investigation it was concluded

that nuclear stopping plays a key role for the calculation of angular momentum.

## 1.8 Review of experimental attempts on nuclear flow

Collective flow and its components were measured experimentally by many collaborations due to its attractive features. The list of different experimental collaborations where several accelerators were built are as follow

• EOS, collaboration at Lawrance Berkely National laboratory's Bevalac heavy-ion accelerator facility [133].

• FOPI and ALADiN (A Large Acceptance Dipole Magnet) collaboration at Gesellschaft fur Schwerionenforschung (GSI) Darmstadt, Synchrotron for heavy-ions (SIS) accelerator facility [134, 135].

• LBNL, Lawrence Berkeley National Laboratory collaboration and Plastic Ball at Bavalac accelerator [83].

• AGS, Alternating Gradient Synchrotron at Brookhhaven National Laboratory two experiments, E877 and E895 were performed [136].

• Diogene collaboration at Saturne Synchrotron in Sachley France [82].

• STAR collaboration at National Superconducting Cyclotron Laboratory, Michigan State University (USA) [137, 138].

The detailed study made by these collaboration are discussed below:

The Plastic Ball collaboration [139], showed two different collective effects for the first time: the bounce off and the side-splash of the participants for the reactions ${}^{40}_{20}Ca+{}^{40}_{20}Ca$ and ${}^{92}_{41}Nb+{}^{92}_{41}Nb$ at 400 MeV/nucleon. FOPI collaboration [135] studied the sideward flow without reaction plane reconstruction and compared their results with the theoretical predictions. EOS collaboration [133] had measured fragment flow in 1995, using reaction ${}^{197}_{79}Au+{}^{197}_{79}Au$ with beam energy 0.25A to 1.15 GeV/nucleon. First measurement of directed flow for protons, deuterons, tritium, ${}^{3}He$, ${}^{4}He$, and Li was observed.

Interesting experiments in the year 1996-97, were carried out at National Superconducting Cyclotron Laboratory (NSCL) at Michigan State University (USA) $4\pi$ ar-

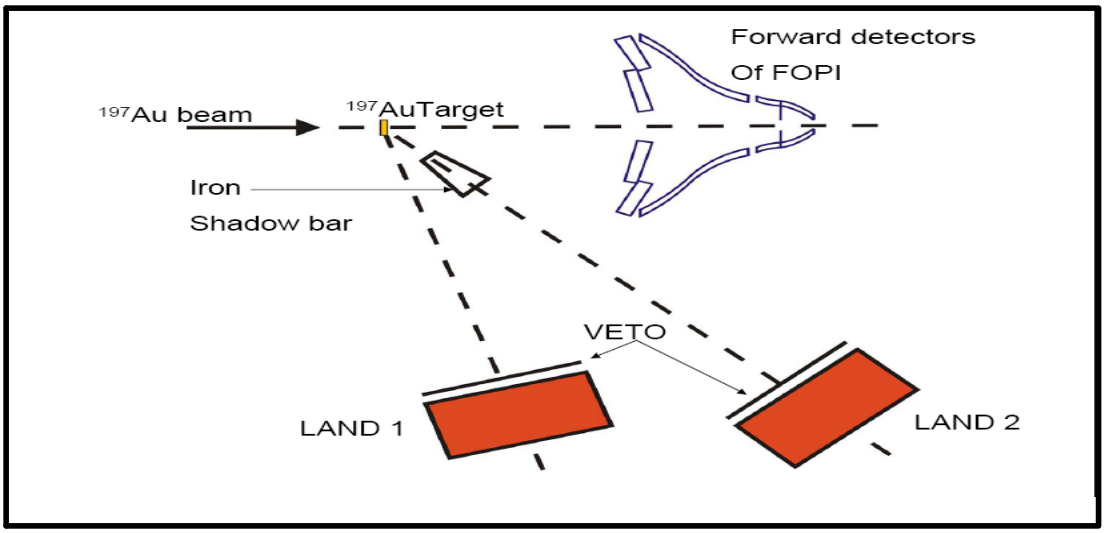


**Figure 1.15:** Sketch of FOPI detector. The figure is taken from the Ref. [134]

ray. Initially, disappearance of transverse flow for the reaction ${}^{40}_{18}Ar + {}^{45}_{21}Sc$ and impact parameter dependence was investigated [137,138]. Their results concluded that balance energy depends upon impact parameter of the nuclear reaction. Isospin dependence of collective transverse flow for the reactions ${}^{58}_{26}Fe + {}^{58}_{26}Fe$ and ${}^{58}_{28}Ni + {}^{58}_{28}Ni$ was demonstrated by R. Pak et al., [140,141] and transverse flow for different fragments Z = 1, 2 and 3 was calculated. From experimental demonstration they concluded that neutron-rich system exhibit larger flow.

P. Crochet et al., [142] studied the balance energy and transition energy for the system ${}^{197}_{79}Au + {}^{197}_{79}Au$. It was reported that the balance energy points occurred at lower beam energies than transition energy points. E877 [143], collaboration measured the directed flow for the light nuclei like deuterons, tritium, ${}^{3}He$ and ${}^{4}He$ for four centrality regions. D. J. Magetro [144] studied the transverse flow for the reaction ${}^{197}_{79}Au + {}^{197}_{79}Au$ and they calculated balance energy for the lighter system as well as for heavier system.

First differential directed flow [145] for the symmetric reaction ${}^{197}_{79}Au + {}^{197}_{79}Au$, was studied by FOPI collaboration [146]. The differential directed flow for Z = 1 to Z = 6 particles were calculated. FOPI collaboration also calculated the transitions from in-

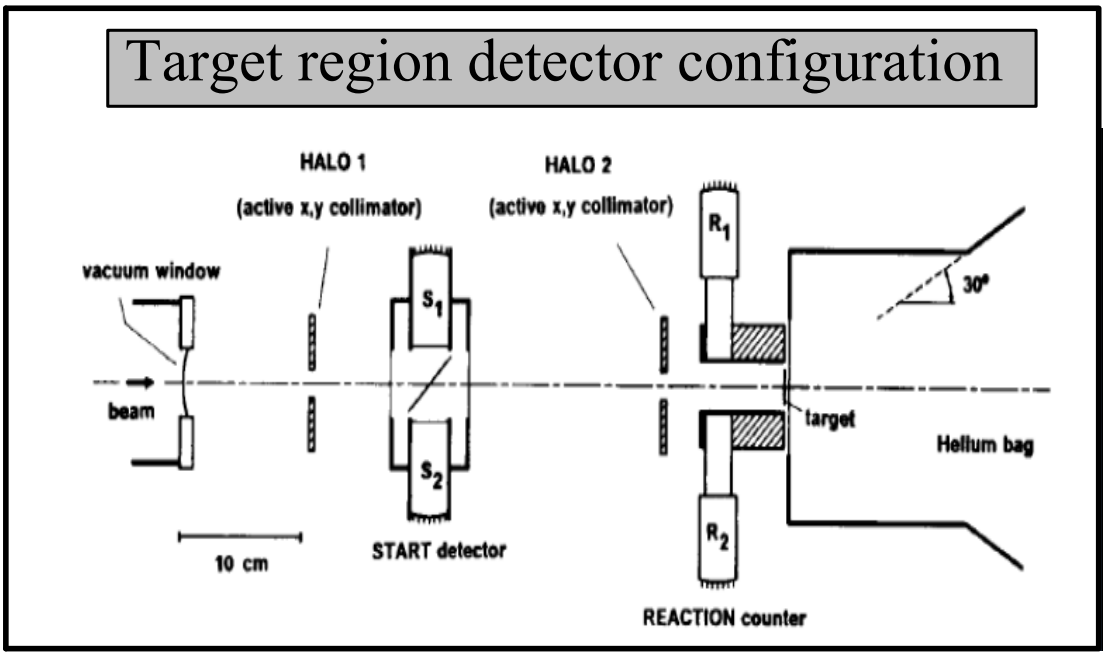


**Figure 1.16:** Target region detector configuration in FOPI detector. The figure is taken from the Ref. [134].

plane to out-of-plane [147] for the reaction ${}^{197}_{79}Au+{}^{197}_{79}Au$. Collaborators concluded that while going from lower to higher incident energies, in-plane to out-of-plane transitions are occurred. As the mass of the system increases, there was systematic decrease in transition energy. In the year 2003 [148] FOPI collaboration calculated the differential directed flow for three nuclear reactions ${}^{197}_{79}Au+{}^{197}_{79}Au$, ${}^{129}_{54}Xe+{}^{132}_{55}CsI$ and ${}^{58}_{28}Ni+{}^{58}_{28}Ni$. Experimental results of directed flow was compared with IQMD model. They conclude that momentum dependent interactions are the only model ingredients which can be used for the reproduction of the data for the following reactions ${}^{197}_{79}Au+{}^{197}_{79}Au$ and ${}^{129}_{54}Xe+{}^{132}_{55}CsI$. The discrepancy occurred in the lighter system ${}^{58}_{28}Ni+{}^{58}_{28}Ni$ needs to be addressed separately.

A new method Lee-Yang zeros was introduced by FOPI collaboration [149] for the first analysis of anisotropic for the reaction ${}^{96}_{44}Ru+{}^{96}_{44}Ru$ at 1.69 GeV/nucleon. INDRA

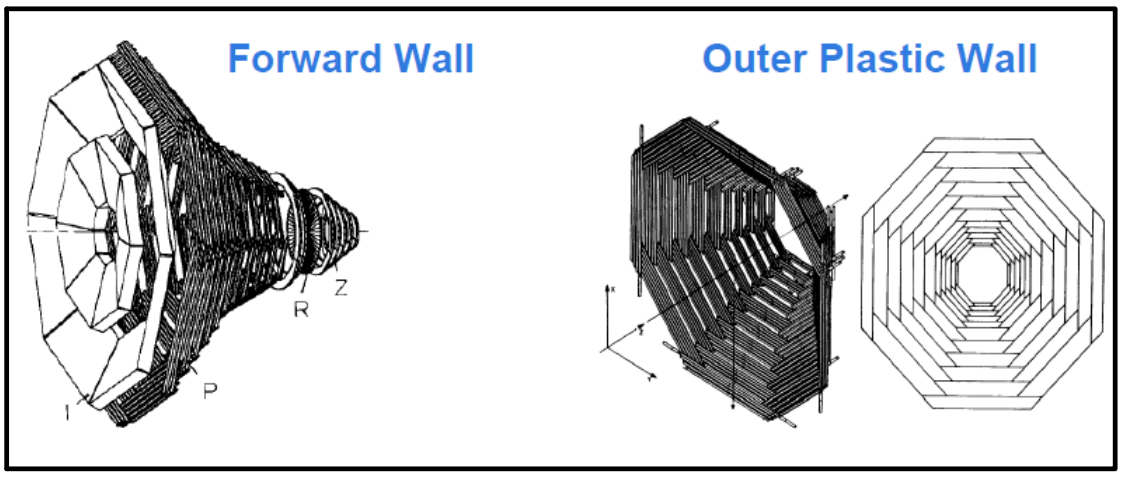


**Figure 1.17:** Reaction-plane detector in forward and outer plastic wall.

collaboration measured the sideward flow around the balance energy [150] for the reactions ${}^{36}_{18}Ar + {}^{36}_{18}Ar$, ${}^{58}_{28}Ni + {}^{58}_{28}Ni$ and ${}^{129}_{54}Xe + {}^{118}_{50}Sn$, at incident energies ranging 30A to 100 MeV/nucleon. Calculated values for the balance energy at central collisions for the three systems was equal to $(82 \pm 4)$ MeV/nucleon for ${}^{36}_{18}Ar + {}^{36}_{18}Ar$ and $(75 \pm 2)$ MeV/nucleon for ${}^{58}_{28}Ni + {}^{58}_{28}Ni$ system. For ${}^{129}_{54}Xe + {}^{118}_{50}Sn$ reaction balance energy was found to be 50 MeV/nucleon.

INDRA and ALADIN collaboration [17] also measured directed and elliptic flow for the mass symmetric system ${}^{197}_{79}Au + {}^{197}_{79}Au$ at intermediate energies where the incident energy varying between 40 MeV/nucleon and 150 MeV/nucleon is taken into account. STAR collaboration [151] studied the anisotropic flow coefficients $v_2$ and $v_4$. They have calculated the ratio $v_4/v_2^2$ in the $20\% - 30\%$ centrality interval. Directed flow of pions, kaons, protons and antiprotons for ${}^{197}_{79}Au + {}^{197}_{79}Au$ system were also measured by STAR collaboration [152]. Higher flow harmonics have been studied by STAR collaboration [153, 154]. Elliptic ($v_2$) and triangular flow ($v_3$) were studied extensively by ALICE (A Large Ion Collider Experiment) collaboration [155]. They have presented the first measurement of transverse momentum $p_t$ and differential triangular flow and observed that $v_3$ have features similar to $v_2$.

Recently, Sushanta et al. [156] studied the nuclear modification factor ($R_{AA}$) and

transverse-momentum spectra for the reaction $^{155}_{82}Pb +^{155}_{82} Pb$ at Large Hardon Collider (CERN), where nuclear modification factor $R_{AA}$, is defined as

$$R_{AA}(p_T) = \frac{(1/N^{evt}_{AA})d^2N_{AA}/dydp_T}{(< N_{coll}/\sigma^{inel}_{NN} >) \times d^2\sigma_{pp}/dydp_T} \tag{1.4}$$

where $d^2N_{AA}/dydp_T$ is the yield and $N^{evt}_{AA}$ is the number of events in nucleus-nucleus collisions. Their study concluded that collective radial flow shows significant and vital role in explaining the transverse-momentum distribution using Boltzmann-Gibbs Blast Wave function.

### 1.8.1 Theoretical attempts

The collective sideward flow was studied theoretically by H. Stocker et al., [157]. Energy spectra and angular distributions, dependence on the impact parameter was predicted. Sideward emission of fragments for the central collisions was compared with available experimental data. P. Danielewicz and G. Odyniec [158] reported that transverse-momentum method is used to analyze collective flow in the $^{36}_{18}Ar +^{36}_{18} KCl$ reaction at 1.8 GeV/nucleon and predicted that collective effects were considerably stronger from the Cugnon cascade model [159]. Transverse momentum distribution was also studied by G. F. Bertsch et al., [160]. It was reported that as the incident energy increases above 100 MeV/nucleon transverse momentum changes sign because of the weak mean field. As the incident energy increases nucleon-nucleon collisions plays vital role. G. Peilert et al., [161] studied the fragment flow for the reactions $^{197}_{79}Au +^{197}_{79} Au$ and $^{93}_{41}Nb +^{93}_{41} Nb$ in the energy range 100 to 800 MeV/nucleon. The disappearance of collective flow was studied by G. D. Westfall et al., [162] for the reactions $^{12}_{6}C +^{12}_{6} C$, $^{20}_{10}Ne +^{26}_{13} Al$, $^{36}_{18}Ar +^{45}_{21} Sc$ and $^{84}_{36}Kr +^{93}_{41}$Nb using Boltzmann-Uehling-Uehlenbeck model. They calculated the balance energy for the above mentioned reactions and scaled the value up to the order of $A^{-1/3}$. The disappearance of flow was also studied by Sven Soff et al., [163] for the reaction $^{40}_{20}Ca +^{40}_{20} Ca$ using QMD model. Their study concludes that balance energy completely lean on impact parameter of the nuclear reaction.

Mass dependence of directed flow was studied by M. J. Huang et al., [164] for the reaction $^{84}_{36}Kr +^{197}_{79} Au$ at an incident energy 200MeV/nucleon. Light mass fragments show

linear dependence and intermediate mass fragments are nearly independent of collective flow. The transversal radial expansion was studied by Voloshin and Zhang [165]. An important features of directed flow and radial transverse flow were studied in the azimuthal distribution.

Isospin-dependent quantum dynamic model was used to determine squeeze-out flow in heavy-ion collision for different input parameters for the reactions ${}^{124}_{50}Sn + {}^{124}_{50}Sn$ and ${}^{124}_{56}Ba + {}^{124}_{56}Ba$. It was found that neutron rich system shows weaker squeeze out flow [166]. D. J. Magestro [167] showed nuclear equation of state parameter i.e., nuclear compressibility ($\kappa$) can be isolated. With increase in the system mass, impact parameter dependence of balance energy weakens. In their calculations, they have used BUU model [168–171] showing the dependence of $E_{bal}$ on $\sigma_{nn}$.

Aman D. Sood et al., [172] considering symmetric colliding nuclei ${}^{12}_{6}C + {}^{12}_{6}C$, ${}^{20}_{10}Ne + {}^{20}_{10}Ne$, ${}^{40}_{20}Ca + {}^{40}_{20}Ca$, ${}^{58}_{28}Ni + {}^{58}_{28}Ni$, ${}^{93}_{41}Nb + {}^{93}_{41}Nb$, ${}^{131}_{54}Xe + {}^{131}_{54}Xe$, ${}^{197}_{79}Au + {}^{197}_{79}Au$ and ${}^{238}_{92}U + {}^{238}_{92}U$ at normalized impact parameter and using different nucleon-nucleon cross sections to study of the energy of vanishing flow. Their study concluded that impact of energy on vanishing flow was very less for both the equation of state as well as momentum dependent interactions.

Isospin effects on balance energy were studied by Sakshi and Sood [173] using IQMD model. The reactions for two sets of isotopic and isobaric pair were: ${}^{26}_{12}Mg + {}^{26}_{12}Mg$, ${}^{65}_{30}Zn + {}^{65}_{30}Zn$, ${}^{91}_{42}Mo + {}^{91}_{42}Mo$, ${}^{117}_{54}Xe + {}^{117}_{54}Xe$, ${}^{164}_{76}Os + {}^{164}_{76}Os$ having N/Z = 0.54 and reactions ${}^{28}_{12}Mg + {}^{28}_{12}Mg$, ${}^{70}_{30}Zn + {}^{70}_{30}Zn$, ${}^{98}_{42}Mo + {}^{98}_{42}Mo$, ${}^{126}_{54}Xe + {}^{126}_{54}Xe$, ${}^{177}_{76}Os + {}^{177}_{76}Os$ having N/Z = 0.54, for N/A = 0.5 reaction are ${}^{26}_{12}Mg + {}^{26}_{12}Mg$, ${}^{58}_{29}Cu + {}^{58}_{29}Cu$, ${}^{72}_{36}Kr + {}^{72}_{36}Kr$, ${}^{96}_{48}Cd + {}^{96}_{48}Cd$, ${}^{120}_{60}Nd + {}^{120}_{60}Nd$, ${}^{135}_{67}Ho + {}^{135}_{67}Ho$ and reactions having N/A = 0.58 are ${}^{24}_{10}Ne + {}^{24}_{10}Ne$, ${}^{58}_{24}Cr + {}^{58}_{24}Cr$, ${}^{72}_{30}Zn + {}^{72}_{30}Zn$, ${}^{96}_{40}Zr + {}^{96}_{40}Zr$, ${}^{120}_{50}Sn + {}^{120}_{50}Sn$ and ${}^{135}_{56}Ba + {}^{135}_{56}Ba$. Their study concluded that isospin effect was not visible for any above mentioned reactions.

Sanjeev et al., [174] used the mid-rapidity region to study the elliptic flow ($v_2$). With the change in mass asymmetry [175] and system size of fragments the transition energy is found to decreases. Production of light mass fragments (LMF's) also exhibits isospin effects in the mid-rapidity region. Elliptic flow ($v_2$) [176] was also studied by

using different form of density dependent symmetry energy.

Elliptic flow associated with neutron and proton was studied by M.D. Cozma [177]. The neutron proton elliptic flow difference (npEFD), $v_2^{n-p}$=$v_2^n - v_2^p$ shows very little dependence on compressibility($\kappa$), Gaussian width (L), NN cross-sections and isospin asymmetric equation of state. In the year 2013, Yan Ting-Zhi [178] studied directed and elliptic flow for the symmetric system $^{197}_{79}Au+^{197}_{79}Au$. It was reported that directed flow occurs because of nucleon-nucleon collision and elliptic flow occurs due to fire-ball expansion and therefore overwhelm system rotation with increase in the energy. Collective flow of light charged particles like proton, neutrons, deuterons, tritium, $^3He$ and $^3He$ in $^{197}_{79}Au+^{197}_{79}Au$ at three different energies 150, 250 and 400 MeV/nucleon were studied by Yongjia Wang et al., [179]. It was concluded that light particles are sensitive to medium modification of nucleon-nucleon cross sections.

In the recent study, correlation between elliptic flow, shear viscosity ($\eta$) and specific viscosity ($\eta/s$) with impact parameter were studied by C. L. Zhou et al., [180] and from the results it was concluded that ratio of elliptic flow with impact parameter ($v_2/b$) decreases linearly with increase in the shear viscosity ($\eta$) but increases with increasing specific viscosity ($\eta/s$).

The balance energy using IQMD model was studied [181] and role of different equation of states has been analyzed. The mass dependence of balance energy at peripheral geometry acts as a probe to study the stiffness and compressibility of nuclear matter. The higher order flow harmonics of identified hadron for the reaction $^{208}_{82}Pb+^{208}_{82}Pb$ at energy 2.76 TeV/nucleon was studied [182] by using event-by-event VISHNU hybrid model. The results were compared with the recent ALICE measurements for the $p_T$ spectra and differential flow harmonics $v_2(p_T)$, $v_3(p_T)$, and $v_4(p_T)$. Using the same event-by-event VISHNU hybrid model [183] the $p_T$-spectra and elliptic flow ($v_2$) of hadrons such as $\Lambda$, $\Xi$ and $\pi$ for the reaction $^{197}_{79}Au+^{197}_{79}Au$ at energy 200 GeV/nucleon were studied and compared with the calculations of STAR experiment. Recently, different flow shapes and higher harmonics in anisotropic transverse collective flow for the reaction $^{197}_{79}Au+^{197}_{79}Au$ at various incident energies were studied [184]. Jet-finder algorithm method was used to study the flow shapes and properties of anisotropic

flow. To study the longitudinal flow fluctuation in heavy-ion collisions Jiangyong Jia et al., [185], studied the several new observables which was motivated from previously CMS collaboration [186] studies. It was proved that these observables are sensitive to the event by event fluctuations and act as a framework to investigate the longitudinal flow fluctuation.

## 1.9 Organization of thesis

The thesis is organized as follow:

• In **chapter 2**, we will describe the various models in brief i.e., IBUU, ImQMD, QMD, FMD and IQMD will be discussed in detail. Also, we shall discuss the secondary approaches (algorithms) such as MST which are used to clusterize the phase space obtained from primary models.

• **Chapter 3**, we have discussed the detail of collision dynamics (central and peripheral collision). The results for $N_{Coll}$ as a function of impact parameter for the mass symmetric reaction $^{197}_{79}Au+^{197}_{79}Au$ at two incident energies i.e., E = 50 and 400 MeV/nucleon is presented. Nucleon which suffer one or more collisions with nucleons of the other nucleus, is usually called a participant nucleon i.e., $N_{part}$. A number of spectator nucleons $N_{spec}$ constitutes the part of the nuclear volume not involved in the interaction. We have also checked the individual contribution of projectile nucleons and target nucleons at lower energy (50 MeV/nucleon) or as well as at higher energy (400 MeV/nucleon). The phase-space evolution for symmetric and asymmetric colliding nuclei have been displayed.

• In **chapter 4**, the stopping observable $< R_E >$, $< R_P >$ and $< varxz >$ are studied. The different nuclear stopping observable exhibit different sensitivities. It is of high interest to learn, which observable is the best to study the nuclear stopping. Initially, time evolution of the stopping observable at incident energies E = 50 MeV/nucleon or 400 MeV/nucleon has been displayed. The variation of three different stopping observable ($< R_E >$, $< R_P >$ and $< varxz >$) has been displayed at initial time step i.e., t = 20 fm/c as well at higher time steps t = 200 fm/c. In the next step, incident energy dependence of nuclear stopping for proton ($^1_1H$), deuterium ($^2_1H$), tritium ($^3_1H$) and the fragment having Z=1 have been studied.

• In **chapter 5**, author has presented the analysis on the nuclear stopping by simulating various type of nuclear reactions. The main aim of the study is to address the significance of mass asymmetry on the projectile stopping and compensate the effect of mass asymmetry by varying the impact parameter. The anisotropy ratio $< R_a >$

is compared with mass asymmetric reactions for which total system mass is kept fixed ($A_{TOT} = 240, 160, 100, 80, 40$) and also when the total mass is floating at incident energies E = 50 and 200 MeV/nucleon. In the next step, $< R_a >$ is compared with 50% of the participant matter ($b/b_{max}@< Part >_{Norm}$) for total mass floating and when the mass is kept fixed ($A_{TOT} = 240$).

• In the **chapter 6**, we present the comprehensive interpretation of the momentum distribution of nucleons participating in different kind of nuclear flow, $< v_1 >$, $< v_2 >$, $< v_3 >$ and $< v_4 >$. The main aim intention is to estimate the participation of nucleons among different harmonics of anisotropic flow and to pin down the correlation between over all rapidity region and mid rapidity region. In the step ahead author has tried to study the characteristics of transition energy. Another feature associated with transition energy is to explore the isospin effects which is also included in the present chapter. Anisotropy ratio $R_N$ for A = 1, 2, 3 and 4 particles for two impact parameter bins have been reported.

• In the **Chapter 7**, author summarizes the results and also contains an outlook of the present work.

# Chapter 2

# Methdology

## 2.1 Introduction

Experimentalist, as well as theoretician in the past few decades, have studied the nuclear reactions from low to relativistic energies. There exists a variety of phenomena from low to relativistic energies [18–20, 111, 187–192]. At low incident energies Pauli principle blocks majority of the scattering nucleons and the physics in this energy region dominates by the attractive mean field. The combined role of attractive mean field and repulsive nucleon-nucleon scattering exists [60, 193, 194] at intermediate energy which is the main focus area of present thesis. The essential condition to construct a relativistic theory in heavy-ion collisions is to describe simultaneous role of mean field and nucleon-nucleon interactions.

Depending upon the interaction of nuclei i.e., either they interact by binary hard collisions or by the superposition of the soft interactions of all nucleons, there are two different approaches to study reaction dynamics of the Heavy-ion Collision. A tool to study the reaction dynamics of heavy-ion collisions from the initial configuration to the final distribution of nucleons in phase-space, by treating the colliding nuclei as a classical N-body system was first studied with the help of Intranuclear Cascade Calculations (INC) [195–197] in the early eighties. The main disadvantage of this model was neither the Pauli blocking of nucleon-nucleon scattering nor an attractive mean field due to nucleons were included in the calculations. Due to the absence of these effects this model is applicable only for the reactions at high beam energies where a large fraction of nucleons are unbounded.

Another description was given by the classical molecular dynamics (CMD) model [198–200]. In this model nucleons interact via classical potentials and no collisions of nucleons is assumed to takes place, like INC it is also an N-body approach. The main drawback of these models is that all the quantum features which are necessary to describe high energy heavy-ion collisions are neglected. The classical potentials can only provide a poor approximation to nucleon-nucleon scattering and nuclear binding energy. Therefore, in order to give the full description of these effects, quantum effects of the nucleons are necessarily be included.

## 2.2 Quantum Molecular Dynamics (QMD) Model

The quantum properties of the nucleons like nucleon-nucleon collisions are successfully introduced by Aichelin and co-workers [60] by solving the time dependent Schrodinger wave equation in the Hartree-Fock approximation. This time dependent Hartree-Fock model (TDHF) has been applied with some success to heavy ion collisions at low incident energies. However, the dynamics at intermediate energies requires the equal weightage to nucleon-nucleon binary collisions as well as mean field. Therefore, the exact information about the real (trajectory of nucleons) and imaginary (nucleon-nucleon collisions) parts of potential is required.

However, isospin degree of freedom is equally important to extract the information about the equation of state (EOS) of neutron rich matter induced by neutron-rich beams (stable or radioactive) at intermediate energy. This isospin degree of freedom enters into the real & imaginary part in terms of iso-vector (symmetry) potential, isospin dependent in-medium nucleon-nucleon cross section and Pauli blocking respectively. The other essential features is to address the time evolution of the phase-space density from the begining (where matter is non-equilibrated) to the final state (where matter is cold and fragmented).

The dynamical transport models employed at intermediate energies are supposed to contain the above said features and can be sub-divided into two classes:

**The models:**

1. Which follow the time evolution of one-body phase space distribution i.e. VUU/BUU, IBUU and SMF.

2. Which are based on N-body molecular dynamics or cascade dynamics i.e. QMD and IQMD.

## 2.3 Importance of Iso-spin dependent models in heavy-ion collisions at intermediate energies

The main goal of studying isospin physics in heavy-ion collisions is to explore the properties of nuclear matter and its equation of state. Various phenomena associated with isospin have been observed in heavy-ion collisions. Iso-spin dependent models tend to explain the essential isospin physics which govern the complex interactions among the neutrons and protons. The entire study of present thesis is carried out by using the Isospin Quantum Molecular Dynamics (IQMD) Model.

### 2.3.1 Different theoretical models based on iso-spin effects

1. **IBUU**

IBUU (isospin-dependent Boltzmann-Uehling-Uhlenbeck), is semi classical transport model in which an isospin and momentum-dependent mean-field of single nucleon potential is used. The isospin degree of freedom has been incorporated in the model by the elementary nucleon-nucleon cross-section and the nuclear mean field. To extract the important information of nuclear matter properties and collision dynamics, IBUU model [201–203], just like BUU model [204, 205] was widely used for simulations. This model provides an explicit sketch of the time dependence one-body distribution function. The Boltzmann-Uehling-Uhlenbeck equation describes the time evolution of the single particle phase-space distribution function and reads as follow:

$$\begin{aligned}\frac{\partial f_1}{\partial t} + v\cdot\nabla_r f_1 - \nabla_r U\cdot\nabla_p f_1 &= \int \frac{d^3\acute{p_1}d^3p_2d^3\acute{p_2}}{(2\pi)^9}\sigma_{12}v_{12}(2\pi)^3\delta^3(p_1+p_2-\acute{p_1}-\acute{p_2}) \\ &\quad\times\left[\acute{f_1}\acute{f_2}(1-f_1)(1-f_2)-f_1f_2(1-\acute{f_1})(1-\acute{f_2})\right].\end{aligned} \tag{2.1}$$

Here $\sigma_{12}$ is the differential cross-section for a certain change of momentum $(p_1, p_2) \rightarrow (p_1^{'}, p_2^{'})$ and $v_{12}$ is the relative velocity for the colliding nucleons.
In this model, $U$ is the mean field, which is a function of the local density. It can be parametrized as an arbitrary function of the density, making possible to model a variety of equations of state. Typically, it can be written as, the sum of three terms:

$$U = V_{Coul} + V_N + V_{Sym}, \tag{2.2}$$

where $V_{Coul}$, $V_N$ and $V_{Sym}$ represents the Coulomb, iso-scaler nucleon potential and the symmetry energy, respectively. The nuclear mean field $U$ including the isospin symmetry term is parametrized as:

$$U(\rho, \tau_z) \;=\; \alpha\left(\frac{\rho}{\rho_0}\right) + \beta\left(\frac{\rho}{\rho_0}\right)^{\gamma} + (1-\rho_0)V_{Coul} + C\frac{\rho_n - \rho_p}{\rho_0}\tau_z. \tag{2.3}$$

Here $\rho_0$ is the normal nuclear matter density, $\rho$, $\rho_n$ and $\rho_p$ are the nucleons, neutron and proton densities, respectively. $\tau_z$ equals to +1 or -1 for neutrons or protons, respectively. The $V_{Coul}$ as discussed above is the Coulomb potential. Its strength $C$ can be deduced from experiments (e.g. nuclear symmetry energies, optical potentials for nucleon scatterings, excitation of analog states in (p,n) reactions). In the IBUU model the cross-section of neutron-proton collisions is about three times that of neutron-neutron and proton-proton cross-section ($\sigma_{np} = 3\sigma_{nn} = 3\sigma_{pp}$).

**Comparison of IQMD model with IBUU model**

The main drawback of BUU model is density fluctuations. The density fluctuations lead to the fragment production, are suppressed in the BUU equation [206–209]. To overcome these drawbacks, alternate model like, Isospin dependent Quantum Molecular Dynamics (IQMD) model has been developed to address the density fluctuations.

2. **ImQMD**

The quantum molecular dynamics (QMD) [60] model was proposed for simulating the heavy-ion collisions (HICs) at intermediate energies. The improved quantum molecular dynamics model (ImQMD) [210] is extended to the field of low energy heavy ion fusion reaction research based on the QMD model.Since the QMD model is suitable

for medium and high energy heavy ion collision studies, it is quite difficult to apply the QMD model to low energy fusion reactions. To extend the QMD model for the study of heavy-ion reactions at energies around the Coulomb barrier, the ImQMD [210] model was proposed based on the QMD framework with some modifications:

• The standard Skyrme interactions is adopted for describing the bulk properties and the surface properties of nuclei.

• To consider the fermionic properties of nucleons when Fermi constraint is used.

• The mass dependence of the wave-packet width is used so that the surface properties of finite nuclei and the fluctuations in the reactions are better described.

• The momentum dependence of the nucleon-nucleon interactions is involved in this ImQMD model based on Skyrme interactions.

A further improvement in ImQMD model is made by same group [211] to study the dynamical process of fusion reactions keeping in view the stability of individual nucleus [212, 213]. This model has also been used in studying isospin effects in reaction dynamics [214,215]. The ImQMD model is mainly applied to study heavy-ion collisions at intermediate and low energies. The model is widely used for heavy ion near-base fusion reaction and strong damping reaction of giant composite system.

### 3. **FMD**

The model of Fermionic Molecular Dynamics (FMD) was suggested in 1990 [216–218], in order to describe the heavy-ion reactions in the energy region below particle production and ground state properties of atomic nuclei. When classical dynamics is applied to the atoms and molecules, the study is called as 'molecular dynamics [219]. Fermion molecular dynamics (FMD) is a quasi-classical method for treating quantum-mechanical systems by using classical equations of motion along with momentum-dependent model potentials added to the usual Hamiltonian. These model potentials constraint the motion of nucleons by satisfying the Heisenberg uncertainty principle and the Pauli exclusion principle. Classical points in the phase space is replaced by wave packets and thereby introducing quantum properties into classical molecular dynamics. Fermionic Molecular Dynamics model [216–218, 220] for fermions was investigated

thoroughly which works with antisymmetrized manybody states composed of localized single particle wave packets. Various phenomena like shell effects, cluster structure, incomplete fusion, dissipative binary collisions and multi-fragmentation are addressed by FMD. In FMD model each particle follows a single trajectory which cannot split into two or more with certain amplitudes like in the quantum case. By using the concept of time averaging, thermodynamic equilibrium properties can be determined by using FMD.

4. **AMD**

Antisymmetrized molecular dynamics was used to define the microscopic simulation framework for heavy ion reactions. AMD [221–225] is similar to the Fermionic molecular dynamic (FMD) with respect to the choice of the trial state and includes random branching between trial states. FMD approach is based on width parameter and in case of AMD width is constant.The essential properties of nuclear ground states is reproduced by this model. For the reproduction of fragment nuclide distribution AMD was verified as an excellent simulation framework for heavy ion reactions and at the same time it is expensive when applied to heavier systems. AMD simulation method does not assume any clusters but can describe the shell effects and the clustering effects in the case when they should appear in the simulation. In the next section, we will discuss the Isospin quantum dynamics model (IQMD) and its numerical realizations in detail.

## 2.4 Isospin Quantum Molecular Dynamics (IQMD) Model

Isospin-dependent Quantum Molecular Dynamics (IQMD) model is an extension and improved version of the QMD model which incorporates the isospin degree of freedom and is developed by Hartnack et. al. [194]. The isospin degree of freedom enters into the calculations viz. in both cross section and mean field [72, 226]. Since it is an extension of QMD model and also consists of three steps namely:

• Initialization

• Propagation

• Nucleon-Nucleon collisions

In the first step, one has to generate the nuclei also known as initialization. After the initialization, nuclei propagate under the influence of surrounding mean field. This is termed as propagation. In the last step, nucleons are finally bounded to collide if they come too close to each other. In the following subsections, all the three steps are elaborated in details.

### 2.4.1 Initialization

Both in QMD as well as in IQMD models, the nucleons are represented by Gaussian wave packets which interact by mutual two and three body forces. The model simulates the heavy-ion collisions on an event by event basis and as a consequence preserves the correlations and fluctuations. In IQMD model, the centroids of Gaussians in a nucleus are randomly distributed in a phase space sphere ($r < RA^{1/3}$ and $p \leq p_F$, where $\acute{A}$ is the mass number of nucleus under consideration) corresponding to the ground state density. The wave function for $i^{th}$ nucleon which has a mean position $r_i(t)$ and mean momentum $p_i(t)$ is given by:

$$\psi_i(r,\ p_i(t),\ r_i(t)) \ = \ \frac{1}{(2\pi L)^{3/4}} exp\left[\frac{i}{\hbar}\ p_i(t)\cdot r \ - \ \frac{(r \ - \ r_i(t))^2}{4L}\right] \tag{2.4}$$

The parameter L, is related to the extension of the wave packet in phase-space and is a measure of interaction range of nucleons. In the QMD model, L is 1.08 $fm^2$ and is independent of system size, whereas in the IQMD model, L varies with size of the system. This system mass dependence of L is introduced so as to obtain maximum stability of density profile equals to 8.66 $fm^2$ for Au+Au and 4.33 $fm^2$ for Ca+Ca and lighter nuclei, and in between these two values for intermediate mass.

As the model is semi-classical, therefore to keep the formulation as close as possible to classical transport theory, we use the Wigner densities instead of wave functions which correspond to the phase-space densities in classical mechanics. The Wigner

representation of $A_P + A_T$ nucleon system is given by

$$f_i(r,p,t) = \frac{1}{\pi^3\hbar^3}\ e^{-(r-r_i(t))^2\frac{2}{L}}\ e^{-(p-p_i(t))^2\frac{L}{2\hbar^2}}. \tag{2.5}$$

where $r_i(t)$ and $p_i(t)$ define the classical orbit or the center of the Gaussian wave packets in phase-space. The parameter L is assumed to be independent of time. The Wigner distribution of Gaussian wave packets obeys the Uncertainty relation:

$$\Delta x \Delta p_x \geq \tfrac{1}{2}\hbar.$$

In order to initialize a nucleus, we have to assign the co-ordinates and momenta to all nucleons. In three dimensional space (inside a sphere with radius $R = 1.12A^{1/3}$), the centers of Gaussian wave packet $r_i$ are uniformly distributed in polar co-ordinates by

$$\begin{aligned} r &= R\ x_1^{1/3}, \\ cos\theta &= 1\ -\ 2x_2, \\ \phi &= 2\pi\ x_3 \end{aligned}$$

where $x_1$, $x_2$ and $x_3$ are the random numbers. The co-ordinates of nucleons are rejected if the distance between them is less than 1.5 fm. The nucleons are initialized in accordance with the liquid drop model. Each nucleon occupies a volume of $h^3$, so that phase-space is uniformly filled. The center of each Gaussian wave packet $p_i$ are uniformly distributed in polar co-ordinates

$$\begin{aligned} p_i &= p_F(r_i)x_4^{1/3}, \\ cos\theta &= 1\ -\ 2x_5, \\ \phi &= 2\pi x_6 \end{aligned}$$

where, $x_4$, $x_5$ and $x_6$ are again the random numbers. In order to obtain a smoother distribution of nucleons in phase-space, we have introduced a minimum distance $d_{min}$ and require nucleons in phase-space to satisfy

$$|r_i - r_j|^2|p_i - p_j|^2 \geq d_{min} \tag{2.6}$$

Typically only 1 out of 50,000 initializations is accepted under the present criteria. The accepted configurations are quite stable.

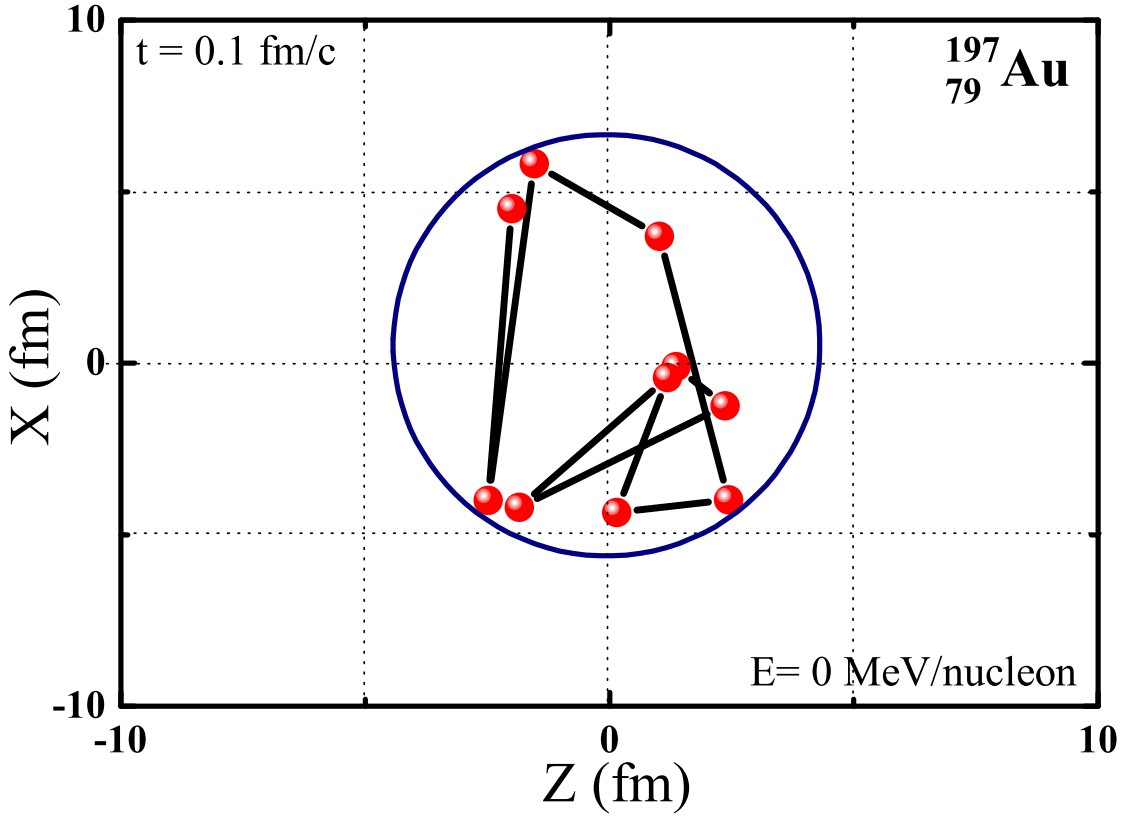


**Figure 2.1:** Trajectory of single nuclei of $^{197}_{79}Au$ at incident energy E= 0 MeV/nucleon.

In the Fig 2.1, trajectory of single nuclei of $^{197}_{79}Au$ at incident energy E = 0 MeV/nucleon has been shown. Here, author has demonstrated the ground state properties of the single nucleus at initial time, t = 0.1 fm/c. Fig 2.1 shows how the single nucleon moves in the potential generated by all its fellow nucleons in the $^{197}_{79}Au$ nucleus. The line joining the nucleons show how they are moving inside the nucleus. Whenever the nucleons comes close to the surface of the $^{197}_{79}Au$ nuclei, it gets pulled back by the other nucleons. The nucleons are confined within the sphere because no collisions are taking place.

The density profile of single nuclei's for the system $^{50}_{20}Ca$, $^{96}_{36}Kr$, $^{124}_{50}Sn$ and $^{197}_{79}Au$ is plotted in the Fig 2.2. To make density profile as accurate as possible, density fluc-

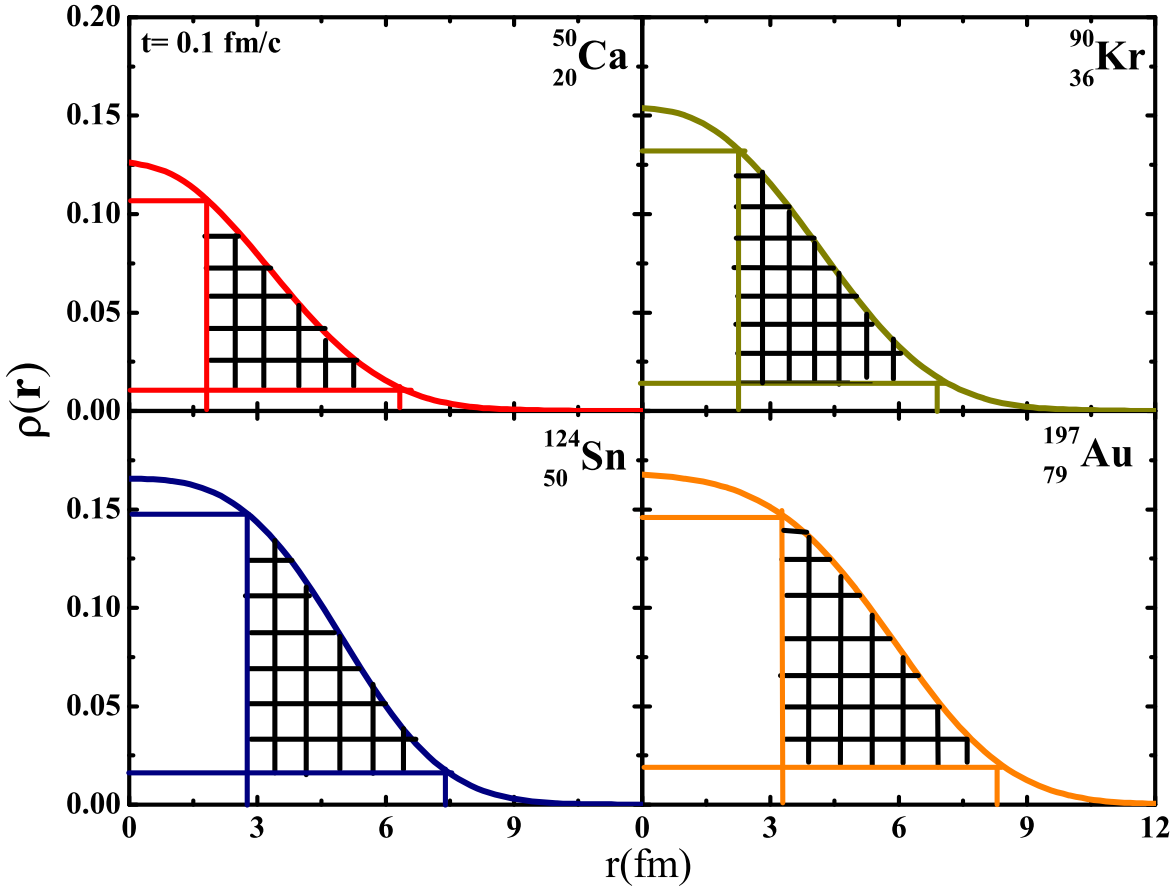


**Figure 2.2:** Density of nucleons in Ca, Kr, Sn and Au nuclei plotted versus radial distance from the center.

tuations is maximum at the centre of all the systems and is nearly same for all the systems under study at r = 0 fm. This is because the volume of the nucleus is proportional to the number of nucleons, thereby the density of nucleons is nearly same in the interior. As we move away from the centre of nuclei towards the surface of the system the density profile falls and attains minimum at the surface. The behavior is similar for all the systems under observations. The value of the density $\rho$ varies for different systems (Ca to Au) from 0.12 to 0.17 $fm^{-3}$.

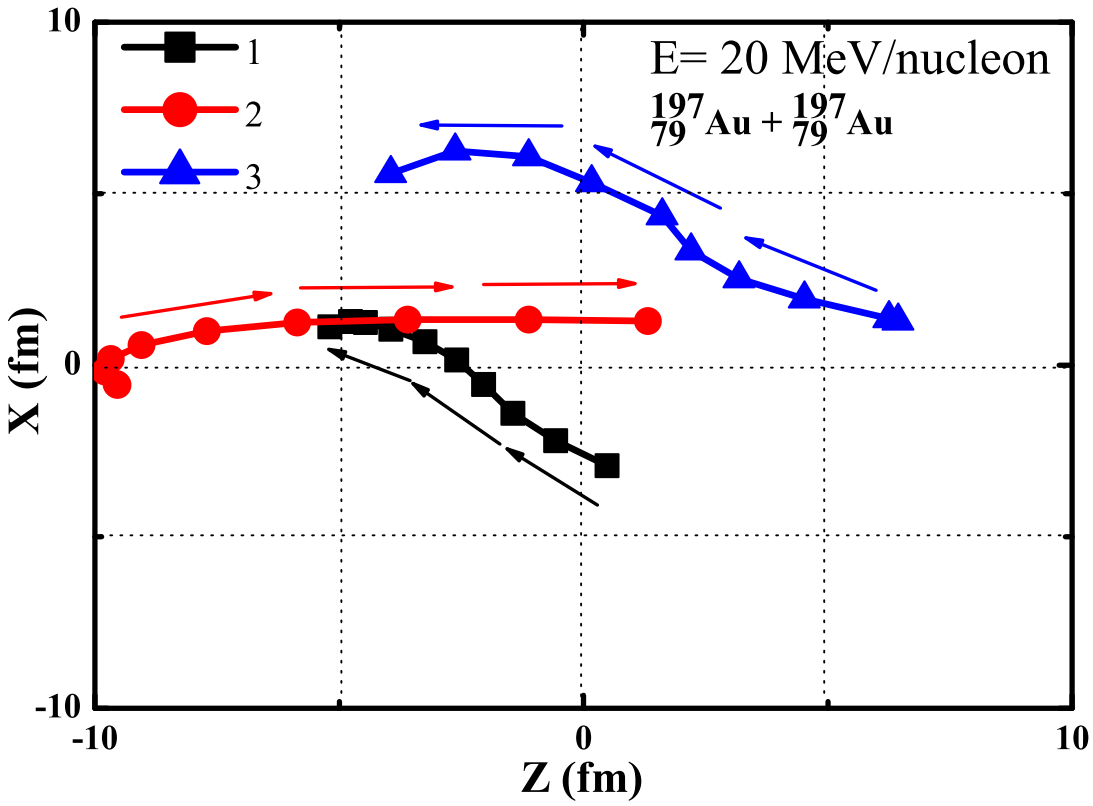


**Figure 2.3:** Trajectory of nucleons for the reaction $^{197}_{79}Au +^{197}_{79} Au$ at incident energy E = 20 Mev/nucleon, under the influence of different collision constraints.

### 2.4.2 Propagation

In the Fig 2.3 author has shown the propagation of nucleons under the influence of different collision constraints. The black curve shows the trajectory of those nucleons which undergoes only one collision, red curve corresponds to those nucleons which undergoes two collisions and blue line corresponds to three collisions respectively. The distance covered by the nucleons which suffers only one collisions is lesser as compared to one which suffers two or three collisions. The direction of propagation of nucleons under the influence of different collision constraints are shown by solid arrows.

Nuclei which have been successfully initialized are then boosted towards each other with

proper center-of-mass velocity using relativistic kinematics. The centers of projectile and target move along Coulomb trajectories upto a distance of 2 fm between the surface of projectile and target. The equation of motion of many body system is then calculated by mean of a generalized variational principle. We start from the action

$$S = \int_{t_1}^{t_2} \mathcal{L}[\Phi, \Phi^*] d\tau, \tag{2.7}$$

with the Lagrange functional

$$\mathcal{L} = \langle \Phi | i\hbar \frac{d}{dt} - H | \Phi \rangle, \tag{2.8}$$

The time evolution is obtained when the action is stationary under the allowed variation of the wave function

$$\delta S = \delta \int_{t_1}^{t_2} \mathcal{L}[\Phi, \Phi^*] dt = 0 \tag{2.9}$$

Which yields an Euler Lagrange equation for each parameter $\lambda$ as follow

$$\frac{d}{dt} \frac{\partial \mathcal{L}}{\partial \dot{\lambda}} - \frac{\partial \mathcal{L}}{\partial \lambda} = 0 \tag{2.10}$$

If the true solution of the Schrödinger equation is contained in the restricted set of wave function $\psi(r, p_i(t), r_i(t))$, this variation of the action gives the exact solution of the Schrödinger equation. For the coherent states and for the Hamiltonian of the form,

$$H_N = \sum_i T_i + \frac{1}{2} \sum_{i,j;i \neq j} V(r_i(t) - r_j(t)) \quad (i = 1, N) \tag{2.11}$$

The potential energy $V(r_i(t) - r_j(t))( \equiv V_{ij})$ between two particles is obtained by folding the two-body interaction with the densities of both particles. i.e.,

$$V(r_i(t) - r_j(t)) = \int f_i(r_i, p_i; t) f_j(r_j, p_j; t) V(r_i, r_j) d^3r_i d^3r_j d^3p_i d^3p_j \tag{2.12}$$

Using classical Liouville equation, we find that the equations of motion of $r_i$ and $p_i$ shows similar structure like classical Hamilton equations (provided the Hamiltonian can be written as in Eqn.2.11). The nucleons of the target and projectile interact via two and three body Skyrme interactions, Yukawa potential and momentum dependent interactions. The isospin degree of freedom is treated explicitly by employing a symmetry potential and explicit Coulomb forces between protons of colliding target and

projectile.

The hadrons propagate using Hamilton equations of motion

$$\dot{r}_i = \frac{\partial H_N}{\partial p_i}; \dot{p}_i = \frac{-\partial H_N}{\partial r_i} \tag{2.13}$$

Suppose the Hamiltonian for the system is given by local Skyrme nucleon-nucleon interaction consisting of two-body and three-body interactions only:

$$V_{loc} = t_1\delta(r_1 - r_2) + t_2\delta(r_1 - r_2)\delta(r_1 - r_3) \tag{2.14}$$

where $t_1$ and $t_2$ are (two) and (three) body coefficients, respectively. It is well known that three-body part of above equation is equivalent to a density-dependent two-body force, however, the IQMD is an N-body theory. Therefore, we prefer to use the three-body form rather than the density-dependent form. For three-body interactions (which includes three Gaussian overlap), the Hamiltonian becomes

$$H_N = \sum_i \frac{p_i^2(t)}{2m} + \frac{1}{2}\sum_{i,j;i\neq j} V_{ij} + \frac{1}{3!}\sum_{i,j,k;i\neq j\neq k} V_{ijk} \equiv \sum_i H_i \tag{2.15}$$

where

$$H_i = T_i + \frac{1}{2}\sum_{j;j\neq i} V_{ij} + \frac{1}{3!}\sum_{j,k;j\neq k\neq i} V_{ijk} \tag{2.16}$$

where $V_{ij}$ is potential between two particles and is obtained by folding two-body interaction with densities of both the particles as mentioned in Eqn.2.12. $V_{ijk}$ is the potential among three particles and is obtained by folding three-body interaction with the densities of the three particles and is written as

$$V_{ijk} = \int f_i(r_i, p_i; t) f_j(r_j, p_j; t) f_k(r_k, p_k; t) V(r_i, r_j, r_k) d^3r_i d^3r_j d^3r_k d^3p_i d^3p_j d^3p_k \tag{2.17}$$

For the two-body interaction represented by second term of Eqn.2.16and according to Eqn.2.12, we can write,

$$\begin{aligned}
\frac{1}{2}\sum_{j;i\neq j} V_{ij} &= \frac{1}{2}\sum_{j;i\neq j} \int f_i(r_i,p_i;t)\ f_j(r_j,p_j;t)\ V(r_i,r_j) \qquad (2.18)\\
&\quad \times\ d^3r_i\ d^3r_j\ d^3p_i\ d^3p_j \\
&= \frac{1}{2}\sum_{j;i\neq j}\int f_i(r_i,p_i;t)\ f_j(r_j,p_j;t)\ t_1 \\
&\quad \times\delta(r_i-r_j)d^3r_i\ d^3r_j\ d^3p_i\ d^3p_j \\
&= \frac{1}{2}\sum_{j;i\neq j}\ t_1\int f_i(r_i,p_i;t)\ f_j(r_j,p_j;t) \\
&\quad \times\ d^3r_i\ d^3p_i\ d^3p_j \\
&= \frac{1}{2}\sum_{j;i\neq j}\ t_1\int \frac{1}{(\pi\hbar)^3}e^{-(r-r_i(t))^2 2/L}e^{-(p-p_i(t))^2L/2\hbar^2} \\
&\quad \times\frac{1}{(\pi\hbar)^3}e^{-(r-r_j(t))^2 2/L}\ e^{-(p-p_j(t))^2L/2\hbar^2}\ d^3r_i\ d^3p_i\ d^3p_j \\
&= \frac{1}{2}\sum_{j}\ t_1\frac{1}{(4\pi L)^{3/2}}e^{-(r_i-r_j)^2/4L} \\
&= \frac{t_1}{2}\sum_{j;i\neq j}\rho_{ij} \qquad (2.19)
\end{aligned}$$

where, the interaction density $\rho_{ij}$ is given by:

$$\rho_{ij} = \int d^3r\ \rho_i(r)\ \rho_j(r) = \frac{1}{(4\pi L)^{3/2}}e^{-(r_i-r_j)^2/4L} \qquad (2.20)$$

The three-body interactions can be calculated as follows:

$$\begin{aligned}
\frac{1}{3!}\sum_{j,k;i\neq j\neq k} V_{ijk} &= \frac{1}{3!}\sum_{j,k;i\neq j\neq k}\int f_i(r_i,p_i,t)\ f_j(r_j,p_j,t)\ f_k(r_k,p_k,t)\ V(r_i,r_j,r_k) \\
&\quad \times d^3r_i\ d^3r_j\ d^3r_k\ d^3p_i\ d^3p_j\ d^3p_k \\
&= \frac{1}{3!}\sum_{j,k;i\neq j\neq k}\int f_i(r_i,p_i,t)\ f_j(r_j,p_j,t)\ f_k(r_k,p_k,t)\ t_2 \\
&\quad \times\delta(r_i-r_j)\ \delta(r_i-r_k)d^3r_i\ d^3r_j\ d^3r_k\ d^3p_i\ d^3p_j\ d^3p_k \\
&= \frac{1}{3!}\frac{t_2}{(2\pi L)^3\cdot 3^{3/2}}\sum_{j,k;i\neq j\neq k} e^{-\left[(r_i-r_j)^2+(r_i-r_k)^2+(r_k-r_j)^2\right]/6L} \\
&= \frac{1}{3!}\frac{t_2}{(2\pi L)^3 3^{3/2}}\sum_{j,k;i\neq j\neq k} e^{-\left[(r_i-r_j)^2+(r_i-r_k)^2\right]/6L\times\frac{3}{2}} \\
&= \frac{1}{3!}\frac{t_2\ (4\pi L)^{3/2\times 2}}{(2\pi L)^3\cdot 3^{3/2}}\left[\sum_{j\neq i}\frac{1}{(4\pi L)^{3/2}}e^{-(r_i-r_j)^2/4L}\right]^2 \\
&= \frac{1}{3!}\frac{t_2\ 2^3}{3^{3/2}}\left[\sum_{j\neq i}\rho_{ij}\right]^2
\end{aligned} \tag{2.21}$$

From the above equations, we have noticed that for three-body interactions, the mean field can be written as $[\sum_{j\neq i}\rho_{ij}]^2$.

The total baryon-baryon potential in IQMD model can be given as:

$$V^{ij}(\vec{r}'-\vec{r}) = V^{ij}_{Skyrme}+V^{ij}_{Yukawa}+V^{ij}_{Coul}+V^{ij}_{mdi}+V^{ij}_{sym} \tag{2.22}$$

The detail regarding these potentials is discussed below:

In nuclear matter where the density is constant, the interaction density coincides with the single particle density and $V^{(2)}_{loc}$ as well as $V^{(2)}_{Yuk}$ are directly proportional to $(\frac{\rho}{\rho_o})$. The three-body part of the interaction $V^{(3)}_{loc}$ is proportional to $(\frac{\rho}{\rho_o})^2$. In nuclear matter, the local potential energy has the form

$$V_{loc} = \frac{\alpha}{2}\left(\frac{\rho}{\rho_o}\right) + \frac{\beta}{\gamma+1}\left(\frac{\rho}{\rho_o}\right)^2 \tag{2.23}$$

The above potential has two free ($\alpha$ and $\beta$) parameters, which can be fixed as per the requirement. For normal nuclear matter density the average binding energy should be -16 MeV and total energy should have a minimum at $\rho_o$. In order to investigate the

influence of different compressibilities, one can generalize the above potential energy to

$$V_{loc} = \frac{\alpha}{2}\left(\frac{\rho}{\rho_o}\right) + \frac{\beta}{\gamma+1}\left(\frac{\rho}{\rho_o}\right)^{\gamma} \tag{2.24}$$

This equation leads to the nuclear equation of state which connects the pressure and energy. In the study of heavy-ion collisions, one usually uses the so-called the Skyrme parameterization of nuclear equation of state (EOS) which contains two sets of parameter giving the correct binding energy and saturation density. However, two different types of incompressibility $K$, one corresponds to soft EOS with $K$ = 200 MeV (at smaller value of $\gamma$), another corresponds to hard EOS with $K$ = 380 MeV (at larger value of $\gamma$). The total Skyrme potential then can be written as:

$$V^{Skyrme} = \sum_{j;i\neq j} t_1\delta(r_i - r_j) + t_2\delta(r_i - r_j)\rho^{\acute{\gamma}-1}((r_i + r_j)/2) \tag{2.25}$$

We have a finite range Yukawa term $V^{Yuk}$, and Coulomb interaction $V^{Coul}$ which reads as:

$$V^{Yuk} = t_3\frac{exp\{-|r_i - r_j|\}/\mu}{|r_i - r_j|/\mu} \tag{2.26}$$

$$V^{Coul} = \frac{Z_i Z_j\ e^2}{|r_i - r_j|} \tag{2.27}$$

The Yukawa potential is also a short ranged potential in IQMD model with $t_3$= -6.66 MeV and $\mu$ = 0.4 fm (in QMD, $\mu$ = 1.5 fm). It has been added to existing potential to improve the surface properties of the interaction which are very important to study multi-fragmentation.

When momentum-dependent potential (which is optional) is introduced, one has to readjust the parameters of the Skyrme interaction so as to have correct saturation properties for the normal nuclear matter and the same incompressibilities as those of the soft and hard EOS. The parameterized form of the momentum-dependent interactions which is fitted with the experimental data [227, 228] and is given as:

$$V^{MDI} = \sum_{j;i\neq j} t_4 ln^2(t_5(p_i - p_j)^2 + 1)\delta(r_i - r_j) \tag{2.28}$$

where $t_4$ = 1.57 MeV and $t_5 = 5 \times 10^{-4}\ MeV^{-2}$. The new parameter sets with the momentum dependence are called SMD and HMD, respectively. All these set of

**Table 2.1:** Parameter sets used in the IQMD model [194].

| EOS | $\alpha$(MeV) | $\beta$(MeV) | $\gamma$ | $\delta$(MeV) | K(MeV) |
|---|---|---|---|---|---|
| S | -356 | 303 | 1.17 | | 200 |
| SMD | -390 | 320 | 1.14 | 1.57 | 200 |
| H | -124 | 71 | 2.00 | | 380 |
| HMD | -130 | 59 | 2.09 | 1.57 | 380 |

parameters are listed in Table 2.1 along with with incompressibilities. As we have already stated that, the isospin effects in the IQMD model enters via Coulomb and Symmetry potential. In the present model, we have used real charge i.e. for proton $Z_{proton} = 1$ and for neutron $Z_{neutron} = 0$ to include the isospin dependence of Coulomb potential. On the other hand in the QMD model, we have used effective charge ($Z_{eff}$) for all the nucleons without distinguishing among protons and neutrons. The symmetry potential which appears due to protons and neutrons is included and is given by

$$V^{sym} = \sum_{j;i\neq j} t_6(1/\rho_0)T_{3i}T_{3j}\delta(r_i - r_j) \tag{2.29}$$

where $t_6$ = 100 MeV and $T_{3i}$ and $T_{3j}$ denote the isospin projection of $i^th$ and $j^th$ particle (being +1/2 for protons and -1/2 for neutrons, respectively). The Symmetry and Coulomb potentials are isospin dependent and however Skyrme, Yukawa and momentum-dependent potentials are isospin independent. For a nucleus in its ground state, the expectation value of the total Hamiltonian corresponds to its total binding energy. While comparing with the Bethe-Weizsäcker mass formula, the kinetic energy, the Skyrme interaction and the momentum-dependent interactions contributes to the volume energy. The Yukawa interaction contributes to the surface and volume energy, and the symmetry interactions to the volume symmetry energy. There is no term corresponding to the pairing energy, since it corresponds to a global property of the nucleus which would be difficult to model by microscopic local forces.

Therefore, the total baryon-baryon potential in IQMD model can be written as:

$$\begin{aligned} V^{ij}(\vec{r}' - \vec{r}) &= V^{ij}_{Skyrme} + V^{ij}_{Yukawa} + V^{ij}_{Coul} + V^{ij}_{mdi} + V^{ij}_{sym} \\ &= \left[ t_1 \delta(\vec{r}' - \vec{r}) + t_2 \delta(\vec{r}' - \vec{r}) \rho^{\gamma - 1} \left( \frac{\vec{r}' + \vec{r}}{2} \right) \right] \\ &+ \left[ t_3 \frac{exp(|\vec{r}' - \vec{r}|/\mu)}{(|\vec{r}' - \vec{r}|/\mu)} \right] + \left[ \frac{Z_i Z_j e^2}{|\vec{r}' - \vec{r}|} \right] \\ &+ \left[ t_4 ln^2 [t_5 (\vec{p}' - \vec{p})^2 + 1] \delta(\vec{r}' - \vec{r}) \right] \\ &+ \left[ t_6 \frac{1}{\rho_0} T_3^i T_3^j \delta(\vec{r}_i' - \vec{r}_j) \right] \end{aligned} \tag{2.30}$$

### 2.4.3 Nucleon-Nucleon collisions

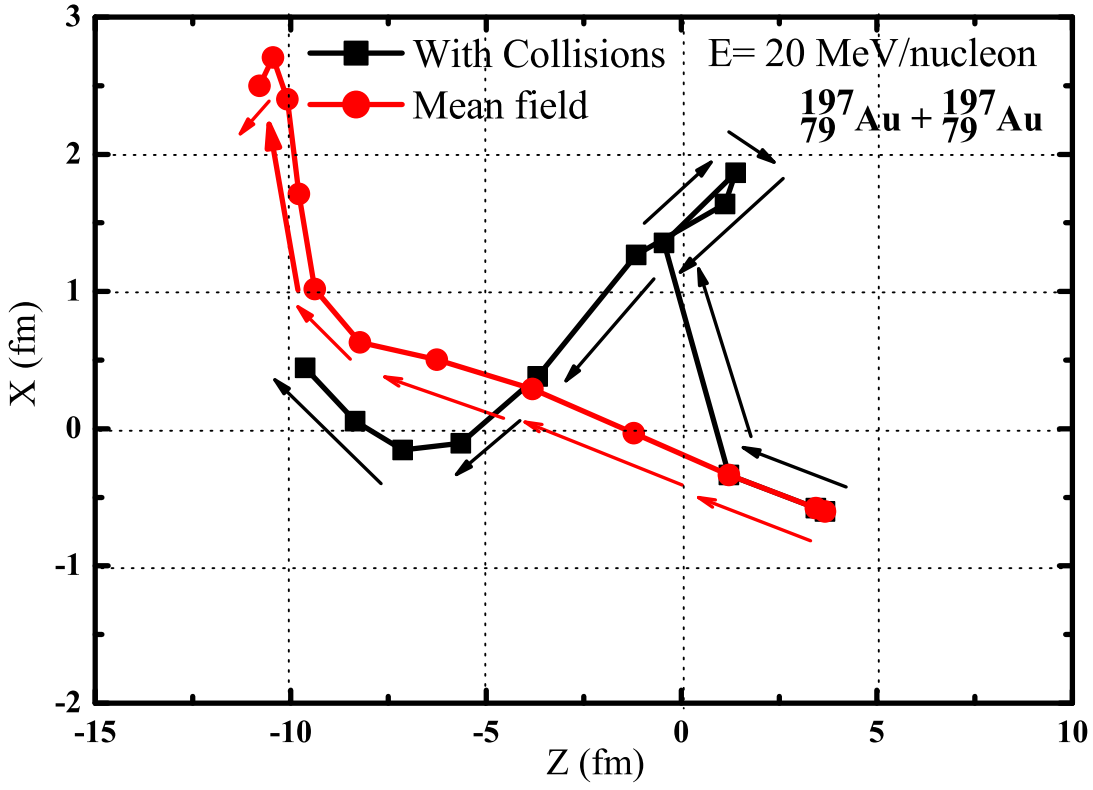


**Figure 2.4:** Trajectory of nucleons for the reaction $^{197}_{79}Au + ^{197}_{79}Au$ at incident energy E = 20 MeV/nucleon, under the influence of collisions and mean field.

In the Fig 2.4, trajectory of nucleons for the reaction $^{197}_{79}Au +^{197}_{79} Au$ at incident energy E = 20 MeV/nucleon, under the influence of collisions and mean field have been shown. The nucleons which do not suffer any collisions and moving under the influence of only mean field in a specified direction and represented by red curve. However the nucleons which suffers multiple collisions and moves randomly in the presence of mean field are shown by the black curves. The path followed by these nucleons is more random as compared to the nucleons which do not suffer any collision.

Two nucleons are supposed to suffer a binary collision if the distance between their centroid is fulfilled by condition

$$|r_i - r_j| \leq \sqrt{\frac{\sigma_{tot}}{\pi}}, \quad \sigma_{tot} = \sigma(\sqrt{s}, type) \tag{2.31}$$

where "type" denotes the ingoing collision partners (N-N, N-$\Delta$, N-$\pi$,....).

Total cross section is the sum of the elastic and inelastic cross sections

$$\sigma_{tot} = \sigma_{el} + \sigma_{inel} = \sigma_{el} + \sum_{channels} \sigma_i \tag{2.32}$$

In addition to nucleons and deltas (as in QMD model), pions are also formed in the IQMD model via the decay of delta resonances. The following inelastic channels are explicitly taken into account and constitute the imaginary part of the pion optical potential

$$\begin{aligned} &N\ N \rightarrow\ \Delta\ N\ (hard - delta\ production) && (a)\\ &\Delta \rightarrow\ N\ \pi\ (delta\ decay) && (b)\\ &\Delta\ N \rightarrow\ N\ N\ (delta\ absorption) && (c)\\ &N\ \pi \rightarrow\ \Delta\ (soft - delta\ production) && (d) \end{aligned} \tag{2.33}$$

Elastic $\pi\ -\ \pi$, $\pi\ -\ N$, $\pi\ -\ \Delta$, $\Delta\ -\ \Delta$, $\Delta\ -\ N$ scattering is not taken into account. Experimental cross sections are used for processes (a) and (d) [226, 229], as well as for the elastic NN collisions. Inaccessible reactions like $\Delta$N$\rightarrow\ NN$ are calculated from their reverse reactions ( $NN\ \rightarrow\ \Delta N$) using modified detailed balance formula [230].

**Table 2.2:** a(s) and b(s) as a function of the center of mass energy

| $x = \sqrt{s}\ (GeV)$ | $a\ (fm)$ | $b$ |
|---|---|---|
| 2.104 - 2.12 | $294.6(x-2.014)^{2.578}$ | $19.71(x-2.014)^{1.551}$ |
| 2.12 - 2.43 | $\frac{0.01224}{(x-2.225)^2\ +\ 0.004112}$ | $19.71(x-2.014)^{1.551}$ |
| 2.43 - 4.50 | $\left(\frac{2.343}{x}\right)^{43.17}$ | $33.14\ arctan(0.5404(x-2.146)^{0.9784})$ |

The angular distribution for the elastically scattered nucleons is given by [195]:

$$\frac{d\sigma_{el}}{d\Omega} \sim e^{A(s)t} \tag{2.34}$$

where,

$$t = -2p^2(1-cos\theta) \quad and \quad A(s) = 6\frac{[3.65(\sqrt{s}-1.8766)]^6}{1+[3.65(\sqrt{s}-1.8766)]^6} \tag{2.35}$$

$\sqrt{s}$ is the center of mass (c.m.) and energy is measured in GeV.

The inelastic channel is treated in an analogous fashion. The parametrization suggested by Huber and Aichelin [231] is used: fitted differential cross-sections are extracted from one boson exchange (OBE) calculations:

$$\frac{d\sigma_{in}}{d\Omega} \approx a(s)exp\left[b(s)cos\theta\right] \tag{2.36}$$

The $a(s)$ and $b(s)$ are functions of $\sqrt{s}$ and vary in their definition for different intervals of $\sqrt{s}$ (see table 2.2). $\theta$ is the polar angle.

In the next step, to identify the isospin effects, we compare the cases when the isospin dependence of nucleon-nucleon cross-section channel is either turned on $\sigma_{iso}$ ($\sigma_{np} = 3\sigma_{nn} = 3\sigma_{pp}$) [194] or off $\sigma_{noiso}$ ($\sigma_{np} = \sigma_{nn} = \sigma_{pp}$). In the Fig 2.5, we have shown the variation of allowed collisions $dN_{coll}/dt$, for the reaction $^{197}_{79}Au + ^{197}_{79}Au$ at low incident energy E = 50 MeV/nucleon (below the balance energy) and at higher incident energy E = 400MeV/nucleon (above the transition energy). In general, neutron-proton ($\sigma_{np}$) cross-section is larger with a factor of 2 to 3 than that of the proton proton cross section ($\sigma_{pp}$) and neutron-neutron ($\sigma_{nn}$) cross-section [232]. At lower incident energies

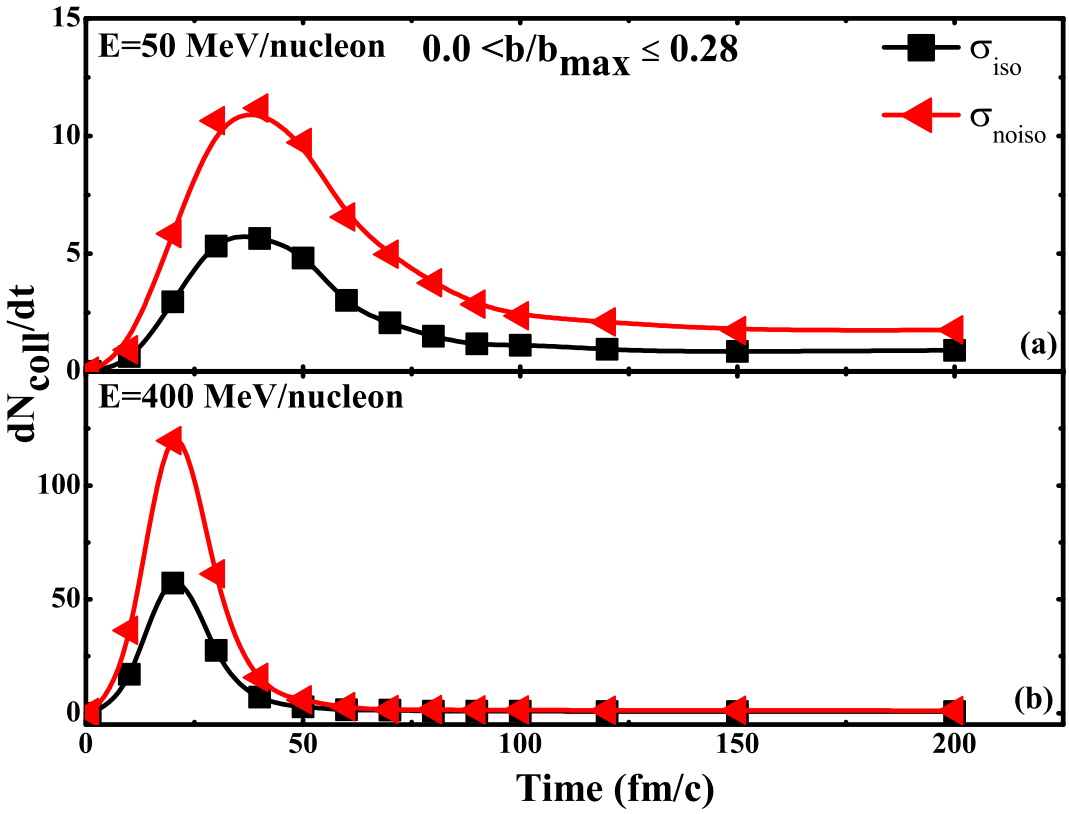


**Figure 2.5:** The rate of allowed collisions $dN_{coll}$ = dt versus reaction time for the reaction $^{197}_{79}Au +^{197}_{79} Au$, at incident energies E = 50 MeV/nucleon and 400 MeV/nucleon [21].

a broader Gaussian shape is observed which clearly indicates the ongoing interactions among the nucleons and less thermalization. Therefore maximum number of collisions occurred between 30-40 fm/c. At higher incident energy (E=400 MeV/nucleon), reaction finishes much earlier as compared to lower incident energy (E=50 MeV/nucleon) and maxima occurs between 20-30 fm/c. At lower as well as higher incident energy, one can clearly see the difference due to isospin dependent and isospin independent nucleon-nucleon cross sections.

Fig 2.6, shows similar results as depicted in the Fig 2.5, the only difference is, we are enhancing and reducing the scaled Gaussian width (SGW = 0.8, 1.0 and 1.2). Scaled Gaussian width stand for the ratio of enhanced or reduced value of Gaussian width to

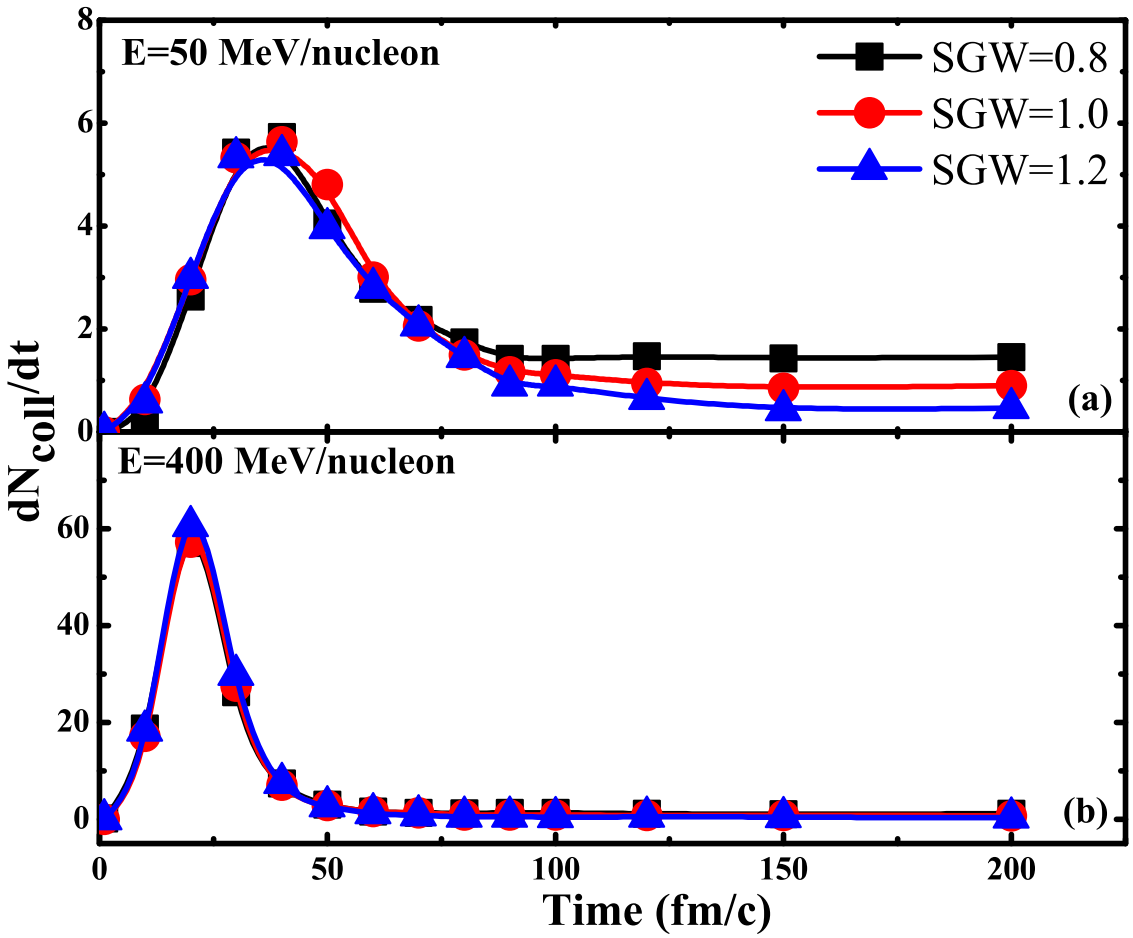


**Figure 2.6:** The rate of allowed collisions $dN_{coll}$ = dt versus reaction time for the reaction ${}^{197}_{79}Au + {}^{197}_{79}Au$, at incident energies E = 50 MeV/nucleon and 400 MeV/nucleon [21].

actual value of Gaussian width used in IQMD model [233]. To obtained maximum stability of the nucleus, we have always used the mass dependence Gaussian width. Effect of scaled Gaussian width (SGW) on fragment production and there flow in heavy-ion collision, has been already studied [233]. In the Fig. 2.6, we have shown the variation of allowed collisions $dN_{coll}/dt$, for the reaction ${}^{197}_{79}Au + {}^{197}_{79}Au$ at low incident energy E = 50 MeV/nucleon (where the role of mean field is strong) and at higher incident energy E = 400 MeV/nucleon (where the nucleon-nucleon collisions play the strong role). At E = 50 MeV/nucleon, nucleon-nucleon collisions undergoes longer time span (broader

the Gaussian width) and there is slight difference in collision rate due to small changes in the Gaussian widths. While at incident energy E = 400 MeV/nucleon the reaction finishes much earlier (shorter Gaussian width) and negligible difference is seen on the collision rate due to changes made in the Gaussian width.

## 2.5 Pauli blocking

The nucleons are fermions, therefore Pauli principle (a quantum feature) is an important ingredient in the reaction dynamics. It is difficult to include the Pauli blocking properly in classical approaches because it has no classical equivalence. To overcome this, only average phenomenological treatments are usually attempted [234–237]. In such a case, the basic idea is to prevent nucleons from being in overpopulated regions of phase space. With the inclusion of this methodology, whenever a binary collisions occurs the phase space around the scattering partners is checked. For simplicity, each nucleon is assumed to occupy a sphere in the coordinate and momentum space. The results of the Pauli blocking ratio are exactly similar to the one calculated by the overlapping of the Gaussian and is less time consuming. The fractions $P_1$ and $P_2$ of the final phase space are calculated for each of the two scattering partners which is already occupied by other nucleons. A binary collision is blocked with a probability:

$$P_{block} \;=\; 1 - [1 - min(P_1, 1)][1 - min(P_2, 1)] \tag{2.37}$$

and correspondingly allowed with a probability $(1 - P_{block})$. For a nucleus in its ground state, where all collisions should be blocked ideally, the average blocking probability $< P_{block} >$ is about 0.96. In the case of complete blocking, this factor should be equal to one.

## 2.6 Different Methods of Clusterization

The above mentioned models are "primary models" that are used to generate the phase space of nucleons. We need "secondary models" to clusterize the nucleons into

fragments. After getting the final outcome of the reaction clusterization approach plays a significant role. In the following subsections, the secondary models are used to clusterize the phase space of nucleons and are discussed below in subsections.

### 2.6.1 Minimum Spanning Tree (MST) method

The MST [60, 238–242] is one of the method of analysis which is most extensively used to clusterize the nucleons. In MST method, two nucleons share the same fragment if their centroids are closer than a certain distance $d_{min}$.

$$| \vec{r}_i - \vec{r}_j | \leq d_{min} \tag{2.38}$$

where $\vec{r}_i$ and $\vec{r}_j$ are the spatial positions of both nucleons. The value of $d_{min}$ can vary between $2-4$ fm. However, minimum spanning tree method cannot be used to address the time scale as it yields big fragments during the early stage of the reaction. This clusterization method can only be used to analyze asymptotic configurations in which the fragmenting system can be viewed as a very dilute mixture of free particles and almost equilibrated fragments. To study the time of fragment formation, one needs to device a method which should be able to detect the overlapping of fragments.

# Chapter 3

# Collision dynamics

## 3.1 Introduction

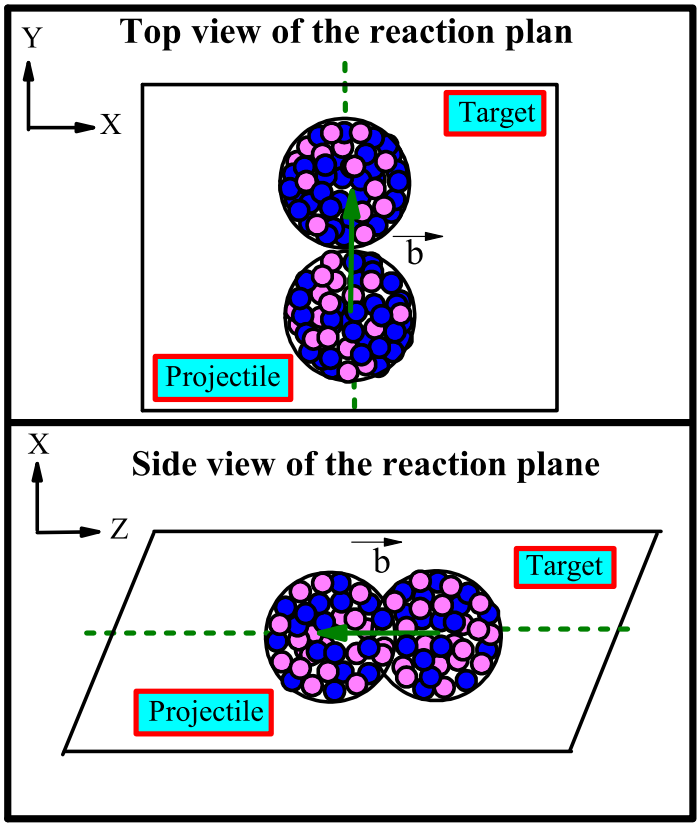


**Figure 3.1:** Top and side view of the reaction plane.

Collision dynamics is an essential and influential feature of heavy-ion nuclear re-

actions. According to geometrical concept the interaction between two nuclei depends firmly on the impact parameter of the reaction. From the physics point of view, when straight lines are drawn from the center of the two nuclei along Z-axis the transverse distance between these straight lines is known as impact parameter. Impact parameter provides the information about centrality of the nuclear reaction. In general, the range of the impact parameter for the central collision is $0 \leq \widehat{b} \leq 0.3$, for the semi-central $0.3 \leq \widehat{b} \leq 0.6$ and for the peripheral collision the range is $0.6 \leq \widehat{b} \leq 0.9$, ($\widehat{b} = b/b_{max}$, $b_{max} = 1.12(A_P^{1/3} + A_T^{1/3})$) where, $A_P$ and $A_T$ are the masses of projectile and target respectively. In Fig 3.1, we have shown the top and side view of the collision in reaction plane. Proper selection of the impact parameter bin is very important because stopping power, nuclear flow and compression depends on the overlapping of colliding nuclei [243–247].

Fig 3.2, describes the geometrical description of the collision process. Initially, two nuclei are far apart from each other. After the collision, nucleons which participate in the collision process are known as participant nucleons and the rest of the nucleons which do not participate in the collision process are known as spectator nucleons.

### 3.1.1 Central collisions

A central collision or head on collision leads to maximum overlapping between the colliding nuclei, thereby resulting in more participant and less spectators nucleons. The study of nuclear matter in extreme states of density and temperature, at small impact parameters (i.e., central collisions) are the main area of interest. Central collisions boast to have a wide range of multiple phenomenon [248]. In such types of collision target and projectile form maximum possible overlapping zone, therefore in the collision process the maximum number of nucleons participate. At a low energy range, central collision leads to fusion. At higher bombarding energies, central collision results in complete disassembly of the system. To study the highly excited compressed hadronic matter and the quark-gluon plasma, central collisions are most appropriate tools [249] in nuclear physics. In Fig 3.3, the geometrical arrangement of central collisions is shown.

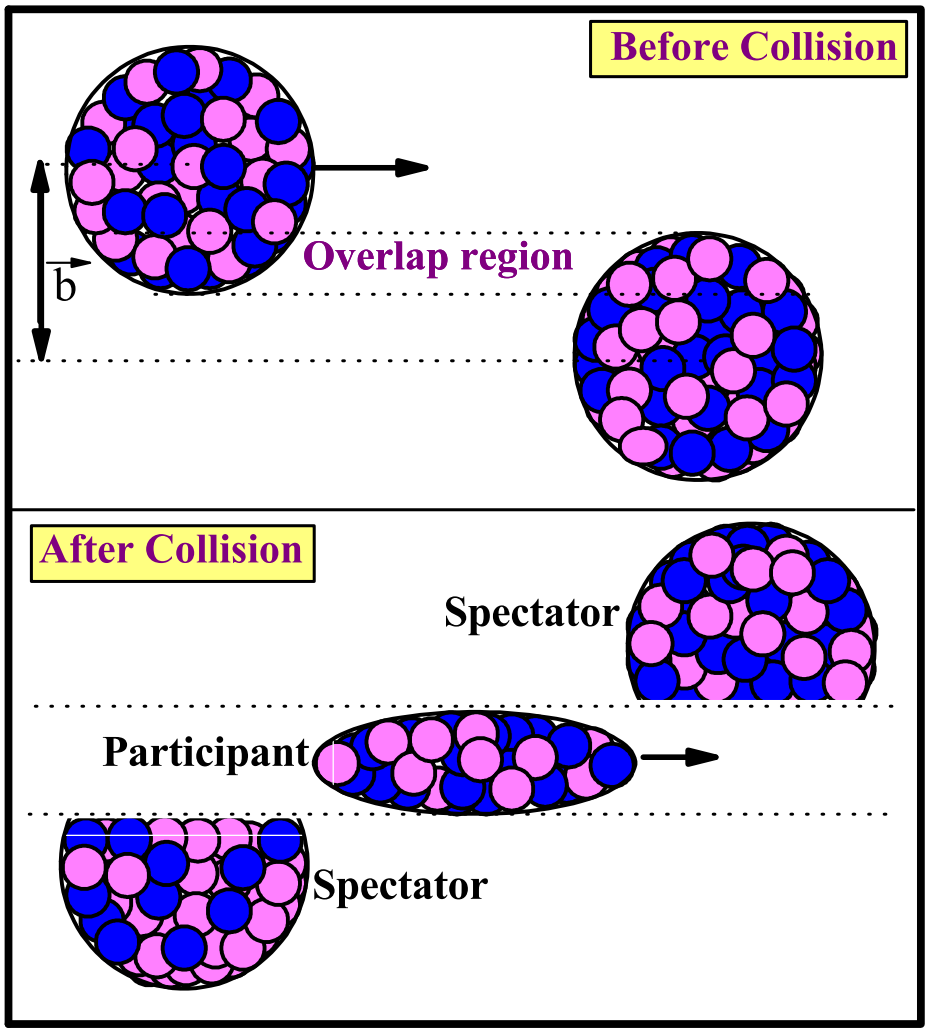


**Figure 3.2:** Geometrical description before and after collision.

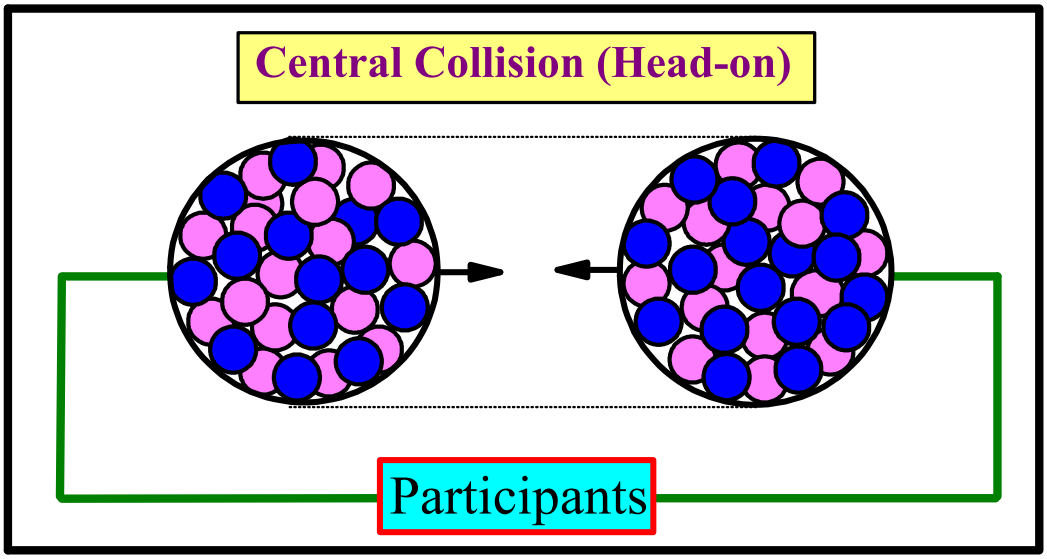


**Figure 3.3:** Geometrical arrangement of central collision.

### 3.1.2 Peripheral collisions

A collision far from the center is known as peripheral collision. In these collisions there are less number of participating nucleons and more number of spectator nucleons. The amount of momentum and energy transfer [250] in such type of collisions is very small. The excited fragments are pushed towards the forward hemisphere resulting into non uniform emissions of the fragments [250]. At low incident energies peripheral collisions results into deep inelastic interactions and at a high bombarding energies, it results into fragment production [249]. Author has displayed the block diagram for peripheral collision in Fig 3.4. In the peripheral collision lesser number of nucleons participate in collision dynamics as compared to central collisions.

### 3.1.3 Probability of occurrence of collisions at different impact parameters

In the Fig 3.5, author has displayed the probability of collisions with the number of nucleons participating nucleons at different conditions. It is further observed that

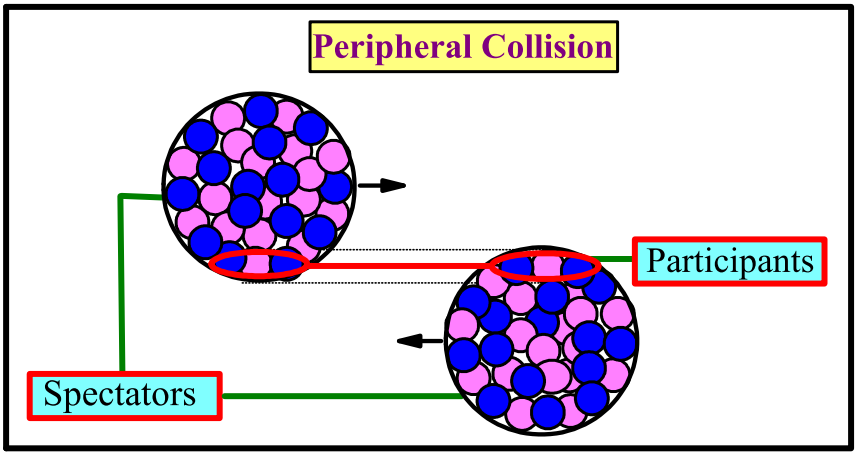


**Figure 3.4:** Schematic diagram of participant and spectator matter during peripheral collisions.

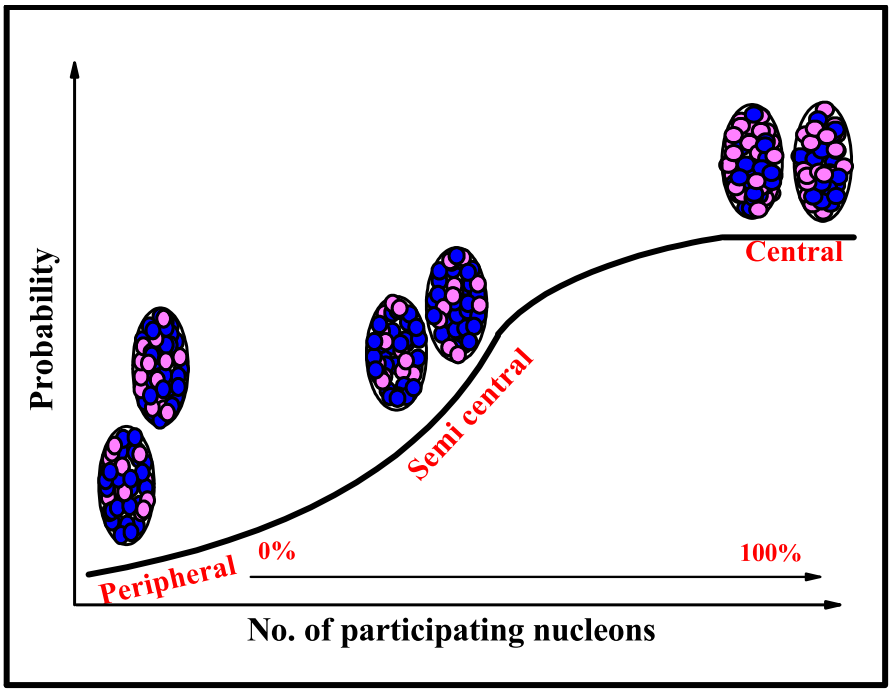


**Figure 3.5:** Probability of collisions at different impact parameters.

number of collisions are not same at different collision conditions. While changing in the impact parameter i.e., from central to semi-central and from semi-central to peripheral, the probability of nucleons participating in collision dynamics decreases. The black solid arrow shows the percentage of participating nucleons during the collision process, which is 100% at central impact parameter and 0% at peripheral impact parameter. The impact parameter investigation manifest the initial geometry of the collision zone, rooted from nuclear structure and used to explore the final stage of heavy-ion collisions [251].

## 3.2 Three dimensional trajectory of nucleons

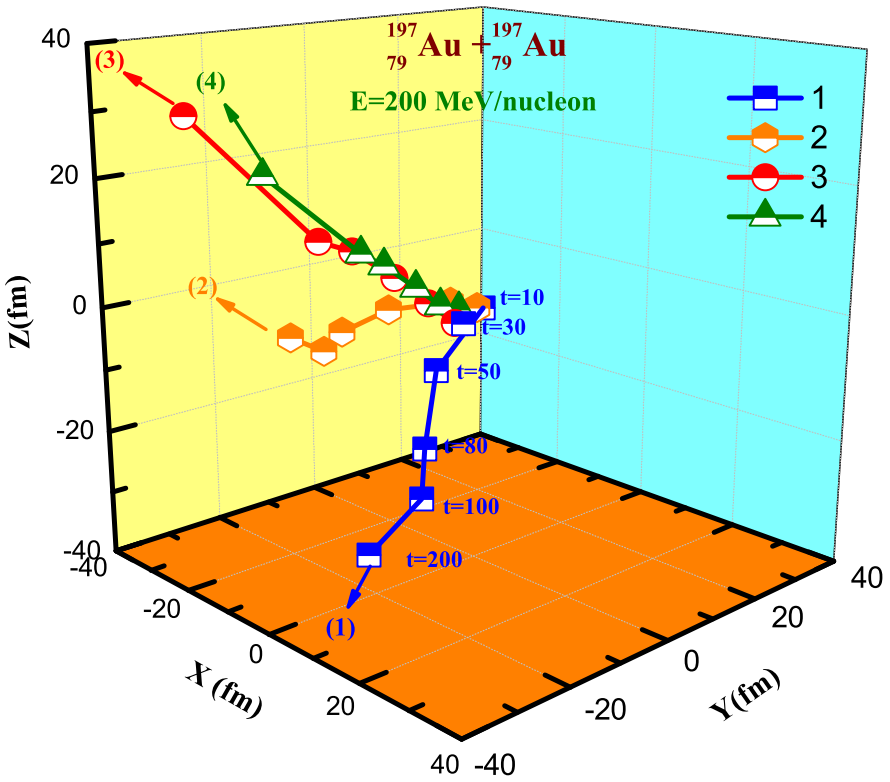


**Figure 3.6:** The 3-D snapshot shows the trajectory of nucleons at E = 200 MeV/nucleon for the reaction $^{197}_{79}Au +^{197}_{79} Au$.

**Table 3.1:** List of the whole impact parameter range.

| *S. No.* | *Impact parameter* | *Fraction of participants* |
|---|---|---|
| $BIN(I)$ | $0 < \hat{b} \leq 0.28$ | 1 |
| $BIN(II)$ | $0.28 < \hat{b} \leq 0.39$ | 0.8569 |
| $BIN(III)$ | $0.39 < \hat{b} \leq 0.48$ | 0.7141 |
| $BIN(IV)$ | $0.48 < \hat{b} \leq 0.56$ | 0.5713 |
| $BIN(V)$ | $0.56 < \hat{b} \leq 0.62$ | 0.4285 |
| $BIN(VI)$ | $0.62 < \hat{b} \leq 0.76$ | 0.2857 |
| $BIN(VII)$ | $0.76 < \hat{b} \leq 0.88$ | 0.1428 |
| $BIN(VIII)$ | $0.88 < \hat{b} \leq 1.0$ | 0 |

In Fig 3.6, one can clearly see the drifting of nucleons in the transverse direction, in three dimensional plot which shows the trajectory of the nucleons. In Fig 3.6, nucleons trajectory ia depicted for the symmetric reaction $^{197}_{79}Au +^{197}_{79} Au$ at six different time steps varying from 10 fm/c to 200 fm/c for the central collisions. We keep track of haphazardly selected the nucleons from the target and projectile which undergoes at least five collisions. The nucleons trajectory is shown using the solid arrows. It is observed that nucleons show more deviation in first few fm/c of the reaction in comparison to the rest of the path covered by nucleons.

The whole impact parameter range have been divided into eight bins. The selection of impact parameter bins is based on the data extracted from experimental measurements [137]. The impact parameter range is binned in eight classes (Table 3.1), so that the total number of collisions varying from the central part to peripheral can be divided. Depending upon the impact parameter of the colliding nuclei, the type of nuclear reactions can be distinguished and dynamical properties of the reaction can be discussed by studying their coordinate and momentum space (phase space).

Recently, the importance of impact parameter selection in heavy-ion collisions was discussed thoroughly by Li et al., [252]. A nucleon that suffer one or more collisions with nucleons of other nuclei are termed as participant nucleons. The volume of the initial overlap region is expressed via the number of participant nucleons denoted as

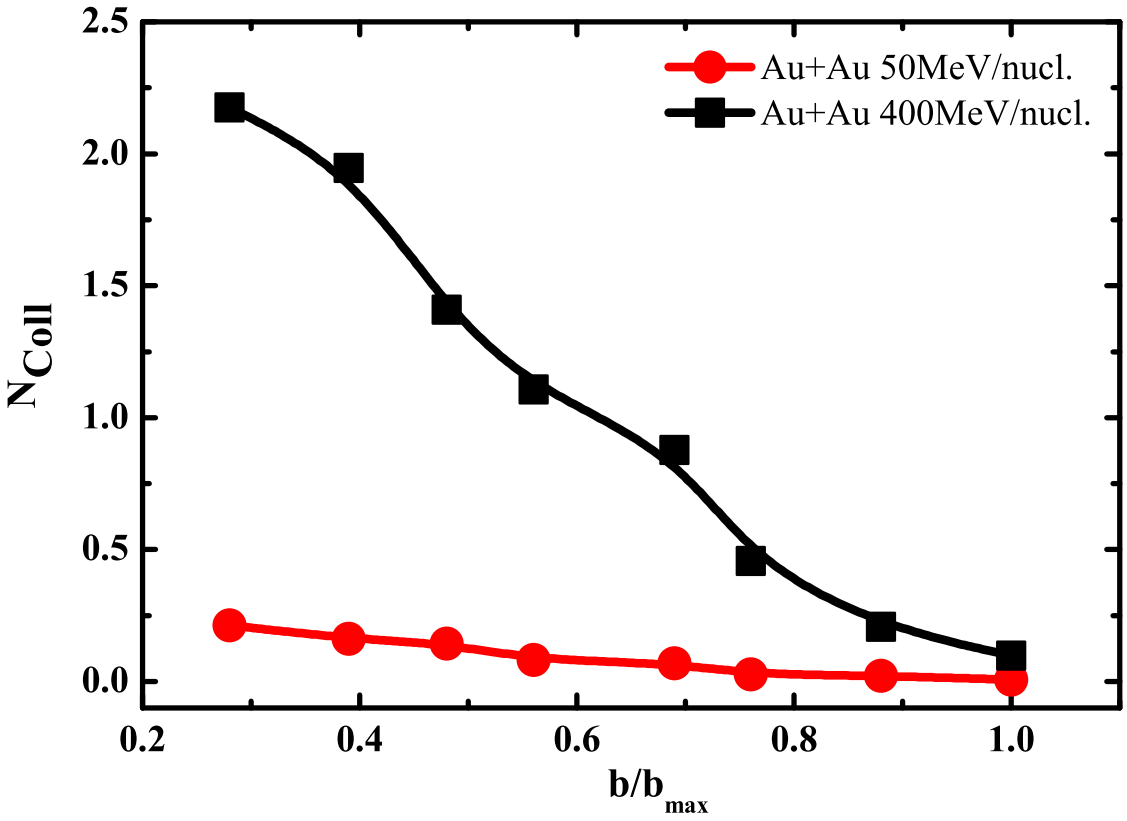


**Figure 3.7:** $N_{Coll}$ as the function of scaled impact parameter for the reaction $^{197}_{79}Au +^{197}_{79} Au$, at an incident energies E = 50 MeV/nucleon and E = 400 MeV/nucleon [20].

$N_{part}$ [253–255]. A number of binary nucleon-nucleon collisions are usually denoted as $N_{coll}$ [255]. If A is the mass of the colliding nuclei then number of spectator nucleons ($N_{spec}$) constituting the part of the nuclear volume, and not involved in the collisions is defined as $N_{spec}$ = 2A - $N_{part}$ [256]. In the Fig 3.7, we have displayed the results for $N_{Coll}$ as a function of scaled impact parameter for the mass symmetric reaction $^{197}_{79}Au +^{197}_{79} Au$. Calculations have been performed at two incident energies i.e., for E = 50 MeV/nucleon and 400 MeV/nucleon. At lower incident energies, reaction dynamics are directed by the mean field only and binary collisions are suppressed due to Pauli

blocking. The situation changes drastically at higher energy because of large number of nucleon-nucleon (NN) collisions and hence the net participant number of nucleon increases. As the impact parameter increases, the interaction zone between the projectile and target nuclei decreases, and hence there is decrease in the rate of nucleon-nucleon collisions due to small overlapping region. One can clearly see that the number of binary nucleons at E = 400 MeV/nucleon, is larger than at E = 50 MeV/nucleon. With an increase in the impact parameter, binary collisions are decreases and fall in the curves is clearly seen.

In the Fig 3.8, the results are displayed for $N_{Part}$ as a function of scaled impact

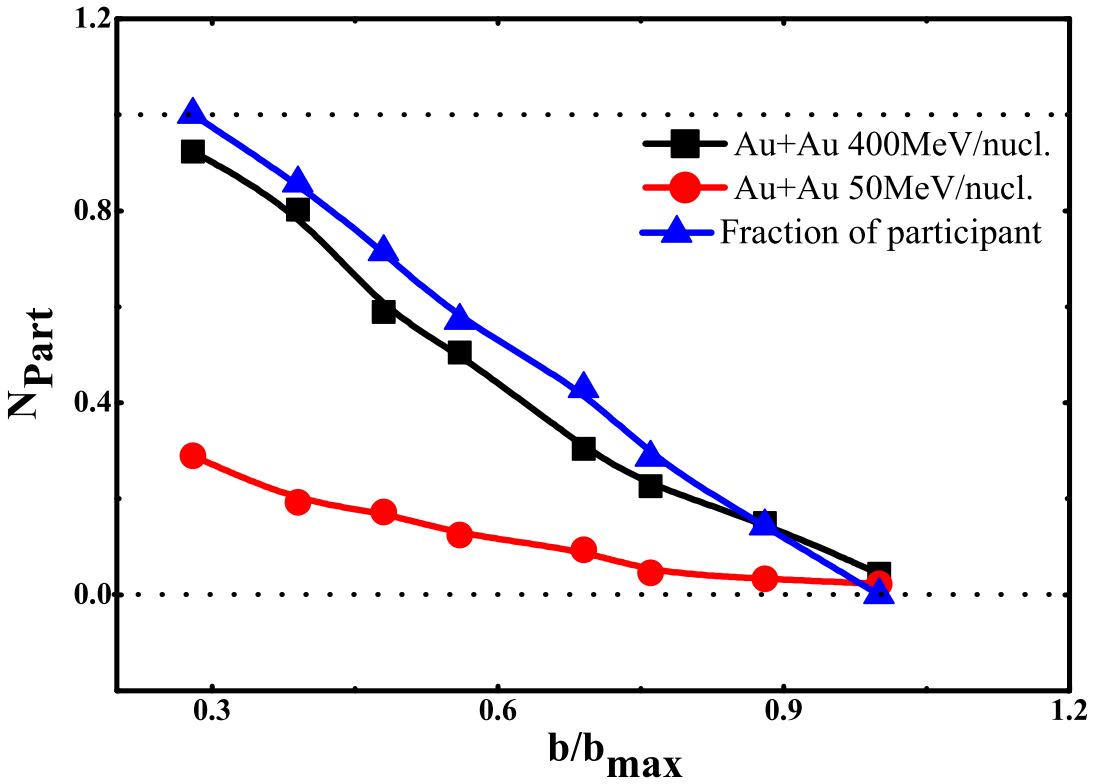


**Figure 3.8:** $N_{Part}$ as the function of scaled impact parameter for the reaction ${}^{197}_{79}Au + {}^{197}_{79}Au$, at an incident energies E = 50 MeV/nucleon and E = 400 MeV/nucleon [20].

parameter, for the mass symmetric reaction ${}^{197}_{79}Au + {}^{197}_{79}Au$ and the results obtained are compared with the theoretical participant fraction. We have derived the theoretical participant percentage distribution directly from the basic postulate of statistical me-

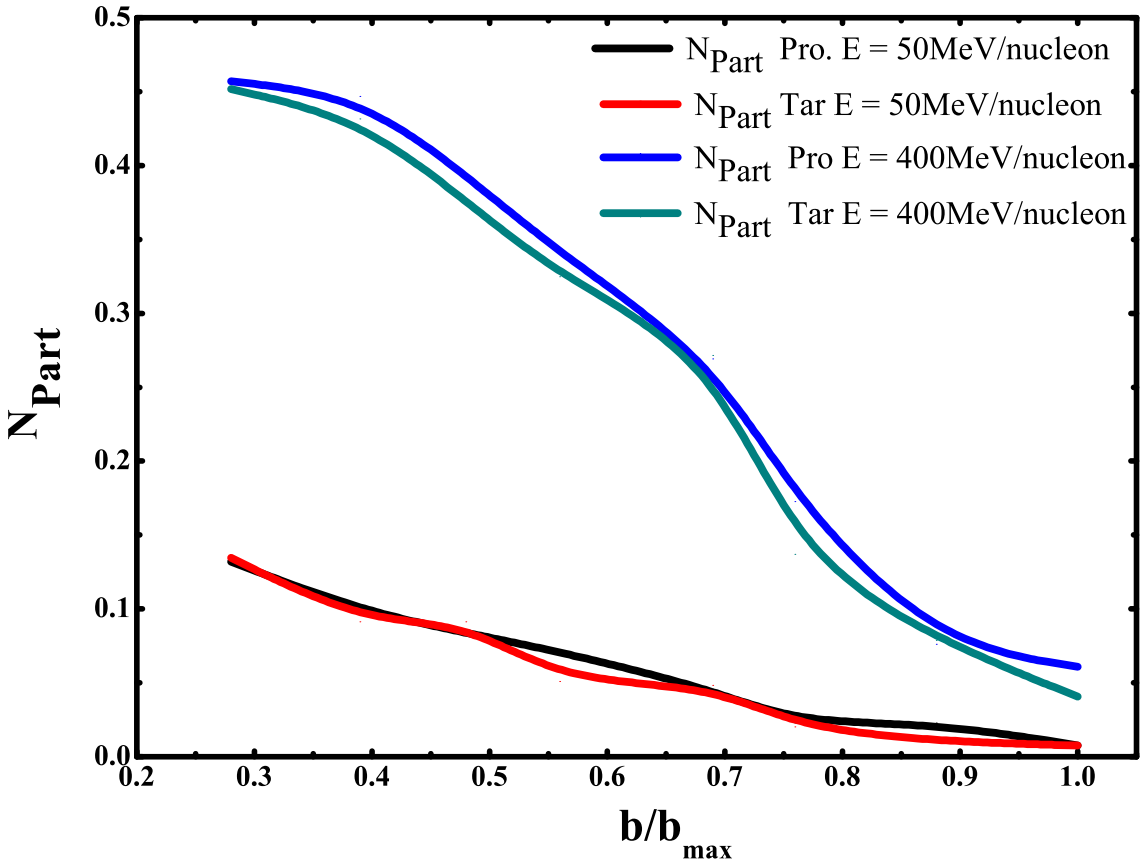


**Figure 3.9:** $N_{Part}$ as the function of impact parameter for the reaction ${}^{197}_{79}Au + {}^{197}_{79}Au$, at an incident energies E = 50 MeV/nucleon and E = 400 MeV/nucleon [20].

chanics using the principal of equal priori probability. The theoretical calculated values fractions of participant are mentioned in the Table 3.1, and theoretical fraction participant occurring an event is 100% and non-occurring is 0%. For impact parameter bin, $0 < \hat{b} \leq 0.28$ maximum number of collisions are observed and for bin $0.88 < \hat{b} \leq 1.0$ i.e., at peripheral collisions the target and projectile scarcely hits each other, so the theoretical participant percentage of collisions is minimized (say $\approx 0\%$). One can clearly see that at higher energies theoretical participant percentage perfectly matches with the IQMD model results. The trend of the curves at lower as well as higher incident energies are same. Only difference is that at lower energies their are small number of participating nucleons as compared to higher energies. The percentage change in the

$N_{part}$ with impact parameter bins from $0 < \hat{b} \leq 0.28$ to $0.88 < \hat{b} \leq 1.0$, in case of two incident energies is 69% and 50% respectively. The percentage change in $N_{Part}$ decreases as we move from the $BIN(I)$ to $BIN(VIII)$, because the participant matter decreases while moving from the central collisions to peripheral one.

In the Fig 3.9, author has displayed the $N_{Part}$ for both the target and projectile, as a function of impact parameter. Author has checked the individual contribution of projectile nucleons and target nucleons at lower incident energy (50 MeV/nucleon) or as well as at higher incident energy (400 MeV/nucleon). One can clearly see that at both the energies, contribution of projectile nucleons or target nucleons is same throughout the whole impact parameter range [20].

## 3.3 Fraction of participant and spectator matter in central collision

In Fig 3.10, author has tried to calculate the fraction of participant projectile (Part-Pro) nucleons, spectator projectile (Spect-Pro) nucleons, participant target (Part-tar) nucleons and target spectator (Spect-Tar) nucleons for the reaction ${}^{12}_{6}C + {}^{197}_{79}Au$ at an incident energy E = 10, 20, 30, 40, 50 and 100 MeV/nucleon. With increase in incident energy, spectator matter decreases and participant matter increases. This is because with increase in incident energy the excitation among the nucleons increases. It is further observed from the Fig 3.10 (a), with increase in the incident energy participant matter of projectile increases and maximum increase in the participant matter is seen and lies in between 20 fm/c to 100 fm/c, this is because nucleons suffer multiple collisions. Spectator matter of projectile decreases with increase in the incident energy as one can see clearly seen from the Fig 3.10 (b). Similar behavior is seen in the case of target participant matter Fig 3.10 (c) and target spectator matter in the Fig 3.10 (d). The fraction of participant matter is more for projectile which means the smaller projectile completely contribute in participant zone while reverse is true in the case of the target.

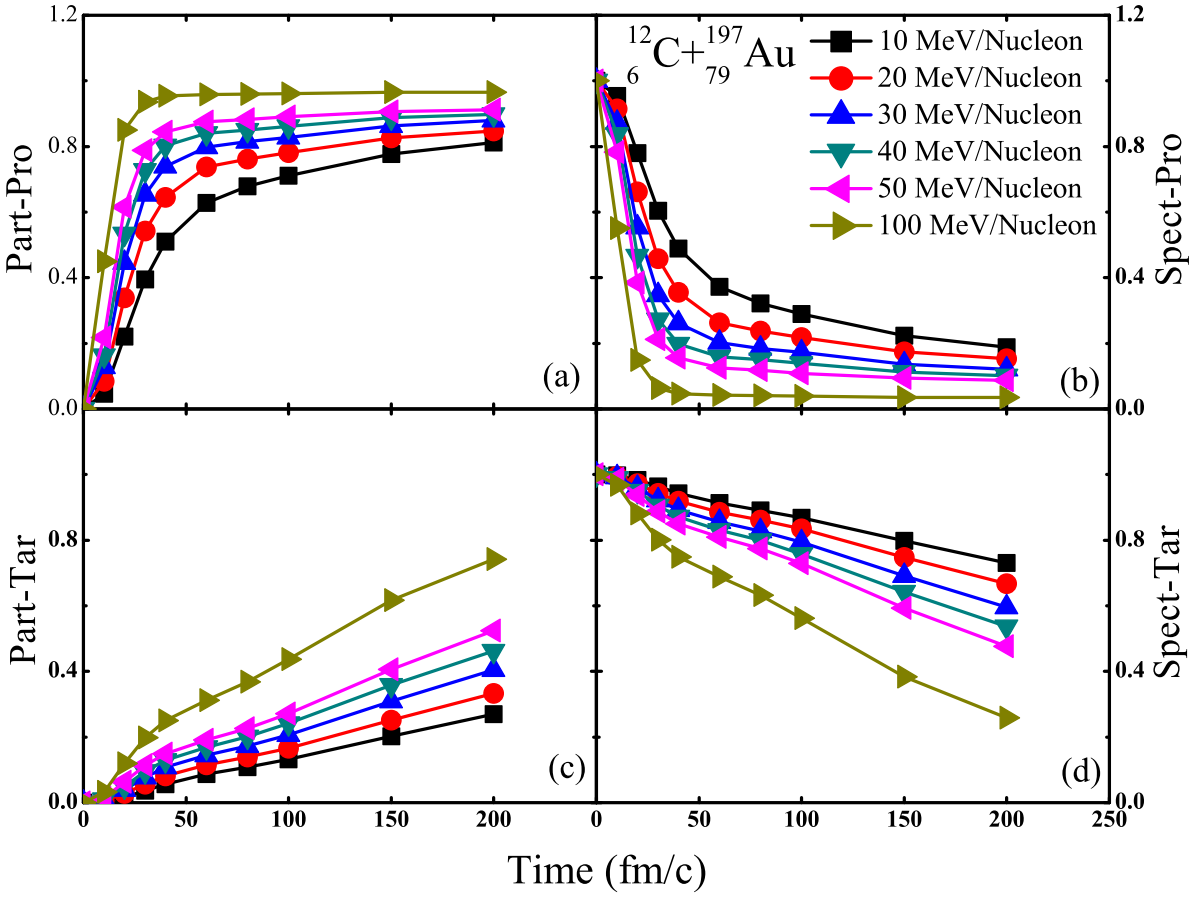


**Figure 3.10:** Participant and spectator matter for central collision for the asymmetric reaction at an incident energy in between E = 10 MeV/nucleon to 100 MeV/nucleon.

## 3.4 The coordinate space evolution for symmetric colliding nuclei for different impact parameter bins

In the Fig 3.11, the coordinate space of nucleons for symmetric reaction $^{197}_{79}Au + ^{197}_{79}Au$ has been displayed at different impact parameter bins as (shown in the Table 3.1) respectively. During the initial phase of the reaction, projectile and target are separated in the coordinate space and the whole matter is in the form of spectator only. At t = 0.1 fm/c, the projectile and target are properly initialized and approaching towards

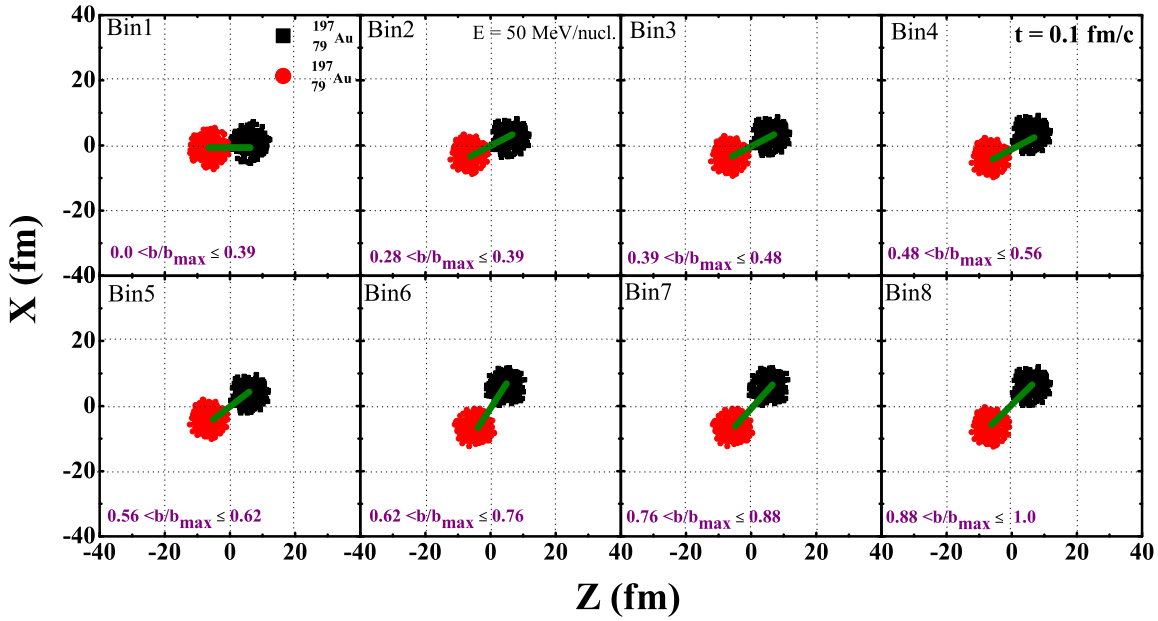


**Figure 3.11:** Coordinate space of a single event for the reactions $^{197}_{79}Au + ^{197}_{79}Au$, at incident energy of 50 MeV/nucleon for eight impact parameter bins [20].

each other. One can clearly see that the position coordinates of projectile and target nucleons are changing with the impact parameters, i.e., the line joining the centers of projectile and target changes their orientation with impact parameters. There is change in the angle w.r.t Z-axis, BIN(I) = $0^0$, BIN(II) = $26^0$, BIN(III) = $30^0$, BIN(IV) = $36^0$, BIN(V) = $42^0$, BIN(VII) = $51^0$ and BIN(VIII) = $55^0$. The change in the angle between projectile and target is not linear. As the impact parameter increases, the angle between the projectile and target increases. One can see the as one move from BIN(I) to BIN(VIII) participant matter decreases and spectator matter increases [20]. The participant nucleons give rise to a high density and volume known as the fireball. Nucleons outside the overlapping region of the two nuclei are unaffected by the collisions except for Coulomb-interactions and they retain their initial momentum and correlations.

### 3.4.1 The coordinate space evolution for mass symmetric nuclear reactions

Depending upon the impact parameter of the reaction, the type of nuclear reactions can be distinguished and dynamical properties of the reaction can be discussed by studying their phase space. The phase space of nucleons provide adequate acceptable illumination about the trajectories of the nucleons. The phase space shows the time evolution of the nucleons of the system. With the help of phase space, one can study the collision dynamics via individual nucleon-nucleon collisions and associated changes. In case of mass symmetric nuclear collisions, the contribution from the target and projectile are almost same. In the Fig 3.12, the phase space of nucleons for symmetric reaction ${}^{197}_{79}Au + {}^{197}_{79}Au$ has been displayed at t = 0.1, 10, 20, 40, 60, 80, 100 and 200 fm/c respectively.

At t = 0.1 fm/c, the projectile and target are properly initialized and lifted towards one another. After the overlapping stage, repulsion is generated among the projectile as well as target nucleons. As the reaction proceeds, the nucleons of both the projectile and target start interacting with each other. The projectile nucleons travel towards the target and because of strong density gradient at the surface of the projectile they experience strong transverse thrust. From the Fig 3.12, one can see that mass symmetric nuclear collisions leads to spherical distribution. This is due to equal number of nucleons present in the target and projectile. Subsequently, as the time approaches saturation point i.e., at t = 200fm/c, the emission of either fragments or nucleons takes place.

### 3.4.2 The coordinate space evolution for mass asymmetric nuclear collisions

In the Fig 3.13, phase space is displaying the time evolution for the mass asymmetric system ${}^{12}_{6}C + {}^{197}_{79}Au$, at E = 100 MeV/nucleon. We have simulated a single event of the reaction at a scaled impact parameter $\hat{b} = 0.6$. Evidently rotational effect has been picturised by the phase space evolution. From the Fig 3.13, one can see that highly mass asymmetric nuclear collisions leads to non-spherical distribution of nucleons in

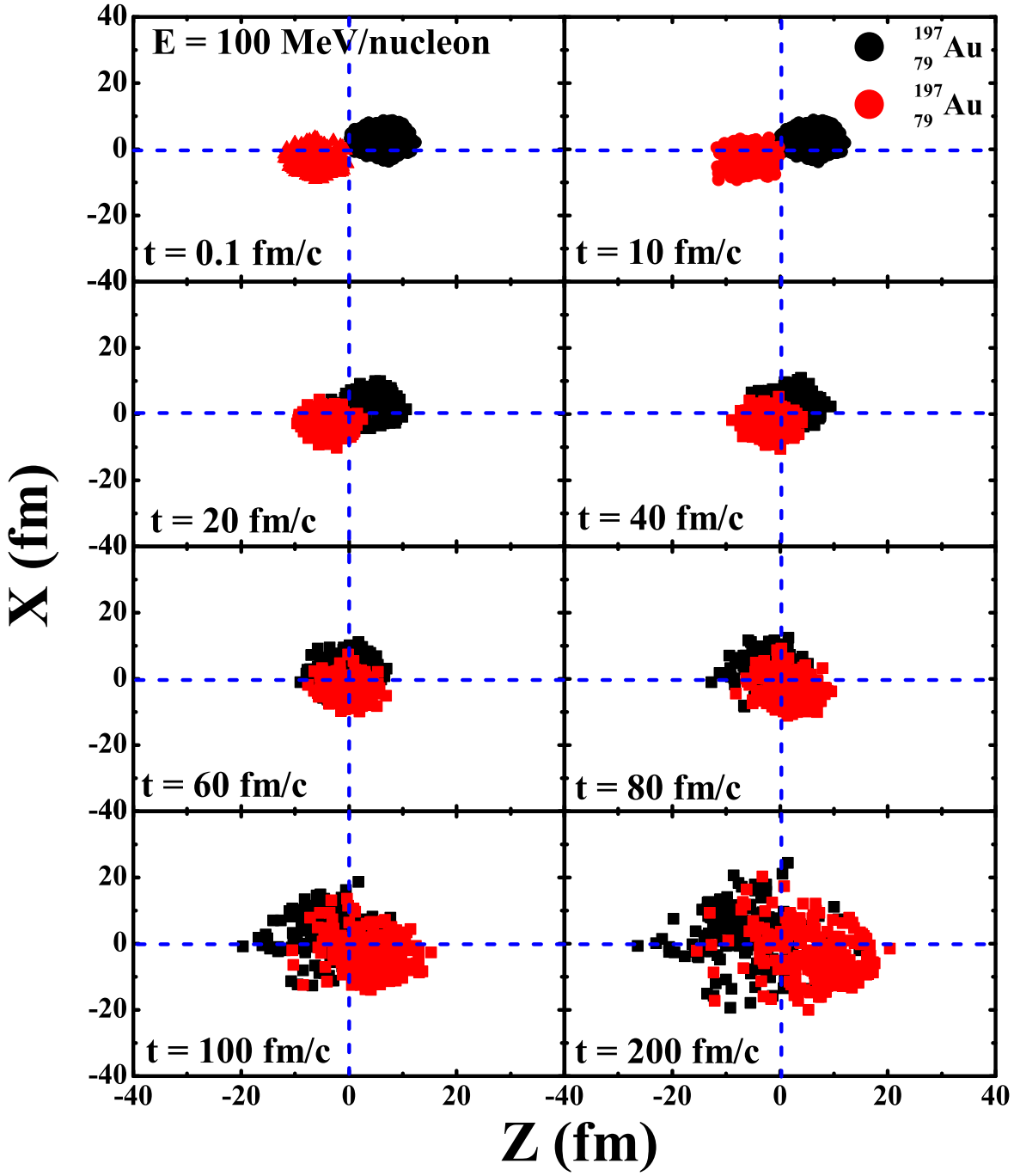


**Figure 3.12:** Coordinate space of a single event for the reactions $^{197}_{79}Au +^{197}_{79} Au$, at an incident energy of 100 MeV/nucleon and impact parameter $\hat{b} = 0.6$.

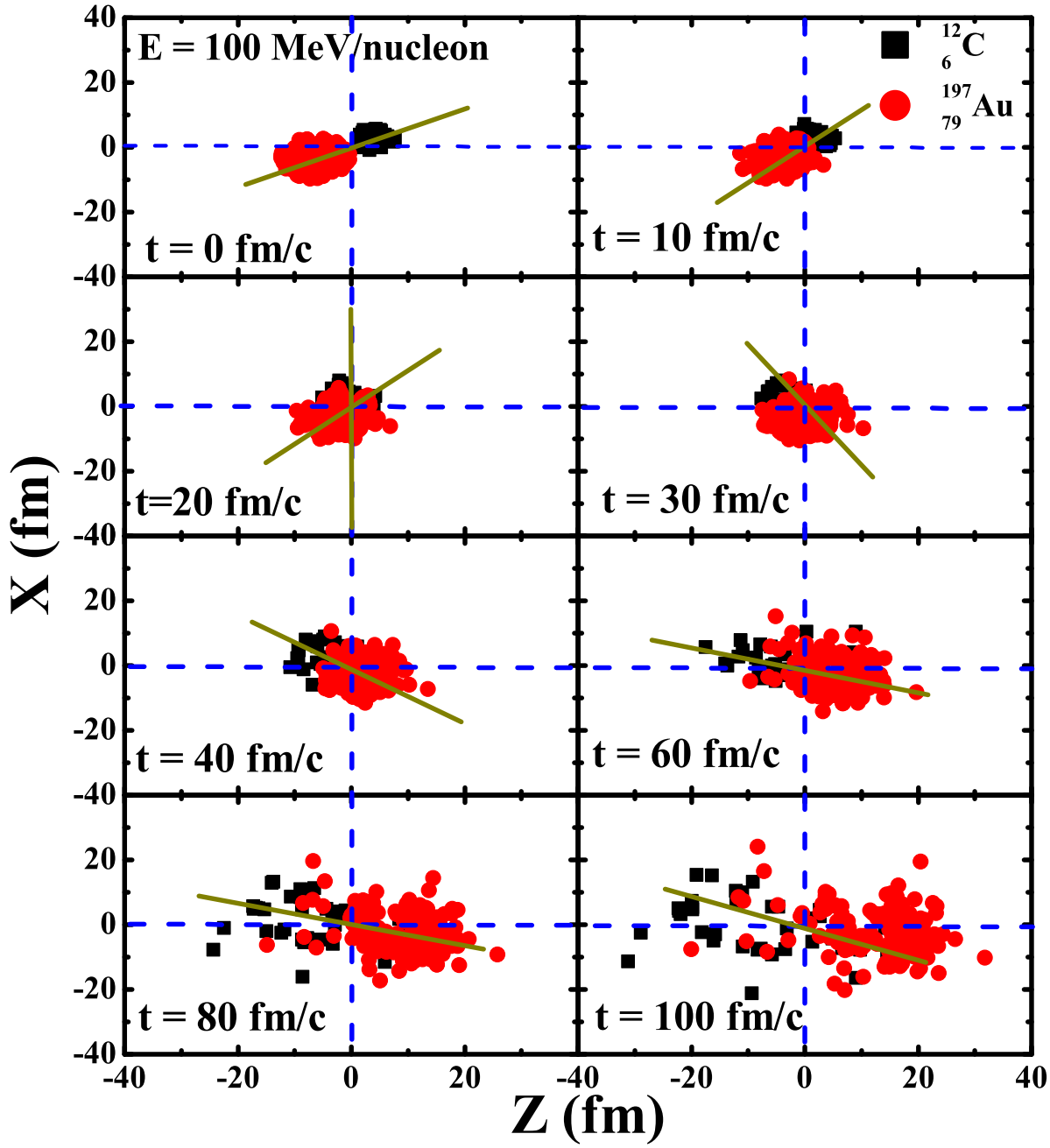


**Figure 3.13:** Coordinate space of a single event for the reactions $^{12}_{6}C +^{197}_{79} Au$ at incident energy of 100 MeV/nucleon and $\hat{b} = 0.6$.

the coordinate space. In the coordinate space of the reaction $^{12}_{6}C +^{197}_{79} Au$ the projectile $^{12}_{6}C$ tends to rotate about the target $^{197}_{79}Au$. Therefore, contribution of participant and

spectator matter will also be different.

## 3.5 Conclusions

In the present chapter we have analyzed the fraction of participant and spectator nucleons for the central collision. Our detailed study concludes that, initially at t = 20 fm/c participant matter is less and spectator matter is more. On the other hand for higher time step i.e., at t = 200 fm/c multiple collisions ceases. With decrease in size of the projectile, the overall interaction volume becomes small, so the rate of nucleon-nucleon collision decreases, thus leading to formation of lesser participant matter and greater amount of spectator matter. The number of binary collisions increases with an increase in the incident energy and decreases with the increase in impact parameter. At lower energies as well as at higher energies, the contribution of projectile nucleons and target nucleons that participate in collisions are almost same throughout the whole impact parameter range. Mass symmetric nuclear reactions lead to a spherical distribution, while highly mass asymmetric collisions lead to a non-spherical distribution in the co-ordinate phase.

# Chapter 4

# Optimization of nuclear stopping observables and memory loss

## 4.1 Introduction

The mainly observed phenomena in the intermediate energy region are collective flow [88, 257, 258], nuclear stopping [19–21, 124, 259], fragmentation [260, 261] and isospin effects [262–265] etc. The study is significant due to the presence of both nuclear mean field and nucleon-nucleon collisions. In this chapter, author has discussed the nuclear stopping in detail while, the collective flow is studied in the next chapter. Nuclear reactions are requisite to demonstrate the relative motion and stopping of fragments in HIC's from lower to higher incident energies. Information about the EOS of nuclear matter, in-medium nucleon-nucleon (NN) cross section, and the level of equilibration reached in nuclear reactions [266–268] can be extracted from nuclear stopping. Bauer and Bertsch [96, 269] in 1988 investigated that nuclear stopping in heavy-ion collisions is determined by the mean field and in-medium nucleon-nucleon(NN) cross-sections. When the target and projectile collide with each other, the participating nucleons transfer a larger fraction of their kinetic energy into other degrees of freedom. The initial energy is redistributed over the other new degrees of freedom and depends on the strength of stopping. At sufficiently high energy and density the nucleons loses their correlations. At low incident energies due lack of nucleon-nucleon collisions, interactions among the nucleons remain intact. On increasing the incident energy, the correlations between the nucleons break down and hence nucleons lose their initial

correlations or memories [13]. In heavy ion collisions the nuclear stopping has been studied by rapidity constraints or by asymmetry of nucleonic distribution. In the next section, author will discuss in detail various stopping parameters.

## 4.2 Overview of various stopping observables

In the literature, many observable have been suggested to study the phenomenon of nuclear stopping [19]. The degree of nuclear stopping obsessed by rapidity distribution [97, 98, 270] is given by the relation:

$$Y(i) = \frac{1}{2} ln \left[ \frac{E(i) + p_z(i)c}{E(i) - p_z(i)c} \right] \tag{4.1}$$

where $E(i)$ is the total energy and $p_z(i)$ is the longitudinal momentum of the $i^{th}$ particle. For the present study nuclear stopping observables have been developed, one of them is energy-based isotropy ratio and another one is momentum based. The detailed study on these parameters have been discussed in ref. [18, 19, 116] in detail.

One observable is studied on the energy-based isotropy ratio:

$$R_E = \left[ \frac{1}{2} \frac{(\sum_i |E_\perp(i)|)}{(\sum_i |E_\parallel(i)|)} \right] \tag{4.2}$$

where $E_\perp(i)$ and $E_\parallel(i)$ are transverse and longitudinal kinetic energy for the $i^{th}$ particle respectively. Another definition of stopping observable on momentum base is $R_P$ [116],

$$R_P = \left[ \frac{2}{\pi} \frac{(\sum_i |p_\perp(i)|)}{(\sum_i |p_\parallel(i)|)} \right] \tag{4.3}$$

where summation runs over all the nucleons.

Another way of looking into equilibrium can be accomplished through rapidity distributions ratio between width of transverse to longitudinal variance of rapidity distribution i.e., $< varxz >$. Mathematically, it is represented as

$$varxz = \frac{\sigma^2(x)}{\sigma^2(z)} \tag{4.4}$$

This formalization of nuclear stopping has been opted by INDRA [18], ALADIN and FOPI [14, 109, 271] collaborations. The value of $< varxz > = 1$, $< 1$ and $> 1$ indicates complete stopping, partial transparency and super stopping respectively [120]. Single

Gaussian shape have been observed of the rapidity distribution for complete stopping. Narrower Gaussian distribution intimate better nuclear stopping in comparison to broader Gaussian distribution. These observables mentioned in the above equations have been used in various studies and have been reported in literature [18, 116].

## 4.3 Results and discussion

The reactions ${}^{197}_{79}Au + {}^{197}_{79}Au$, ${}^{181}_{73}Ta + {}^{197}_{79}Au$, ${}^{129}_{54}Xe + {}^{129}_{50}Sn$, ${}^{58}_{28}Ni + {}^{58}_{28}Ni$, ${}^{36}_{18}Ar + {}^{58}_{28}Ni$ and ${}^{36}_{18}Ar + {}^{36}_{18}KCl$ at $\hat{b} = 0.0$ are simulated in the present analysis [19]. Incident energy varies between 10 MeV/nucleon and 1000 MeV/nucleon.

## 4.4 Time evolution of stopping observable $R_E$

In Fig 4.1, time evolution of the stopping observable $R_E$ has been displayed for the reactions ${}^{197}_{79}Au + {}^{197}_{79}Au$ and ${}^{58}_{28}Ni + {}^{58}_{28}Ni$ at two incident energies. At lower incident energies reaction dynamics are governed by the mean field and binary collisions among nucleons are suppressed because of Pauli blocking. Hence, mean field takes longer time to thermalize the colliding nuclear matter. At higher incident energies the value of stopping observable start decreasing indicating the partial transparency. From the Fig 4.1, one can concludes that in case of the heavier system the value of stopping observable at both the energies E = 50 MeV/nucleon and 400 MeV/nucleon is more as compared to the lighter system mass (shown by red arrows), which means that heavier system takes longer time to equilibrate as compared to lighter one. Lighter system (${}^{58}_{28}Ni + {}^{58}_{28}Ni$) equilibrate at t = 70 fm/c and t = 90 fm/c corresponding to the incident energies E = 50 MeV/nucleon and 400 MeV/nucleon, while heavier system equilibrate at t = 200 fm/c and t = 225 fm/c corresponding to the incident energies taken in case of lighter systems.

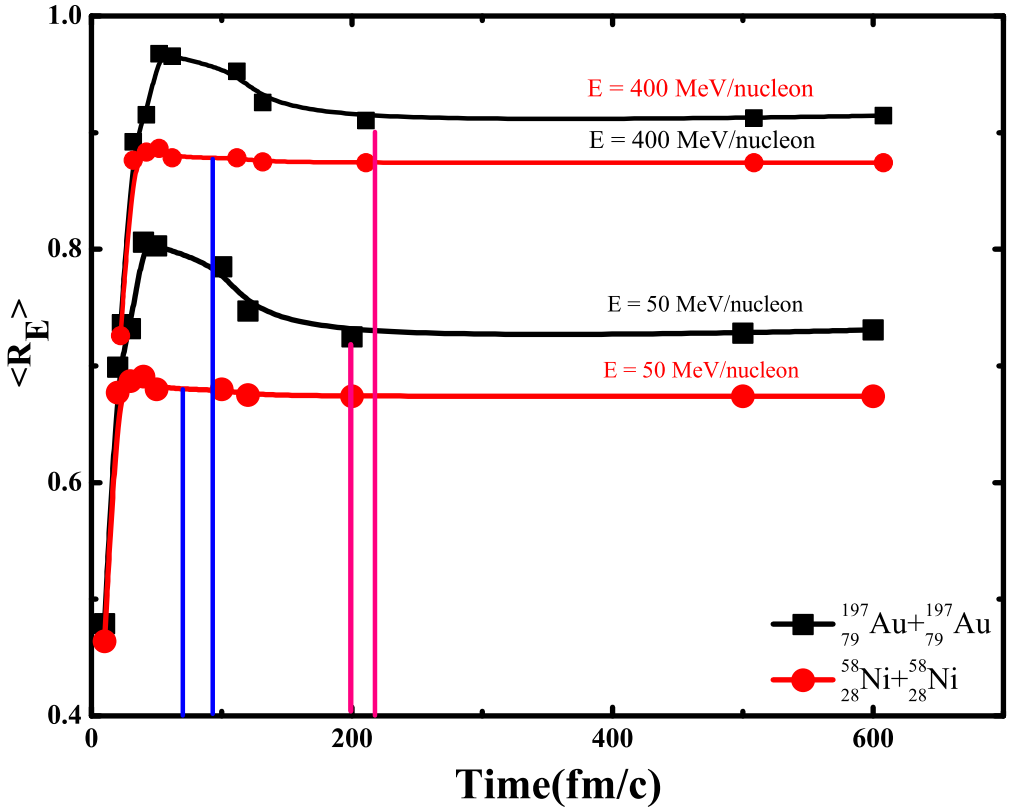


**Figure 4.1:** Time evolution of nuclear stopping observable $< R_E >$ for the reaction ${}^{197}_{79}Au + {}^{197}_{79}Au$ and ${}^{58}_{28}Ni + {}^{58}_{28}Ni$ at incident energy 50 MeV/nucleon and 400 MeV/nucleon.

## 4.5 Energy dependence of stopping observables

At very low energy the phenomenon of collision between nucleus-nucleus takes place. As the energy increases role of mean field start decreasing and collisions among nucleons starts taking place. One can clearly see a dip around Fermi energy, but as the incident energy further increases, the value of stopping increases for all the observable as shown in the Fig 4.2. The maxima in nuclear stopping value takes place around 500 MeV/nucleons. Further with increase in incident energy nuclear stopping value decreases. The decrease in the value of stopping observable is observed because nucleon-nucleon cross-section decreases with energy. One can conclude that nucleons experience more transparency.

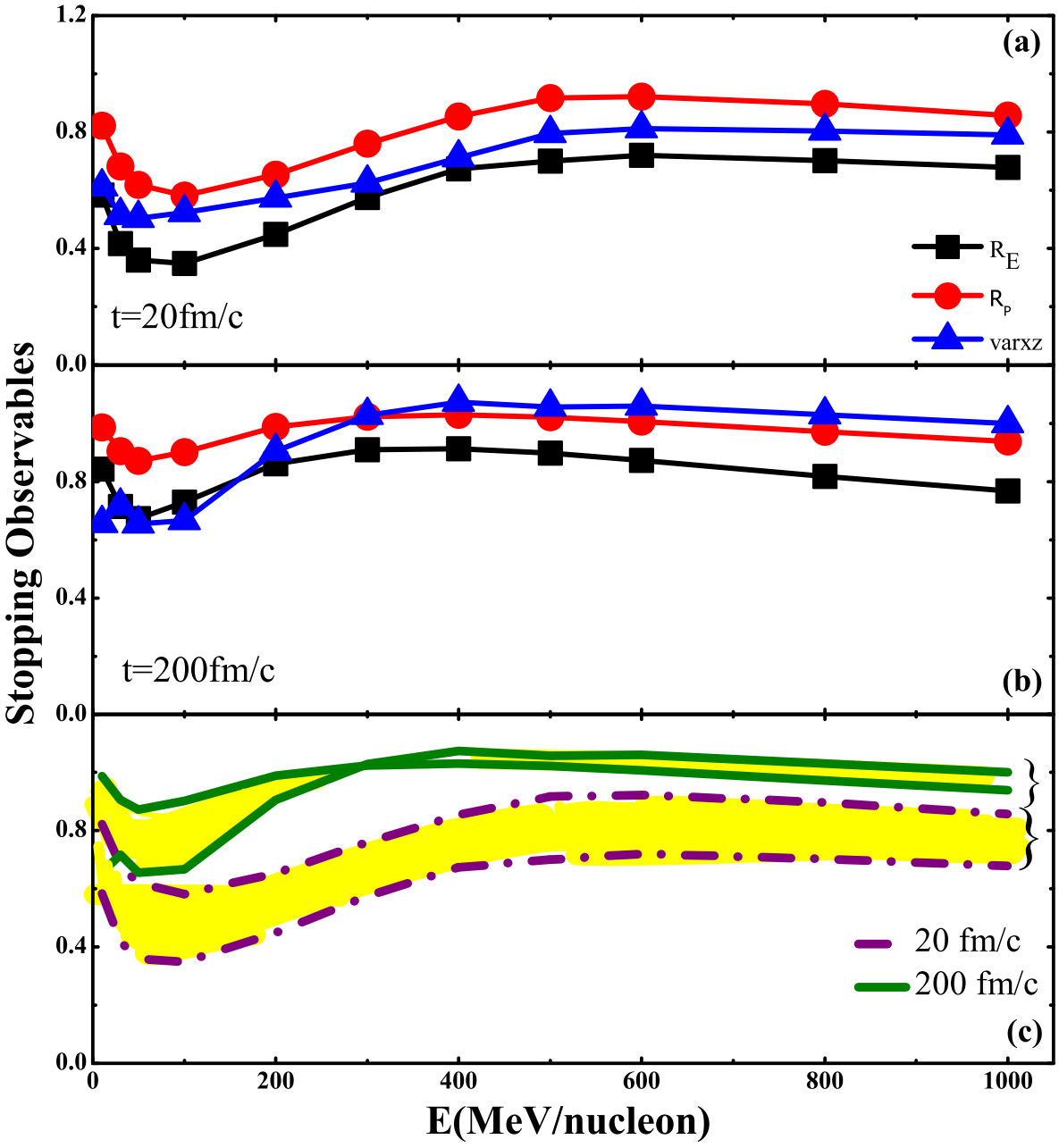


**Figure 4.2:** Incident energy dependence of nuclear stopping observables at t = 20 fm/c and t = 200 fm/c for the reaction $^{197}_{79}Au +^{197}_{79} Au$.

In Fig 4.2, the variation of three different stopping observable ($< R_E >$, $< R_P >$ and $< varxz >$) has been displayed at initial time step i.e., t = 20 fm/c as well as at higher time step t = 200 fm/c. From the Fig 4.2 (a) it is clear that, at initial time step (t

= 20 fm/c) the value of nuclear stopping is less at all energies because the collisions among the nucleons are still taking place i.e., the system is still in volatile stage. In the Fig 4.2 (b), stopping observable at saturation time step (t = 200 fm/c) has been displayed. One can see the similar trend at both the time steps. The difference in three nuclear stopping observable values is not distinguishable as observed in Fig 4.2 (a and b). In the Fig 4.2 (c), the difference in stopping values for initial time step and saturation time step has been displayed, author has merged two graphs just for the sake of comparison. The variation of stopping observable at lower time interval is more sharp as compared to variation at 200 fm/c. In case of initial time step (t = 200 fm/c) the variation in the value of stopping observable spreads over a wide range at lower energies but at higher time step (200 fm/c) the variation is restricted to a very small range as collisions ceases at saturation time. This shows that colliding systems takes time to achieve complete equilibrium. Moreover, dynamics at lower energies are governed by fragment phase space, while dynamics at higher energies are dominated by stopping due to nucleon phase space [272]. Nuclear stopping observable $< varxz >$ in the present study is found to exhibit more variation in stopping value as compared to other observables, which can be clearly seen in Fig 4.2 (c).

## 4.6 Optimization of nuclear stopping due to collisions

It would be interesting to see how longitudinal and transverse momentum is acquired by nucleons under different collision constraints. Nucleons lose a part of their energy in the collision and drifts in the transverse direction. In general, the collision rate depends on the density of participant zone, which is maximum in central collisions. The collision rate first increases with incident energy and then decreases. This is due to the fact that nucleon-nucleon cross section is energy as well as isospin dependent [124]. Also, the collision rate increases with mass of colliding partners. The amount of energy lost by incident nucleons is describe by the nuclear stopping. Now, it would be of great interest to ruminate that how many collisions are sufficient to stop a nucleon. Earlier

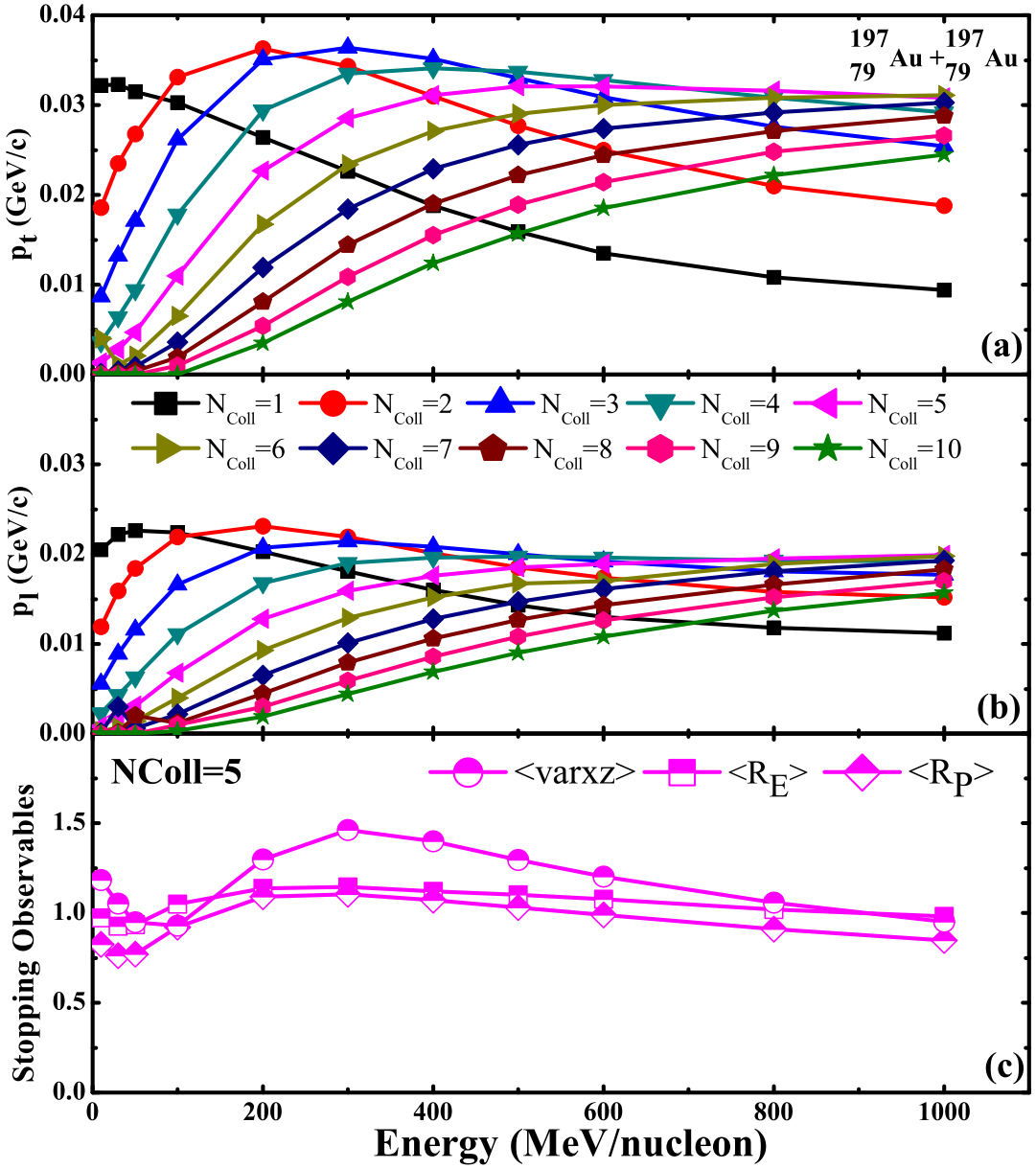


**Figure 4.3:** (a) The transverse and (b) longitudinal momentum as a function of incident energy for the reaction $^{197}_{79}Au +^{197}_{79} Au$ at different collision constraints. (c) Incident energy dependence of nuclear stopping observables ( $< R_E >$, $< R_P >$ and $< varxz >$) for the reaction $^{197}_{79}Au +^{197}_{79} Au$ at t = 200 fm/c.

studied have been carried out by using QMD model suggest that the nucleons suffering at least ten collisions are most thermalize and hence such nucleons are close to complete equilibrium [273]. After suffering collisions, the nucleons are drifted in transverse

direction. In Fig 4.3 (a), transverse momentum of nucleons and in Fig 4.3 (b), longitudinal momentum of nucleons as the function of incident energy have been displayed. The nuclear stopping is greatly influenced by the transverse component of momentum associated with nucleons. One can see from Fig 4.3 (a) that on an average if a nucleon suffer five collisions, its transverse momentum gets saturated with incident energy. It has been observed that nucleon on average suffering more than five collisions get drifted randomly such that their net transverse momentum decreases. It gives us an idea to include only those nucleons which have suffered five collisions for the estimation of nuclear stopping. In the further analysis we have taken those nucleons into consideration which have suffered at least five collisions. The loss of energy associated with incident nucleons takes place due to collisions among them. Therefore, one has to understand weather the loss of energy increases with increase in number of collisions suffered by a nucleon in Fig 4.3 (c), we have shown the variation of different stopping observable $< R_E >$, $< R_P >$ and $< varxz >$ with energy for collision constraint $N_{coll} = 5$. The value of stopping observable varies with energy and is maximum at the lower incident energy where the nucleon-nucleon collisions are negligible due to Pauli blocking. One can see that at certain energies, the value of stopping is greater than unity implies the preponderance [123, 274]. Stopping observable $< varxz >$, shows maximum sensitivity out of three observables. Therefore, one can conclude that to study nuclear stopping $< varxz >$ is the most important observable.

## 4.7 Stopping due to fragment and nucleon phase space

The calculation of nuclear stopping is influenced by the method used for analysis and depends on some observables. As we know that at lower incident energies most of the nucleons are in the bound state. The probability of drifting of individual nucleons due to nucleon-nucleon collisions is very small due to Pauli blocking. Therefore, calculations for stopping observable based on fragment phase space is more accurate, but as the incident energy increases, the rate of nucleon-nucleon collisions increases

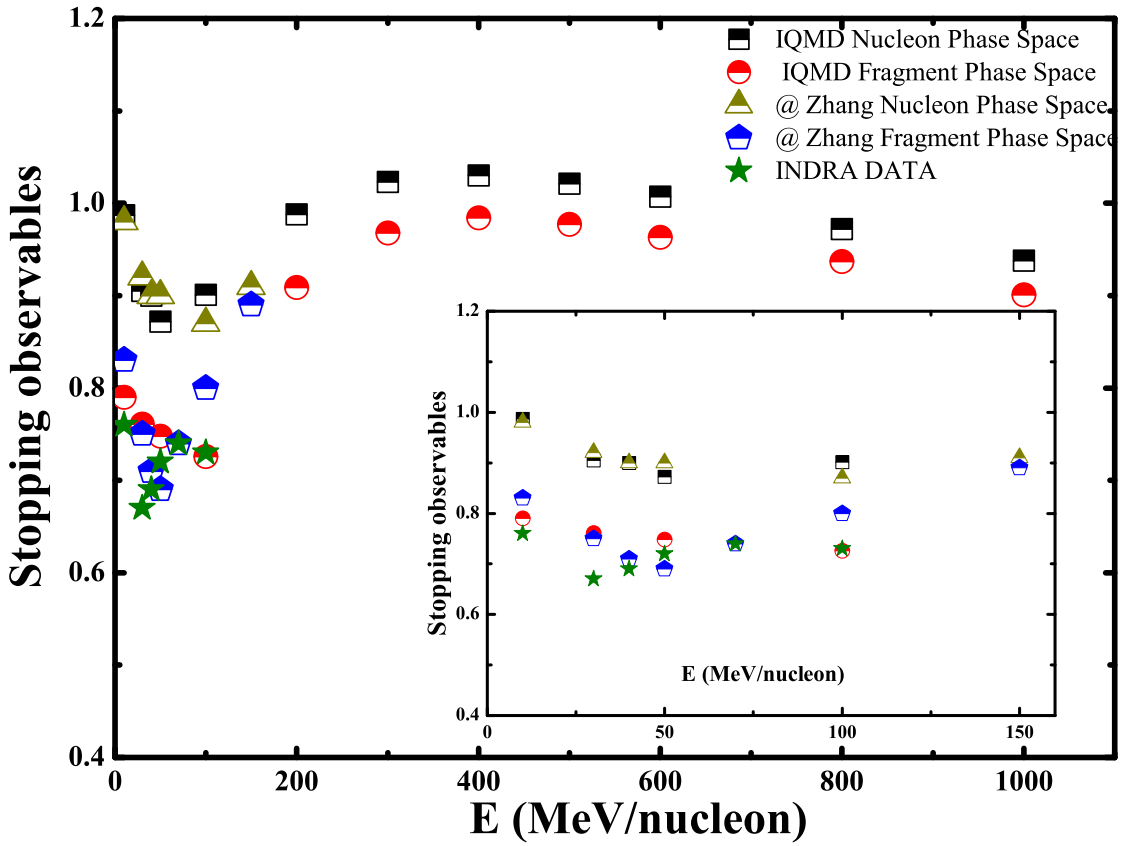


**Figure 4.4:** Incident energy dependence of nuclear stopping parameters for nucleon phase space and fragment phase space [272].

and hence more nucleons suffers drift from their original path. Therefore, nuclear stopping observable based on nucleon phase space is more appropriate. In Fig 4.4, author has shown the comparison between experimental values and predictions on the basis of IQMD calculations, the nucleon phase space and fragment phase space for central collision. At lower incident energies experimental results are comparable with theoretically calculated results of IQMD. At higher incident energies, one can clearly see the different tend for both nucleon phase space and fragment phase space. Inset of Fig 4.4, clearly depicts the comparison between experimental values and predictions of IQMD calculation at lower incident energies. Author has compared the results with INDRA [18] data and with Zhang et al. [272] results.

## 4.8 Nuclear Stopping due to neutrons and protons

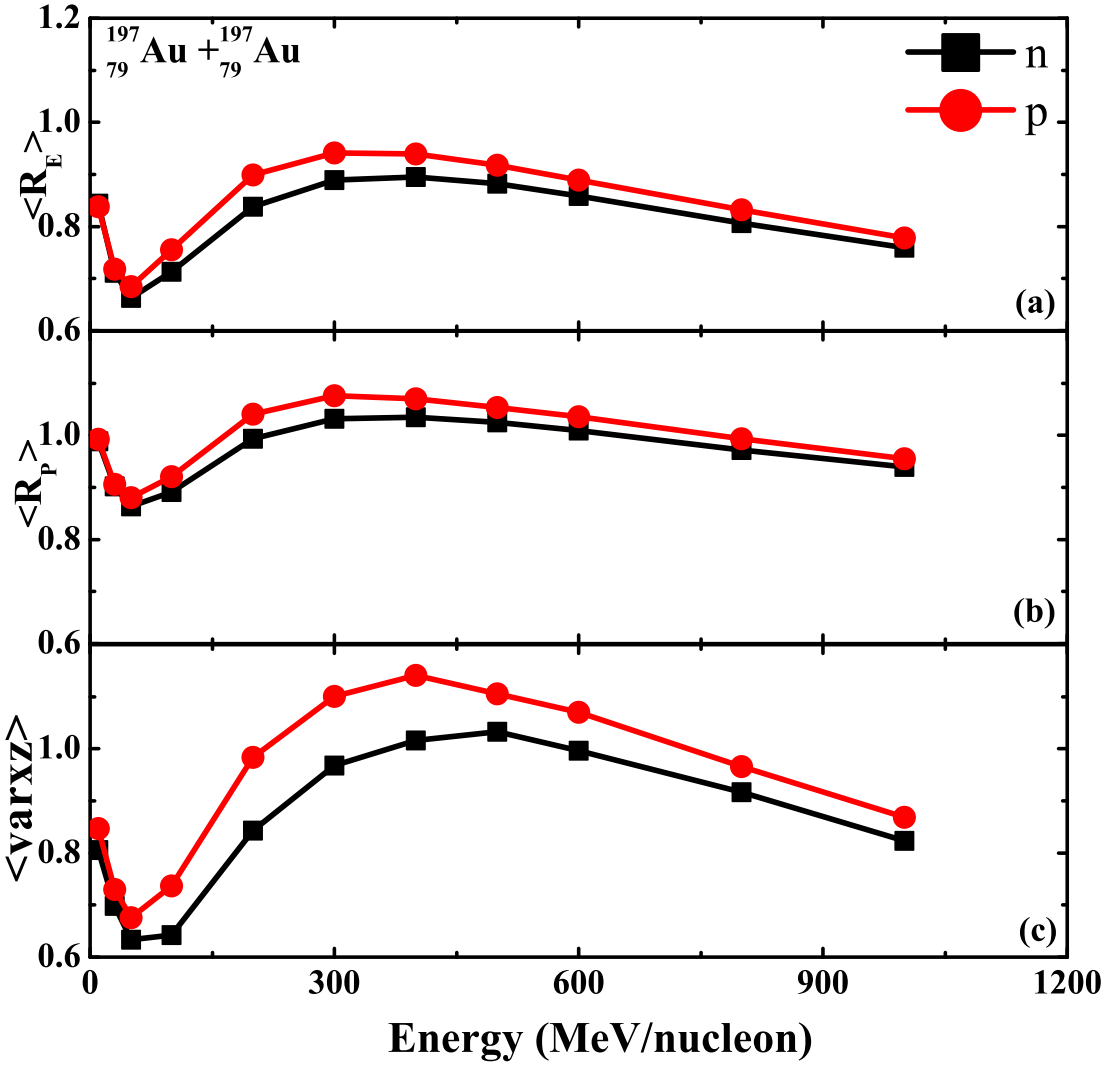


**Figure 4.5:** The incident energy dependence of nuclear stopping observable ($< R_E >$, $< R_P >$ and $< varzx >$) for protons and neutrons for the reaction $^{197}_{79}Au +^{197}_{79} Au$ at t = 200 fm/c.

It would be interesting to see the influence of isotopic contents on nuclear stopping reproduced by different observable from Fig 4.5. Due to the presence of isospin dependent nucleon-nucleon potential and cross section, the stopping due to protons and neutrons differ. Coulomb interaction potential and symmetry energy plays different roles at different energy ranges [123]. In Fig 4.5, author has presented the nuclear

stopping associated with protons and neutrons as a function of incident energy for stopping observable $< R_E >$, $< R_P >$ and $< varxz >$. Here attempts have been made to investigate the role of isospin content in heavy ion collisions by calculating the value of stopping observable for protons and neutrons for the reaction ${}^{197}_{79}Au + {}^{197}_{79}Au$. The contribution in stopping of protons and neutrons have been extracted from nn, pp and np collisions. The np collisions are not excluded from the value of stopping observable. One can see that the protons have larger value of $< R_E >$, $< R_P >$ and $< varxz >$ as compared to neutrons. The larger value of stopping observable for protons is due to the repulsion produced by Coulomb and symmetry potentials. The protons being a charged particles are stopped by the target protons strongly than the neutral particles neutrons due to additional repulsive interactions. The difference is more in case of $< varxz >$ as compared to other stopping observables $< R_E >$ and $< R_P >$ for protons rather than neutrons. The observable based on rapidity distribution is found to be more sensitive to isospin content of the colliding nuclei while studying nuclear stopping. Influence of isospin contents on nuclear stopping can be studied using neutron rich nuclei. In other words, one can say that stopping associated with protons and neutrons can be worn as an inquest for symmetry energy at higher incident energies. From the above discussion it is concluded that $< varxz >$ is most sensitive for studying the nuclear stopping.

### 4.8.1 Isospin mixing

In the step ahead, we have tried to check the sensitivity of $< varxz >$ in the Fig 4.6 and displayed as a function of incident energy for the pair of isotopes (${}^{197}_{79}Au + {}^{197}_{79}Au$ and ${}^{179}_{79}Au + {}^{179}_{79}Au$) and isobars (${}^{124}_{47}Ag + {}^{124}_{47}Ag$ and ${}^{124}_{50}Sn + {}^{124}_{50}Sn$). Author has chosen stable isotope and isobar pairs in the present investigation. In the upper panel, the proton number is kept fixed and neutron number is varied. In the lower panel, author has varied the proton number as well as neutron number. Nuclear stopping is found to be dependent strongly on the isospin content of colliding nuclei. There is large difference in the value of $< varxz >$, which appears in the upper panel. Protons being charged particles repels each other and results in more drifting of curve in the

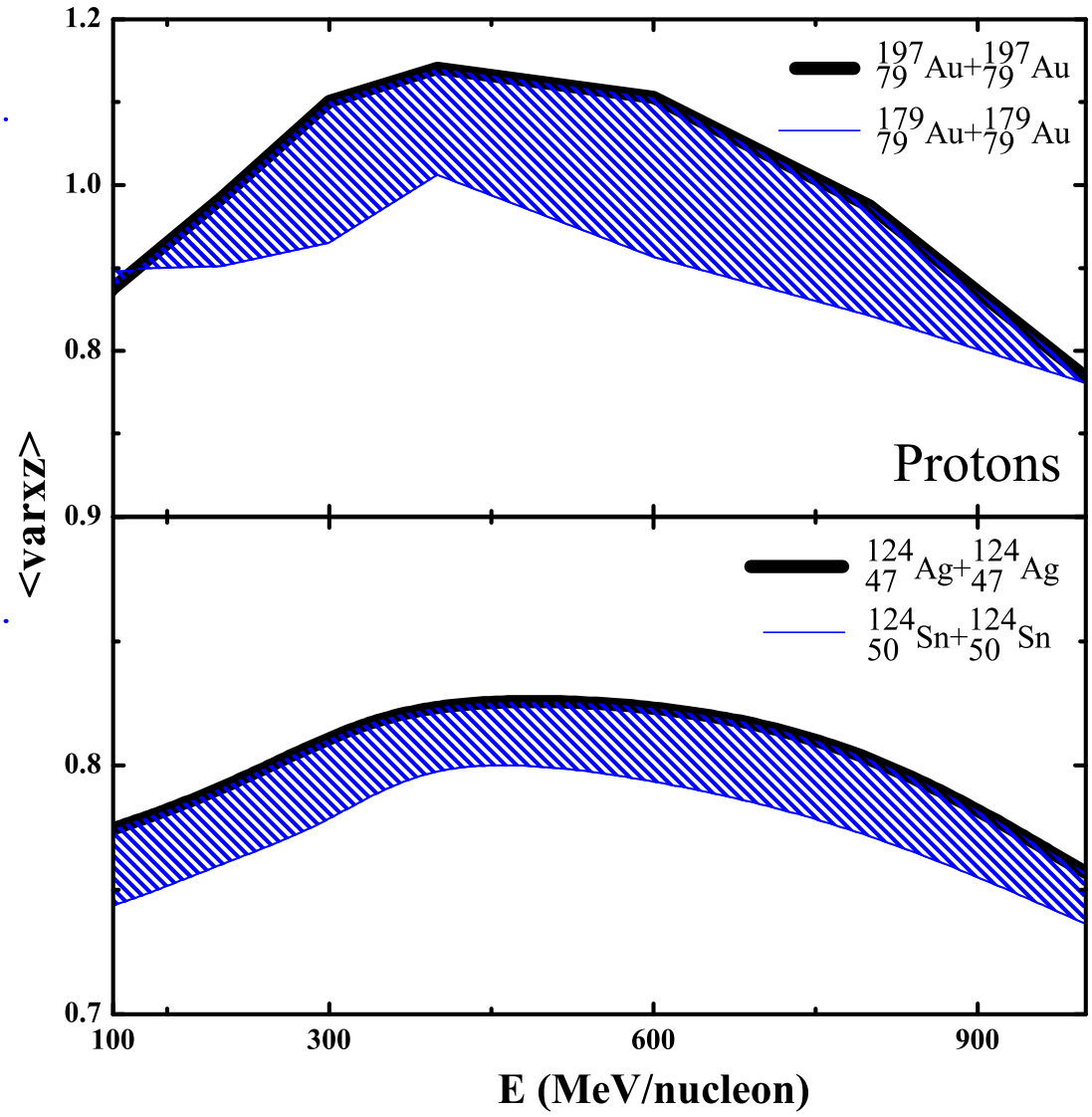


**Figure 4.6:** Incident energy dependence of $< varxz >$ for the reactions $^{197}_{79}Au +^{197}_{79} Au$, $^{179}_{79}Au +^{179}_{79} Au$, $^{124}_{47}Ag +^{124}_{47} Ag$ and $^{124}_{50}Sn +^{124}_{50} Sn$ for protons.

transverse direction, which is clearly seen in the upper panel. In order to extract the complete information, the ratio of proton to neutron have been varied between 1.4 to 1.6 in case of isobars and 1.2 to 1.5 in case of isotopes. The shaded region exhibits the range of nuclear stopping value due to other combination of isotopes and isobars on nuclear stopping.

In the Fig 4.7 (a and b), we have displayed the rapidity distribution for the pair of iso-

bars ($^{124}_{47}Ag+^{124}_{47}Ag$ and $^{124}_{50}Sn+^{124}_{50}Sn$) and isotopes ($^{197}_{79}Au+^{197}_{79}Au$ and $^{179}_{79}Au+^{179}_{79}Au$). In the case of isobars, one can see two broader Gaussian shape peaks, but in case of isotopes single narrow Gaussian distribution is observed. The relative difference between the peaks of isobars and isotopes is 25% and 5.6% respectively. In the middle panel $R_{iso}$, is the ratio of rapidity distribution of two isobars ($^{124}_{47}Ag+^{124}_{47}Ag$ and $^{124}_{50}Sn+^{124}_{50}Sn$) and two isotopes ($^{197}_{79}Au+^{197}_{79}Au$ and $^{179}_{79}Au+^{179}_{79}Au$) and is defined by the following formulas [19]:

$$R_{iso} = \left[\frac{(dN/dy)_{^{124}_{47}Ag+^{124}_{47}Ag}}{(dN/dy)_{^{124}_{50}Sn+^{124}_{50}Sn}}\right] \tag{4.5}$$

and

$$R_{iso} = \left[\frac{(dN/dy)_{^{197}_{79}Au+^{197}_{79}Au}}{(dN/dy)_{^{179}_{79}Au+^{179}_{79}Au}}\right] \tag{4.6}$$

Fig 4.7 (c and d), shows the behavior of $R_{iso}$, in both the cases of isotopes and isobars. It is clear that $R_{iso}$ shows almost similar behavior in both the cases. However, the values of $R_{iso}$ in case of isotopes is slightly higher than values of isobars. These values are closer to unity. In case when full mixing is achieved in the collisions, the variation of $R_{iso}$ as a function of rapidity is flat at intermediate energies. Our interpretation are further strengthened when we display $R_{mix}$ as a function of rapidity for the pair of isotopes and isobars. The ratio $R_{mix}$ is defined by the formulas [19]:

$$\begin{aligned} R_{mix} = &\left[\frac{2\times(dN/dy)_{mix}}{(dN/dy)_{^{124}_{47}Ag+^{124}_{47}Ag}-(dN/dy)_{^{124}_{50}Sn+^{124}_{50}Sn}}\right] \\ &-\left[\frac{(dN/dy)_{^{124}_{47}Ag+^{124}_{47}Ag}}{(dN/dy)_{^{124}_{47}Ag+^{124}_{47}Ag}-(dN/dy)_{^{124}_{50}Sn+^{124}_{50}Sn}}\right] \\ &-\left[\frac{(dN/dy)_{^{124}_{50}Sn+^{124}_{50}Sn}}{(dN/dy)_{^{124}_{47}Ag+^{124}_{47}Ag}-(dN/dy)_{^{124}_{50}Sn+^{124}_{50}Sn}}\right] \end{aligned} \tag{4.7}$$

$$R_{mix} = \left[\frac{2 \times (dN/dy)_{mix}}{(dN/dy)_{^{197}_{79}Au+^{197}_{79}Au} - (dN/dy)_{^{179}_{79}Au+^{179}_{79}Au}}\right] - \left[\frac{(dN/dy)_{^{197}_{79}Au+^{197}_{79}Au}}{(dN/dy)_{^{197}_{79}Au+^{197}_{79}Au} - (dN/dy)_{^{179}_{79}Au+^{179}_{79}Au}}\right] - \left[\frac{(dN/dy)_{^{179}_{79}Au+^{179}_{79}Au}}{(dN/dy)_{^{197}_{79}Au+^{197}_{79}Au} - (dN/dy)_{^{179}_{79}Au+^{179}_{79}Au}}\right] \tag{4.8}$$

where, mix can be either $^{124}_{47}Ag +^{124}_{47} Ag$ or $^{124}_{50}Sn +^{124}_{50} Sn$ in case of isobars and $^{197}_{79}Au +^{197}_{79} Au$ or $^{179}_{79}Au +^{179}_{79} Au$ case of isotopes. The ratio $R_{mix}$ in Fig 4.7 (e and f), shows almost similar behavior as a function of rapidity as shown by $R_{iso}$. Due to the highest sensitivity shown by $< varxz >$ among the stopping observable, we have concentrated our study on $< varxz >$, observable which can be extracted from the rapidity distribution.

## 4.9 Comparison with experimental data

It would be interesting to see how accurately one can reproduce the experimental data of stopping observable, using $< varxz >$. In Fig 4.8, a complete systematic study of nuclear stopping has been carried out for mass symmetric and nearly mass symmetric reactions. Reactions are chosen in accordance with reported theoretical results and the available experimental data [111]. The total mass of the colliding systems is varied from 72 to 394, while the incident energy is varied from 10 MeV/nucleon to 200 MeV/nucleon. In this whole study, we have extracted the physical results when the system is in the freeze-out stage i.e., at 200 fm/c. When incident energy is varied from 10 MeV/nucleon to 40 MeV/nucleon, a sharp decrease in the stopping value is observed. Above the Fermi energy, reaction dynamics are dominated by nucleon-nucleon (NN) collisions. At lower incident energies mean field takes longer time to thermalize the nuclear matter. It is clear from the Fig 4.8, that as one move from lighter system to the heavier system, the stopping increases irrespective of the incident energy. Thus nucleons of the heavier systems are easily stopped as compared to lighter systems. The nuclear stopping increases with increase in system mass, as nuclear stopping is related

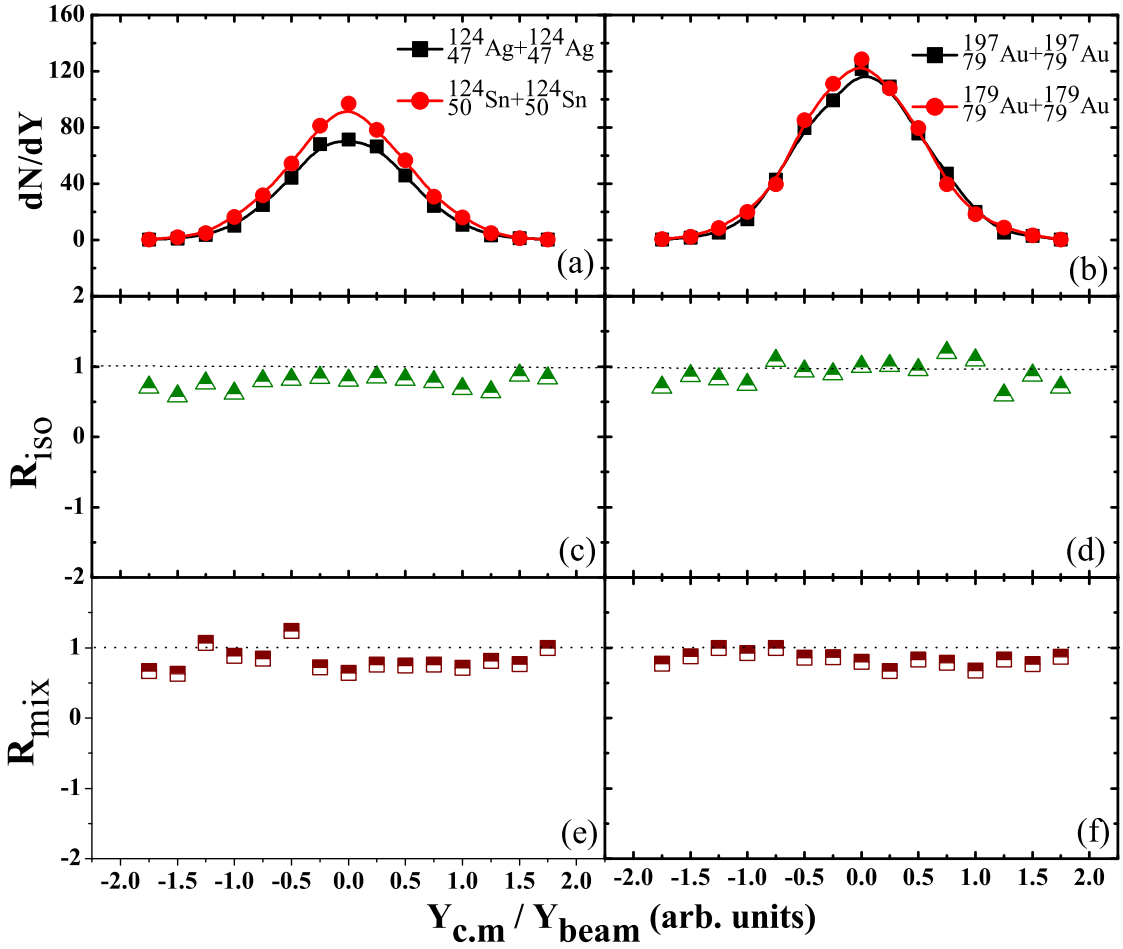


**Figure 4.7:** Observable extracted from rapidity distribution. Each row of the panel shows respective results of $dN/dY$, $R_{iso}$ and $R_{mix}$.

to the collision realm. We have also compared our theoretical results of $< varxz >$ with the experimental findings of INDRA collaboration [18,111,116,275,276] and FOPI collaboration [109]. In case of reaction $^{36}_{18}Ar +^{58}_{28} Ni$, our results are closer to INDRA data as compared to Liu et al. [116] because instead of using soft equation of state, hard equation of state was used by Liu et al. [116]. In the INDRA experiment systematic errors have been estimated by varying the multiplicity constraints for lighter systems ($^{36}_{18}Ar +^{58}_{28} Ni$ and $^{36}_{18}Ar +^{36}_{18} KCl$) by 1 unit and by 2 to 3 units for heavier systems ($^{129}_{54}Xe +^{129}_{50} Sn$ and $^{197}_{79}Au +^{197}_{79} Au$) in order to change all the cross sections in the same proportion. Ying Yuan et al. [276] used four different equation of states (EoS) namely: H-EoS, S-EoS, HM-EoS, and SM-EoS respectively. Their study concluded that hard

EOS shows higher stopping value than the soft EOS. Further INDRA experimental results support the soft equation of state (S-EOS). In the present investigation theoretical predictions are closer to experimental data points for incident energies ranging from 20 MeV/nucleon to 100 MeV/nucleon. In the case of $^{197}_{79}Au + ^{197}_{79}Au$ system, our results are very close to the INDRA and FOPI collaborations, so we conclude that $< varxz >$ is the best observable to study the nuclear stopping. Theoretical error bars on predicted nuclear stopping observable have been added using statistical methods to

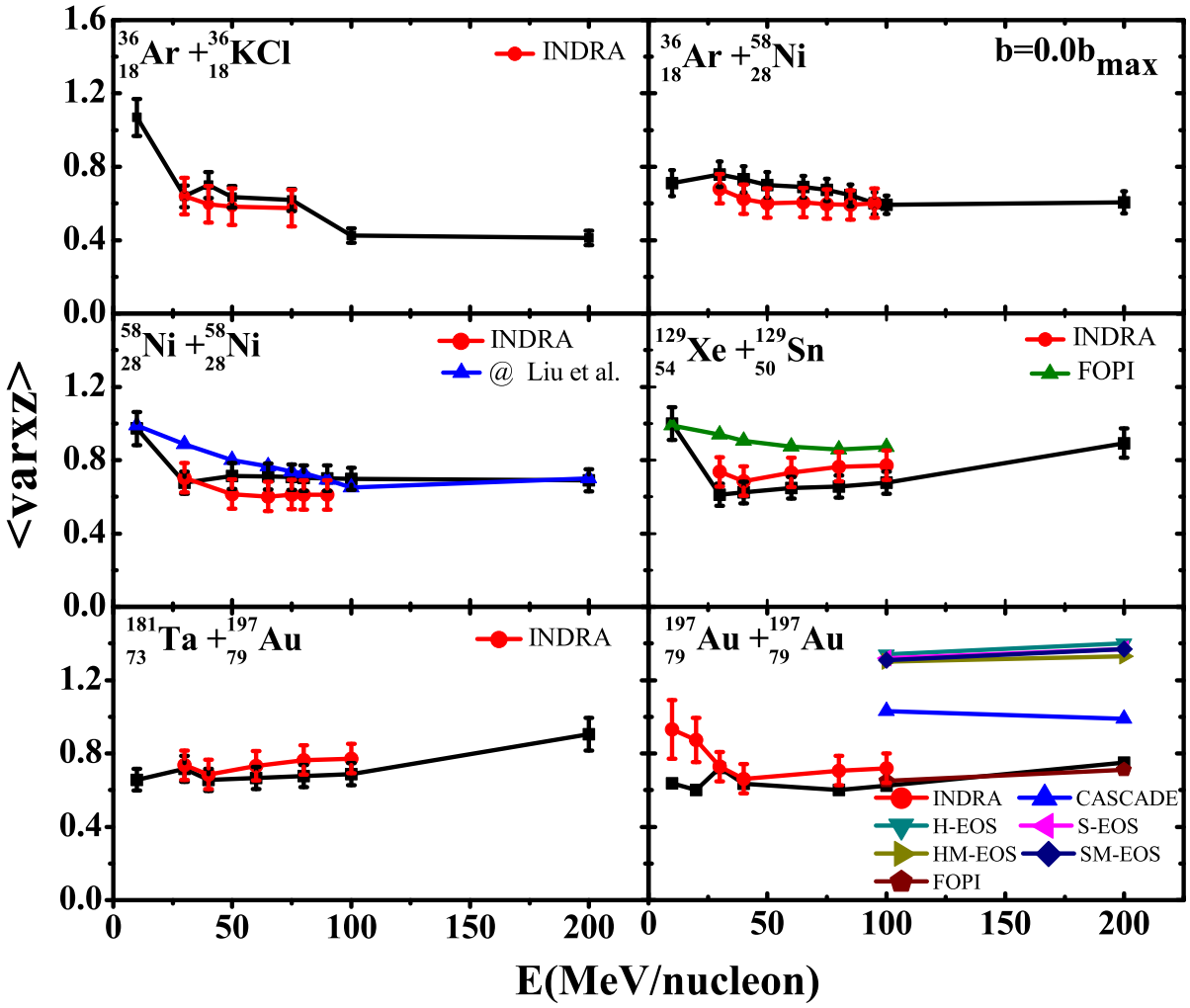


**Figure 4.8:** Incident energy dependence of nuclear stopping observable $< varxz >$, for the reactions $^{197}_{79}Au+^{197}_{79}Au$, $^{181}_{73}Ta+^{197}_{79}Au$, $^{129}_{54}Xe+^{129}_{50}Sn$, $^{58}_{28}Ni+^{58}_{28}Ni$, $^{36}_{18}Ar +^{58}_{28}Ni$ and $^{36}_{18}Ar +^{36}_{18}KCl$ at $\hat{b} = 0.0$.

study correlations between various observables. So one can significantly enhance the feedback between experiment and nuclear modeling. Basically, errors bars are graphical representation of how much the data varies. The comparison testifies that the trend of theoretical findings reproduced by $< varxz >$ is similar to the experimental data.

### 4.9.1 System mass dependence

The variation of nuclear stopping with mass reveals significant information. From the Fig 4.9 (a, b, c and d), it is observed that nuclear stopping depends on the mass of

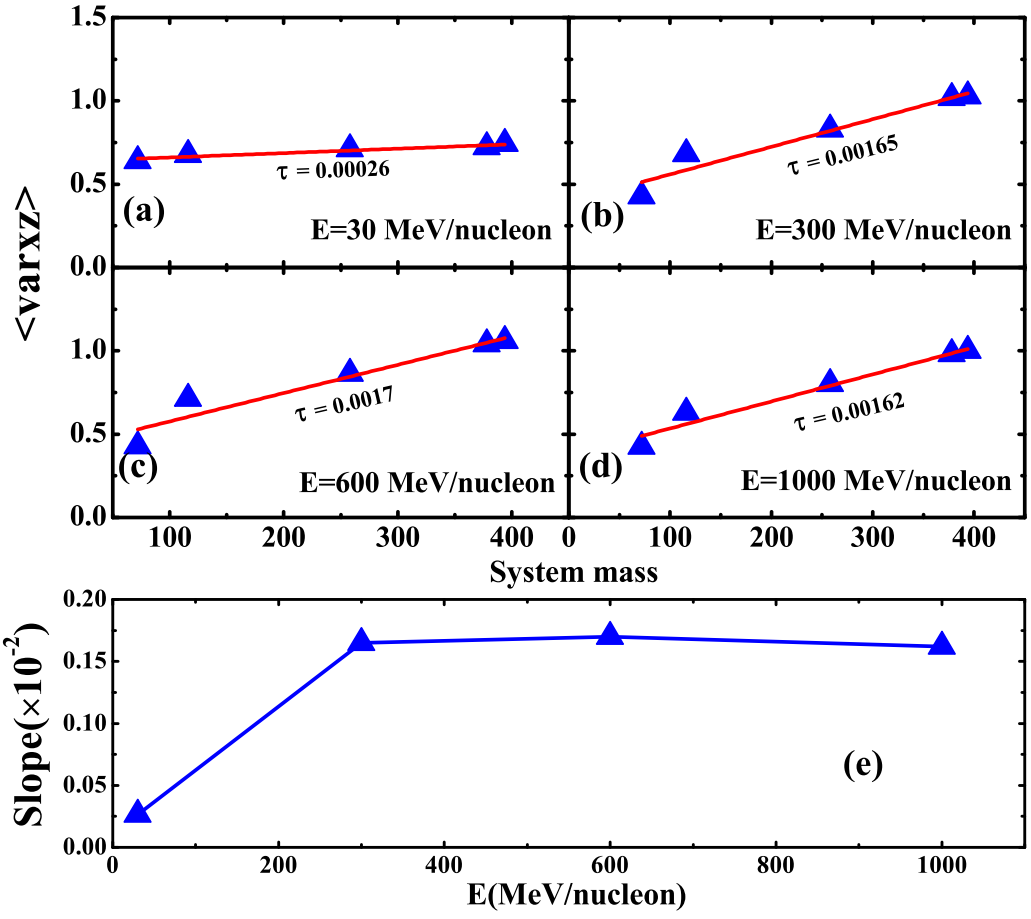


**Figure 4.9:** System mass dependence of nuclear stopping observables at different energies (30, 300, 600 and 1000 MeV/nucleon) and (e) slope of nuclear stopping parameter's as a function of incident energy.

colliding nuclei as well as on the incident energy. The mass dependence of nuclear stopping would give us an idea about the role of Coulomb interaction potential and the symmetry potential. In Fig 4.9 (a, b, c and d), the variation of nuclear stopping with the mass of colliding nuclei have been displayed from energies 30 MeV/nucleon to 1000 MeV/nucleon. In the Fig 4.9 (a), the role of the mean field on nuclear stopping can be observed. At lower incident energy only the mean field control the reaction dynamics therefore variation with mass is very small, but in Fig 4.9 (b, c and d), the role of the nucleon-nucleon cross section, Coulomb as well as symmetry potentials can be seen since slope changes with energy. This is because at higher energies these interactions play a significant role. If one looks at Fig 4.9 (e), the slope of $< varxz >$ as a function of system mass has been plotted and it is found that at lower incident energies the variation in slope is more as compared to higher energies. This is due the fact that mean field, Pauli blocking and fragment phase space plays a significant role in nuclear stopping. At higher energies, the fragment phase space behaves similar to nucleon phase space and hence less variation in stopping observable can be seen. The slope of the curves shown in Fig 4.9 (a, b, c and d) is calculated and one can see that variation in the slope value is more in lower energy range and their is very small change in slope value at higher energies as shown in Fig 4.9 (e). This is because, reaction dynamics changes drastically from mean field to nn collisions.

Therefore, in the next step, incident energy dependence of nuclear stopping for the fragment having Z = 1, proton ($^1_1H$), deuterium ($^2_1H$) and tritium ($^3_1H$) have been displayed in the Fig 4.10. On plotting $< varxz >$ separately as a function of energy, one can see that comparison with experimental data is fairly good [109]. In the case of protons, the value of $< varxz >$ is slightly higher than experimental data at lower incident energies. At higher incident energies the magnitude of nuclear stopping is small as compared to experimental finding. A remarkable feature is similarity in the behavior of three isotopes, but a closer look reveals that there are some subtle difference in the shapes of the $< varxz >$. The maximum value of stopping has been obtained around 400 MeV/nucleon. Also, when energy exceeds above 400 MeV/nucleon, the value of nuclear stopping falls gradually because at higher energies nucleons pass each

other without suffering any collisions. Theoretical error bars have been added using statistical methods.

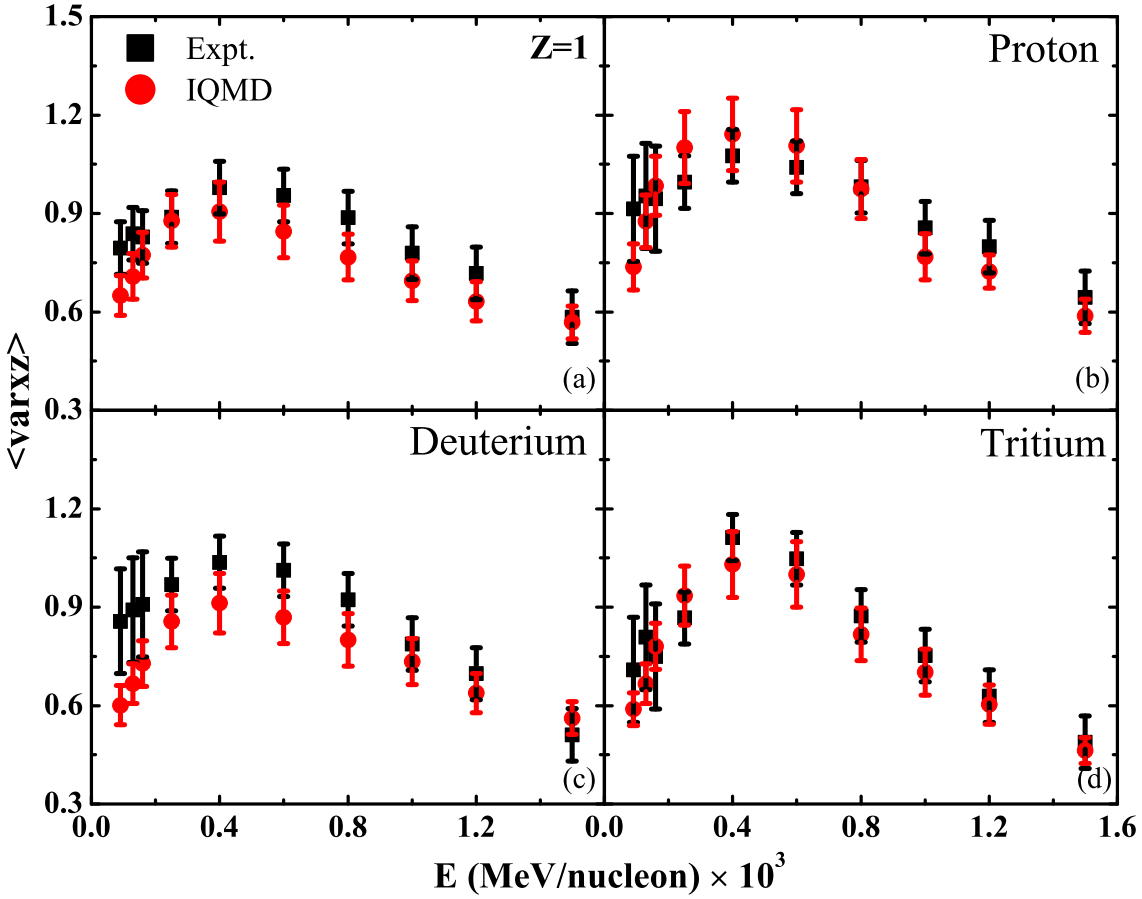


**Figure 4.10:** The variation of incident energy dependence on $< varxz >$ for the reaction $^{197}_{79}Au +^{197}_{79} Au$ and for the fragments having Z = 1, proton, deuterium and tritium.

## 4.10 Correlation with fragment production

An interesting feature of nuclear stopping is to look at the production of fragments from the participant zone, which can be used as a barometer to estimate the nuclear stopping using $< varxz >$ as an observable. In our earlier studies [123], it has been

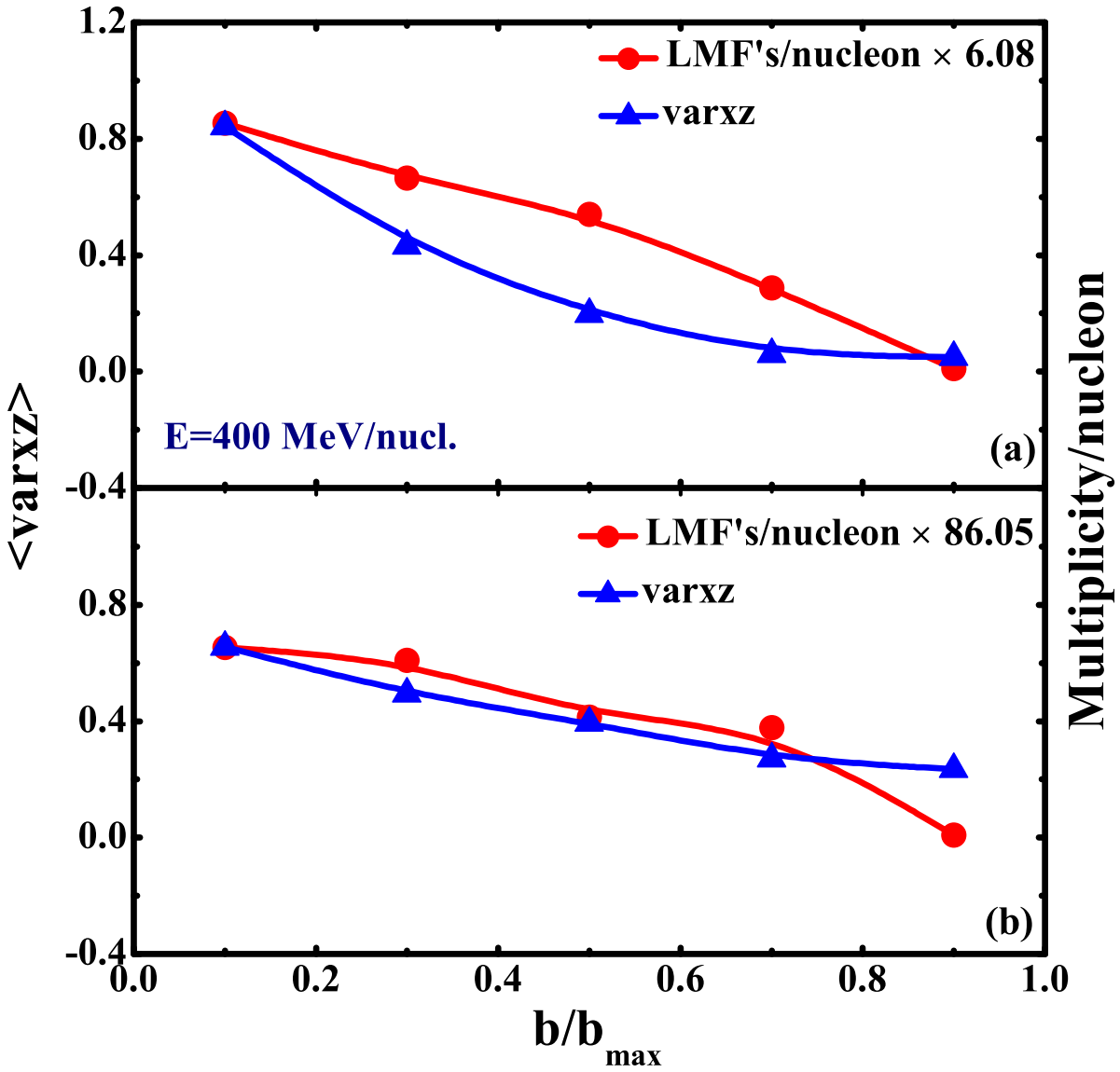


**Figure 4.11:** The scaled LMF's/nucleon as well as nuclear stopping observable $< varxz >$ as a function of normalized impact parameter at an incident energy of 400 MeV/nucleon.

reported that stopping observable R and average multiplicity of the light mass fragments (LMF's) do not show the similar trend. It was assumed that LMF's originate from the participant zone. As shown in the Fig 4.11 (a), there is no correspondence interpolated between $< varxz >$ and multiplicity of light mass fragments (LMF's) as a function of impact parameter. Here, in the present study we have normalized the LMF's with $< varxz >$ with the variation of impact parameter. Multiplicity of LMF's

decreases with increase in the impact parameter as a result, the participant matter decreases and leads to the formation of more number of heavier mass fragments. A visible difference occurs between the value of nuclear stopping observable $< varxz >$ and the multiplicity of the light mass fragment (LMF's). Therefore, in Fig 4.11 (b), we have considered the LMF's only originated from participant zone. One can see that there is a close agreement between LMF's and $< varxz >$. As we have discussed before that nucleons which suffered atleast five collisions are better stopped. Now one can also say that LMF's are formed by the nucleons suffering collisions and their initial correlations are broken. Therefore one can observe that LMF's production is highly correlated with global nuclear stopping.

## 4.11 Memory loss

The incomplete stopping clearly indicates that in central collisions the nucleons do not lose all memories or correlations with respect to the entrance channel. Due to lack of nucleon-nucleon collisions at lower energies the correlation among the nucleons remains intact. But as the energy increases, the correlations among the nucleons break down and hence nucleons lose their memory. The memory loss ratio can be written as [13]:

$$R_{ml} = \left[\frac{R_E - R_E^{entr}}{1 - R_E^{entr}}\right] \tag{4.9}$$

In recent study, it was concluded that $< varxz >$ is the more sensitive parameter to study the nuclear stopping, so author has calculated the memory loss using the $< varxz >$ stopping observable defined as [19]:

$$R_{ml} = \left[\frac{< varxz > - < varxz >^{entr}}{1 - < varxz >^{entr}}\right] \tag{4.10}$$

### 4.11.1 Time evolution of memory loss

In the Fig 4.12, time evolution of the memory loss ratio $R_{ml}$ for the reaction $^{197}_{79}Au +^{197}_{79} Au$ at E = 60 MeV/nucleon is calculated. One can see $< R_{ml} >$, diversify drastically during the high density phase (30-80 fm/c), once this phase is over, no

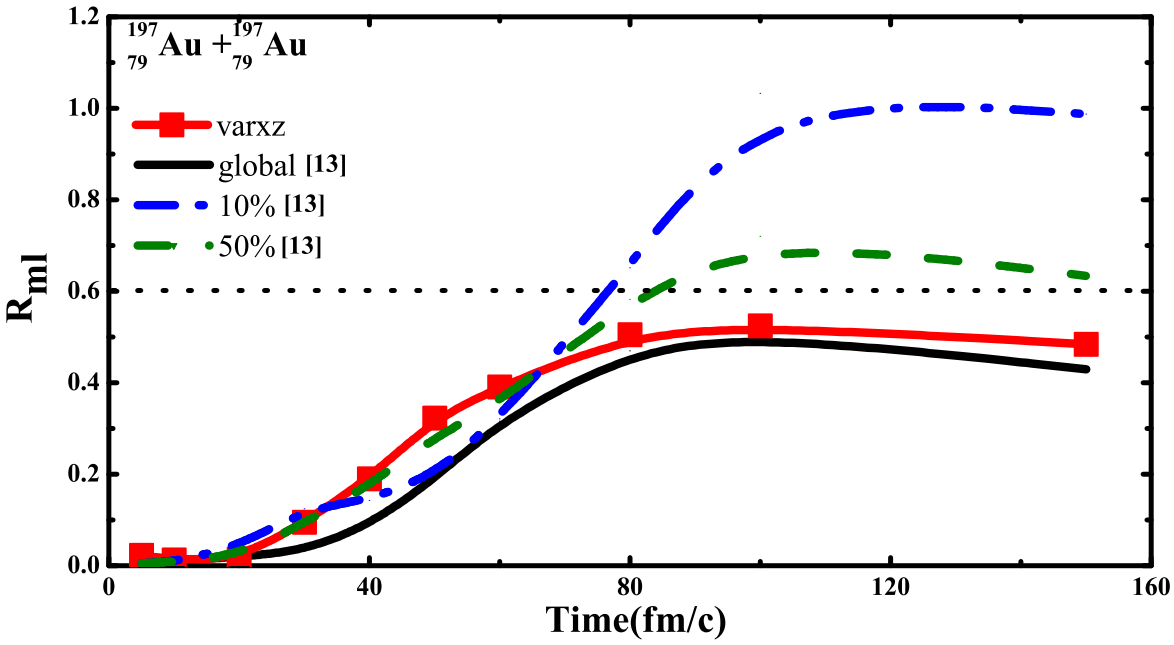


**Figure 4.12:** Time evolution of memory loss ratio $R_{ml}$ for the reaction $^{197}_{79}Au$ +$^{197}_{79}$ $Au$ in case of theoretical and experimental data at E = 60 MeV/nucleon.

more shift appear in the magnitude of the observable. Time evolution using stopping observable $< varxz >$ has been displayed and compared with the Jun Su et al. [13] calculations. The solid red line represents the memory loss due to global nuclear stopping. The dashed green line and the dotted purple line represent the central region including 50% and 10% of the nucleon, respectively. Memory loss has been calculated using $< varxz >$, observable and the results obtained are more closer to the Jun Su et al. [13]. From the Fig 4.12, it is clear that at central impact parameter more number of nucleons lose their memory as compared to those reactions which takes place at peripheral impact parameter. The value of $R_{ml}$ does not reach unity. It is further observed that only maximum 60 % of the nucleons lose their memory.

### 4.11.2 Incident energy dependence of memory loss

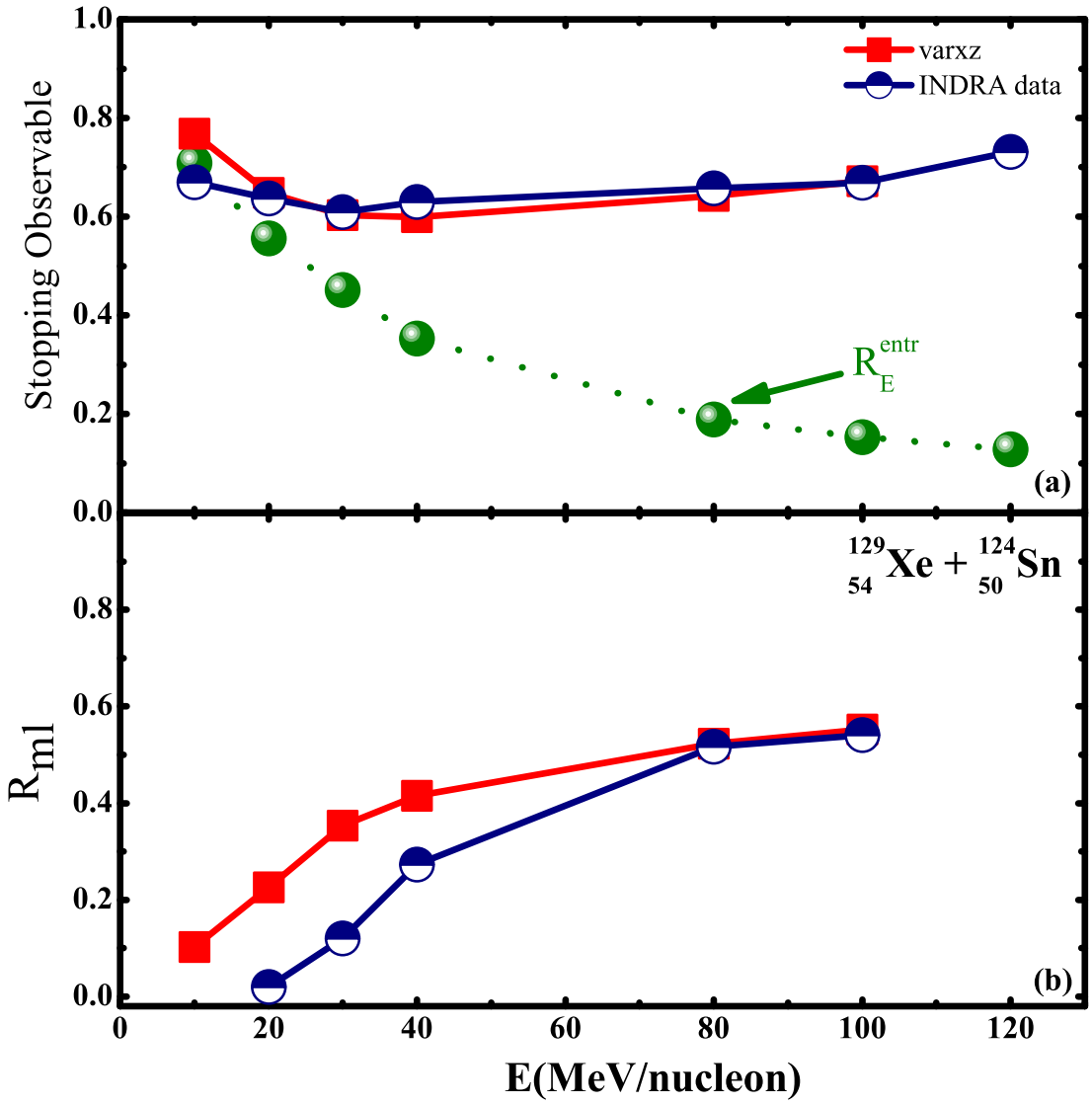


**Figure 4.13:** (a) Nuclear stopping observable in central collisions for the reactions $^{129}_{54}Xe +^{121}_{50} Sn$, (b) Memory loss as a function of incident energy for the reaction $^{129}_{54}Xe +^{121}_{50} Sn$.

In the Fig 4.13 (a), the nuclear stopping observable as a function of incident energy is displayed for the reaction $^{129}_{54}Xe+^{121}_{50} Sn$. The lower dashed curve represents the expected value of stopping for the entrance channel ($R_E^{entr}$) when the nucleon-nucleon collisions are switched off. We have compared theoretical calculations of $< varxz >$

with experimental data (INDRA Collaboration) [111] in the present study. It is observed that below the Fermi energy the theoretical and experimental points are close to the entrance channel $R_E^{entr}$ and in case of incident energy higher than Fermi energy the points are far away from the $R_E^{entr}$. This is because at the lower incidence energies, nucleon-nucleon collisions are suppressed and nucleons retain their initial memories. At higher incident energies, the value of nuclear stopping observable as well as experimental points are far from the isotropy ratio $R_E^{entr}$. In the Fig 4.13 (b), author has calculated the memory loss for the reaction $^{129}_{54}Xe +^{121}_{50} Sn$ using theoretical values and compared with experimental data w.r.t entrance channel and concluded that values of memory loss calculated theoretically are greater than the values calculated using experimental data at lower incident energies. However, memory loss in case of nuclear stopping observable $< varxz >$, are closer to the values calculated using the experimental data at higher incident energies.

In the Fig 4.14, author has calculated the memory loss of participating matter and spectator matter respectively. The nucleons those have suffered at least one collision are treated as participant nuclear matter and the remaining nucleons contributes to the spectator nuclear matter [256]. The value of memory loss enhances with increase in incident energy and then falls since the nucleon-nucleon cross-section decreases at higher energies. It is clearly seen that participant nucleons loses more memory as compared to spectator matter. The participant matter increases due to increased rate of nucleon-nucleon collisions at $\widehat{b} = 0.0$ with an increase in the incident energy.

To determine the memory loss as a function of collisions suffered by nucleons, simulations have been performed for different set of reactions having different total mass. In the Fig 4.15 (a), we have shown the allowed collisions as a function of system mass, for various reactions $^{197}_{79}Au+^{197}_{79}Au$, $^{150}_{60}Nd+^{150}_{60}Nd$, $^{131}_{54}Xe+^{118}_{50}Sn$, $^{100}_{40}Zr+^{100}_{40}Zr$, $^{58}_{28}Ni+^{58}_{28}Ni$, and $^{40}_{18}Ar +^{45}_{21} Sc$. We observe that the value of the allowed collisions increases with increase in the system mass. This is due to the larger interaction volume in heavier nuclei, resulting in collisions for a longer time. In the Fig 4.15 (b), memory loss as the function of system mass dependence has been plotted. One can see the value of memory loss increases as the system mass increases. With variation in system mass

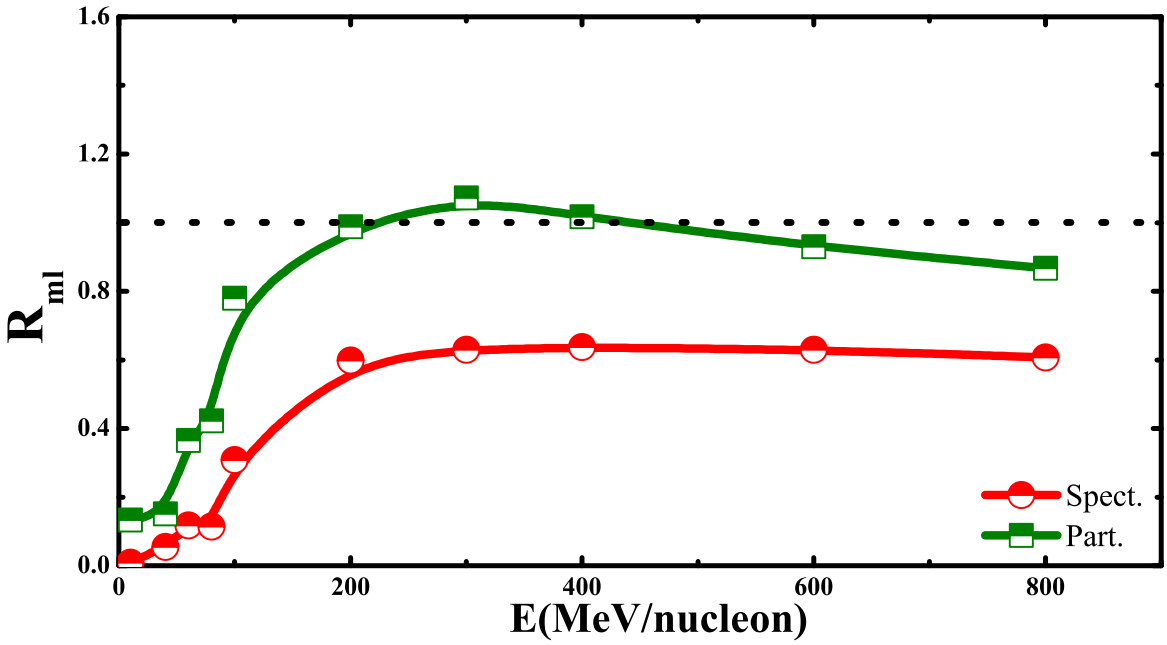


**Figure 4.14:** Memory loss as a function of incident energy for the reaction ${}^{197}_{79}Au + {}^{197}_{79}Au$ both for participant and spectator matter.

from 95 to 394, the change in the values of allowed collisions and memory loss are 72% and 33% respectively. Although allowed collisions and memory loss increases linearly as the function of system mass, the direct correlation between allowed collisions and memory loss can not be established. The nucleons in the bulk of colliding nuclei suffer less number of collisions and the nucleons on surface of nuclei suffer more collisions.

## 4.12 Summary

In this chapter, we have carried out systematic investigation for the nuclear stopping observables $R_E$, $R_P$ and $< varxz >$ for mass symmetric and nearly mass asymmetric reactions. It has been concluded that nucleons suffering at least five number of collisions are more thermalized and contributes in nuclear stopping. The value of nuclear stopping observable in the case of protons is higher than the neutrons. Nuclear stop-

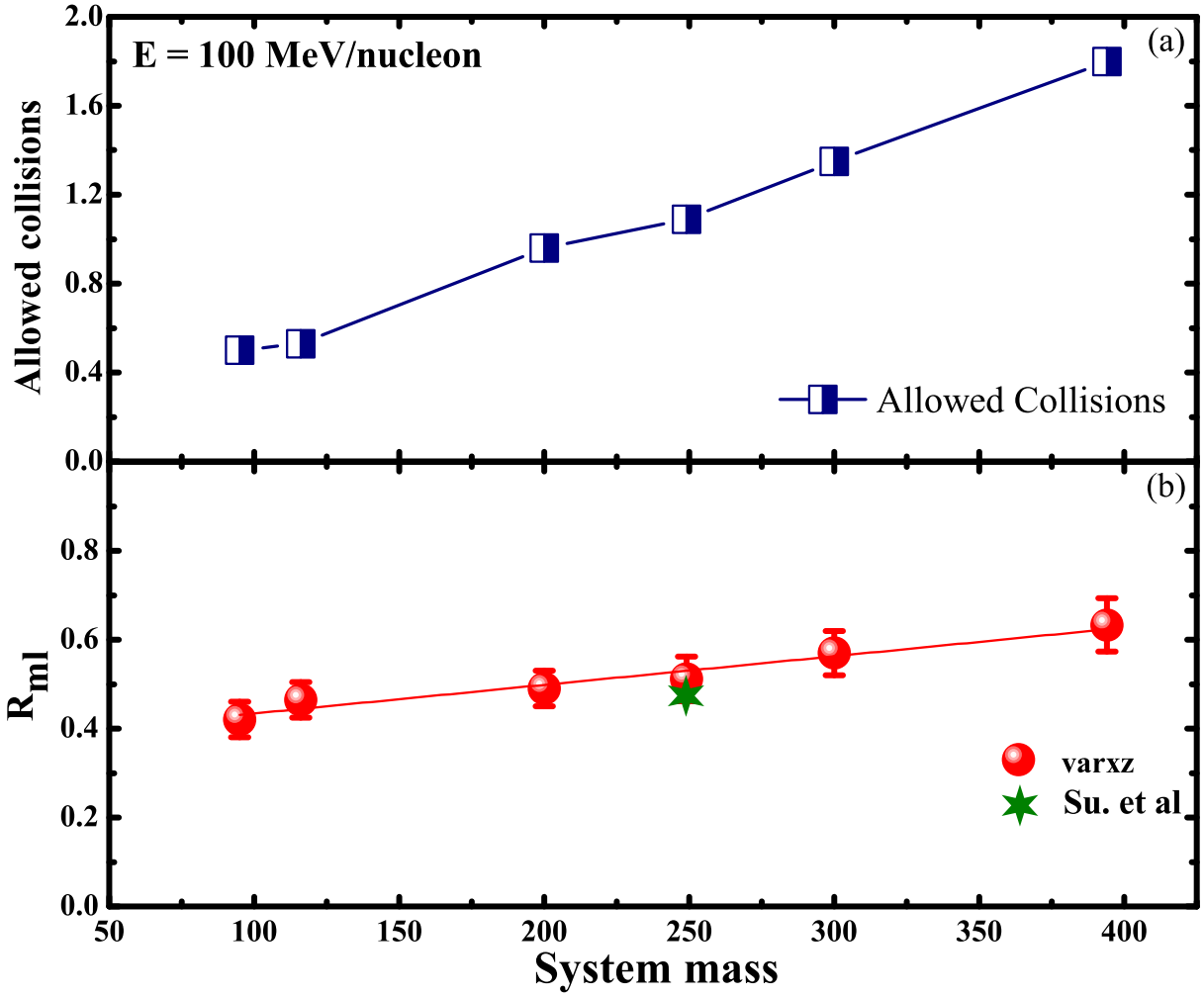


**Figure 4.15:** (a) Allowed collisions as the function of system mass at incident energy E = 100 MeV/nucleons (b) memory loss as a function of system mass dependence at incident energy E = 100 MeV/nucleons.

ping is found to increase with the composite mass of the system because the nuclear stopping phenomena are related to the collision zone. Moreover $< varxz >$ is the more sensitive observable to study the nuclear stopping. LMF's production is found to be associated with global nuclear stopping.

Nucleons forming the light mass fragments lose their memory with increase in energy. Memory loss is strongly dependent upon the impact parameter. Spectator matter keeps

more memories than that of participant matter. With the increase in system mass allowed collisions as well as memory loss increases. Finally, direct correlation between memory loss and number of colliding nucleons can not be established.

# Chapter 5

# Interplay between mass asymmetry and impact parameter on nuclear stopping

One of the essential observable, of intermediate energy is nuclear stopping that reveals the degree of thermalization and equilibration in a reaction. Nuclear stopping is influenced by large amount of the dissipated energy in central heavy ion collisions and constrains the different reaction mechanisms over large domains of incident energies [14, 18]. It also provides enlightenment about the nuclear equation of state, nucleon-nucleon cross section as well as the degree of equilibrium reached in heavy-ion collisions. Reaction dynamics depends crucially on various entrance channel parameters including mass asymmetry that plays a decisive role in a reaction [277, 278]. This fact has also been supported by experiments [279–281]. Reaction dynamics involved in the mass symmetric reactions are different than those observed in mass asymmetric reactions. In the mass symmetric reactions excitation energy is deposited as compression energy whereas in asymmetric reactions it leads to thermal excitation energy. Nuclear stopping for mass asymmetric nuclear reactions have been studied by V. Kaur et al., [126]. Their findings revealed that collision in symmetric systems leads to maximum nuclear stopping and decreases as one deviates from mass asymmetry. In another study, the requirement of a very heavy system in the entrance channel was essential to achieve complete stopping as reported by Puri et al., [273] for the reactions of Xe+Sn. Interestingly, none of the above reported studies on nuclear stopping were performed

**Table 5.1:** List of various mass asymmetric reactions with fixed total mass.

| $SNo.$ | $A_{TOT} = 240$ | $A_{TOT} = 160$ | $A_{TOT} = 100$ | $A_{TOT} = 80$ | $A_{TOT} = 40$ |
|---|---|---|---|---|---|
| $\eta = 0.1$ | ${}^{108}_{48}Cd + {}^{132}_{56}Ba$ | ${}^{70}_{32}Ge + {}^{90}_{40}Zr$ | ${}^{45}_{19}K + {}^{55}_{25}Mn$ | ${}^{36}_{18}Ar + {}^{44}_{20}Ca$ | ${}^{17}_{8}O + {}^{23}_{11}Na$ |
| $\eta = 0.3$ | ${}^{84}_{38}Sr + {}^{156}_{66}Dy$ | ${}^{54}_{26}Fe + {}^{106}_{48}Cd$ | ${}^{34}_{18}Ar + {}^{66}_{30}Zn$ | ${}^{28}_{14}Si + {}^{52}_{24}Cr$ | ${}^{14}_{7}N + {}^{26}_{12}Mg$ |
| $\eta = 0.5$ | ${}^{60}_{28}Ni + {}^{180}_{74}W$ | ${}^{40}_{20}Ca + {}^{120}_{52}Te$ | ${}^{25}_{12}Mg + {}^{75}_{33}As$ | ${}^{20}_{10}Ne + {}^{60}_{28}Ni$ | ${}^{10}_{5}B + {}^{30}_{14}Si$ |
| $\eta = 0.7$ | ${}^{36}_{18}Ar + {}^{204}_{82}Pb$ | ${}^{24}_{12}Mg + {}^{136}_{58}Ce$ | ${}^{14}_{7}N + {}^{86}_{36}Kr$ | ${}^{10}_{5}B + {}^{70}_{32}Ge$ | ${}^{6}_{3}Li + {}^{34}_{16}S$ |

with fixed target mass and varying projectile mass. The main intent of the present investigation in this chapter is to elaborate, significance of mass asymmetry on the projectile stopping and compensate the effect of mass asymmetry by impact parameter.

## 5.1 Results and discussions

Mass asymmetric reactions ${}^{12}_{6}C + {}^{197}_{79}Au$ ($\eta = 0.8$), ${}^{26}_{13}Al + {}^{197}_{79}Au$ ($\eta = 0.7$), ${}^{40}_{18}Ar + {}^{197}_{79}Au$ ($\eta = 0.6$), ${}^{56}_{26}Fe + {}^{197}_{79}Au$ ($\eta = 0.5$), ${}^{83}_{36}Kr + {}^{197}_{79}Au$ ($\eta = 0.4$), ${}^{96}_{40}Zr + {}^{197}_{79}Au$ ($\eta = 0.3$), ${}^{131}_{54}Xe + {}^{197}_{79}Au$ ($\eta = 0.2$), ${}^{197}_{79}Au + {}^{197}_{79}Au$ ($\eta = 0.0$) at incident energies between 40 and 1000 MeV/nucleon, for impact parameter range:

$$b/b_{max}(\widehat{b}) = 0,\ 0.3,\ 0.6,\ \text{and}\ 0.9;$$

have been simulated. In all these reactions, the total system mass ($A_{TOT} = A_T + A_P$) is floating. For a comparative study, various mass asymmetric reactions with fixed total mass have also been analyzed. Particularly, the reactions are listed in the Table 5.1 :

We define mass asymmetry parameter as:

$$\eta = \frac{A_T - A_P}{A_T + A_P};$$

where $A_P$ and $A_T$ are the masses of projectile and target respectively. In the present study, soft momentum-dependent equation of state [282–284], has been used to study nuclear stopping in various mass asymmetric reactions.

## 5.2 Mass asymmetry dependence of the normalized participant and spectator matter

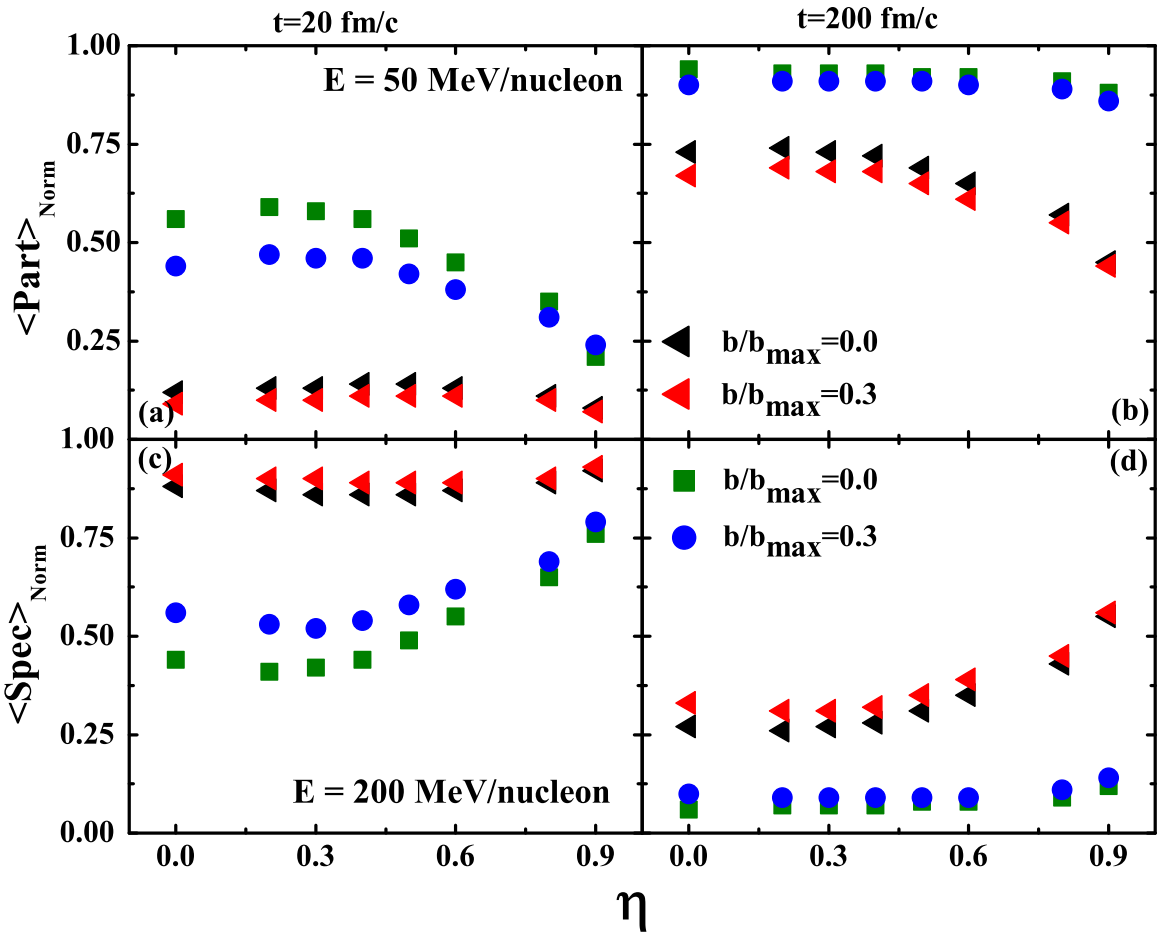


**Figure 5.1:** Analysis of mass asymmetry dependence of the normalized participant (a and b) and spectator matter (c and d) in terms of nucleon-nucleon collisions at two different time scales t = 20 fm/c and t = 200 fm/c.

The mass asymmetry dependence of normalized participant and spectator nuclear matter have been shown in Fig 5.1, at two incident energies E = 50 MeV/nucleon and 200 MeV/nucleon. Initially, author have checked the relative contribution of various mass asymmetric reactions towards the participant-spectator matter for initial time steps i.e., at t = 20 fm/c as well as for higher time steps t = 200 fm/c [285]. The nucleons which have suffered at least one collision are treated as participant nuclear

matter and the remaining nucleons contributes to the spectator nuclear matter [286]. Another definition is based on rapidity range i.e., the nucleons which are present in the mid rapidity zone are treated as participant matter and those which belongs to target like, projectile rapidity region are treated as spectator. In case of mass symmetric nuclear reactions the range of mid-rapidity region is equal on both side of zero rapidity point, while in case of mass asymmetric nuclear reactions the range of mid-rapidity zone is not equal w.r.t zero rapidity point.

The participant and spectator matter is then averaged over all nucleons and labeled as $< Part >_{Norm}$ and $< Spec >_{Norm}$. From the Fig 5.1, it is clear that the participant as well as spectator matter is highly dependent on the size of the projectile. It is obvious that the spectator matter and the participant matter will respond in an opposite manner to each other. At t = 20 fm/c, participant matter is small as the collision among the nucleons are going on but spectator matter is more. The situation changes as the reaction proceeds from t = 20 fm/c to t = 200 fm/c, where large number of nucleons suffer collisions and hence net number of participant number of nucleons increases. As the size of the projectile decreases, the interaction region between the projectile and target nuclei also decreases, due to decrease in the interactions among nucleons, the rate of nucleon-nucleon collisions decreases. Thus leading to the formation of smaller participant matter and larger fraction of spectator matter. This mass asymmetry dependence of the participant and spectator matter is clearly visible at 50 MeV/nucleon in Fig 5.1 (a and b) and at 200 MeV/nucleon as shown in Fig 5.1 (c and d). As the incident energy increases the participant matter increases which is due to the increased rate of nucleon-nucleon collisions at $\widehat{b} = 0.0$ and for $\widehat{b} = 0.3$.

For a broader view of the equilibrium process, one needs to supplement nuclear stopping with the other observable, for example anisotropy ratio $< R_p >$ already defined in the pervious chapter [18]. The main factor on which $< R_p >$ depends is the incident energy and the impact parameter.

## 5.3 Time evolution of stopping parameter $< R_p >$

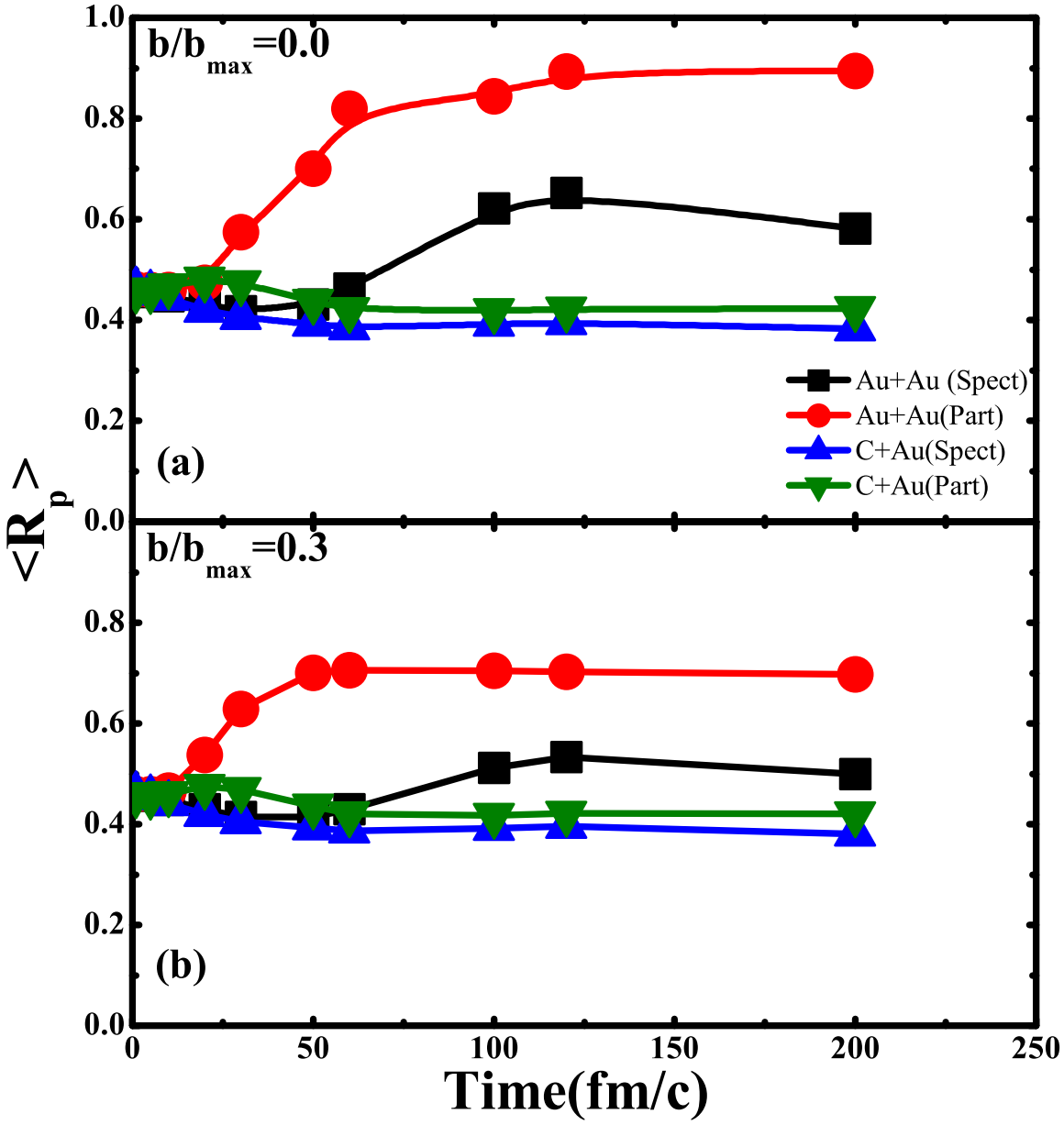


**Figure 5.2:** Time evolution of stopping parameter ($< R_p >$) at a scaled impact parameters, $\hat{b} = 0.0$ and 0.3.

In the Fig 5.2, we have displayed the time evolution of stopping parameter $< R_p >$. One can notice that complete stopping is observed for central collision due to maximum overlap and larger participant zone is produced for heavier system $^{197}_{79}Au + ^{197}_{79}Au$ than

lighter system ${}^{12}_{6}C + {}^{197}_{79}Au$. A net decrease in stopping values is observed while going from scaled impact parameter $\hat{b} = 0.0$ to 0.3 as shown in the lower panel of Fig 5.2.

Fig 5.3 (a), displays the percentage of the normalized participant matter at an inci-

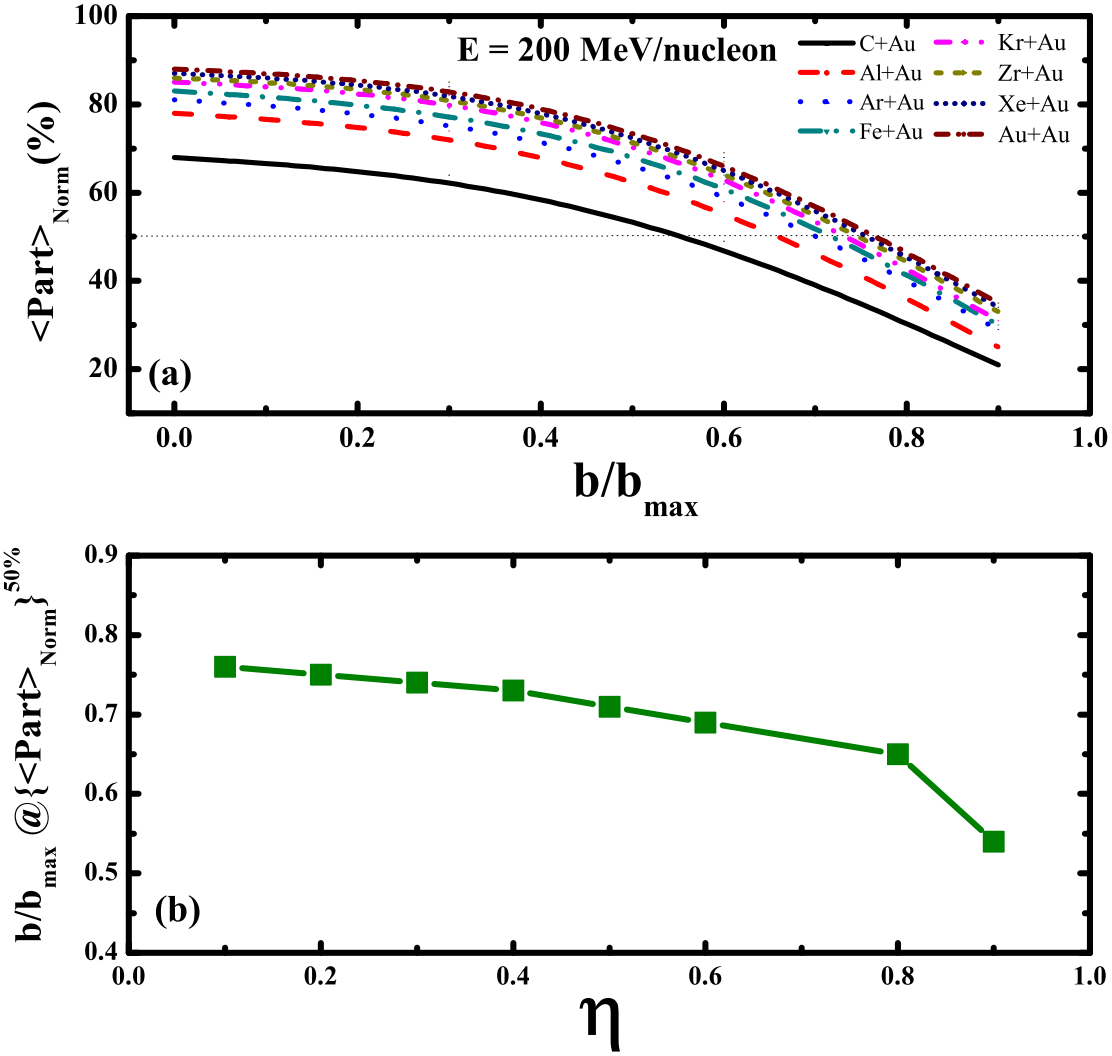


**Figure 5.3:** (a) The participant zone in percentage as a function of impact parameter and (b) Impact parameter for normalized participant nuclear matter as a function of mass asymmetry.

dent energy of 200 MeV/nucleon at different colliding impact parameters for various colliding partners: ${}^{12}_{6}C + {}^{197}_{79}Au$, ${}^{26}_{13}Al + {}^{197}_{79}Au$, ${}^{40}_{18}Ar + {}^{197}_{79}Au$, ${}^{56}_{26}Fe + {}^{197}_{79}Au$, ${}^{83}_{36}Kr + {}^{197}_{79}Au$, ${}^{96}_{40}Zr + {}^{197}_{79}Au$, ${}^{131}_{54}Xe + {}^{197}_{79}Au$ and ${}^{197}_{79}Au + {}^{197}_{79}Au$. From Fig 5.3 (a), it is clear that in all the mass asymmetric reactions, the net participant matter decreases with impact

parameter as the overlapping region between the projectile and target decreases. This means that for achieving equal participant zone in the considered mass asymmetric reactions, different impact parameters should be taken. The net participant matter decreases more sharply in case of $(C + Au)$ i.e., in case where mass asymmetry is more than other reactions where mass asymmetry is less

In Fig 5.3 (b), we have displayed impact parameter as a function of mass asymmetry at which normalized participant matter becomes 50% (labeled as $b/b_{max}@ < Part >^{50\%}_{Norm}$). It is clear that $b/b_{max}@ < Part >^{50\%}_{Norm}$ decreases with mass asymmetry. To achieve 50% matter as a participant matter in the collision of $^{12}C +^{197} Au$, the reaction should be carried out for semi-central collisions, whereas for $^{197}Au +^{197} Au$, the impact parameter should be peripheral one. The impact parameters needed for the other reactions to take place should lies in between the reactions $^{197}_{79}Au+^{197}_{79}Au$ and $^{12}_{6}C+^{197}_{79}Au$. If we treat the nuclear matter from target and projectile on equal footing, one can study nuclear stopping of nuclear matter and additionally some rotational effects. This study may be useful for the experimentalist as they can look for projectile stopping along with projectile fragmentation.

## 5.4 Incident energy dependence for various reactions

In Fig 5.4, we display anisotropy ratio as a function of incident energy for the following reactions $^{197}_{79}Au +^{197}_{79} Au$, $^{131}_{54}Xe +^{197}_{79} Au$, $^{83}_{36}Kr +^{197}_{79} Au$, $^{56}_{26}Fe +^{197}_{79} Au$, $^{40}_{18}Ar +^{197}_{79} Au$ and $^{12}_{6}C +^{197}_{79} Au$. The trend of $< R_p >$ with incident energy [272] is clearly visible in the case of $^{197}_{79}Au+^{197}_{79} Au$, $^{131}_{54}Xe+^{197}_{79} Au$, and $^{83}_{36}Kr+^{197}_{79} Au$. One can observe the transition from lower to high incident energies. The nuclear stopping is found to decrease steeply for low incident energy (100 MeV/nucleon), where Pauli blocking dominates, and for higher incident energies nuclear stopping increases because nucleon-nucleon collisions plays an important role. The steep decrease for the reactions $^{83}_{36}Kr +^{197}_{79} Au$ is caused by the increased mean-free-path of the nucleon increases and nucleon-nucleon cross-section decreases. This leads to passing of the nucleons close to each other without

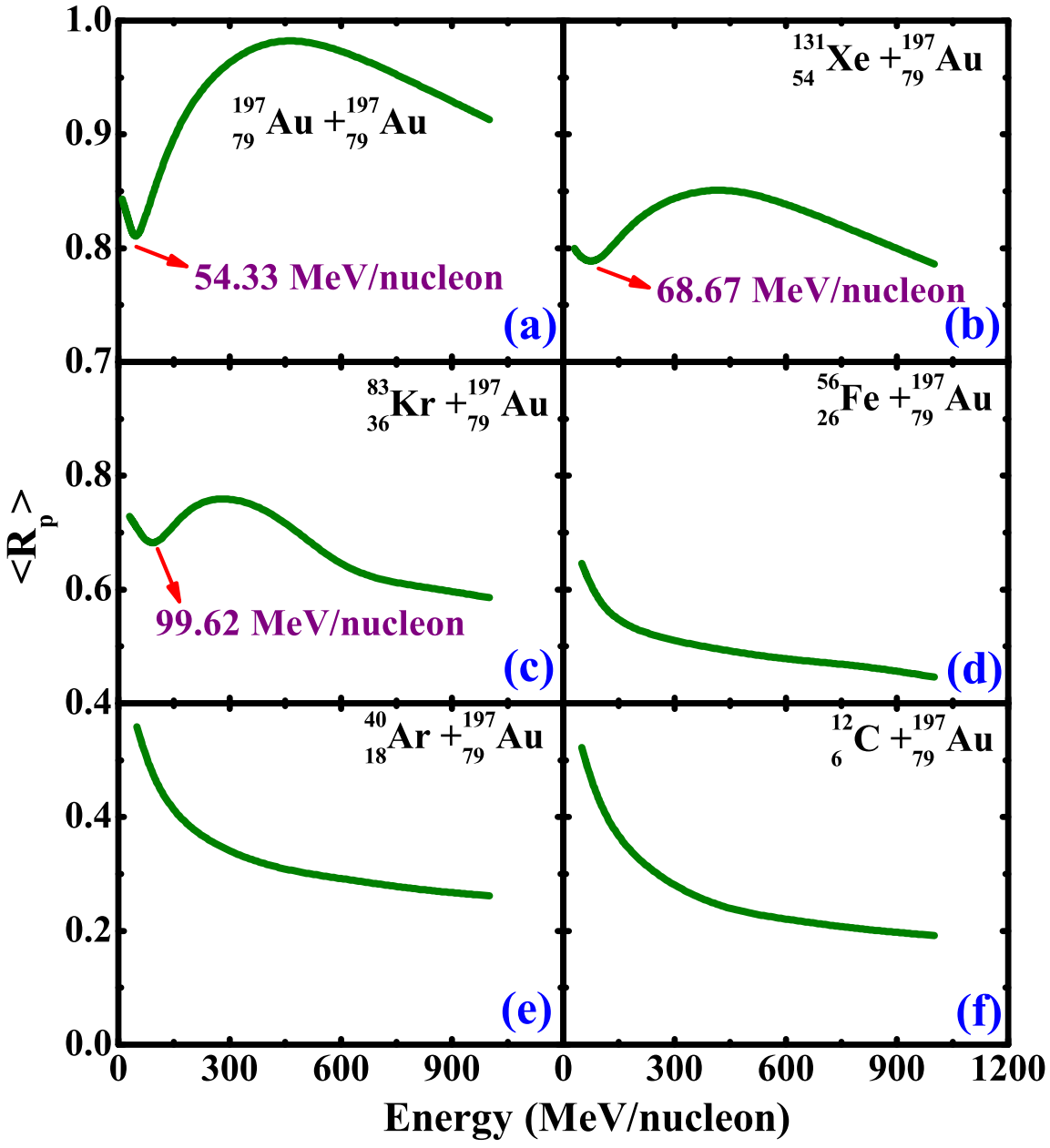


**Figure 5.4:** The anisotropy ratio $< R_p >$ as a function of incident energy for the reactions (a) $^{197}_{79}Au +^{197}_{79} Au(a)$, $(b)$, $^{131}_{54}Xe +^{197}_{79} Au$,$(c)$ $^{83}_{36}Kr +^{197}_{79} Au$, $(d)$ $^{56}_{26}Fe +^{197}_{79} Au$, $(e)$ $^{40}_{18}Ar +^{197}_{79} Au$ and $(f)$ $^{12}_{6}C +^{197}_{79} Au$, at zero impact parameter.

interactions. The incident energy at which $< R_p >$ shows minima, increases with the decrease in the size of the projectile. For reactions $^{56}_{26}Fe +^{197}_{79} Au$, $^{40}_{18}Ar +^{197}_{79} Au$ and $^{12}_{6}C +^{197}_{79} Au$ an exponential decrease in $< R_p >$ can be seen instead of usual dip around

100 MeV/nucleon. Here, the mass asymmetry effects are strongly observed. Time interval during which the maximum number of collisions occurred among projectile and target nucleons for the reactions are $^{197}_{79}Au +^{197}_{79} Au$, $^{131}_{54}Xe +^{197}_{79} Au$ and $^{83}_{36}Kr +^{197}_{79} Au$ in comparison to $^{56}_{26}Fe +^{197}_{79} Au$, $^{40}_{18}Ar +^{197}_{79} Au$ and $^{12}_{6}C +^{197}_{79} Au$. This is because of the large number of nucleons involved in the former case.

Fig 5.5 (a), displays the variation of anisotropy ratio $< R_p >$ with incident energy for

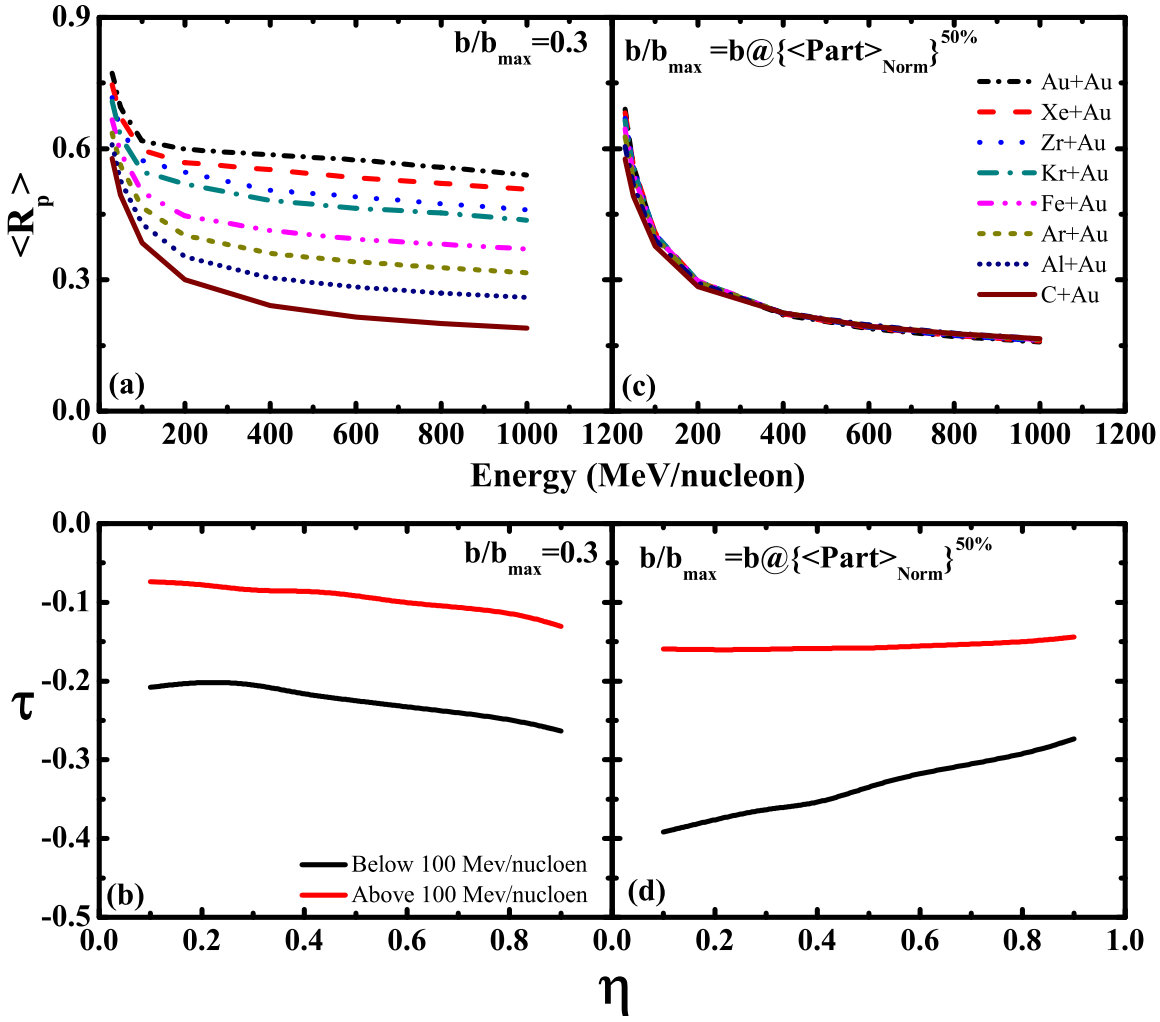


**Figure 5.5:** (a) The anisotropy ratio $< R_p >$ as a function of incident energy for different mass asymmetric reactions and (b) the value $\tau$ extracted from Fig.5 (a), as a function of mass asymmetry. In the panels (c) anisotropy ratio $< R_p >$ as a function of incident energy for different mass asymmetric reactions, at $\hat{b} = b@< Part >_{Norm}$ 50% and (d) the value $\tau$ extracted from Fig.5 (c), as a function of mass asymmetry

various reactions mentioned above at $\widehat{b} = 0.3$. Following conclusions have been drawn:

1. The behavior of anisotropy ratio $< R_p >$ is different at different incident energies. The nucleon-nucleon cross-section becomes almost independent as the incident energy increases which tends to increase the longitudinal momentum of nucleons and hence there is a decrease in the anisotropy ratio. This observation is valid for all the considered mass asymmetric reactions. This trend of $< R_p >$ under present investigation is similar as reported in Ref. [287, 288], for symmetric colliding nuclei.

2. The heavier projectile induced reactions tends to attain better equilibrium as compared to reactions induced by lighter projectile because of the larger interaction volume and hence more nucleon-nucleon collisions takes place in the former case.

In the Fig 5.5 (a), as the mass asymmetry increases from the reaction ${}^{197}_{79}Au + {}^{197}_{79}Au$ to ${}^{12}_{6}C + {}^{197}_{79}Au$, there is decrease in the anisotropy ratio $< R_p >$. More decrease is seen in case of highly mass asymmetric reaction because less number of nucleons are present in the projectile. Further, it is encouraging to analyze reactions at different impact parameters for different reactions based on the choice of 50% participant matter as shown in Fig 5.5 (c). It is clear that for a fixed amount of participant matter, the degree of equilibrium achieved is almost same for all the reactions. The nuclear stopping which is basically the transfer of longitudinal momentum to transverse momentum is related to the number of participants in the system. One can make inferences from Fig 5.5 (a and c) that up to incident energy 100 MeV/nucleon, there is a sudden decrease in the nuclear stopping for all the reactions, whereas above 100 MeV/nucleon, there is a gradual decrease in the nuclear stopping value. This is because of the fact that below Fermi energy mean field plays its important role and hence Pauli blocking dominates. Above Fermi energy nucleon-nucleon collisions start dominating and role of Pauli blocking decreases. This energy dependence of nuclear stopping is fitted by the power law as: $< R_p > \propto E^{\tau}$ for all systems under consideration. Due to the different behavior of stopping in different energy regimes, the value of the parameter

$\tau$ is fitted for two energy regions: from 40 to 100 MeV/nucleon and from 100 to 1000 MeV/nucleon. The value of $\tau$ extracted from Fig 5.5 (a and c) is shown in the Fig 5.5 (b and d) respectively. The non zero values of slope in Fig 5.5 (b), for above and below E = 100 MeV/nucleon is observed. However, change in the slope is marginal because of the effective contribution of participant zone as shown in the Fig 5.5 (d). Comparing Fig 5.5 (b and d) indicates that mass asymmetry can be compensated by varying the impact parameter. The spectator matter does not changes in the same ratio as the mass asymmetry changes.

In the Fig 5.6 (a), author has displayed the time evolution of stopping observable $< R_p >$ for the reaction ${}^{197}_{79}Au + {}^{197}_{79}Au$ and ${}^{12}_{6}C + {}^{197}_{79}Au$. It has been observed that the value of nuclear stopping is more in case of heavier system as compared to lighter one. In case of ${}^{197}_{79}Au + {}^{197}_{79}Au$, 394 nucleons are involved in the reaction but in case of ${}^{12}_{6}C + {}^{197}_{79}Au$, only 209 nucleons are involved. In later case, ${}^{12}_{6}C$ being very small projectile might be fused inside the heavier target ${}^{197}_{79}Au$, hence less stopping is being observed. Also, at low incident energies reaction dynamics are directed by the mean field only and binary collisions are suppressed as a result of Pauli blocking. Hence mean field takes longer time to thermalize the colliding nuclei. Therefore nuclear stopping is almost same for both the reactions at low incident energy, as the reaction proceeds due to nucleon-nucleon collisions, there is 50% enhancement in the nuclear stopping observable value as $\eta$ varies from 0.9 to 0.0.

In the Fig 5.6 (b), we have displayed the results for two reactions ${}^{197}_{79}Au + {}^{197}_{79}Au$ and ${}^{12}_{6}C + {}^{197}_{79}Au$ at impact parameter $b/b_{max}@< Part >_{Norm} = 50\%$. We compensate the effect of mass asymmetry by impact parameter of the reaction. One can clearly see that difference between the values of stopping observable ($< R_p >$) is very small as compared to the values shown in Fig 5.6 (a). It is clear from the 5.6 (b) that for a fixed amount of participant matter, the degree of equilibrium achieved has slight difference, this difference might be due to the rotational effect. The rotation of the participating nucleons are more for highly mass asymmetric reactions, due to the partial overlap, which leads to lesser destruction of co-relation among the nucleons. When a small projectile ${}^{12}_{6}C$ hits on a heavier target ${}^{197}_{79}Au$, at a non zero impact parameter,

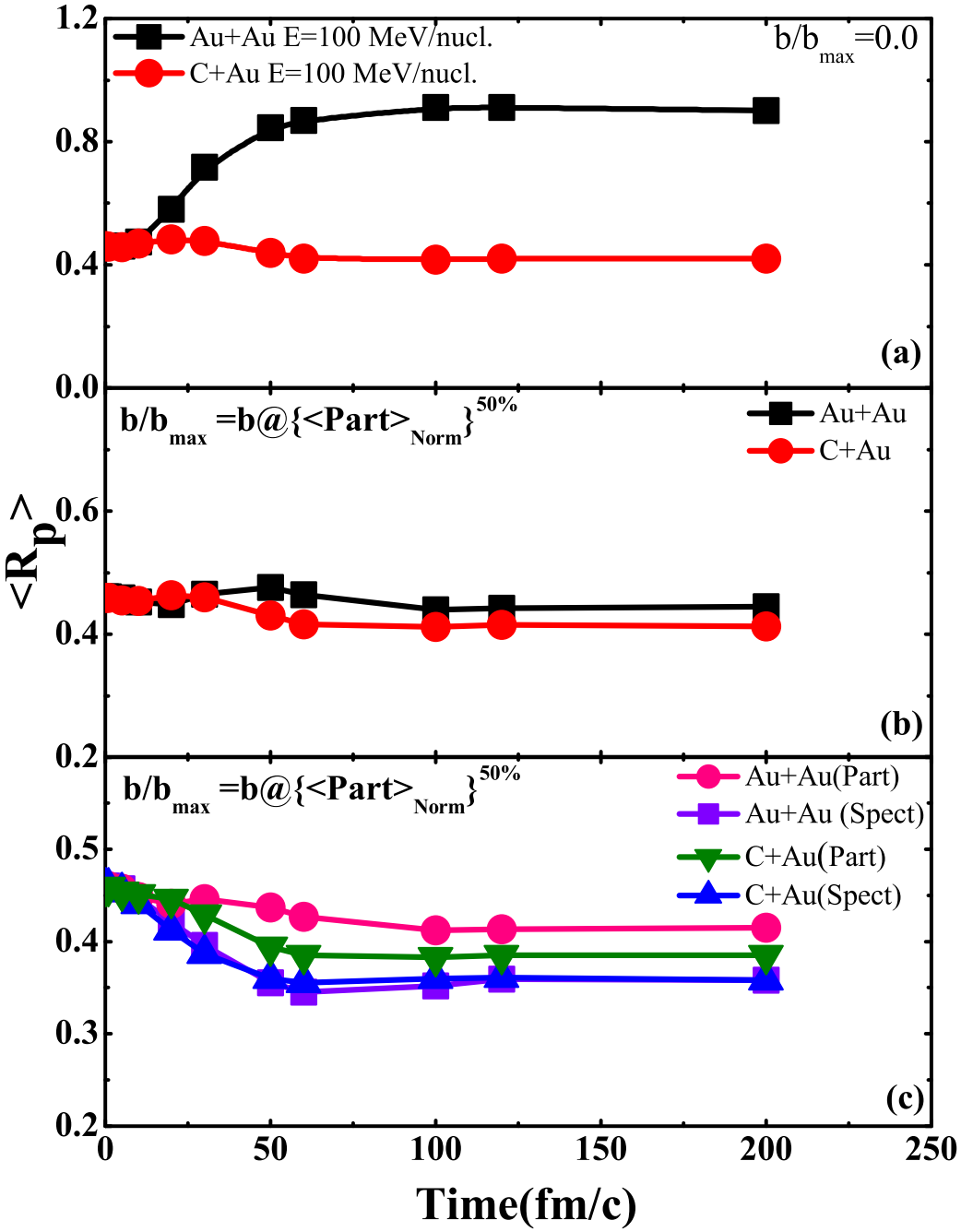


**Figure 5.6:** (a) Time evolution of stopping observable ($< R_p >$) at colliding geometry, $\hat{b} = 0.0$ (b) at colliding geometry $b/b_{max}@< Part >_{Norm} = 50\%$ and (c) colliding geometry $b/b_{max}@< Part >_{Norm} = 50\%$ both for participant and spectator matter for (Au+ Au) and (C + Au).

the system gets rotated. Azimuthal distribution demonstrates the existence of the flow [289]. In the next step, contribution of participant matter and spectator matter is seen for the mass symmetric and mass asymmetric reaction.

In the Fig 5.6 (c) time evolution of stopping observable ($< R_p >$) at impact parameter $b/b_{max}@< Part >_{Norm} = 50\%$ is shown. Participant and spectator part of the highly asymmetric reaction ${}^{12}_{6}C + {}^{197}_{79}Au$, lies in between the participant and spectator part of highly symmetric reaction. One can clearly see from the Fig 5.6 (c), that the value of $< R_p >$, for the participant part of the reaction ${}^{197}_{79}Au + {}^{197}_{79}Au$ is more as compared to the participant part of the reaction ${}^{12}_{6}C + {}^{197}_{79}Au$, and there is a large difference between the participant matter of both the reactions. Spectator part of the reaction ${}^{197}_{79}Au + {}^{197}_{79}Au$ lies below the spectator part of the reaction ${}^{12}_{6}C + {}^{197}_{79}Au$ for initial time steps, but at higher time steps negligible change is seen. Since the total stopping is due to the contribution from participant and spectator nucleons. Thus it has been observed from Fig 5.5 (c), that almost same value of stopping can be achieved if we compensate the mass asymmetry with impact parameter. One can conclude that the mass asymmetry can be compensated with the impact parameter.

## 5.5 Anisotropy as a function of mass asymmetry parameter

In the Fig 5.7, initially, $< R_p >$ is correlated with mass asymmetric reactions for which total system mass is kept fixed ($A_{TOT} = 40, 80, 100, 160, 240$) and for the case when total mass is floating at incident energies E = 50 MeV/nucleon and 200 MeV/nucleon respectively. Secondly, $< R_p >$ is compared with 50% of the participant matter ($b/b_{max}@< Part >_{Norm}$) for two different cases (a) total mass is floating and (b) for total system when mass is kept fixed ($A_{TOT} = 240$). The Fig 5.7, clearly depicts that $< R_p >$ exhibits the similar trend with $\eta$ for both types of mass asymmetric reactions. One can see that at E = 50 MeV/nucleon, the magnitude of $< R_p >$ is larger for the reactions with floating system mass (most equilibrated) as compared to the fixed one (lesser equilibrated). At E = 200 MeV/nucleon the magnitude of $< R_p >$, for the reactions with floating system mass (most equilibrated) varies with the mass asymmetry.

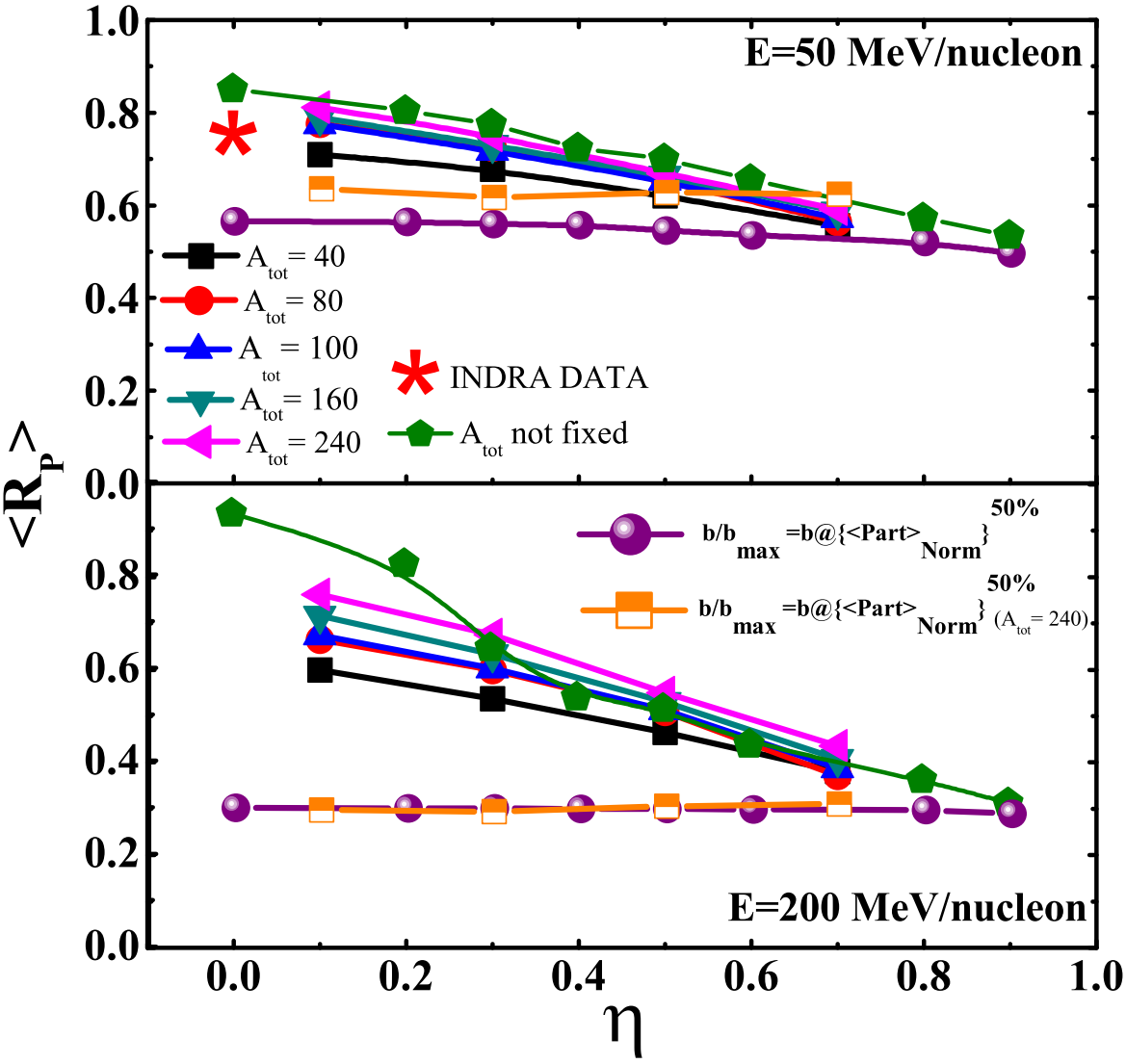


**Figure 5.7:** The anisotropy ratio $< R_p >$ as a function of mass asymmetry parameter for two types of reactions: (a)total mass fixed at incident energy E = 50 MeV/nucleon (b) with total system mass floating at an incident energy E = 200 MeV/nucleon.

The value of nuclear stopping decreases with the increase in the mass asymmetry. In the upper panel least equilibration is there for $A_{TOT} = 40$ which clearly signifies the dependence of $< R_p >$ on the total number of nucleons. This mass dependence of $< R_p >$ is dominating for central impact parameters.

However, when author deals with 50% of the participant matter ($b/b_{max}$@<

$Part >_{Norm}$) for which total mass is floating and total system mass is kept fixed ($A_{TOT} = 240$) at incident energies E = 50 MeV/nucleon and 200 MeV/nucleon, it is found that at lower energies, floating system mass has less stopping as compared to the fixed ($A_{TOT} = 240$) mass system. Total mass in case of floating system is varied from 394 to 209, whereas in fixed mass case, mass is 240. It was already predicted that nuclear stopping increases with increase in number of nucleons, but at low energies due to dominance of strong mean field less stopping is achieved in the case when total mass is floating as compared to the case when total mass is kept fixed when geometry is compensated with 50% of the participant matter ($b/b_{max}@< Part >_{Norm}$). At E = 200 MeV/nucleons, one can clearly see that stopping value remain same even when total mass of the system is kept constant or total mass is floating because at higher energies mean field and nucleon-nucleon collision plays its contribution. Our theoretical simulated results are compared with available INDRA data [111].

## 5.6 Summary

We conclude that mass asymmetry of the reaction (or size of the projectile) has a remarkable influence on the dynamics of the reaction. Thus, while studying various phenomena of heavy-ion reactions at intermediate energies, the mass asymmetry of the reaction should be properly taken into account. However, the mass asymmetry parameter can be compensated with impact parameter. The nuclear reactions with lighter projectile are far from equilibrium and vice versa. The compensation of the geometrical effects helps to achieve an almost similar amount of equilibrium in mass symmetric as well as mass asymmetric reactions. $< R_p >$ is always found to be larger for the reactions with floating system mass (most equilibrated) as compared to the system whose mass is fixed (lesser equilibrated). However the complete equilibrium is absent in both the cases.

# Chapter 6

# Correlation between anisotropic flow and participant nucleons

## 6.1 Introduction

The multiple nucleon-nucleon collisions leads to momentum anisotropy and hence collective flow. The collective flow provides a measure of rescattering in non central collisions. It is basically generated due to the pressure gradient originating from nucleon-nucleon collisions and hence acts as a promising tool to obtain information on the nuclear equation of state. Collective flow is of various types, namely radial flow, directed flow, elliptic flow, triangular flow, quadrangular flow and higher order anisotropic flow. Directed flow is sensitive to the compressibility of highly thermalized nuclear matter. On the other hand elliptic flow can be used to study the influence of isospin degree of freedom on reaction dynamics. The higher order components of anisotropic flow are important to understand the scaling, i.e., the relationship between the momentum of nucleons constituting the fragments [290]. A large number of attempts have been made both theoretically and experimentally [16,17,162,167,175,291] to study the collective flow. The first harmonics i.e., directed flow is sensitive towards compressibility of highly thermalized nuclear matter, whereas the second harmonics i.e., elliptical flow can be used to investigate the influence of isospin degree of freedom on reaction dynamics. The higher order components of anisotropic flow are important to understand the scaling. It has been observed that collective transverse flow is dependent on the system size [257], incident energy [16,17], colliding geometry [137,140,141]

and isospin content of the colliding nuclei [262, 263]. Mathematically, anisotropic flow can be defined as the different $n^{th}$ harmonic coefficient $v_n$ of an azimuthal Fourier expansion of the particle invariant distribution [73].

$$\frac{dN}{d\phi} \propto [1 + 2\sum_{n=1}^{\infty} v_n \cos(n\phi)] \tag{6.1}$$

where $\phi$ is the azimuthal angle between the transverse momentum of the particles and the reaction plane. The first harmonic coefficient $v_1$ represents the directed flow, second harmonic coefficient $v_2$ represents elliptic flow, third harmonic coefficient $v_3$ represents triangular flow and fourth harmonic coefficient $v_4$ represents the quadrangular flow respectively and are represented by following equations [292]:

$$v_1 = \langle \cos\phi \rangle = \langle \frac{p_x}{p_t} \rangle \tag{6.2}$$

$$v_2 = \langle \cos 2\phi \rangle = \langle \frac{p_x^2 - p_y^2}{p_t^2} \rangle \tag{6.3}$$

$$v_3 = \langle \cos 3\phi \rangle = \langle \frac{p_x^3 - 3p_x p_y^2}{p_t^3} \rangle \tag{6.4}$$

$$v_4 = \langle \cos 4\phi \rangle = \langle \frac{p_x^4 - 6p_x^2 p_y^2 + p_y^4}{p_t^4} \rangle \tag{6.5}$$

where, $p_x$ and $p_y$ are the projection of nucleons momentum both parallel as well as perpendicular to the reaction plane respectively and $p_t = \sqrt{p_x^2 + p_y^2}$ is the transverse momentum.

## 6.2 Different Harmonics

Anisotropic flow is the flow corresponding to the first two harmonics derived from equation no. (6.1), and is known either directed flow or elliptic flow. Anisotropic flow plays a very important role in heavy-ion collision dynamics. Nuclear mean field produces two effects at low incident energies:

• First projectile nucleons are allowed to deflect towards the target and therefore called as negative directed flow [293].

• The projectile and target forms a rotating system which leads to particle formation

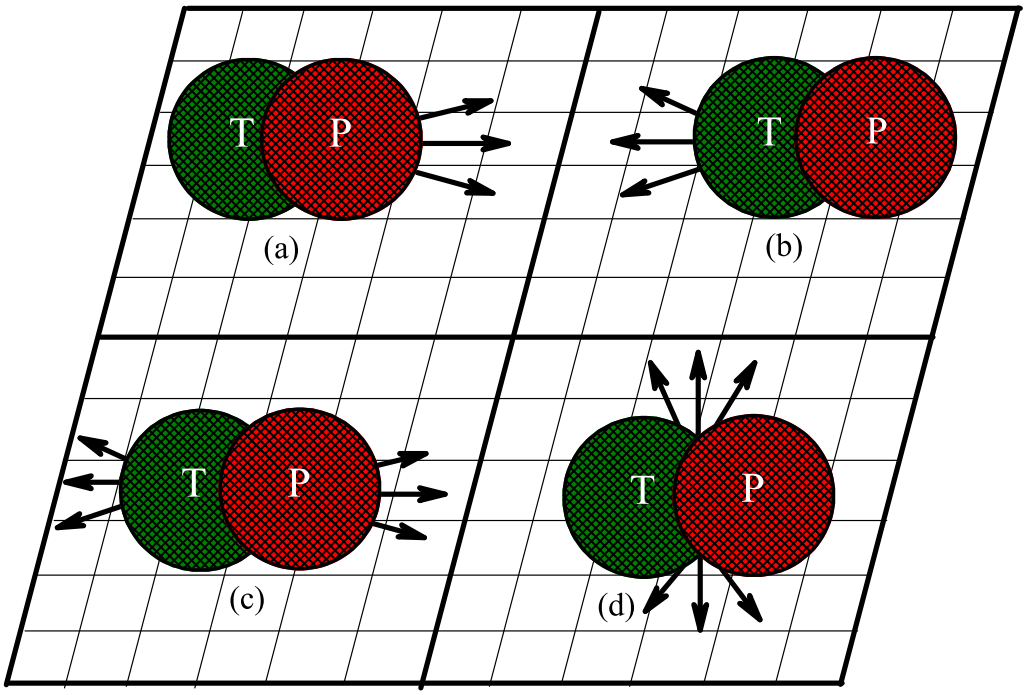


**Figure 6.1:** Azimuthal anisotropy viewed in the transverse plane. Directed flow on the projectile side of mid-rapidity, (a) positive and (b) negative. Bottom panel shows (c) elliptic flow in-plane or positive and (d) out-of-plane or negative.

and in-plane elliptic flow [294–296].

At higher incident energies, due to nucleon-nucleon collisions:

• The projectile and target are deflected apart from each other due to generated positive pressure and corresponds to positive directed flow.

• The projectile and target overlap each other and participant region which is compressed and spectator nucleons producing out-of-plane negative elliptic flow [83].

It is worth mentioning here that both directed and elliptic flow are significant observables for studying the intermediate energy heavy ion collision dynamics. The directed flow which is also known as in-plane or sidewards flow refers to the preferential emission of particles within and to a particular side of the reaction plane as shown in the Fig

6.1 (a and b). In the Fig 6.1 (c and d), in-plane and out-of-plane elliptic flow is shown. In the Fig 6.1 T denotes target and P denotes projectile.

### 6.2.1 Directed flow

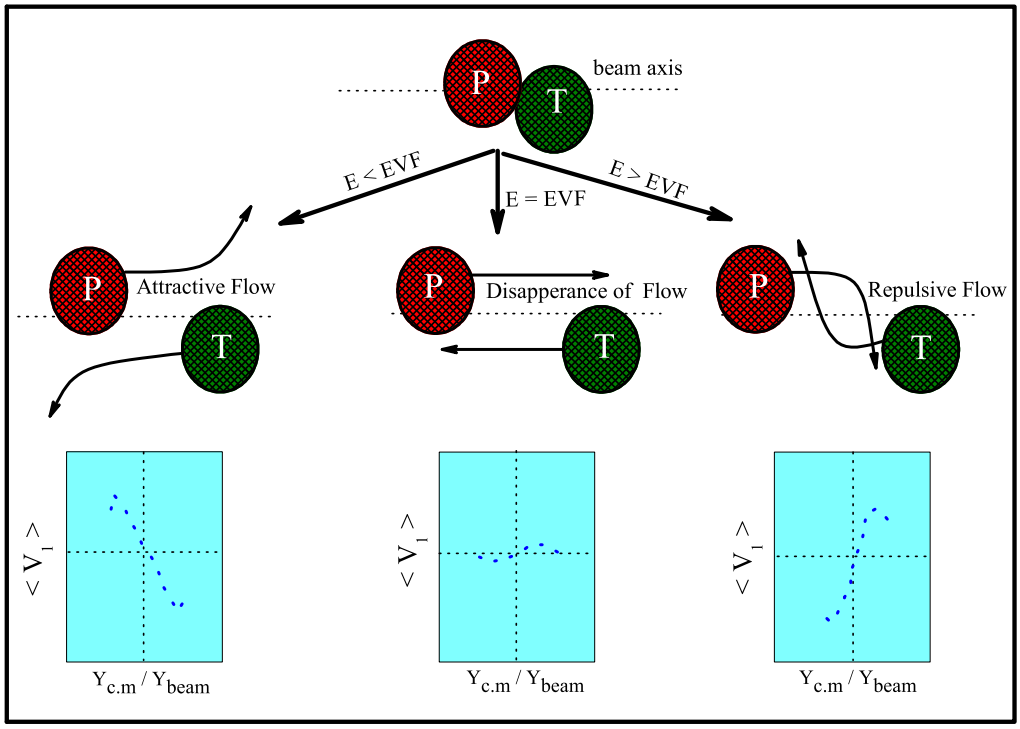


**Figure 6.2:** Pictorial view of the energy dependence of directed flow.

A significant information about the radial and directed flow could be revealed from the anisotropy of the particles [73]. It was experimentally observed that the mean transverse momentum changes its sign from negative to positive as the bombarding energy is increased above 100 MeV/nucleon [297]. Nuclear interactions are mostly dominated at lower incident energy due to attractive mean field and therefore deviating the particles towards the negative angles [298]. At intermediate energy the nucleons mean field and nucleon-nucleon scattering starts dominating and the particles are emitted towards the positive angles [299]. The attractive interactions are balanced at a certain energy with repulsive interactions, therefore net transverse flow vanishes. Such incident energy is

termed as the energy of vanishing flow (EVF) or balance energy ($E_{bal}$) [59]. A schematic illustration of directed flow is given in Fig 6.2. At higher incident energies particles are forced to move in forward hemisphere making in-plane flow positive. Extensive efforts have been made in the last few years to understand the diminishing of flow and to measure the balance energy. The study of balance energy have been made by varying the impact parameter and over a wide range of masses by various researchers in the past.

### 6.2.2 Elliptic flow

The elliptic flow which is basically an output of the counter-balancing force between the spectator matter and the expansion of the participant matter is found to saturate earlier in case of heavier fragments in contrast to the case of lighter ones [123]. This may be due to slower movement of the heavier fragments which consists of large number of nucleons moving collectively with respect to each other. There is a cogent and convincing divergence between the elliptic flow associated with free nucleons to the nucleons which are bounded and moves collectively forming a cluster of fragments.

Fig 6.3 shows two different signatures of the elliptic flow:

• The in plane bounce-off [300] flow caused by the compressed matter.

• The squeeze-out [301] flow of the participant matter perpendicular to the reaction plane.

Fig 6.4 illustrates the formation of the compressed region in a non-central nuclear collisions and the subsequent emission of particles from the participant (mid-rapidity) region.

## 6.3 Results and discussion

In this chapter complete systematic study of balance and transition energies for the collision of nearly symmetric nuclei i.e., for the reactions $^{197}_{79}Au + ^{197}_{79}Au$, $^{150}_{60}Nd + ^{150}_{60}Nd$, $^{131}_{54}Xe + ^{118}_{50}Sn$, $^{100}_{40}Zr + ^{100}_{40}Zr$, $^{58}_{28}Ni + ^{58}_{28}Ni$, and $^{40}_{18}Ar + ^{45}_{21}Sc$ have been undertaken. The whole impact parameter has been divided into seven bins - BIN(I), BIN(II), BIN(III), BIN(IV), BIN(V), BIN(VI) and BIN(VII) i.e., $0 < \hat{b} \leq 0.28$, $0.28 < \hat{b} \leq 0.39$, $0.39 <$

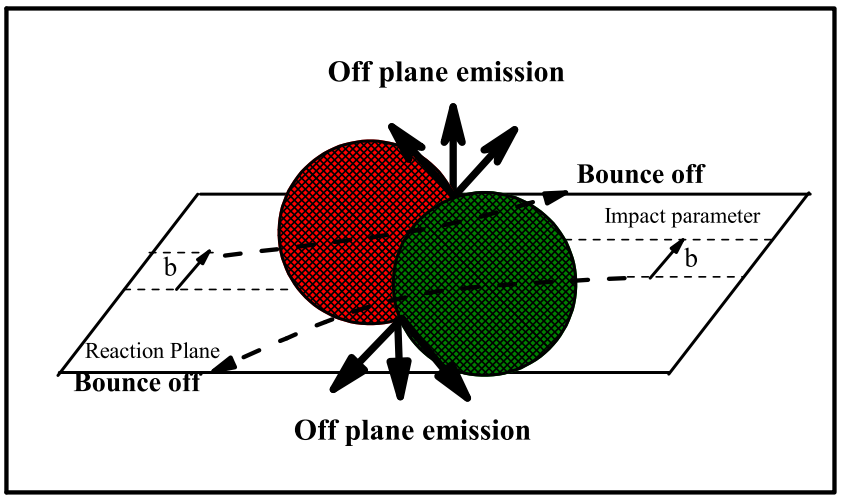


**Figure 6.3:** In-plane bounce-off caused by compression and squeeze-out caused by enhanced emission of light particles perpendicular to plane close to mid-rapidity.

$\hat{b} \leq 0.48$, $0.48 < \hat{b} \leq 0.56$, $0.56 < \hat{b} \leq 0.62$, $0.62 < \hat{b} \leq 0.76$ and $0.76 < \hat{b} \leq 0.88$, respectively, where $\hat{b} = b/b_{max}$ with $b_{max} = 1.12(A_1^{1/3} + A_2^{1/3})$. The impact parameter bins selection is based on the constraints laid by the experimental measurements [137]. To study the transverse momentum dependence of nuclear flow, we have divided the entire rapidity into bins, where rapidity is defined as [60]

$$Y_i = \frac{1}{2} \ln \frac{(E(i) + P_z(i)c)}{(E(i) - P_z(i)c)} \tag{6.6}$$

where E(i) and $P_z(i)$ are the energy and longitudinal momentum of the $i^{th}$ nucleon, respectively. The region (-0.1 < $Y_{c.m.}/Y_{beam}$ < 0.1) is identified as mid-rapidity region. Where, the region ($Y_{c.m.}/Y_{beam}$ < -0.1) is define as target like (TL) matter and ($Y_{c.m.}/Y_{beam} > 0.1$) recognized as projectile like (PL) matter.

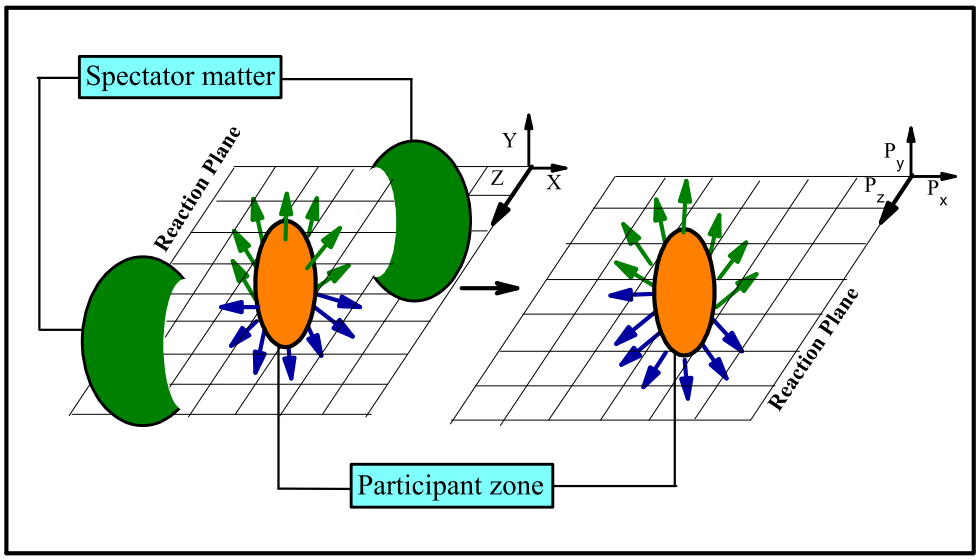


**Figure 6.4:** Non-central collision of two nuclei results in the formation of almond shaped volume. The spatial anisotropy with respect to the X-Z plane (reaction plane) translates into a momentum anisotropy of the produced particles (anisotropic flow).

## 6.4 Rapidity dependence of directed flow

In the Fig 6.5 directed flow ($< v_1 >$) has been displayed as a function of the rapidity for the reaction ${}^{197}_{79}Au + {}^{197}_{79}Au$. The variation of ($< v_1 >$) with $Y_{c.m.}/Y_{beam}$ leads to a well-known S-shape [16], usually deduced with linear fits and is termed as reduced flow. As the incident energy increases the number of nucleon-nucleon collisions increases, resulting into drifting of nucleons in a direction, transverse to the beam direction and thereby affecting the directed flow. The nucleons are drifted along the positive angles at higher incident energies and towards negative angles at lower incident energies. The directed flow is influenced by Coulomb interactions as well as symmetry potential. The repulsive Coulomb interactions increases with peak value of $< v_1 >$ for protons as compared to neutrons [302]. The influence of symmetry energy is found to be small at lower energies. At the incident energies lower than balance energy [303, 304], most of the collisions are suppressed due to Pauli blocking. When incident energy is more than

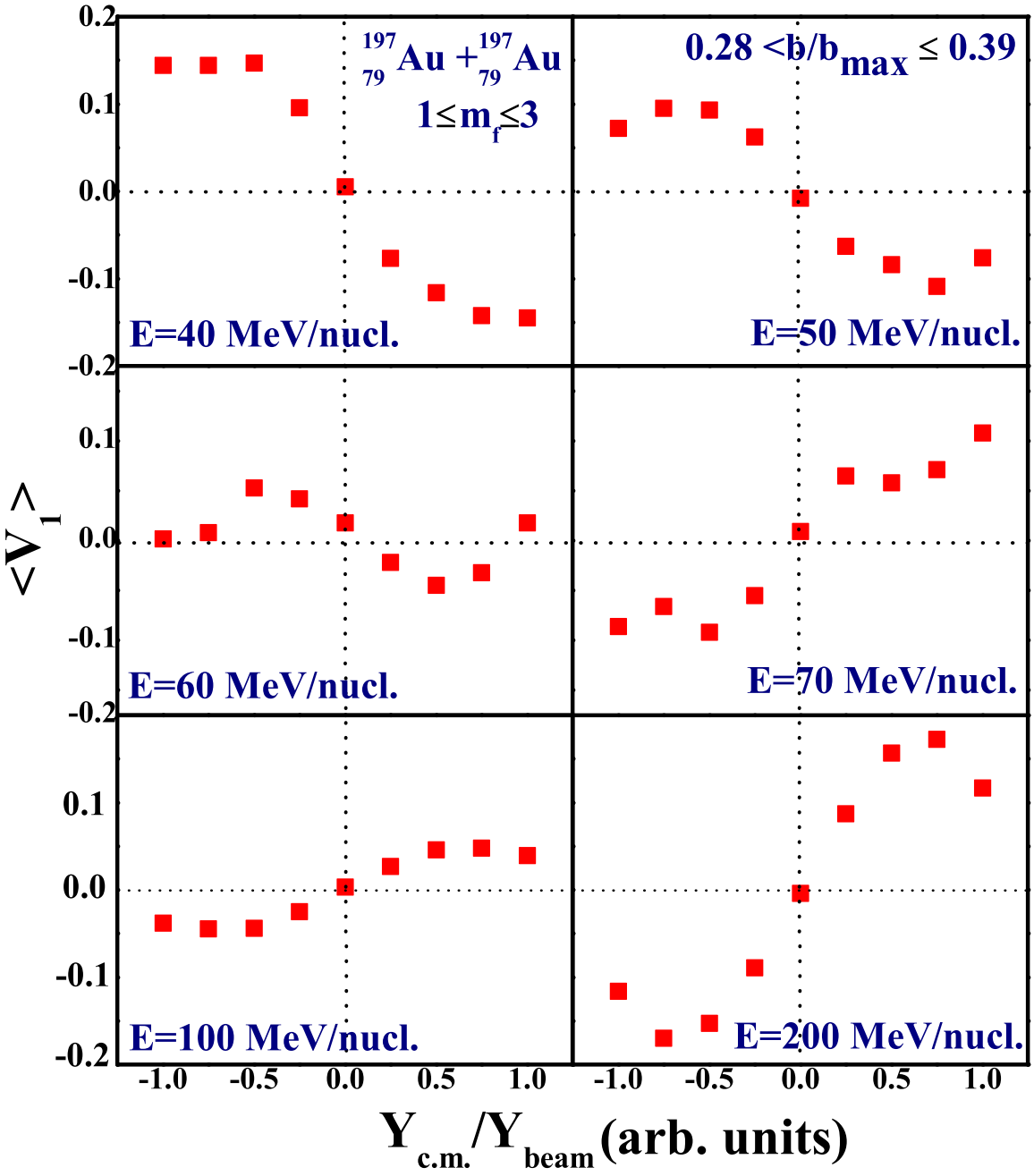


**Figure 6.5:** Rapidity dependence of directed flow observable ($< v_1 >$) for the reaction $^{197}_{79}Au +^{197}_{79} Au$ at a scaled impact parameter $\hat{b}$ = 0.28 - 0.39 and incident energy varying from 40 to 200 MeV/nucleon.

balance energy, both the mean field and the nucleon-nucleon collisions simulate to a remarkable position and one can observe a positive slope. From the Fig 6.5, one can observed that the slope of the directed flow shows transition from negative to positive.

## 6.5 Rapidity dependence of elliptic flow

In the Fig 6.6, author has displayed the variation of elliptic flow ($< v_2 >$) with rapidity $Y_{c.m.}/Y_{beam}$. At low incident energy i.e., E = 50 MeV/nucleon, elliptic flow is positive and one observes a Gaussian shape around mid-rapidity region [16,17,168]. At a certain incident energy, the value of $< v_2 >$ becomes zero i.e., the distribution of nucleons is isotropic in nature. As the incident energy further increases ($< v_2 >$) become negative. The negative value of elliptic flow in the mid rapidity region is the outcome of influential nucleon-nucleon fling counting squeeze-out and shadowing effects. A Gaussian shaped behavior is observed in elliptic flow and this behavior is quite similar to the one obtained by Colona and Toro et al. [258].

## 6.6 Transverse momentum dependence of anisotropic flow

In the Fig 6.7, anisotropic flow as a function of transverse momentum for the system ${}^{197}_{79}Au + {}^{197}_{79}Au$ has been displayed. Higher flow harmonics like triangular flow and quadrangular flow becomes gradually smaller than directed flow and elliptical flow with increase in transverse momentum [290]. Consequently, magnitudes of $< v_1 >$ is higher than $< v_2 >$, $< v_3 >$ and $< v_4 >$. The different $v_n$ harmonics have different dependency on transverse momentum ($p_t$). At low value of transverse momentum ($p_t < 0.4GeV/c$), directed flow ($< v_1 >$) shows highest magnitude as compared to the other higher-order harmonics. It is further perceived that initially all the four types of flow i.e., directed flow, elliptical flow, triangular flow and quadrangular flow have positive value and increases with transverse momentum ($p_t$) and then attains a maxima at a particular transverse momentum thereafter there is subsequent fall in flow with

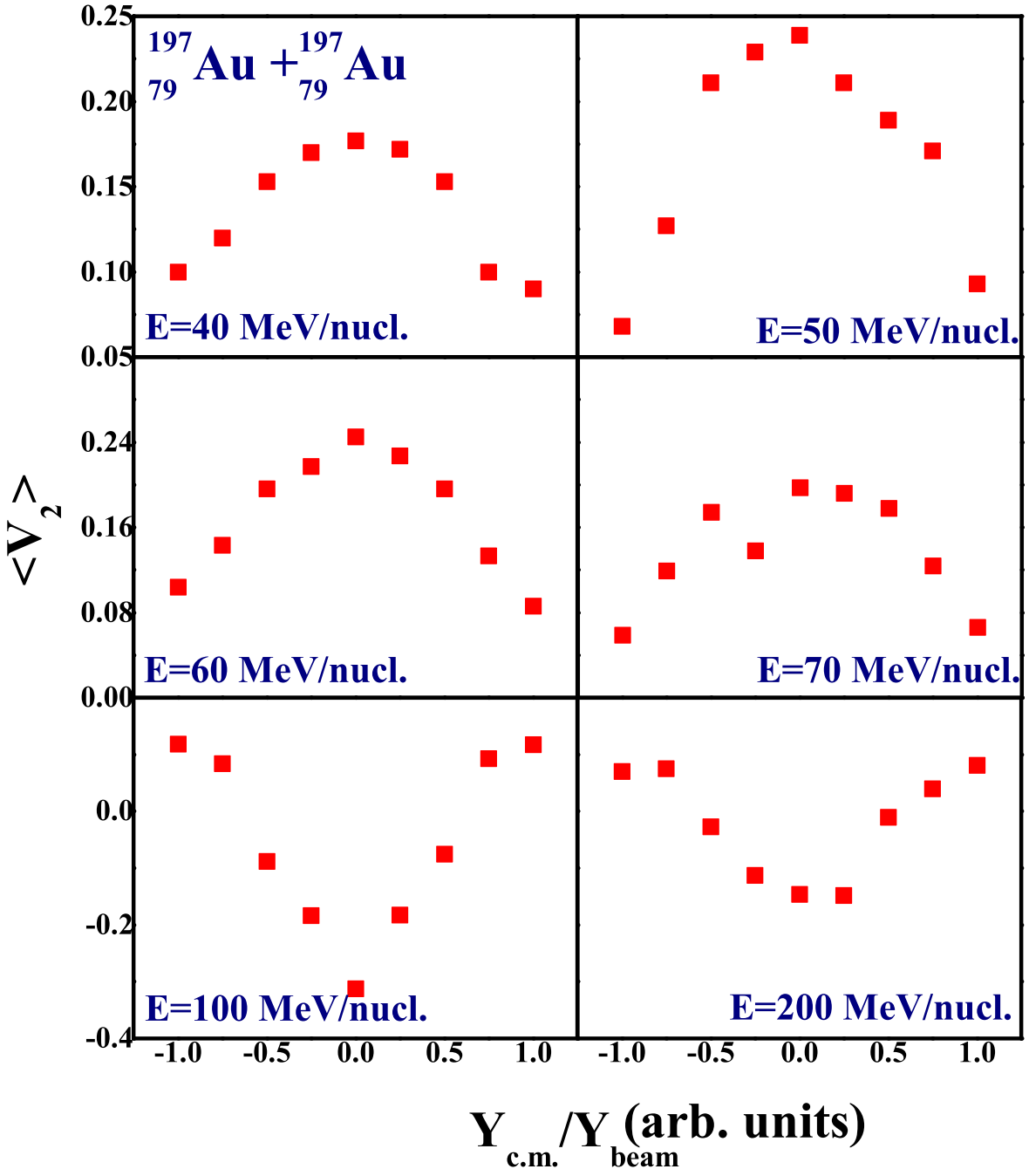


**Figure 6.6:** Rapidity dependence of elliptical flow ($< v_2 >$) for the reaction ${}^{197}_{79}Au + {}^{197}_{79}Au$ at scaled impact parameter of $\hat{b} = 0.28$ - 0.39 and an incident energy from 40 to 200 MeV/nucleon.

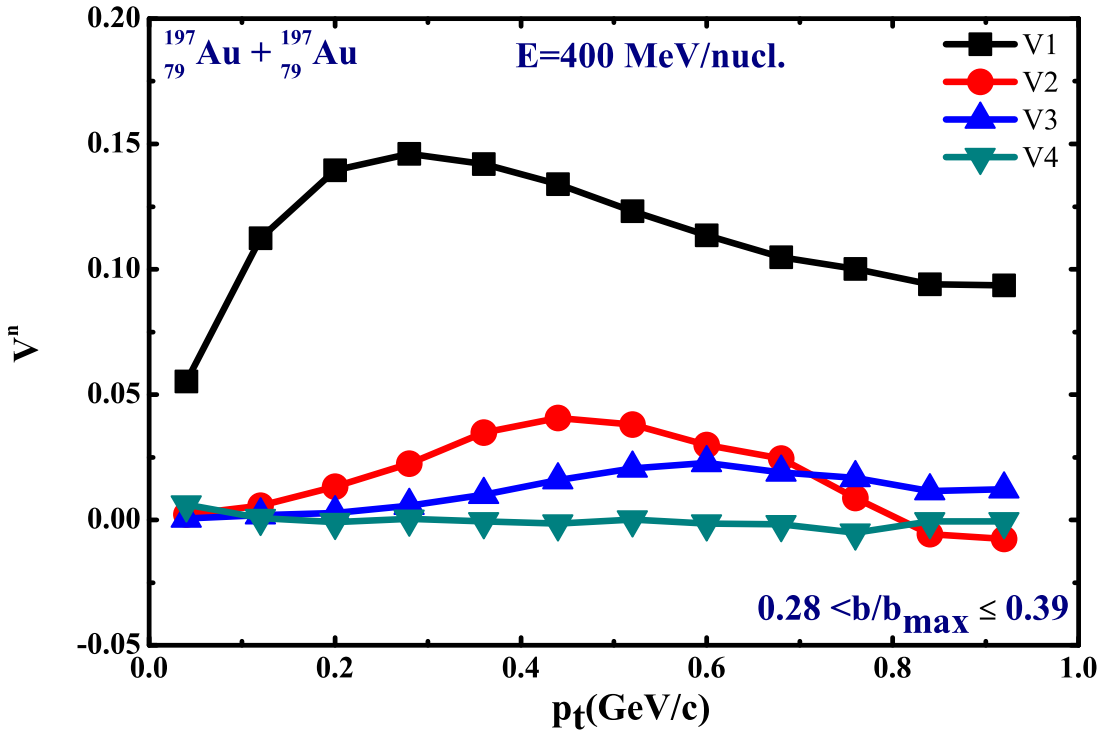


**Figure 6.7:** Anisotropic flow as a function of transverse momentum ($p_t$) for the reaction $^{197}_{79}Au +^{197}_{79} Au$ at a scaled impact parameter $\hat{b}$ = 0.28 - 0.39 and at an incident energy of 400 MeV/nucleon.

increasing transverse momentum ($p_t$).

### 6.6.1 Phase space analysis of anisotropic flow

In the Fig 6.8, we have displayed three-dimensional view of directed flow $< v_1 >$ in momentum space for the specified transverse momentum range $0.2 < p_t < 0.3$ (GeV/c) at centrality $0.28 < \hat{b} \leq 0.39$ using incident energy of 400 MeV/nucleon. Nucleons represented within the circle are those nucleons which participate in the directed flow. Similarly, in the Fig 6.9, three-dimensional view of elliptic flow has been displayed and nucleons which participate in the elliptic flow form elliptic shape. Identical studies have been performed for the triangularity and triangular flow. In the Fig 6.10, three dimensional view of the triangular flow for momentum range $0.4 < p_t < 0.5$ GeV/c, has been displayed. We have joined the lines in such a way so that particle lies maximum within the triangular region. In the Fig 6.11, quadrangular flow is displayed. The

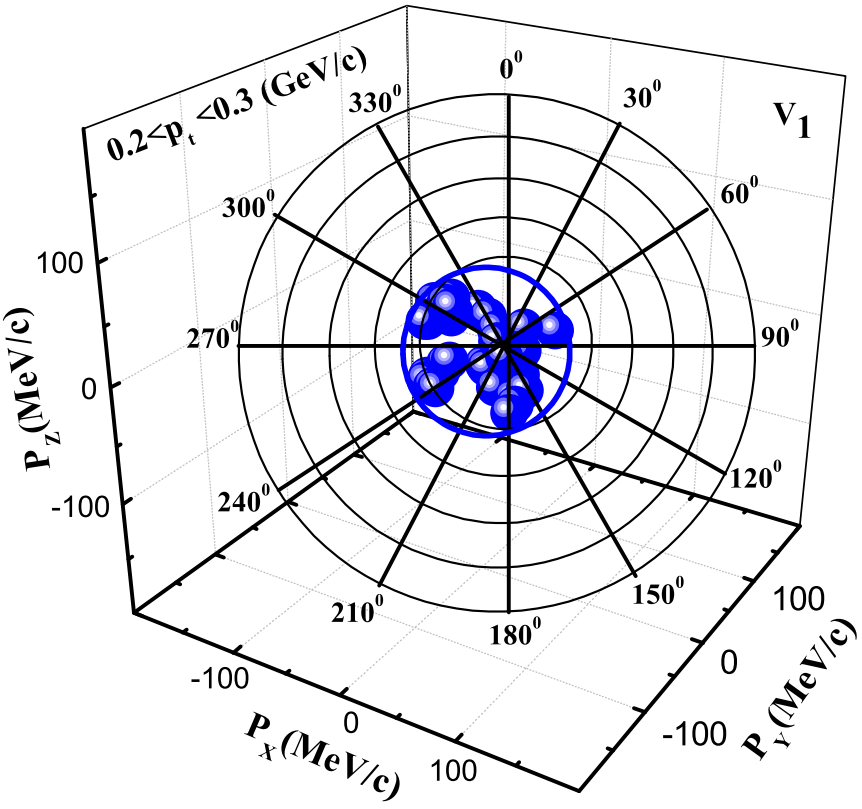


**Figure 6.8:** Three-dimensional view of directed flow $< v_1 >$, in momentum space for the transverse momentum range $0.2 < p_t < 0.3$ (GeV/c) at centrality $0.28 < \hat{b} \leq 0.39$ for fixed value of incident energy 400 MeV/nucleon.

anisotropic flow can be studied as the transverse momentum and demonstrated to be a very promising tool for elucidating flow and useful to understand reaction dynamics of nucleons.

### 6.6.2 Three-dimensional view of elliptic flow

In the Fig 6.12, we have displayed three-dimensional view of elliptic flow $< v_2 >$ at impact parameter $0.28 < \hat{b} \leq 0.39$ and for fixed value of incident energy 400 MeV/nucleon. Nucleons represented within the circle are those nucleons which participate in the elliptic flow and forms ellipsoidal shape. Author has rotated the central part of three-

dimensional Figure through the various angles, it is observed that only the orientation of the elliptic flow changes but the distribution remains same.

## 6.7 Balance and transition energy as a function of impact parameter

It would be interesting to see the dependence of balance and transition energy on the impact parameter of the nuclear reaction. In the Fig 6.13, author has made a systematic investigation of the directed as well as elliptic flow for Z = 1 and Z = 2 particles for different reactions. The observed values of $E_{bal}$ and $E_{trans}$ are shown at the higher side

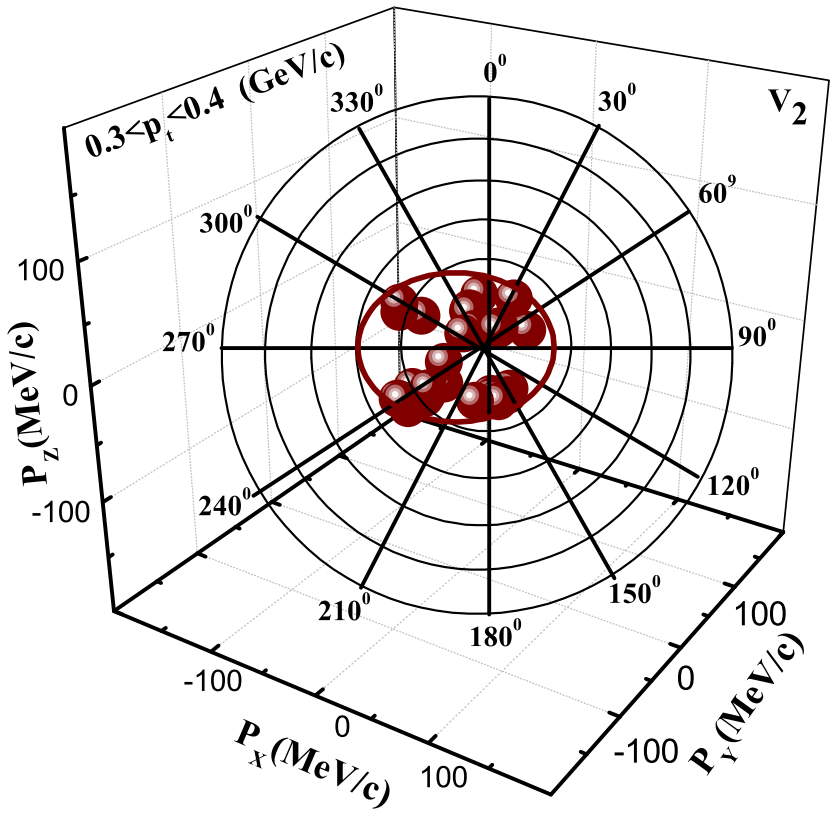


**Figure 6.9:** Three-dimensional view of elliptic flow $< v_2 >$, in momentum space for the transverse momentum range $0.3 < p_t < 0.4$ (GeV/c) at centrality $0.28 < \hat{b} \leq 0.39$ using incident energy 400 MeV/nucleon.

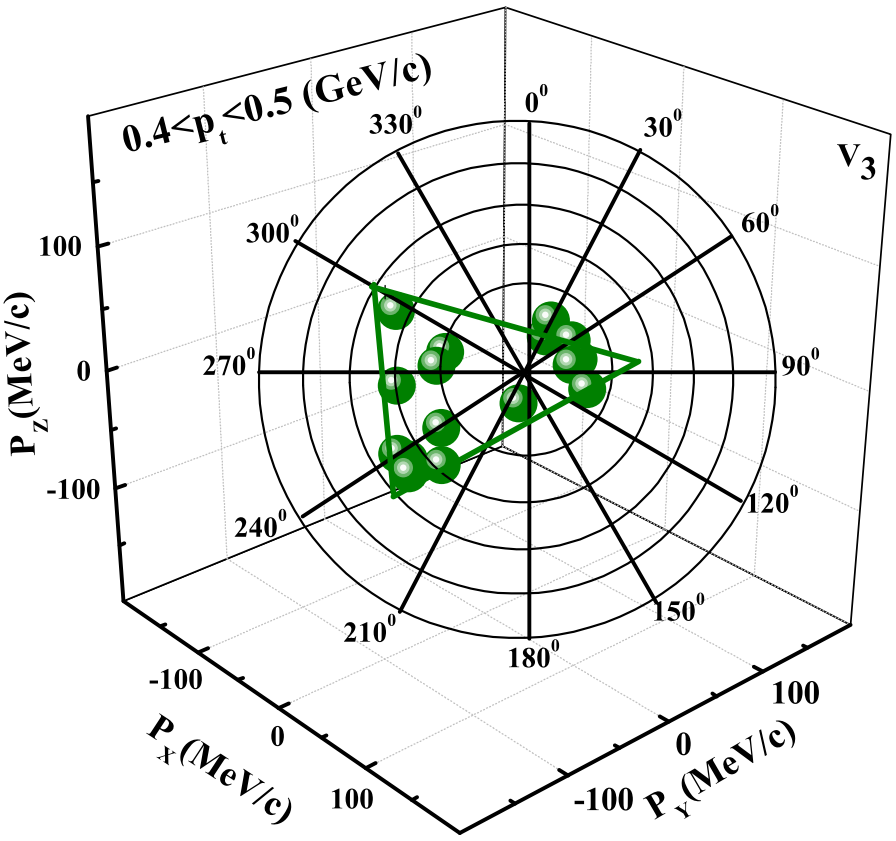


**Figure 6.10:** Three-dimensional view of triangular flow $< v_3 >$, in momentum space for the transverse momentum range $0.4 < p_t < 0.5$ (GeV/c) at centrality $0.28 < \hat{b} \leq 0.39$ using incident energy 400 MeV/nucleon.

of each impact parameter bin. For each curve, slope has been calculated. The value of $\tau_{E_{bal}}$ for different reactions over the whole colliding geometry is found to vary from $\tau = +0.80$ to $\tau = +1.22$. The values of slope of $E_{trans}$ varies from $\tau = +0.55$ to $\tau = +0.89$ for different masses [306].

It has been observed that the role of Coulomb repulsion increases with an increase in the impact parameter of the reaction [263]. The influence of symmetry energy on $E_{bal}$ is uniform for the mass range at all the impact parameters. This is due to decrease in participant zone in peripheral collisions that decreases the extent of nucleon-nucleon collisions and as a result higher energy is vital to overthrow the attractive nuclear forces. As a result the effect of Coulomb repulsion in the heavier system will increase

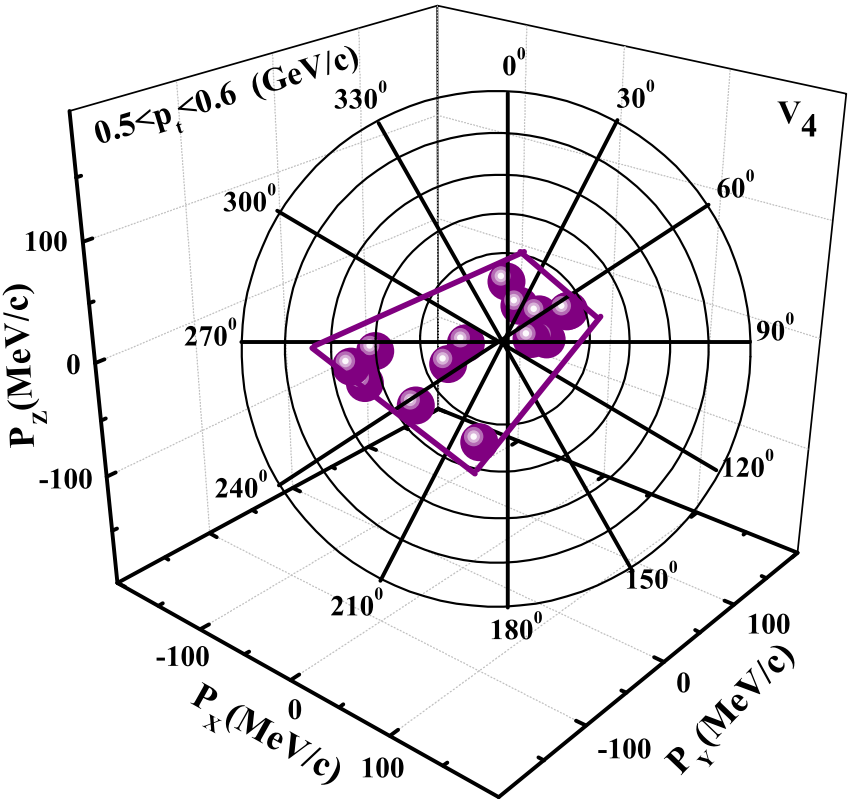


**Figure 6.11:** Three-dimensional view of quadrangular flow $< v_4 >$, in momentum space for the transverse momentum range $0.5 < p_t < 0.6$ (GeV/c) at centrality $0.28 < \hat{b} \leq 0.39$ using incident energy 400 MeV/nucleon.

with impact parameter. In the Fig 6.13, author has compared the theoretical results with the experimental data [17,137,140,141,305]. One can therefore concludes that at the transition energy system achieves higher density. Therefore, elliptic flow is more appropriate and desirable tool to study the equation of state and influence of isospin content of the colliding nuclei.

## 6.8 System mass dependence

In the Fig 6.14, the balance energy and transition energy are plotted as a function of system mass. As the system mass increases the balance as well as transition energies are found to decreases. Inference can be made from the graph that the balance and

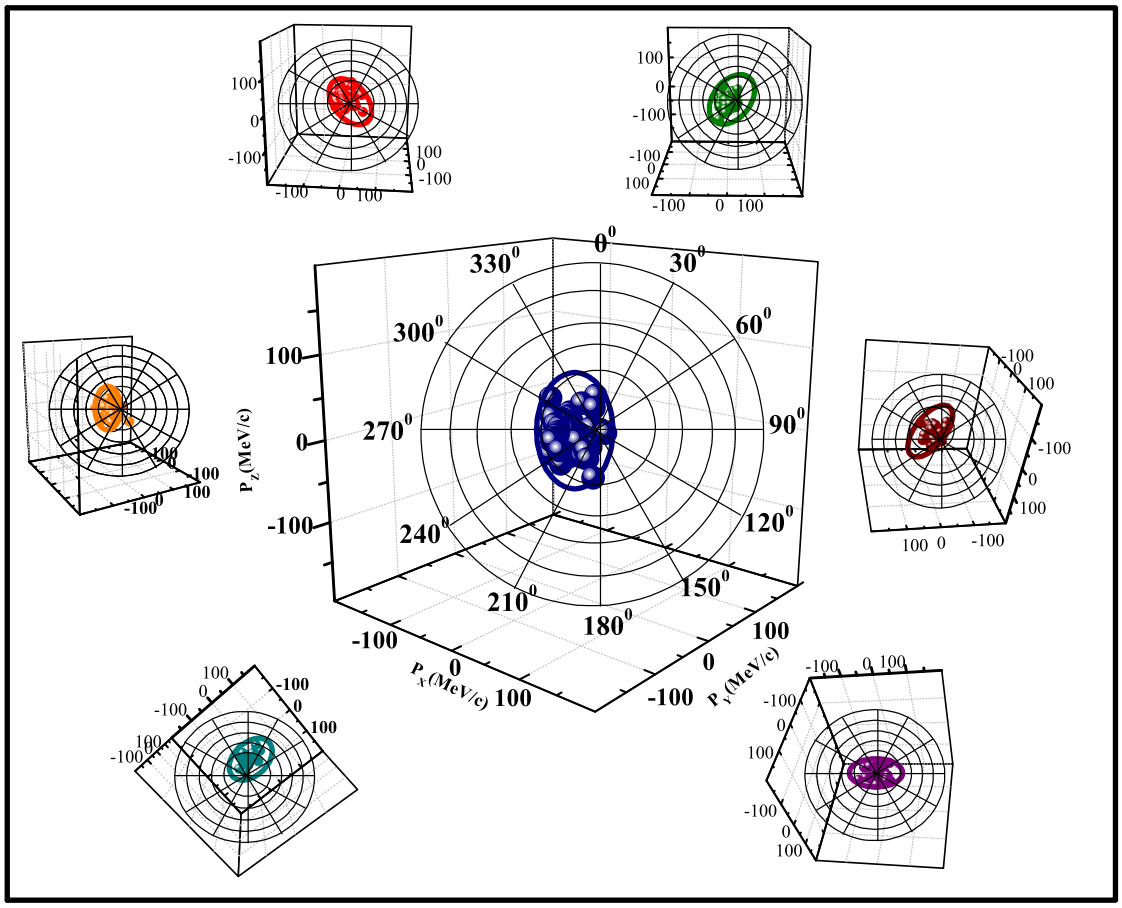


**Figure 6.12:** Three-dimensional view of elliptic flow $< v_2 >$, at impact parameter $0.28 < \hat{b} \leq 0.39$ at an incident energy E = 400 MeV/nucleon.

transition energies for Z = 1 particles is greater than that for Z = 2 particles because the net momentum associated with heavier fragments is more as compared to lighter one because Coulomb repulsive interactions plays a dominant role over the symmetry energy at energies near the balance energy [307]. Curves corresponding to Z = 1 and Z = 2 have been fitted using power law. The value of the slopes for $E_{bal}$ are $\tau_{z_1} = -0.39$ and $\tau_{z_2} = -0.34$ respectively. With the increase in incident energy the influence of Coulomb interactions decreases and significant role of symmetry energy starts dominating. Also, Pauli blocking is very less at energies close to transition energies. It has been reported [123] that symmetry energy influence the elliptical flow strongly as compared to Coulomb interactions. In another work it has been reported that transition

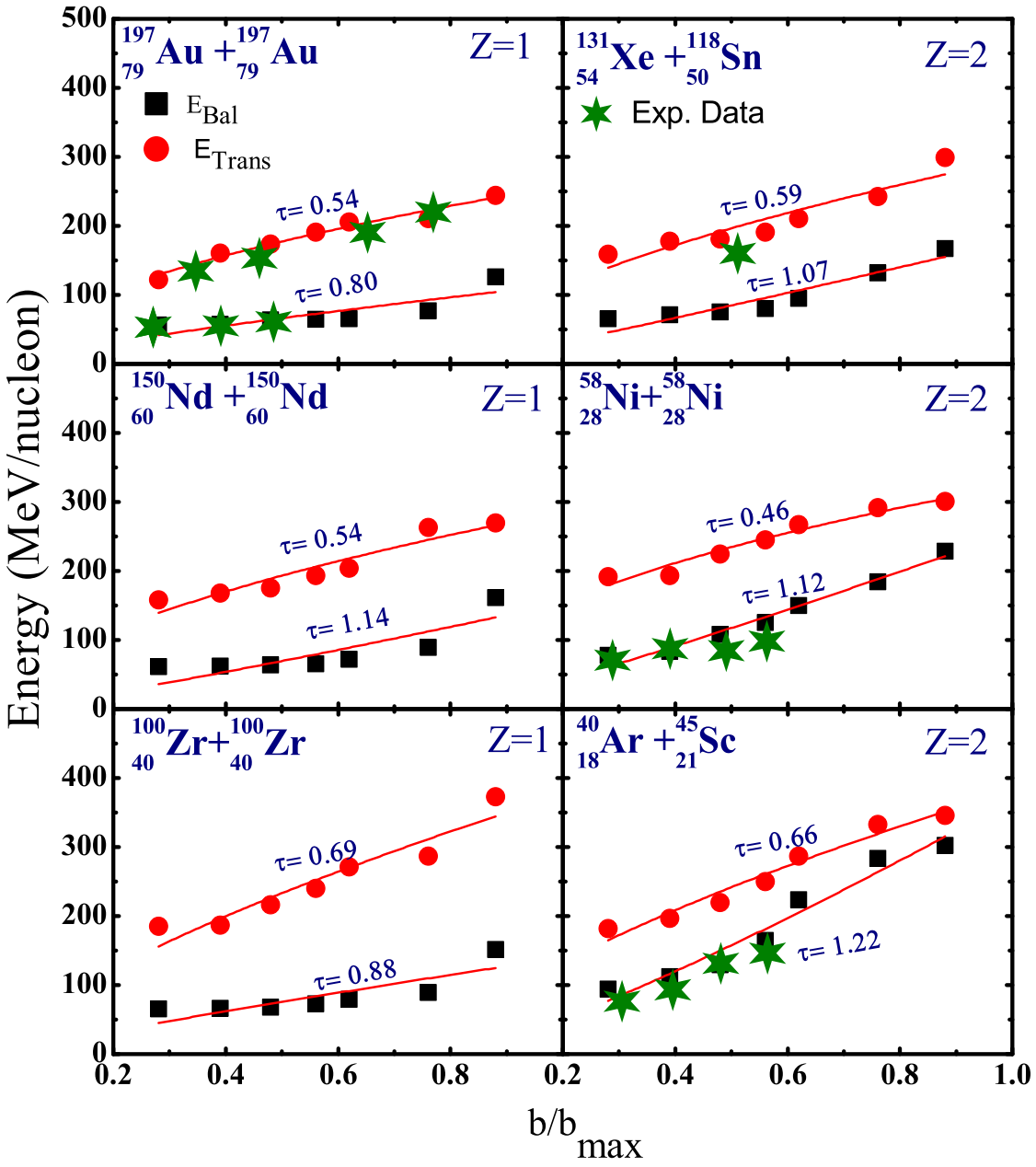


**Figure 6.13:** Energy as a function of scaled impact parameter for the reactions $^{197}_{79}Au +^{197}_{79} Au$, $^{150}_{60}Nd +^{150}_{60} Nd$, $^{131}_{54}Xe +^{118}_{50} Sn$, $^{96}_{40}Zr +^{96}_{40} Zr$, $^{58}_{28}Ni +^{58}_{28} Ni$, and $^{40}_{18}Ar +^{45}_{21} Sc$.

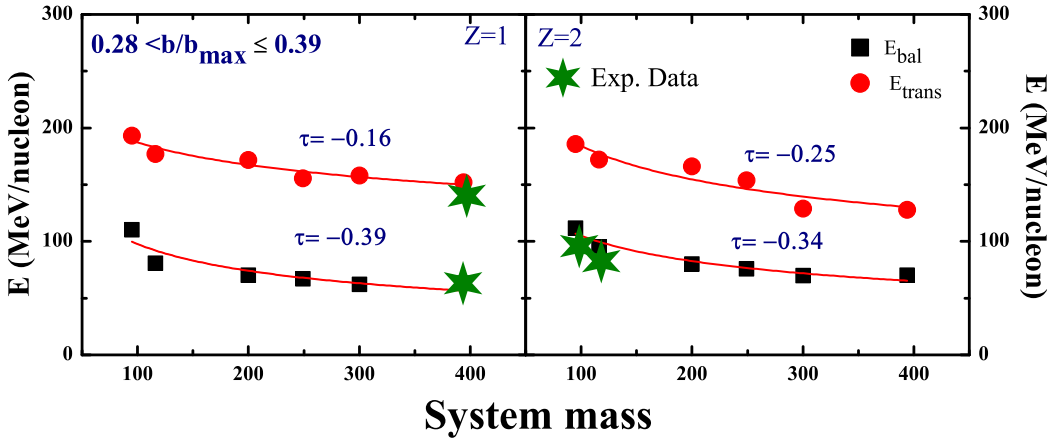


**Figure 6.14:** The variation of balance energy ($E_{bal}$) and transition energy ($E_t$) as a function of system mass.

energy remains almost independent of isospin contents of the colliding nuclei [308], but does depend on the isospin dependence of nucleon-nucleon cross section. The power law equation fits for transition energy curves of Z = 1 and Z = 2 particles and having slope $\tau_{z_1} = -0.16$ and $\tau_{z_2} = -0.25$ respectively. If we compare the slope of $E_{bal}$ with $E_{trans}$, one can see that $E_{bal}$ decreases faster as compared to $E_{trans}$ for the combined system mass. This is due to the nonlinear behavior of Coulomb repulsive interactions at lower incident energies than that of symmetry potential at higher incident energies.

## 6.9 Influence of isospin content on reaction dynamics

Another feature associated with transition energy calculations is to explore the isospin effects. Elliptic flow can be divided into contributions gained due to neutrons and protons. For the calculations of elliptic flow neutron and proton, isospin dependent cross section has been used, where $\sigma_{np} = 3\sigma_{nn} = 3\sigma_{pp}$. While calculating the elliptic flow for protons and neutrons, interactions among nn and pp has been taken into account. In Fig 6.15, the difference between the elliptic flow ($< v_2 >$) due to protons

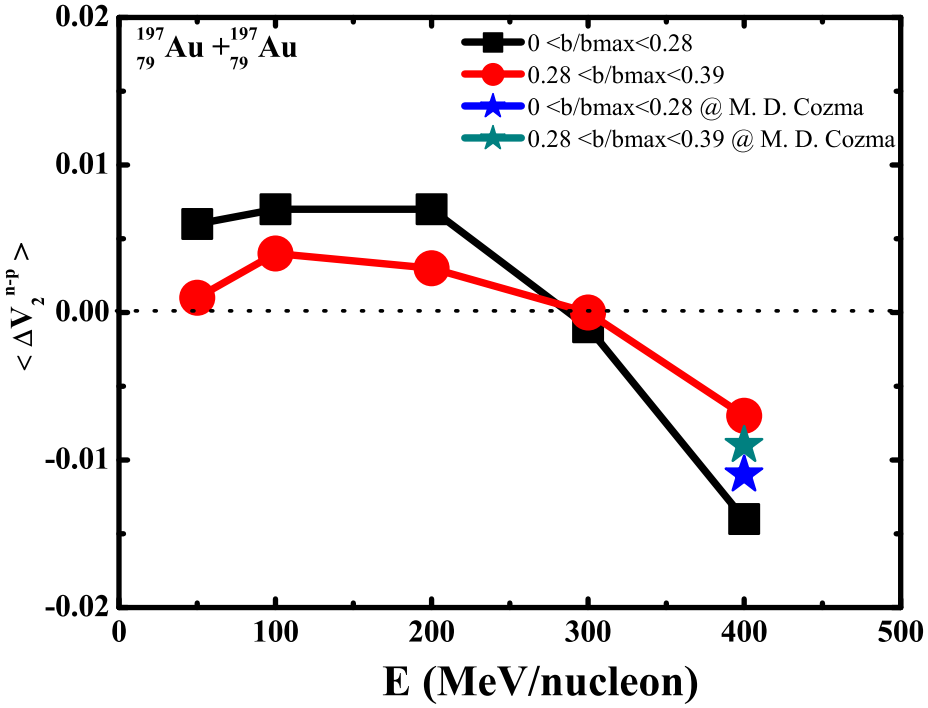


**Figure 6.15:** Relative change in elliptic flow due to protons and neutrons as a function of Incident energy for the reaction $^{197}_{79}Au +^{197}_{79} Au$ at t = 200 fm/c.

and neutrons have been shown by employing two different impact parameter bins. The difference of elliptic flow associated with neutron and proton becomes negative above 320 MeV/nucleon. The averaged change $\langle \triangle\ {v_2}^{n-p} \rangle = \langle {v_2}^n \rangle$ - $\langle {v_2}^p \rangle$ i.e., the change in the elliptical flow for neutrons and protons have been calculated. The difference is more at lower impact parameter and reduces at higher value of impact parameter, because less number of nucleons participating in flow at peripheral collisions as compared to central one. Therefore behavior of $\langle {v_2}^n \rangle$ is expected to be similar to $\langle {v_2}^p \rangle$. It has been observed that $\langle {v_2}^n \rangle$ is more than $\langle {v_2}^p \rangle$ (not shown in the figure) because for neutrons, symmetry energy is repulsive and for proton symmetry energy is attractive. This is because protons feel extra repulsion due to Coulomb interactions and hence transition energies is lower for them. The increase in the impact parameter leads to shifting of transition points due to decrease in the influence of Coulomb interactions and due to increasing role of the symmetry energy starts dominating [262, 309]. This means that study of transition energy associated with proton and neutron can be helpful in

understanding the influence of Coulomb and symmetry energy. Author has compared the theoretical results with experimental data obtained by M. D. Cozma [310].

## 6.10 Transition energy as a function of transverse momentum

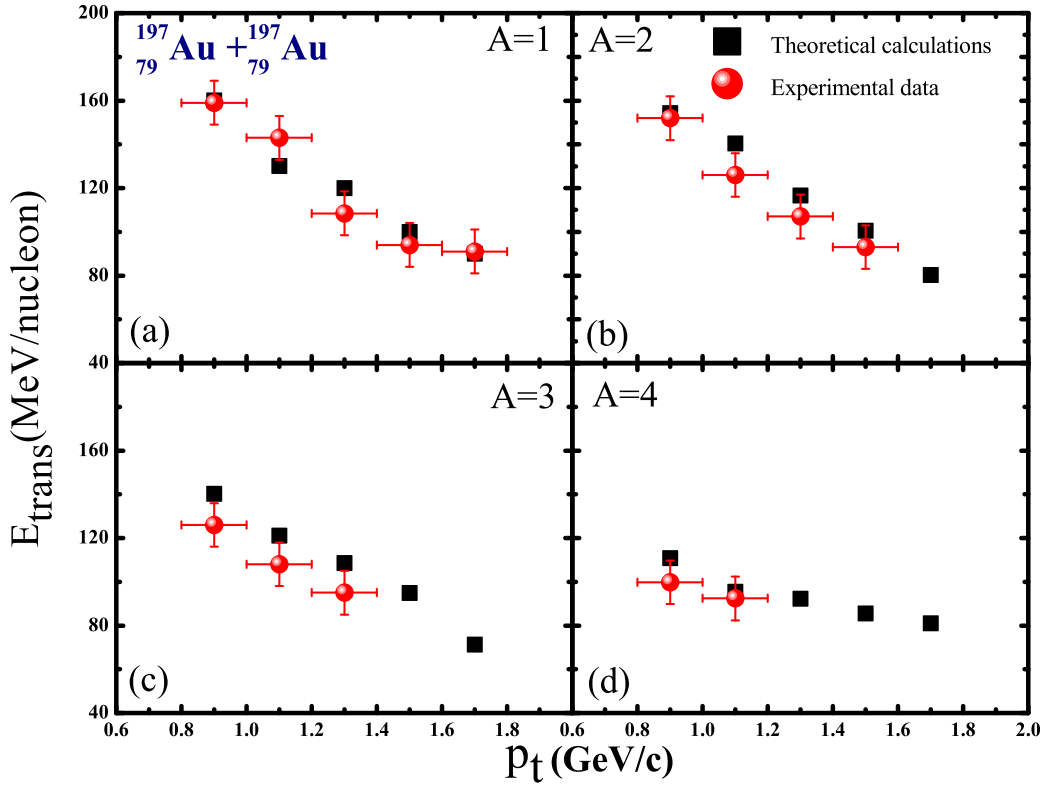


**Figure 6.16:** The transition energy as a function of the transverse momentum for different type of particles (A = 1, 2, 3 and 4) for the reaction $^{197}_{79}Au+^{197}_{79}Au$.

Transition energy as a function of transverse momentum $p_t$ for different particle type (A = 1, 2, 3 and 4) and for the reaction $^{197}_{79}Au+^{197}_{79}Au$ has been comprehensively investigated. Transition energy is closely related to in-plane to out-of-plane transition of nuclear flow. Moreover, experimental observations have put constraints on the transverse momentum of the nucleons depending on the efficiency of detectors. The fragments consisting of nucleons have large value of transverse momentum associated

with them as compared to free nucleons and hence have smaller values of transition energy. In Fig 6.16, transition energy is displayed for different particle types (A = 1, 2, 3 and 4). Experimentally, it is possible to extract data for transition energy at a certain transverse momentum. In Fig 6.16, continuous decrease of the transition energy is clearly observed. The difference in $E_{trans}$ value for different particles decreases with increase in value of $p_t$. At a large value of $p_t$, the contribution comes from large expansion velocities during the early expansion phase of the fireball [311]. The theoretical results presented here are also compared with the experimental data [87] for A = 1, 2, 3 and 4 fragments. Author observed that results obtained from theoretical predictions (black symbols) and experimental (red symbols) data follows the similar trend for all the fragments under consideration.

## 6.11 Anisotropy ratio $R_N$ as a function of incident energy

An anisotropy ratio $R_N$ which is also called as squeeze out ratio is another important feature associated with elliptical flow. The squeeze out ratio can be correlated with shadowing phenomenon of nuclear matter. The anisotropy ratio gives information about the squeeze-out of nucleons and lighter mass fragments. The previous studies have been made to pin down the squeeze-out of neutrons [312] and charged particles [313], have shown their dependence on transverse momentum of nucleons. Light mass fragments are emitted from participant zone, therefore squeeze out ratio is calculated for A = 1, 2, 3 and 4 particles. In the Fig 6.17 (a and b), we have plotted $R_N$ with incident energy for A = 1, 2, 3 and 4 particles for two different impact parameter bins. The squeeze-out ratio $R_N$ is connected with the elliptical flow through the relation given by [313]

$$R_N = \frac{(1 - 2v_2)}{(1 + 2v_2)} \tag{6.7}$$

For lower beam energy limit i.e., up to $\sim$ 100 MeV/nucleon, $R_N < 1$, because $v_2 > 0$. Due to mean field effects at lower energies the colliding system tends to rotate

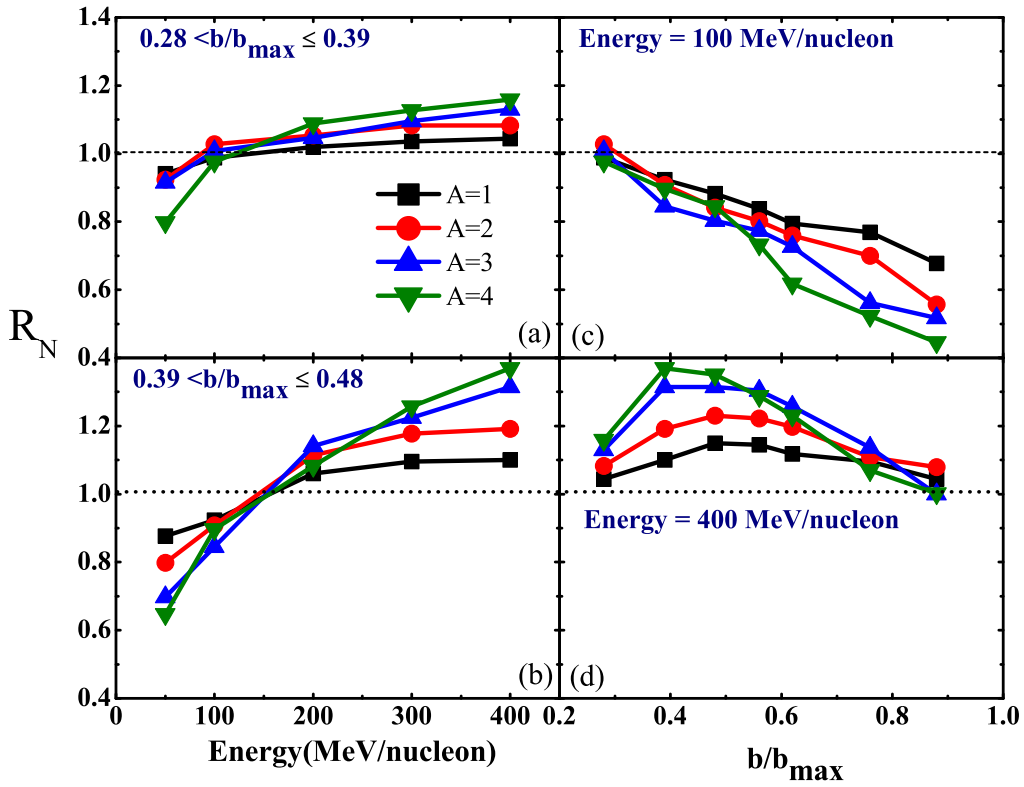


**Figure 6.17:** Anisotropy ratio $R_N$ as a function of energy (a and b) and impact parameter (c and d) for different particle type (A = 1,2,3 and 4) for the reaction ${}^{197}_{79}Au + {}^{197}_{79}Au$.

and emit particles predominantly in the reaction plane due to dominance of centrifugal forces. At higher incident energies $v_2 < 0$ and $R_N > 1$, leads to squeeze out of nucleons/fragments out-of-plane. This squeeze out is the result of the competition between mean field and nucleon-nucleon collisions. The out of plane emission again shows a decrease in number of nucleons with increase in energy. This occurs when $v_2$ reaches its maximum negative value. It is further observed that out of plane squeeze out is achieved above 100 MeV/nucleon at both the impact parameter ranges. From Fig 6.17 (a and b), it has been revealed that squeeze out effect and emission of light mass fragments are correlated with each other. Therefore, more squeeze out is observed at higher energies. In Fig 6.17 (c and d), $R_N$ as a function of impact parameter for two different incident energies has been displayed. At E = 100 MeV/nucleon, there is no

squeeze out as shown in Fig 6.17 (c). $R_N$ increases because of the disappearance of anisotropy in any central collision, therefore as $v_2 \rightarrow 0$ gives $R_N \rightarrow 1$ and not because of enhancement of out-of-plane emission $R_N > 1$. At the higher incident energies E = 400 MeV/nucleon maximum value of $R_N$ is achieved at a scaled impact parameter of $0.48 < \hat{b} \leq 0.56$, this is due to the shadowing effect. If $v_2$ is calculated at still higher impact parameter, then squeeze out effect decreases as energy transferred to participant zone is less and hence the reaction dynamics prefers in-plane emission.

## 6.12 Correlation between $N_{Part}$ and elliptic flow

In the Fig 6.18, author has displayed the elliptic flow and $N_{Part}$, as a function of impact parameter. At incident energy (E = 50 MeV/nucleon) in Fig 6.18 (a), elliptic flow ($< v_2 >$) and $N_{Part}$ cross each other while, in the Fig 6.18 (b), at higher incident energy (E = 400 MeV/nucleon) elliptic flow ($< v_2 >$) and $N_{Part}$ do not cross each other. Transition from the mean field phenomena to nucleon-nucleon collisions are clearly observed. At lower incident energies, reaction dynamics are governed by the mean field and binary collisions are suppressed due to Pauli blocking whereas at higher incident energies because of the nucleon-nucleon (NN) collisions, number of participant nucleon increases. In the inset of Fig 6.18 (a) and (b) elliptic flow as a function of impact parameter has been shown. At incident energy E = 50 MeV/nucleon, elliptic flow increases with increase in the impact parameter while at incident energies E = 400 MeV/nucleon, elliptic flow shows decreasing trend with increase in impact parameter [20].

## 6.13 Correlation between nuclear stopping and elliptic flow

In the Fig 6.19, to check the correlation between nuclear stopping and elliptic flow, author have plotted stopping parameter ($< R_E >$) as the function of elliptic flow ($< v_2 >$)

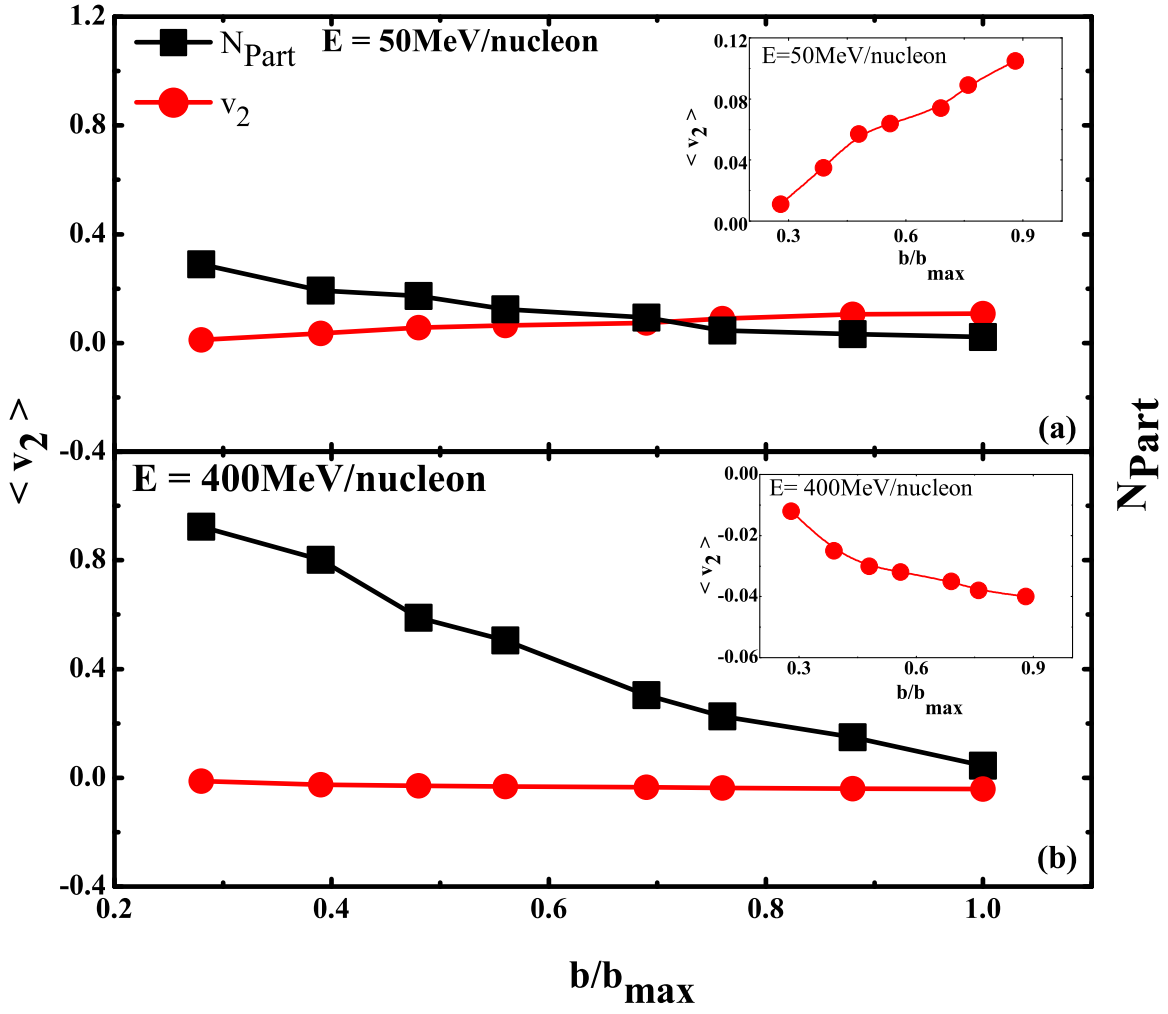


**Figure 6.18:** Elliptic flow ($< v_2 >$) as well as $N_{Part}$ as a function of scaled impact parameter for the reaction $^{197}_{79}Au +^{197}_{79} Au$, at an incident energies E = 50 MeV/nucleon and E = 400 MeV/nucleon.

for the reaction $^{197}_{79}Au +^{197}_{79} Au$. At lower incident energy i.e., E = 50 MeV/nucleon as well as at higher incident energy i.e., E = 400 MeV/nucleon, elliptic flow shows dependence on the nuclear stopping observables. We have shown the correlation between two important observables viz nuclear stopping and elliptic flow below the transition energy and above the transition energy. Elliptic flow is a mid-rapidity phenomenon and nuclear stopping is a global phenomenon. To compare nuclear stopping and elliptic flow, author has calculated the nuclear stopping due to mid-rapidity zone. One can clearly see that the value of nuclear stopping observable $< R_E >$ is higher because at

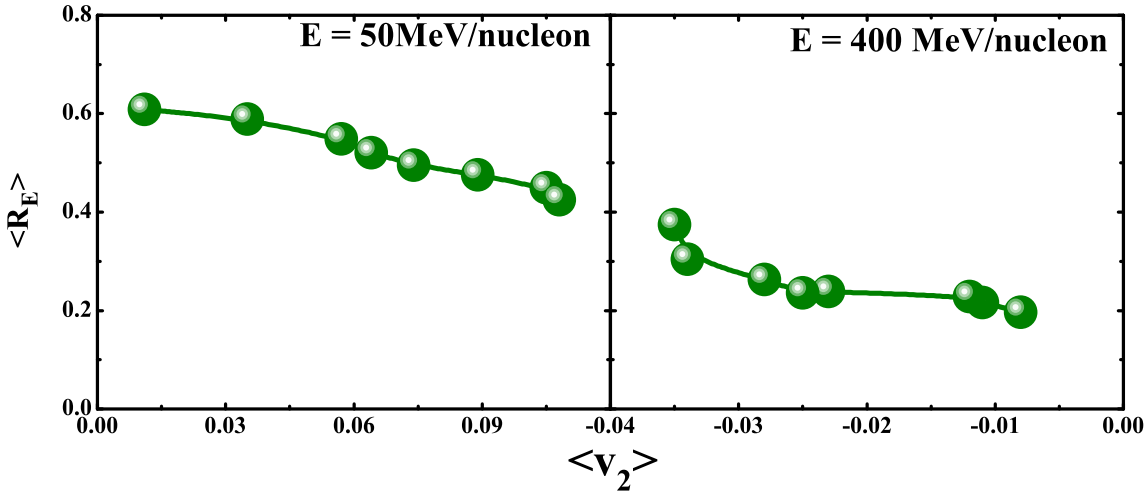


**Figure 6.19:** Stopping parameter ($< R_E >$) as a function of elliptic flow ($< v_2 >$) for the reaction $^{197}_{79}Au+^{197}_{79}Au$, at an incident energies E=50 MeV/nucleon and E=400 MeV/nucleon.

low incident energy nuclear stopping is governed via fragment phase space. At higher incident energy the value of nuclear stopping is less due to nucleons phase space [20].

## 6.14 Relative participation of nucleons in different components of flow

Now, we would like to draw attention towards the comparison of calculated value of different harmonics of flow (difference between % change in over all rapidity region and mid rapidity region) with actual value of Fourier coefficient of flow $< v_1 >$, $< v_2 >$, $< v_3 >$ and $< v_4 >$. On expanding the cosine term of the Fourier series as:

$$< v_1 > = \frac{1}{1!} = 1$$
$$< v_2 > = \frac{1}{2!} = 0.5$$
$$< v_3 > = \frac{1}{3!} = 0.16$$
$$< v_4 > = \frac{1}{4!} = 0.04$$

One can clearly see from the Fig 6.20, that mathematical values over estimate the model values. Here, we have scaled down model calculations w.r.t the Fourier coeffi-

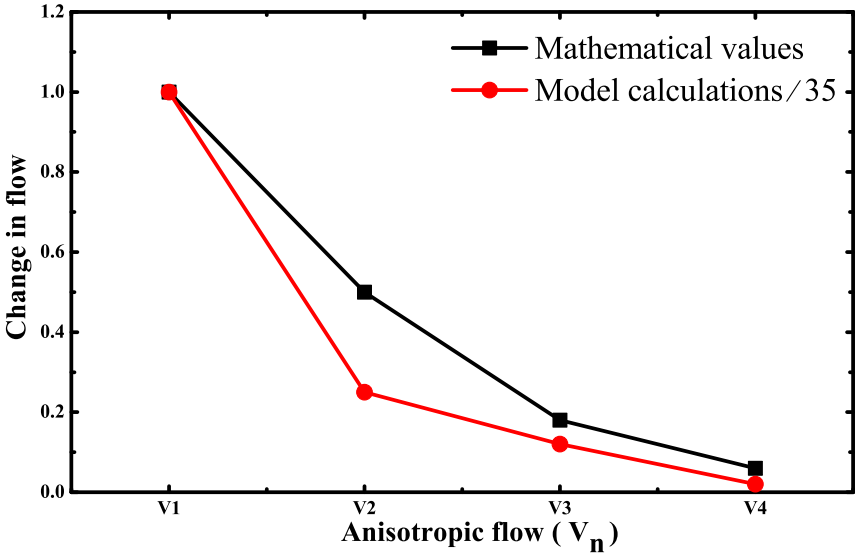


**Figure 6.20:** Relative participation of nucleons among different components of flow [290].

cients by the factor 35. It is simply mathematical scaling. The percentage change in the model calculation and Fourier coefficient decreases with increase in the order of harmonics [290]. These type of studies will be helpful to pin down the scaling among different harmonics for different particles. Consequently, this information will be useful to experimentalist to decide how many collisions among the nucleons they need to perform to get clear signals of higher harmonics of anisotropic flow.

## 6.15 Summary

Our study concludes that there is a broad plateau between the balance energy and transition energy. Author has summate the wealth of unique information relevant to the balance energy and transition energies. Both transition and balance energy found to be decrease with decrease in the impact parameter for any colliding system and the rate of decrease in balance energy is faster than transition energy as the system mass increases. At higher energies, $R_N$ first rises and then fall with light mass fragments (A = 1, 2, 3 and 4). Intermediate energy phenomenon's elliptic flow and nuclear stopping

shows strong correlation with $N_{part}$. The higher harmonics i.e., $< v_3 >$ and $< v_4 >$ have smaller contribution than $< v_1 >$ and $< v_2 >$. The percentage of nucleons participating in flow decreases with increasing order of the harmonics of collective flow.

# Chapter 7

# Summary and outlook

*"The most beautiful thing we can experience is the mysterious. It is the source of all true art and science: Albert Einstein*

## 7.1 Summary

Summarizing, the objectives of the present thesis a comprehensive blueprint of nuclear flow and nuclear stopping have been carried out. Study has been made adopting the Isospin-dependent Quantum molecular dynamics (IQMD) model. In the introductory part basic heavy-ion physics is discussed. Various phenomena that occurs at intermediate energies (Nuclear stopping, Collective flow and multi-fragmentation) have been discussed thoroughly.

Initially the study of basic collision dynamics has been carried out. Present study concludes that there is a broad plateau between the collision dynamics and its correlation with two most important phenomena of intermediate energy i.e., elliptic flow and nuclear stopping. The number of binary collisions increases with an increase in the incident energy and decreases with the impact parameter. At lower energies as well as at higher energies, the contribution of projectile nucleons and target nucleons that participate in collisions are almost same throughout the whole impact parameter range for mass symmetric nuclear reactions. Elliptic flow and nuclear stopping shows strong correlation with $N_{part}$.

After the detailed study on collision dynamics, we have carried out systematic investi-

gations for the nuclear stopping observable $R_E$, $R_P$ and $< varxz >$ for mass symmetric and nearly mass symmetric reactions. Iso-spin mixing have been studied by using pairs of isotopes and isobars. Author concludes that nucleons suffering at least five collisions are more thermalize and contributes in nuclear stopping. The value of nuclear stopping in the case of protons is higher than that of the neutrons. In our investigation, we have observed that $< varxz >$ is the most sensitive observable to study the nuclear stopping. Our study reveals that the LMF's production from the participant zone is immensely associated with global nuclear stopping. In the next part of our study memory loss of nucleons in nuclear stopping have been calculated.

Further, nuclear stopping is calculated for mass asymmetric reactions, where the total system mass is kept fixed ($A_{TOT} = 240, 160, 100, 80, 40$) and also for the total mass is floating at E = 50 MeV/nucleon and 200 MeV/nucleon. The compensation of the geometrical effects helps to achieve an almost similar amount of equilibrium in mass symmetric as well as mass asymmetric reactions. This study is useful for the experimentalist as they can look for projectile stopping along with projectile fragmentation. In the last section of the thesis, author has demonstrated the phenomenon of collective flow. Study concludes that, there is a broad plateau between both the balance energy and transition energy. We summate wealth of unique information relevant to the balance energy and transition energies. We conclude that the balance energy and transition energy are found to increase with the impact parameter for any colliding system. As the mass of colliding nuclei increases, the rate of decrease in balance energy is faster than transition energy. The calculations have been made for the anisotropy ratio $R_N$ is an another way to express the squeeze out ratio ($< v_2 >$) for light mass fragments (A = 1, 2, 3 and 4). Consequently, magnitude of directed flow ($< v_1 >$) is more than elliptic flow ($< v_2 >$), triangular flow ($< v_3 >$) and quadrangular flow ($< v_4 >$). Different $v_n$ harmonics shows different dependency on transverse momentum ($p_t$).

## 7.2 Outlook

In addition to our study, further research and elaboration in intermediate energy domain can be carried out in future. One can look for isospin-mixing effects while studying the pairs of mirror nuclei, in which the number of proton and neutrons are interchanged. The study will be helpful in the discovery of many isotopes, which could have great applications in the field of medicine and material science.

Mass asymmetry can be compensated by varying the colliding geometry, while rotational effects are present. The rotational effects in case of highly mass asymmetric colliding nuclei can be further studied as a topic of further interest.

Memory loss in nuclear stopping gives us an idea of correlation that how many nucleons loose their correlations while undergoing collisions with nucleons of parent nuclei. Further, work in this direction can be presented by checking how many nucleons loose their memories with respect to the entrance channel. Anisotropic flow will provide us with an opportunity to significantly improve our understanding on the properties of nuclear matter. Overall, authors are hopeful that from their study the theoretical and experimental issues covered here will make an impact on the future studies of heavy-ion physics and leads to further studies that will help us to understand more about the origin of collectivity.

# Bibliography


[1] Henri Becquerel, Comptes Rendus **122**, 420 (1896).

[2] F. W. Aston, Nature **128**, 725 (1931).

[3] M. Curie, Compt. Rend. Acad. Sci. **126**, 1101 (1898).

[4] F. W. Aston, Nature **129**, 649 (1932).

[5] W. Marckwald, Phys. Z. **4**, 51 (1902).

[6] E. Rutherford, Phil. Mag. **8**, 636 (1904).

[7] E. Rutherford, Nature **71**, 341 (1905).

[8] E. Rutherford, Phil. Mag. **10**, 290 (1905).

[9] S. J. Sanders, Phys. Rev. C **44**, 2676 (1991).

[10] T. Matsuse *et al.*, Phys. Rev. C **55**, 1380 (1997).

[11] Raj K. Gupta *et al.*, Nucl. Phys. A **738**, 479 (2004).

[12] Ishita Sharma *et al.*, Int. J. Mod. Phys. E **26**, 1750077 (2017).

[13] Jun Su *et al.,* Phys. Rev. C **87** 017602 (2013).

[14] W. Reisdorf *et al.*, Nucl. Phys. A **848**, 366 (2010).

[15] X. Lopez *et al.*, Phys. Rev C **76**, 052203(R) (2007).

[16] A. Andronic *et al.*, Phys. Lett. B **612**, 173 (2005).

[17] J. Lukasik *et al.*, Phys. Lett. B **608**, 223 (2005).

[18] G. Lehaut *et al.*, Phys. Rev. Lett. **104**, 232701 (2010).

[19] Deepshikha and S. Kumar, Nucl. Phys. A **975**, 27 (2018).

[20] Deepshikha and S. Kumar, Nucl. Phys. A **977**, 69 (2018).

[21] Deepshikha and S. Kumar, Nucl. Phys. A **978**, 13 (2018).

[22] Deepshikha and S. Kumar, Nucl. Phys. A **983**, 240 (2019).

[23] A. D. Sood and R. K. Puri, Phys. Rev. C **69**, 054612 (2004).

[24] R. Bansal, S. Gautam and R. K Puri, J. Phys. G **41**, 035103 (2014).

[25] A. Adare *et al.*, Phys. Rev. C **99**, 024903 (2019).

[26] R. K. Puri *et al.*, Phys. Rev. C **54**, R28 (1996).

[27] Y. K. Vermani and R. K. Puri, J. Phys. G **36**, 105103 (2009).

[28] S. Kaur and R. K. Puri, Phys. Rev. C **89**, 057603 (2014).

[29] S. Mallik, G. Chaudhuri, and F. Gulminelli, Phys. Rev. C **97**, 024606 (2018).

[30] G. Chaudhuri and S. Mallik, Nucl. Phys. A **849**, 190 (2011).

[31] S. Das Gupta, S. Mallik and G. Chaudhuri, Phys. Lett. B **726**, 427 (2013).

[32] G. Chaudhuri and S. Das Gupta, Phys. Rev. C **75**, 034603 (2007).

[33] G. Chaudhuri and S. Das Gupta, Phys. Rev. C **76**, 067601 (2007).

[34] G. Chaudhuri and S. Das Gupta, Phys. Rev. C **80**, 044609 (2009).

[35] C. Hartnack *et al.*, Phys. Rep **510**, 119 (2012).

[36] S. Gautam *et al.*, Phys. Rev. C **83**, 034606 (2011).

[37] A. Bonasera Phys. Rev. C **60**, 065212 (1999).

[38] S. Terranova and A. Bonasera, Phys. Rev. C **70**, 024906 (2004).

[39] Ernest Rutherford, Philosophical Magazine, **21**, 669 (1911).

[40] Ernest Rutherford, Philosophical Magazine, **24**, 669 (1912).

[41] Ernest Rutherford, Philosophical Magazine, **27**, 488 (1914).

[42] Kenneth G. Wilson, Phys. Rev. D **10**, 2445 (1974).

[43] B. Martin and G. Shaw, Particle Physics, Wiley 2nd ed., 2005.

[44] David J. Gross and Frank Wilczek, Phys. Rev. Lett. **30**, 1343 (1973).

[45] G. T. Hooft, Nucl. Phys. B **74**, 413 (1998).

[46] Claudio Nassif *et al.*, Canadian J. Phys. **94**, 740 (2016).

[47] T. Lee and G. Wick, Phys.Rev. D **9**, 2291 (1974).

[48] J. W. Negele, Rev. Mod. Phys. **54**, 913 (1982).

[49] Leo P. Kadanoff, J. Stat. Phys. **137**, 777 (2009).

[50] J. Decharge and D. Gogny, Phys. Rev. C **21**, 1568 (1980).

[51] J. Y. Ollitrault, Eur. J. Phys. **29**, 275 (2008).

[52] C. Gale *et al.*, Int. J. Mod. Phys. A **28**, 1340011 (2013).

[53] I. Arsene *et al.*, Nucl. Phys. A **757**, 1 (2005).

[54] J. Adams *et al.*, Nucl. Phys. A **757**, 102 (2005).

[55] S. H. Kahana, Ann. Rev. Nucl. Part. Sci **39**, 231 (1989).

[56] W. D. Myers and W. J. Swiatecki, Phys. Rev. C **57**, 3020 (1998).

[57] James M. Lattimer *et al.*, Phys. Rev. Lett. **66**, 2701 (1991).

[58] H. A. Bethe, Rev. Mod. Phys. **62**, 801 (1990).

[59] J. J. Molitoris and H. Stocker, Phys. Rev. C **32**, 346 (1985).

[60] J. Aichelin Phys. Rep. **202**, 233 (1991).

[61] B. Jakobsson *et al.,* Nucl. Phys. A **509**, 195 (1990).

[62] H. W. Barz *et al.,* Nucl. Phys. A **548**, 427 (1992).

[63] M. Begemann Blaich *et al.,* Phys. Rev. C **58**, 1639 (1998).

[64] M. Begemann Blaich *et al.,* Phys. Rev. C **48**, 610 (1993).

[65] N. T. B. Stone *et al.,* Phys. Rev. Lett. **78**, 2084 (1997).

[66] M. B. Tsang *et al.,* Phys. Rev. Lett. **71**, 1502 (1993).

[67] S. C. Jeong *et al.,* Nucl. phys. A **604**, 208 (1996).

[68] J. Hubele *et al.,* Phys. Rev. C **46**, R1577 (1992).

[69] Fu Hu Liu *et al.*, Chin. J. Phys. **49**, 601 (2011).

[70] G. Chaudhuri, F. Gulminelli and S. Das Gupta, Phys. Rev. C **80**, 054606 (2009).

[71] Swagata Mallik and Gargi Chaudhuri, Phys. Rev. C **87**, 011602 (2013).

[72] J. Y. Ollitrault, Phys. Rev. D **46**, 229 (1992).

[73] S. Voloshin and Y. Zhang, Z. Phys. C **70**, 665 (1996).

[74] P. Danielewicz and G. Odyniec, Phys. Lett. B **157**, 146 (1985).

[75] C. A. Ogilvie *et al.,* Phys. Rev. C **42**, R10 (1990).

[76] R. K. Gupta *et al.*, Phys. Rev. C **47**, 561 (1993).

[77] R. K. Puri *et al.*, Eur. Phys. Lett. **9**, 767 (1989).

[78] H. Sorge, Phys. Rev. Lett. **78**, 2309 (1997).

[79] M. Bleicher and H. Stocker, Phys. Lett. B **526**, 309 (2002).

[80] B. Zhang, *et al.*, Phys. Lett. B **455**, 45 (1999).

[81] D. J. Magestro, Ph.D Thesis, MSU (2000).

[82] M. Demoulins *et al.,* Phys. Lett. B **241**, 476 (1990).

[83] H. H. Gutbrod *et al.,* Phys. Lett. B **216**, 267 (1989).

[84] H. A. Gustafsson *et al.,* Phys. Rev. Lett. **52**, 1590 (1984).

[85] H. H. Gutbrod *et al.,* Phys. Rev. C **42**, 640 (1990).

[86] A. M. Poskanzer and S. Voloshin, Phys. Rev. C **58**, 1671 (1998).

[87] A. Andronic *et al.*, Nucl. Phys. A **679**, 765 (2001).

[88] Yingxun Zhang and Zhuxia Li, Phys. Rev. C **74**, 014602 (2006).

[89] Deepshikha and S. Kumar, AIP Proc. **1953**, 140027 (2018).

[90] Deepshikha and S. Kumar, AIP Proc. **2006**, 030005 (2018).

[91] Deepshikha and S. Kumar, AIP Proc. **2050**, 020014 (2018).

[92] Lie Wen Chen and Che Ming Ko, Phys. Rev. C **73**, 014906 (2006)

[93] Lie Wen Chen and Che Ming Ko, Phys. Rev. C **73**, 044903 (2006).

[94] Jun Xu, and Che Ming Ko, Phys. Rev. C **84**, 044907 (2011).

[95] Y. G. Ma *et al.,* Nucl. Phys. A **787**, 611c (2007).

[96] W. Bauer, Phys. Rev. Lett. **61**, 2534 (1988).

[97] J. K. Dhawan, *et al.*, Phys. Rev. C **74**, 057901 (2006).

[98] P. B. Gossiaux and J. Aichelin, Phys. Rev. C **56**, 2109 (1997).

[99] R. E. Renfordt *et al.*, Phys. Rev. Lett. **53**, 763 (1984).

[100] R. K. Tripathi *et al.*, Phys. Rev. C **8**, 129 (1973).

[101] J. Aichelin *et al.*, Phys. Rev. C **37**, 2451 (1998).

[102] Z. X. Li *et al.*, Phys. Rev. C **44**, 824 (1991).

[103] F. Rami *et al.,* Phys. Rev. Lett. **84**, 1120 (2000).

[104] B. Hong *et al.,* Phys. Rev. C **66**, 034901 (2002).

[105] A. Gobbi *et al.,* Nucl. Instrum. Methods Phys. Res. A **324**, 156 (1993).

[106] J. Ritman, Nucl. Phys. B **44**, 708 (1995).

[107] D. Best *et al.,* Nucl. Phys. A **625**, 307 (1997).

[108] B. Hong *et al.,* Nucl. Phys. A **721**, 317 (2003).

[109] W. Reisdorf *et al.,* Phys. Rev. Lett. **92**, 232301 (2004).

[110] A. Andronic *et al.,* Eur. Phys. J. A **30**, 31 (2006).

[111] O. Lopez, D. Durand et al., Phys. Rev. C **90**, 064602 (2014).

[112] Micghal Gryzinski, The Physical Rev. **107**, 1471 (1957).

[113] W. D. Wilson *et al.,* Phys. Rev. B **15**, 5 (1977).

[114] H. Stocker *et al.,* Phys. Rev. Lett. **52**, 1594 (1984).

[115] B. A. Li *et al.,* Nucl. Phys. A **630**, 556 (1998).

[116] J. Y. Liu *et al.,* Phys. Rev. Lett **86**, 975 (2001).

[117] Yang Yan-Fang *et al.,* Chin. Phys. Lett. **18**, 1040 (2001).

[118] Liu Jian-Ye *et al.,* Chin. Phys. Lett. **21**, 1914 (2004).

[119] J. K. Dhawan *et al.,* Phys. Rev. C **74**, 057901 (2006).

[120] Y. Zhang *et al.,* Phys. Rev. C **75**, 034615 (2007).

[121] Fen fu *et al.,* Phys. Lett. B **666**, 359 (2008).

[122] S. Kumar *et al.,* Chin. Phys. Lett. **27**, 062504 (2010).

[123] S. Kumar *et al.,* Phys. Rev. C **81**, 014601 (2010).

[124] A. Jain *et al.,* Phys. Rev. C **84**, 057602 (2011).

[125] A. Jain *et al.,* Phys. Scr. **85**, 065306 (2012).

[126] V. Kaur *et al.,* Nucl. Phys. A **861**, 37 (2011).

[127] K. S. Vinayak *et al.,* J. Phys. G **39**, 095105 (2012).

[128] K. S. Vinayak *et al.,* Phys. of Atomic Nuclei **76**, 286 (2013).

[129] K. S. Vinayak *et al.,* Eur. Phys. J. A **48**, 96 (2012).

[130] Yong-Zhong Xing *et al.,* Chin. Phys. Lett. **33**, 122501 (2016).

[131] Z. Basrak *et al.*, Phys. Rev. C **93**, 054609 (2016).

[132] G. Tian *et al.,* Phys. Rev. C **95**, 044613 (2017).

[133] M. D. Partlan *et al.,* Phys. Rev. Lett. **75**, 2100 (1995).

[134] https://www.gsi.de/work/forschung/cbmnqm/fopi.htm.

[135] V. Ramillien *et al.,* Nucl. Phys. A **587**, 802 (1995).

[136] C. Pinkenburg Phys. Rev. Lett. **83**, 1295 (1990).

[137] R. Pak *et al.,* Phys. Rev. C **53**, R1469 (1996).

[138] R. Pak *et al.,* Phys. Rev. C **54**, 2457 (1996).

[139] H. A. Gustafsson *et al.,* Phys. Rev. Lett. **52**, 1590 (1984).

[140] R. Pak *et al.,* Phys. Rev. Lett. **78**, 1022 (1997).

[141] R. Pak *et al.,* Phys. Rev. Lett. **78**, 1026 (1997).

[142] P. Crochet *et al.,* Nucl. Phys. A **624**, 755 (1997).

[143] J. Barrette *et al.,* Phys. Rev. C **59**, 884 (1999).

[144] D. J Magestro *et al.,* Phys. Rev. C **61**, 021602(R) (2000).

[145] Q. Pan and P. Danielewicz, Phys. Rev. Lett. **70**, 2062 (1993).

[146] A. Andronic *et al.,* Phys. Rev. C **64**, 041604(R) (2001).

[147] A. Andronic *et al.,* Nucl. Phys. A **679**, 765 (2001).

[148] A. Andronic *et al.,* Phys. Rev. C **67**, 034907 (2003).

[149] N. Bastid *et al.,* Phys. Rev. C **72**, 011901(R) (2005).

[150] D. Cussol *et al.,* Phys. Rev. C **65**, 044604 (2002).

[151] Yuting Bai *et al.,* J. Phys. G. **34**, S903 (2007).

[152] Aihong Tang *et al.,* Jour. of Phys: Conf. Series **230**, 012018 (2010).

[153] Paul Sorensen, J. Phys. G. **38**, 124029 (2011).

[154] L. Adamczyk *et al.,* Phys. Rev. C **88**, 014904 (2013).

[155] Mikoaj Krzewicki, J. Phys. G. **38**, 124047 (2011).

[156] Sushanta Tripathy *et al.*, Eur. Phys. J. A **53**, 99 (2017).

[157] H. Stocker *et al.,* Phys. Rev. Lett. **44**, 725 (1980).

[158] P. Danielewicz and G. Odyniec, Phys. Lett. B **157,** 146 (1985).

[159] J. Cugnon, Nucl. Phys. A **387**, 191 (1982).

[160] G. F. Bertsch *et al.*, Phys. Lett. B **189,** 384 (1987).

[161] G. Peilert *et al.*, Phys. Phys. C **39**, 1402 (1989).

[162] G. D. Westfall *et al.,* Phys. Rev. Lett. **71**, 1986 (1993)

[163] Sven Soff *et al.,* Phys. Rev. C **51**, 3320 (1995).

[164] M. J. Huang *et al.,* Phys. Rev. Lett. **77**, 3739 (1996).

[165] S. Voloshin and Y. Zhang Z. Phys. C **70**, 665 (1996).

[166] Feng Shou Zhang *et al.*, Eur. Phys. J. A **9**, 149 (2000).

[167] D. J. Magestro *et al.*, Phys. Rev. C **62**, 041603(R) (2000).

[168] D. Klakow *et al.*, Phys. Rev. C **48**, 1982 (1993).

[169] W. Bauer, Phys. Rev. Lett. **61**, 2534 (1988).

[170] C. Gale *et al.*, Phys. Rev. C **35**, 1666 (1987).

[171] C. Gale *et al.*, Phys. Rev. C **41**, 1545 (1990).

[172] A. D. Sood and Rajeev K. Puri, Phys. Rev. C **73**, 067602 (2006).

[173] S. Gautam and A. D. Sood, Phys. Rev. C **82**, 014604 (2010).

[174] S. Kumar *et al.*, Phys. Rev. C **81**, 014601 (2010).

[175] V. Kaur *et al.*, Phys. Lett. B **697**, 512 (2011).

[176] K. S. Vinayak and S. Kumar, Eur. Phys. J. A **47**, 144 (2011).

[177] M. D. Cozma, Phys. Lett. B **700**, 139 (2011).

[178] Yan Ting-Zhi, Chin. Phys. C **37**, 014105 (2013).

[179] Yongjia Wang *et al.*, Phys. Rev. C **89**, 034606 (2014).

[180] C. L. Zhou *et al.*, Phys. Rev. C **90**, 057601 (2014).

[181] R. Bansal and S. Gautam, Phys. Rev. C **91**, 024615 (2015).

[182] Hao-jie Xu *et al.*, Phys. Rev. C **93**, 064905 (2016).

[183] Xiangrong Zhu and Huichao Song, Jour. of Phys. Conf. Series **668**, 012080 (2016).

[184] Danut Argintaru, *et al.*, Eur. Phys. J. A **53**, 6 (2017).

[185] Jiangyong Jia *et al.*, J. Phys. G **44**, 075106 (2017).

[186] V. Khachatryan *et al.*, Phys. Rev. C **92**, 034911 (2015).

[187] H. Boal *et al.,* Rev. Mod. Phys. **62**, 553 (1990).

[188] U. Heinz and B. Jacak, Annu. Rev. Nucl. Part. Sci. **49**, 529 (1999).

[189] U. A. Wiedemann and U. Heinz, Phys. Rep. **319**, 145 (1999).

[190] A. Kaur *et al.,* Phys. Atomic. Nucl. **79**, 474 (2016).

[191] M. B. Tsang *et al.*, Phys. Rev. C **40**, 1685 (1989).

[192] S. Kaur *et al.*, Phys. Rev. C **90**, 037602 (2014).

[193] H. Stocker and W. Greiner, Phys. Rep. **137**, 277 (1986).

[194] C. Hartnack *et al.*, Eur. Phys. Journal A **1**, 151 (1998).

[195] J. Cugnon *et al.,* Nucl. Phys. A **352**, 505 (1981).

[196] Y. Kitazoe *et al.,* Phys. Rev. C **29**, 828 (1984).

[197] Y. Yariv and Z. Frankel, Phys. Rev. C **20**, 2227 (1979).

[198] L. Wilets *et al.,* Nucl. Phys. A **301**, 359 (1978)

[199] A. R. Bodmer *et al.,* Phys. Rev. C **22**, 1025 (1980)

[200] A. Vicentini *et al.,* Phys. Rev. C **31**, 1783 (1985).

[201] B. A. Li and Sherry J. Yennello, Phys. Rev. C **52**, 51 (1995).

[202] B. A. Li *et al.,* Phys. Rev. Lett. **76**, 4492 (1996).

[203] B. A. Li *et al.,* Int. Jour. Phys. E **7**, 147 (1998).

[204] G. F. Bertsch *et al.,* Phys. Rev. C **29**, R673 (1984).

[205] J. Aichelin and G. Bertsch, Phys. Rev. C **31**, 1730 (1985).

[206] G. F. Bertsch and Phys. Rep. **160**, 189 (1988).

[207] W. Bauer, G. F. Bertsch and S. Das Gupta, Phys. Rev. Lett. **58**, 863 (1987).

[208] S. Das Gupta, S. Mallik, and G. Chaudhuri, Phys. Lett. B **726**, 427 (2013).

[209] S. Mallik, S. Das Gupta, and G. Chaudhuri, Phys. Rev. C **89**, 044614 (2014).

[210] N. Wang, Z. Li and X. Wu, Phys. Rev. C **65**, 064608 (2002).

[211] N. Wang *et al.,* Phys. Rev. C **69**, 034608 (2004).

[212] J. Bartel *et al.,* Nucl. Phys. A **386**, 79 (1982).

[213] E. Chabanat *et al.,* Nucl. Phys. A **627**,710 (1997).

[214] Y. Zhang *et al.,* Phys. Lett. B **664**, 145 (2008).

[215] L. W. Chen and C. M. Ko, Phys. Lett. B **634**, 205 (2006).

[216] H. Feldmeier, Nucl. Phys. A **515**, 147 (1990).

[217] H. Feldmeier *et al.,* Nucl. Phys. A **586**, 493 (1995).

[218] J. Schnack, H. Feldmeier, Nucl. Phys. A **601**, 181 (1996).

[219] Lawrence Wilets and James S. Cohen, Contemporary Physics **39**, 163 (1998).

[220] H. Feldmeier and J. Schnack, Rev. of Modn. Phys. **72**, 655 (2000).

[221] A. Ono and H. Horiuchi, Phys. Rev. C **53**, 2341 1996.

[222] A. Ono and H. Horiuchi, Phys. Rev. C **53**, 2958 1996.

[223] A. Ono and H. Horiuchi, Phys. Rev. Lett. **68**, 2898 1993.

[224] A. Ono and H. Horiuchi, Prog. Theor. Phys. **87**, 1185 1992.

[225] A. Ono and H. Horiuchi, Phys. Rev. C **47**, 2652 1993.

[226] S. A. Bass *et al.,* Phys. Rev. C **51**, 3343 (1995).

[227] L. G. Arnold *et al.,* Phys. Rev. C **25**, 936 (1982).

[228] G. Passatore, Nucl. Phys. A **95**, 694 (1967).

[229] B. J. VerWest and R. A. Arndt, Phys. Rev. **C 25**, 1979 (1982).

[230] P. Danielewicz and G. F. Bersch, Nucl. Phys. A **533**, 712 (1991).

[231] S. Huber and J. Aichelin, Nucl. Phys. A **573**, 587 (1994).

[232] B. A. Li *et al.,* Phys. Reports **464**, 113 (2008).

[233] Rajni and S. Kumar Eur. Phys. J. A **48**, 19 (2012).

[234] J. Aichelin, *et al.,* Phys. Rev. C **37**, 2451 (1998).

[235] A. Bohnet *et al.,* Phys. Rev. C **44**, 2111 (1991).

[236] Z. X. Li *et al.*, Phys. Rev. C **44**, 824 (1991).

[237] T. Maruyama *et al.*, Phys. Rev. C **42**, 386 (1990).

[238] G. Peilert *et al.,* Phys. Rev. **C 39**, 1402 (1989).

[239] A. Bohnet *et al.,* Nucl. Phys. A **494**, 349 (1989).

[240] L. Neise *et al.,* Nucl. Phys. A **519**, 375 (1990).

[241] M. Berenguer *et al.,* J. Phys. G **18**, 655 (1992).

[242] P. B. Gossiaux and J. Aichelin, Phys. Rev. C **56**, 2109 (1997).

[243] H. W. Barz *et al.,* Nucl. Phys. A **531**, 453 (1991).

[244] W. Bauer *et al.,* Phys. Rev. C **47**, R1838 (1993).

[245] S. C Jeong *et al.,* Phys. Rev. Lett. **72**, 3468 (1994).

[246] P. Danieiewicz, Phys. Rev. C **51**, 716 (1995).

[247] M. A. Lisa *et al.,* Phys. Rev. Lett. **72**, 3468 (1994).

[248] B. M. Badawy, Journal of Nucl. and Radiation Phys. **3**, 31 (2008).

[249] I. A. Pshenichnov *et al.*, Phys. Rev. C **57**, 1920 (1998).

[250] J. Gosset *et al.,* Phys. Rev. C **16**, 629 (1977).

[251] S. Zhang *et al.,* Phys. Rev. C **95**, 064904 (2017).

[252] L. Li *et al.,* Phys. Rev. C **97**, 044606 (2018).

[253] B. Alver *et al.,* Brazilian Jour. of Phys. **37**, 770 (2007).

[254] Aamodt *et al.,* Phys. Rev. Lett. **106**, 032301 (2011).

[255] B. Abelev *et al.,* Phys. Rev. C **88**, 044909 (2013).

[256] A. D. Sood *et al.,* Phys. Rev. C **70**, 034611 (2004)

[257] A. D. Sood *et al.,* Phys. Lett. B **594**, 260 (2004).

[258] L. Scalone *et al.,* Phys. Lett. B **461**, 9 (1999).

[259] Y. Z. Xing *et al.*, Chin. Phys. Lett. **12**, 122501 (2016).

[260] S. Kumar *et al.,* Phys. Rev. C **78**, 064602 (2008).

[261] S. Kaur and R. K. Puri, Phys. Rev. C **87**, 014620 (2013).

[262] S. Gautam, J. Phys. G. **37**, 085102 (2010).

[263] S. Gautam *et al.,* Phys. Rev. C **83**, 014603 (2011).

[264] R. Pak *et al.,* Phys. Rev. Lett. **78**, 1022 (1997).

[265] R. Pak *et al.,* Phys. Rev. Lett. **78**, 1026 (1997).

[266] W. Scheid *et al.,* Phys. Rev. Lett. **32**, 741 (1974)

[267] H. A. Gustafsson *et al.,* Phys. Rev. Lett. **52**, 1590 (1984).

[268] J. J. Molitoris and H. Stocker, Phys. Lett. B **162**, 47 (1985).

[269] G. F. Bertsch *et al.,* Nucl. Phys. A **490**, 745 (1988).

[270] J. Aichelin, Phys. Rep. **202**, 233 (1991).

[271] A. Andronic *et al.*, Eur. Phys. J. A **30**, 31 (2006).

[272] G. Q. Zhang *et al.*, Phys. Rev. C **84**, 034612 (2011).

[273] R. K. Puri and A. D. Sood, Heavy Ion Phys. **16**, 429 (2002).

[274] R. E. Renforolt *et al.*, Phys. Rev. Lett. **53**, 763 (1984).

[275] Li Qing-Feng and Li Zhu-Xia, Chin. Phys. Lett. **19**, 321 (2002).

[276] Ying Yuan *et al.*, Phys. Rev. C **81**, 034913 (2010).

[277] R. K. Puri and N. K. Dhiman, Eur. Phys. J. A **23**, 429 (2005).

[278] S. Goyal, Phys. Rev. C **84**, 044614 (2010).

[279] J. Hubele *et al.*, Phys. Rev. C **46**, 1577 (1992).

[280] A. Schuttauf *et al.*, Nucl. Phys. A **607**, 457 (1996).

[281] R. Wada *et al.*, Phys. Rev C **69**, 044610 (2004).

[282] M. Begemann-Blaich *et al.,* Phys. Rev. C **48**, 2 (1993).

[283] Y. M. Zheng, Phys. Rev. Lett. **83**, 2534 (1999).

[284] Y. Zhang *et al.*, Phys. Rev. C **74**, 014602 (2006).

[285] Deepshikha and S. Kumar, Modn. Phys. Lett. A **33**, 1850201 (2018).

[286] A. D. Sood and R. K. Puri, Phys. Rev. C **70**, 034611 (2004).

[287] Q. F. Li and Z. X. Li, Chin. Phys. Lett. **19**, 321 (2002).

[288] J. Y. Liu, Chin. Phys. Lett. **21**, 1914 (2004).

[289] S. Soff *et al.,* Phys. Rev. C **51**, 3320 (1995).

[290] Deepshikha and S. Kumar, Canadian Journal of Phys. **96**, 1092 (2018).

[291] R. Rogly, G. Giacalone and J. Y. Ollitrault, Phys. Rev. C **98**, 024902 (2018).

[292] S. Voloshin, Phys. Rev. C **55**, R1630 (1997).

[293] M. B. Tsang *et al.,* Phys. Rev. Lett. **57**, 559 (1986).

[294] W. K. Wilson *et al.,* Phys. Rev. C **41**, R1881 (1990).

[295] M. B. Tsang *et al.,* Phys. Rev. Lett **51**, 1846 (1983).

[296] C. B. Chitwood *et al.,* Phys. Rev. C **34**, 858 (1986)

[297] B. A. Li, Phys. Rev. C **48**, 2415 (1993).

[298] M. B. Tsang *et al.,* Phys. Rev. Lett. **57**, 559 (1986).

[299] J. W. Harris, Nucl. Phys. A **471**, 241 (1987).

[300] H. Stocker *et al.,* Phys. Rev. Lett. **44**, 725 (1980).

[301] H. Stocker *et al.,* Phys. Rev C **25**, 1873 (1982).

[302] A. Jain *et al.,* Ann. Phys. **334**, 334 (2013).

[303] D. Krofcheck *et al.,* Phys. Rev. Lett. **63**, 2028 (1989).

[304] A. Bonasera and L. P. Csernai, Phys. Rev. Lett. **59**, 630 (1987).

[305] J. Lukasik *et al.,* Acta Phys. Hung. A **25**, 229 (2006).

[306] Deepshikha and S. Kumar, Int. Jour. Phys. E **27**, 1850084 (2018).

[307] A. D. Sood *et al.,* Phys. Lett. B **594**, 260 (2004).

[308] A. Jain *et al.,* Phys. Rev. C **85**, 064608 (2012).

[309] Wang Yong Jia *et al.,* Science China C **55**, 2407 (2012).

[310] M. D. Cozma, Phys. Rev. Lett. **700**, 139 (2011).

[311] M. Petrovici, *et al.,* Phys. Rev. Lett. **75**, 5001 (1995).

[312] D. Lambrecht *et al.,* Z. Phys. A **350**, 115 (2011).

[313] H. H. Gutbrod *et al.,* Phys. Rev. C **42**, 640 (1990).